Vectorcardiographic evaluation of electrical dyssynchrony and its role in predicting response to cardiac resynchronization therapy

DR OSITA NATHANIEL OKAFOR

Doctor of Medicine

ASTON UNIVERSITY
August 2022

Vectorcardiographic evaluation of electrical dyssynchrony and its role in predicting response to cardiac resynchronization therapy

by

Dr Osita Okafor

Abstract

Cardiac resynchronization therapy (CRT) has become an important therapeutic strategy for heart failure (HF) patients with impaired left ventricular (LV) systolic function and prolonged QRS duration. The benefit of CRT as an adjunct to pharmacological therapy is now well established, with sustained improvements in quality of life, hospitalization rates and mortality. However, even in carefully selected patients, the response to CRT is often unpredictable with a considerable number of nonresponders (30-50%). Although the reasons for this nonresponse are not entirely clear, studies have suggested that non-optimal left ventricular (LV) lead positioning, lack of electrical dyssynchrony, suboptimal device programming and myocardial scar burden play an important role.

More recently, a wealth of evidence has pointed to the limitations of 12-lead electrocardiography, suggesting it may not accurately reflect the presence or complexities of electrical dyssynchrony in the failing heart. As the efficacy of CRT is primarily achieved through LV resynchronization, there has been renewed interest in the development of techniques that enable better characterization of cardiac electric activation patterns and identification of electrical dyssynchrony. This approach would appear logical, given that CRT is primarily an 'electrical therapy', designed to treat an underlying electrical conduction abnormality. Vectorcardiography (VCG), which was first described in 1920, offers an alternative interpretation of the 12-lead ECG. Its resurgence in the field of CRT has emerged from the recognition that VCG parameters can provide information on dyssynchrony beyond that currently provided by the 12-lead ECG. Prominent amongst these is vectorcardiographic QRS area (QRS_{area}), which has been shown to be superior to QRSd and QRS morphology in predicting response to CRT.

The work presented herein is structured into two major sections. First, we investigate the role of QRS_{area} as a novel predictor of response to CRT. Using a combination of different study designs, our results demonstrate that QRS_{area} is a better predictor of CRT response than QRSd and QRS morphology. We also show that CRT-induced ΔQRS_{area} can be used to help quantify LV resynchronization and to predict long-term clinical outcomes following CRT. Importantly, we are the first to show that a concomitant reduction in both QRS_{area} and QRSd is associated with the best clinical outcomes after CRT, indicating that ECG and VCG can be used in conjunction to help improve patient selection for CRT.

In the second part of this thesis, we focus on the development and validation of a novel, vector-based 3D electroanatomical modelling system. Using a novel computational method, ECGSync combines the surface ECG-derived vectorcardiogram with cardiac magnetic resonance imaging to estimate, by inverse solution, the 3-dimensional sequence of LV activation. Accordingly, we show that

ECGSync can noninvasively map ventricular electrical activity and accurately locate the site of latest electrical activation prior to CRT implantation. Furthermore, we demonstrate that novel ECGSync-derived markers of dyssynchrony can help predict CRT response. Our findings suggest that VCG may have great potential to improve the clinical application of CRT.

Dedicated to my wife
and our wonderful daughters – Bella and Sienna

Acknowledgements

First and foremost, I would like to express my gratitude to my supervisor Professor Leyva-Leon for his tireless help, guidance, and advice throughout my period of research. He encouraged and stimulated countless ideas, which ultimately paved the way towards the research studies included in this thesis. I am also indebted to Dr Peter van Damn (Medical Physicist and owner of PEACS, BV). His knowledge and understanding of vectorcardiography proved to be of immeasurable value during the design and conduct of our research studies. Ultimately, the mathematical construct for ECGSync and TSI is based on his unique interpretation of the vectorcardiogram. He provided the software and training required to undertake vectorcardiographic analysis. As new ideas invariably formed, he was always happy to incorporate these ideas into workable software programmes. I am also grateful for the assistance provided by Dr Berthold Stegemann (Senior Principal Scientist, Medtronic), who was instrumental in the design and set-up of our acute haemodynamic studies. Throughout, he was a source of great knowledge and wisdom on all aspects related to cardiac pacing. Particularmention also goes to Dr Stefan Kracker (Clinical Field Engineer, Medtronic), who flew from Germany to provide technical support for our cases. He emphasised the importance of a meticulous approach to data collection, which proved to be of immeasurable value when analysing the results. Dr Hakam Khalidi (Clinical Affairs and Research Specialist, Medtronic) provided logistical support for our acute haemodynamic studies. He was of tremendous help and was always happy to address my queries with respect to the day-to-day conduct of our studies. I am also grateful to Medtronic, who supported this research with an unrestricted educational grant. This afforded me the luxury to pursue a wide range of different research interests. Finally, but by no means least, I owe my deepest and sincerest gratitude to my wife – Dr Bijal Okafor, whose love, support and understanding never wavered during this lengthy period of research. Thank you.

Contents

List of Tables

List of Figures

Acronyms

AAI	Atrial pacing
ACEI	Angiotensin converting enzyme inhibitor
AF	Atrial fibrillation
AHR	Acute haemodynamic response
AP	Anteroposterior
ARA	Angiotensin receptor antagonist
AT	Activation time
ATP	Anti-tachycardia pacing
AUC	Area under the curve
AV	Atrioventricular
A.Z	Dr Abbazin Zegard
BiV	Biventricular pacing
BSPM	Body surface potential mapping
CABG	Coronary artery bypass graft
CI	Confidence interval
CMR	Cardiac magnetic resonance
CRT	Cardiac resynchronization therapy
CRT-D	Cardiac resynchronization therapy with defibrillator
CRT-P	Cardiac resynchronization therapy - pacing
CRT-R	Cardiac resynchronization therapy responders
CRT-NR	Cardiac resynchronization therapy non-responders
CS	Coronary sinus
DCM	Dilated cardiomyopathy
DDDR	Dual chamber pacing with rate response
EAM	Electroanatomical mapping
ECG	Electrocardiogram

ECGMod	ECG-based electroanatomical modelling
ECGI	Electrocardiographic imaging
EDI	Electrical dyssynchrony index
EDL	Equivalent double layer
EGM	Electrogram
EP	Electrophysiologic
F.L	Professor Francisco Leyva
HF	Heart failure
HR	Hazard ratio
ICD	Implantable cardiac defibrillator
ICM	Ischaemic cardiomyopathy
LAO	Left anterior oblique
LBBB	Left bundle branch block
LAS	Latest activated segment
LEAS	Latest electrically activated segment
LMAS	Latest mechanically activated segment
LV	Left ventricle
LVAT	Left ventricular activation time
LV dP/dt	Maximum rate of pressure increase in the left ventricle
LVEDV	Left ventricular end-diastolic volume
LVEF	Left ventricular ejection fraction
LVESV	Left ventricular end-systolic volume
LVFW	Left ventricular free wall
LVPV	Left ventricular pacing vector
MACE	Major adverse cardiovascular events
MRA	Mineralocorticoid receptor antagonist
MRI	Magnetic Resonance Imaging
NHS	National health service
NICD	Nonspecific intraventricular conduction delay

NICE	National Institute of Clinical Excellence
NICM	Non-ischaemic cardiomyopathy
NYHA	New York Heart Association
O.O	Dr Osita Okafor
OR	Odds ratio
QRS_{area}	Vectorcardiographic QRS area
QoL	Quality of life
QUAD	Quadripolar left ventricular lead
QRSd	QRS duration
UK	United Kingdom
RA	Right atrium
RAO	Right anterior oblique
RBBB	Right bundle branch block
RCT	Randomized controlled trial
ROC	Receiver operator characteristics
RV	Right ventricle
RVOT	Right ventricular outflow tract
SAI QRST	Sum absolute QRS-T integral
SCD	Sudden cardiac death
SD	Standard deviation
SDAT	Standard deviation of activation times
TSAT	Transseptal activation time
T_{area}	Vectorcardiographic T-wave area
VCG	Vectorcardiography
VF	Ventricular fibrillation
VO_2	Oxygen consumption
VT	Ventricular tachycardia
VV delay	Interventricular delay
VVI	Right ventricular pacing

Chapter 1

General introduction

1.1. Introduction to heart failure

Heart failure is a complex clinical syndrome that affects up to 1-2% of the adult population ***(Brignole et al., 2013)***. In developed countries, the major aetiological factors for HF include coronary artery disease, chronic hypertension, valvular heart disease and cardiomyopathy. There has been a recent increase in the contribution of coronary artery disease, which now accounts for 70% of all new cases ***(Mahmood et al., 2014; Sutherland, 2010)***. This has resulted from the improved survival of patients following acute myocardial infarction, alongside the advancing age of the general population. Based on current estimates, the prevalence rates for HF are likely to increase over the next 10 years, with hospital admissions projected to rise by over 50% over the next 25 years ***(Gnani et al., 2001; Sutherland, 2010)***. This poses a significant health concern, with HF already placing a substantial economic burden on the National Health Service (NHS) ***(Murray-Thomas and Cowie, 2003)***. In fact, the management costs associated with HF are currently estimated at 1-2% of the annual NHS budget, or around £625 million ***(Murray-Thomas and Cowie, 2003)***. The majority of these costs (approximately 60%) are driven by inpatient care and the high rehospitalization rates, with an average length of stay for a patient admitted with worsening HF of around 5-10 days, with rehospitalisation rates estimated to be as high as 46% within the first 60 days ***(Krumholz et al., 1997)***. On this basis, improving the treatment and prognosis of patients with HF patients is currently considered to be a global health priority ***(Ponikowski et al., 2014)***.

1.2. Heart failure with conduction delay

Approximately one third of patients with HF have evidence of conduction delay on 12-lead electrocardiography (ECG) [i.e. QRS duration >120ms] ***(Zannad et al., 2007)***. Most commonly, this is due to a block in conduction through the left bundle branch system. Studies have shown that the onset of LBBB can adversely affect left ventricular (LV) systolic performance ***(Zannad et al., 2007)***. Certainly, in patients with established LV systolic dysfunction, the presence of a LBBB QRS morphology has been shown to result in more rapid disease progression, reduced heart function, higher risk of ventricular arrhythmias and poor long-term survival rates ***(Duraes et al., 2016; Zannad et al., 2007)***.

1.3. Pathobiology of ventricular dyssynchrony

In the healthy heart, electrical signals propagate rapidly from the sinoatrial node towards specialised conduction pathways located within the inter-ventricular septum, including the bundle of His and the left and right bundle branches [Figure 1.1] (Nguyên et al., 2018b). This rapid conduction of electrical signals is vital to ensure synchronous activation of the left and right ventricles, respectively. A block in conduction through either the right bundle branch or left bundle branch system results in the development of ventricular conduction delay. If this delay is sufficient to disrupt the normal sequence of activation between the atria and ventricles or within the LV, then dyssynchrony can occur. This may manifest as delayed activation of the left ventricle relative to the right ventricle, so-called **interventricular dyssynchrony**, or alternatively, as a delay in activation of the LV septum versus the LV lateral free wall (**intraventricular dyssynchrony**) ***(Varma et al., 2015)***.

Image redacted

Figure 1.1 Cardiac conduction system.
Overview of the components of the cardiac conduction system, including the sinoatrial (SA) node and atrioventricular (AV) node located within the right atrium. The components of the fast-conducting His-Purkinje system include the bundle of His and the left and right bundle branches. Reprinted from ("Easy Notecards," n.d.)

Due to the relationship between electrical activation and mechanical contraction, the presence of electrical dyssynchrony can result in a disorganised mechanical response (Figure 1.2). In patients with intra-LV dyssynchrony, there is typically early activation and shortening of the septum, which occurs at a time when the LV free wall (LVFW) is still relaxed. In this context, septal contraction contributes little to overall mechanical function and represents 'wasted work' ***(Lim et al., 2008)***. Furthermore, early septal contraction without concomitant lateral LV wall activation results in early pre-systolic stretch of late activated segments [Figure 1.2] (Nguyên et al., 2018b). This places the lateral LV wall under greater wall tension, thereby increasing metabolic demands in this region and creating supernormal contraction (due to the Frank-Starling mechanism) (Nguyên et al., 2018b). Although greater energy expenditure is observed in late activated segments, the net effect of poorly synchronized mechanical contraction is a reduction in myocardial efficiency and impaired global LV systolic function ***(Cheng et al., 2009)***. Several studies have corroborated the negative impact of inter- and intraventricular dyssynchrony on LV function. Additionally, ventricular dyssynchrony results in a reduction in LV filling time, impaired diastolic function, exacerbation of diastolic mitral regurgitation, regional and/or global reductions in LV contractility (dP/dt_{max}) and LV ejection fraction (LVEF) ***(Lim et al., 2008)***. These features contribute to the adverse LV remodelling observed in patients with chronic heart failure.

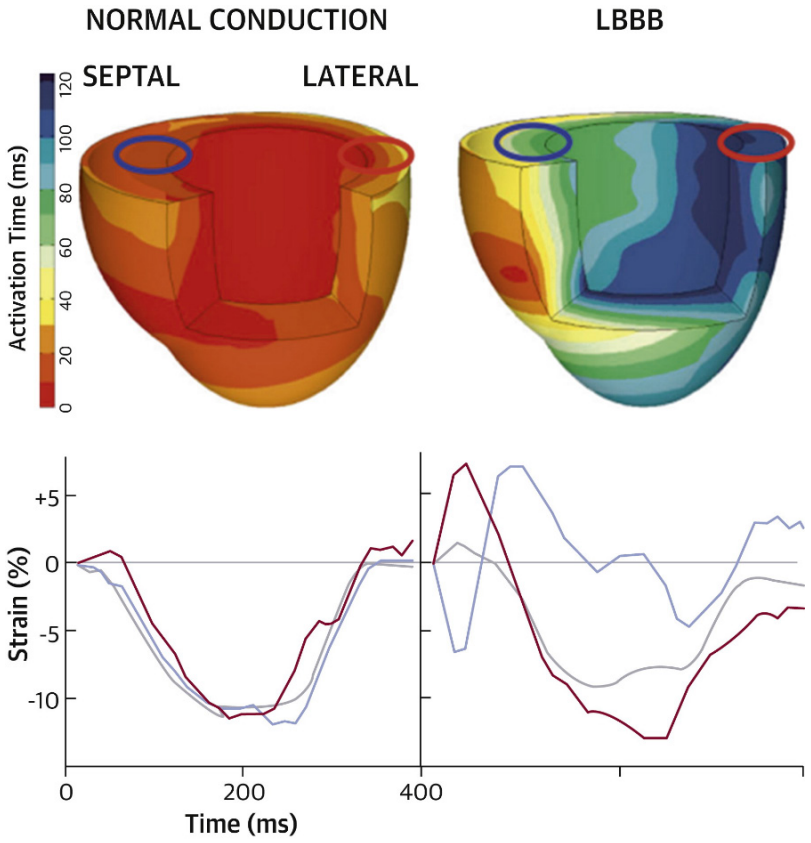

Figure 1.2 LBBB-induced dyssynchrony pattern.

Three-dimensional representation of the activation pattern during normal (top left) and LBBB (top right) activation. These maps show early and synchronous activation of the lateral wall (red circle) relative to the septum (blue circle) during normal LV conduction. In contrast, in a canine model of LBBB, there is early activation and shortening of the septum with delayed activation of the lateral wall. The grey line shows the mean left ventricular strain pattern. Reprinted from Leyva et al (Leyva et al., 2014) and initially adapted from Mills et al (Mills Robert W. et al., 2009).

1.4. Rationale for CRT

Images redacted

Figure 1.3. Trans-venous CRT system.
(Left) Schematic representation of a CRT system. (Right) Chest X-ray of a patient with a wholly transvenous CRT system. Using a left-sided axillary/subclavian vein, three pacing leads have been implanted into the right atrium, right ventricle and left ventricle, respectively.

The aim of CRT is to improve myocardial performance by pre-exciting regions of delayed activation on the LVFW, thereby restoring ventricular synchrony ***(Lim et al., 2008)***. Conventionally, this is achieved by placing a LV lead on the epicardial surface of LVFW (via the coronary sinus [CS]), in conjunction with endocardial right atrial and right ventricular (RV) leads, allowing the left ventricle to be electrically 'resynchronized' (Figure 1.3). Fundamentally, the delivery of biventricular pacing serves to reduce the degree of LBBB-induced dyssynchrony, thereby improving regional and global mechanical function ***(Abraham William T. and Hayes David L., 2003)***. Whilst improvement from CRT is often examined from a mechanical perspective, it is this electrical resynchronization that is thought to underpin its clinical benefits. Immediately following remodelling of electrical activation patterns with the use of CRT, there is a beneficial impact on cardiac function, with improved contractile performance, myocardial efficiency ***(Ellery et al., 2006)***, reduction in mitral regurgitation ***(Breithardt et al., 2003; Vinereanu, 2008)*** and in the longer-term, beneficial geometrical changes of the left ventricle ***(Ellery et al., 2006)***.

1.5. Landmark CRT trials

Although originally devised as a therapeutic strategy for patients with symptomatic bradycardia, significant strides have made in the development of pacemaker technology over the past 20 years. This has enabled the use of biventricular (BiV) pacing as a therapeutic option for HF patients ***(Matsumoto et al)***. The earliest randomized trial designed to prospectively investigate the clinical efficacy of CRT was the 'Multisite Stimulation in Cardiomyopathy' (MUSTIC) study; a multi-centre, randomised, cross-over trial published in 2001 ***(Cazeau et al., 2001)***. A total of 67 patients with advanced heart failure (New York Heart Association [NYHA] class III), LVEF <35% and QRS duration (QRSd) > 150ms were randomised to receive either 3-months of active or inactive CRT ***(Cazeau et al., 2001)***. The delivery of BiV pacing, when compared to no pacing, resulted in significant improvements in walking distance, quality of life and peak oxygen uptake (VO_2) and was associated with reduced hospitalizations ***(Cazeau et al., 2001)***. Similar improvements in walking distance and peak VO_2 were demonstrated in the PATH-HF (Pacing Therapies in Congestive Heart Failure) study ***(Auricchio et al., 2002)***, which evaluated the long-term clinical effects of haemodynamically-optimised CRT. This was the first study to identify that long-term CRT resulted in favourable LV reverse remodelling ***(Auricchio et al., 2002; Leyva et al., 2014)***.

The first large-scale, double-blind study of CRT, the MIRACLE (Multicentre InSync Randomized Clinical Evaluation) trial, randomised 452 patients in sinus rhythm with LVEF <35%, moderate-to-severe HF (NYHA class III-IV) and QRSd ≥ 130ms, to receive either 6-months of BiV or no pacing ***(Abraham et al., 2002)***. The study aimed to assess the therapeutic benefits of CRT but was not powered to address mortality as a primary endpoint. At 6-months follow-up, CRT led to improved quality of life score, walking distance, functional class, and decreased hospitalisations ***(Abraham et al., 2002)***. Furthermore, core analysis of echocardiography data demonstrated improvements in LVEF at 3- and 6-months follow-up, with additional reductions in LV mass, LV end-diastolic volumes (LVEDV), LV end-systolic volumes (LVESV) and severity of mitral regurgitation (MR), confirming the beneficial effects of CRT on reverse LV remodelling ***(Abraham et al., 2002)***.

The CARE-HF (Cardiac Resynchronization – Heart Failure) study was designed to evaluate the mortality benefits of CRT in HF patients with LV systolic dysfunction and QRSd ≥ 120ms, who were already receiving optimal medical therapy (Cleland et al., 2005). Enrolment of CARE-HF subjects required additional evidence of mechanical dyssynchrony, as determined by echocardiography. A total of 813 patients were studied and after a mean follow-up period of 29 months, when compared to medical therapy, the addition of CRT resulted in significant reductions in death from any cause, unplanned cardiovascular hospitalisation and all-cause

mortality ***(Cleland et al., 2005)***. CRT also reduced echocardiographic indices of mechanical dyssynchrony, with reductions in MR severity and beneficial effects on LV reverse remodelling ***(Cleland et al., 2005)***.

The MIRACLE ICD (Multicentre InSync Randomized Clinical Evaluation Implantable Cardioverter Defibrillator) study was one of the earliest studies to evaluate the safety and efficacy of combining implantable cardiac defibrillator (ICD) therapy with BiV pacing ***(Young et al., 2003)***. This multicentre, double-bind RCT was designed to be nearly identical to the original MIRACLE trial, enrolling 369 HF patients with an additional indication for ICD therapy ***(Abraham William T. and Hayes David L., 2003)***. Patients were randomised to receive either 6-months of combined CRT-D (CRT with defibrillator), or ICD therapy alone. At the end of this period, when compared to controls, patients assigned to receive CRT-D demonstrated significant improvements in quality of life, functional status and exercise capacity; comparable to the benefits first observed in the MIRACLE trial. Importantly, the addition of ICD to CRT was safe and did not compromise ICD function, with no difference in the incidence of device-related complications, arrhythmias, detection times for ventricular tachycardia/fibrillation or the number of appropriate and inappropriate shocks ***(Del Negro, n.d.)***. In fact, BiV anti-tachycardia pacing was found to be efficaciously superior then the univentricular (right ventricular) configuration ***(Abraham William T. and Hayes David L., 2003)***. Interestingly, in the VENTAK study, treatment of HF with BiV pacing resulted in a reduced incidence of ICD therapy (including anti-tachycardia pacing and defibrillation), suggesting a protective effect for CRT against ventricular arrhythmias ***(Higgins et al., 2000)***. The authors postulated that improvement in LV performance may have, at least in part, been responsible for this reduced incidence of ICD therapy.

Although the MIRACLE-ICD study found the combination of CRT and ICD to be safe, it was not adequately powered to address reductions in mortality ***(Young et al., 2003)***. Additionally, the relatively short 6-month follow-up period negated a full assessment of late or uncommon complications or reduction in hospitalisation rates ***(Del Negro, n.d.)***. COMPANION (Comparison of Medical Therapy, Pacing and Defibrillation in Heart Failure) was an event-driven study (target > 950 primary events), which was prospectively designed to evaluate the combined primary end-point of all-cause mortality and hospitalisation in patients randomised to receive no pacing (optimal drug therapy only), BiV pacing or biventricular pacing with an ICD ***(Abraham William T. and Hayes David L., 2003; Bristow et al., 2004)***. After enrolling 1520 patients, the study was terminated prematurely due to the finding of a 40% reduction in death or hospitalisation in those allocated to the ICD arm, compared with a 34% reduction in the biventricular arm.

Although these landmark RCT trials established a benefit for CRT in patients with advanced HF (NYHA functional class III-IV), the relative efficacy of CRT in those with milder symptoms (NYHA I-II) was less well established. Some of the early CRT trials (CONTAK-CD and MIRACLE-ICD) extended their inclusion criteria to include those with mild HF symptoms [NYHA functional class II] ***(Abraham et al., 2004; Higgins et al., 2003)***. Within this group, there was evidence to suggest that CRT exerted a beneficial effect on LV reverse remodelling ***(Abraham et al., 2004)***. These findings were corroborated in MIRACLE ICD II (Multicenter InSync ICD Randomized Clinical Evaluation II), which was a double-blind, randomized trial of HF patients with class II symptoms, confirming that CRT resulted in significant improvements in cardiac structure and function over a 6-month follow-up period ***(Abraham et al., 2004)***. Thereafter, several large-scale randomised trials were prospectively designed to evaluate the effectiveness of CRT those with milder HF symptoms (NYHA class I-II), including REVERSE (Resynchronization reVErses Remodelling in Systolic left vEntricular dysfunction), MADIT-CRT (Multicenter Automatic Defibrillator Implantation Trial-Cardiac Resynchronization Therapy) and RAFT (Resynchronization for Ambulatory Heart Failure Trial) ***(Linde et al., 2010; Moss et al., 2009a; Tang et al., 2010)***. The earliest published results came from REVERSE, which randomized 610 patients with NYHA functional class I or II HF to receive 12-months of active or inactive CRT ***(Linde et al., 2010)***. When compared to controls, CRT improved left ventricular remodelling and significantly reduced heart failure hospitalizations but had no effect on quality of life or exercise capacity. This is perhaps unsurprising, given that patients with mild HF, by definition, have minimal or no symptoms.

Thereafter, MADIT-CRT study attempted to define the impact of CRT-D on mortality in HF patients with a wide QRS complex and mild symptoms (NYHA class I-II), randomizing 1,820 patients to receive either CRT-D or ICD alone ***(Moss et al., 2009a)***. There was a significant 34% reduction in the combined endpoint of death or nonfatal HF events in the CRT-D treated group, although this was primarily driven by a 41% reduction in the risk of HF hospitalization. No significant effect on mortality was demonstrated. The lack of a mortality benefit in MADIT-CRT and REVERSE may well be explained by the low background mortality (2-3%) in those with mild HF (NYHA class I-II), as well as the lower reported prevalence of ischaemic cardiomyopathy in these trials ***(Leyva et al., 2014)***.

In the RAFT study, a total of 1798 patients with NYHA class II or III symptoms were randomised to receive either CRT-D or ICD ***(Tang et al., 2010)***. The impact of CRT-D on mortality was assessed over a mean follow-up period of 40 months. In comparison to MADIT-CRT, there was a significantly higher mortality rate observed in RAFT, which was the first study to clearly demonstrate a survival benefit for CRT-D over ICD in patients with mild-to-moderate HF ***(Tang et al., 2010)***. Overall, CRT-D led to significant reductions in the primary endpoints of death or HF hospitalization, which occurred in 33.2% in the CRT-D group and 40.3% in the ICD

group (HR: 0.75, 95% CI: 0.64 to 0.87). Taken together, these landmark trials have confirmed a benefit for CRT in the early stages of HF, with improvements in left ventricular reverse remodelling, HF hospitalization rates and a reduction in total mortality ***(Leyva et al., 2014)***.

Table 1.1. Summary of cardiac resynchronization therapy clinical trials.							
Name	**Year**	**Patients, n**	**Inclusion Criteria**	**LV Lead**	**Unique Design**	**Endpoints**	**Results**
Single-blinded, crossover studies of CRT-pacemaker							
MUSTIC	2001	67	NYHA III; LVEF ≤35%; LVEDD >60 mm; sinus rhythm; QRS ≥150 ms	Transvenous CS LV lead	Use of dedicated CRT-pacemaker generator	Distance walked in 6 minutes	CRT associated with improved exercise tolerance and quality of life in HF patients with intraventricular conduction delay
PATH-CHF	2002	42	NYHA III/IV; sinus ≥55 bpm; PR ≥150 ms; QRS ≥120 ms	Unipolar epicardial (surgical)	2 separate dual-chamber pacemakers implanted	Exercise capacity measures	CRT associated with long-term improvement in the clinical symptoms of HF patients
Double-blinded, non-crossover study of CRT-pacemaker							
MIRACLE	2002	453	NYHA III/IV; LVEF ≤35%; LVEDD >55 mm; sinus rhythm; QRS ≥130 ms 6-min walking distance ≤450 meters	Transvenous CS LV lead	Use of dedicated CRT-pacemaker generator	NYHA class, quality of life, and distance walked in 6 minutes	CRT associated with improvements in NYHA class, distance walked in 6 minutes, and quality of life. CRT also resulted in decreased need for IV medications to treat HF and was associated with fewer hospitalizations
Double-blind, non-crossover study of CRT-defibrillator							

MIRACLE ICD	2003	369	History of VT/VF; NYHA III/IV; LVEF ≤35%; LVEDD >55 mm; sinus rhythm; QRS ≥130 ms 6-min walking distance ≤450 meters	Transvenous CS LV lead	All patients implanted with a CRT-defibrillator; LV pacing turned off in ½ the cohort	NYHA class, quality of life, and distance walked in 6 minutes	CRT associated with improvements in NYHA class, distance walked in 6 minutes, and quality of life
CONTAK CD	2003	490	History of VT/VF; NYHA II/III/IV; LVEF ≤35%; sinus rhythm; QRS ≥120 ms	Unipolar epicardial (surgical) or transvenous CS LV lead	All patients implanted with a CRT-defibrillator; LV pacing turned off in ½ the cohort	Progression of HF, defined as a composite of all-cause mortality, hospitalization for worsening HF, and VT/VF requiring ICD therapy	A non-significant 15% reduction in HF progression observed with CRT
Mortality trials							
COMPANION	2004	1520	NYHA III/IV; LVEF ≤35%; sinus rhythm; PR ≥150 ms; QRS ≥120 ms; Prior HF hospitalization in past 12 months	Transvenous CS LV lead	1:2:2 randomization to guideline-directed medical therapy (GDMT), GDMT + CRT-P, GDMT + CRT-D	Composite of death from any cause or hospitalization for any cause	CRT-P and CRT-D associated with 20% reduction in the primary endpoint
CARE-HF	2005	813	NYHA III/IV; LVEF ≤35%; sinus rhythm; QRS ≥150 ms; select pts with QRS 120-149 ms; LVEDD ≥30 mm (indexed to height)	Transvenous CS LV lead	1:1 randomization to GDMT or GDMT + CRT-P	Composite of death from any cause or hospitalization for any cause	CRT-P associated with a 37% reduction in the primary endpoint as well as 36% reduction in total mortality

REVERSE	2008	610	NYHA I/II, LVEF≤40%; sinus rhythm; QRS ≥120ms, LVEDD ≥55 mm	Transvenous CS LV lead	All patients implanted with a CRT device (± defibrillator) and randomly assigned to CRT-ON or CRT-OFF	Primary endpoint was the HF clinical composite response score. Secondary endpoint was change in left ventricular end-systolic volume index	CRT resulted in significantly lower rates of heart failure hospitalization and improved LV reverse remodeling in patients with mild HF symptoms (NYHA I-II)
MADIT-CRT	2009	1820	NYHA I/II, LVEF≤30%; sinus rhythm; QRS ≥130ms	Transvenous CS LV lead	Patients randomized in a 3:2 ratio to either CRT–D or ICD-only	Death from any cause or nonfatal heart-failure events	CRT-D associated with a 41% reduction in non-fatal heart failure events. Mortality rates were similar across both groups
RAFT	2010	1798	NYHA II/III, LVEF≤30%; sinus rhythm or AF/flutter; QRS ≥120ms (intrinsic) or ≥200ms (paced)	Transvenous CS LV lead	1:1 randomization to CRT-D or ICD	Death from any cause or heart failure leading to hospitalization	CRT-D associated with significantly lower rates of heart failure hospitalization and death
Table taken from Mittal et al (Mittal, 2017)							

1.6. Criteria for patient selection in CRT

The UK's National Institute of Health and Care Excellence (NICE) published their latest guidance on the appropriate use of CRT for HF management in 2014 ***(NICE, 2014)***. This document replaces earlier versions issued by NICE between 2006-2007 (TA95/TA120) ***(BrJCardiol, n.d.)***. According to these latest criteria (TA314), CRT is recommended for patients with severely impaired LV systolic function (LVEF ≤ 35%), NYHA functional class I-IV and evidence of cardiac dyssynchrony (Table 1.2). Typically, a QRSd ≥ 120 ms is used to indicate the presence of electrical dyssynchrony. However, based on the findings of a recent meta-analysis, which has suggested that patients with LBBB appear to derive the greatest benefit from CRT, NICE now place a greater emphasis on the interaction between QRSd and bundle branch block morphology ***(Sipahi et al., 2012)***.

As a result, in those with a moderately prolonged QRSd (between 120-149ms), patient eligibility for CRT is primarily determined by the morphology of the QRS complex. In fact, in those with a LBBB QRS morphology, the use of CRT is recommended for *all* symptomatic patients (NYHA II-IV), irrespective of baseline ECG rhythm (sinus and atrial fibrillation [AF]) or HF aetiology (ischaemic and nonischaemic cardiomyopathy [NICM]). In contrast, patients with a non-LBBB QRS morphology and a QRSd between 120-149ms are only deemed suitable for CRT if they have advanced HF symptoms (NYHA IV). In those with a very prolonged QRSd (≥ 150 ms), NICE now recommend CRT for all patients, irrespective of bundle branch block morphology. This recommendation assumes that many of these patients possess an electrical substrate that is suitable for CRT.

Table 1.2. NICE 2014 selection criteria for CRT

	NYHA			
QRS interval	I	II	III	IV
<120ms	ICD if there is a high risk of SCD			ICD and CRT not indicated
120-149 ms without LBBB	ICD	ICD	ICD	CRT-P
120-149ms with LBBB	ICD	CRT-D	CRT-P or CRT-D	CRT-P
≥150ms with or without LBBB	CRT-D	CRT-D	CRT-P or CRT-D	CRT-P

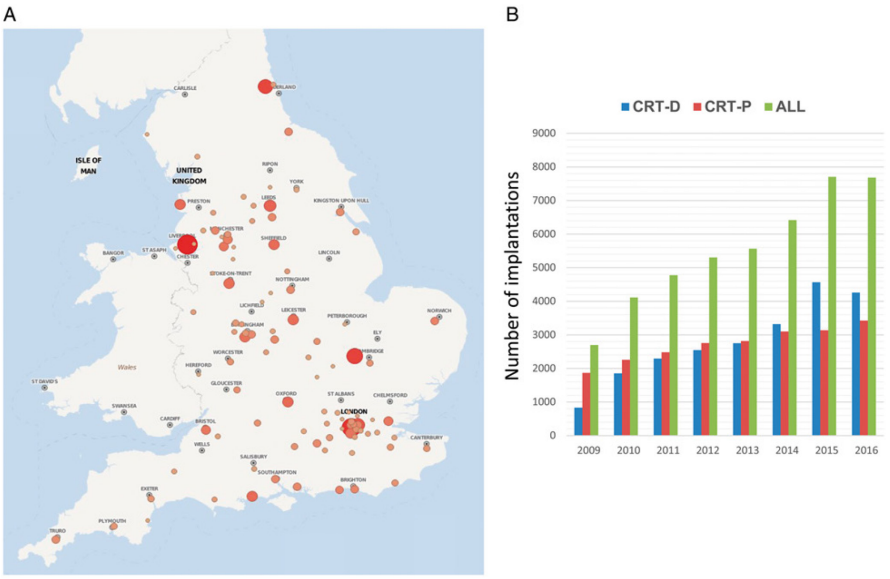

Figure 1.4. CRT implantation rates in the United Kingdom.
(A) shows the distribution of CRT implants across the UK between the period of 2009-2017, with the size and colour of circles proportional to the implant rates. (B) shows bar graphs of the absolute number of CRT implants between 2009-2016, with the y-axis representing the number of implants per year. Reprinted from Leyva et al (Leyva et al., 2019).

1.7. Defining non-response to CRT

Despite careful patient selection for CRT, a considerable proportion of patients fail to derive a significant benefit from CRT (up to 30%). This has led to the concept of 'CRT nonresponders'. Unfortunately, there is no universally agreed definition of CRT response, which makes the process of identifying 'responders' and 'nonresponders' to CRT somewhat challenging ***(Chung et al., 2008; Fornwalt et al., 2010)***. In fact, across the major randomized CRT trials, as many as 17 different criteria have been used to define response to CRT, including those related to improvements in symptoms, exercise capacity, quality of life, LV reverse remodelling rates and the risk of HF hospitalization and mortality ***(Fornwalt et al., 2010)***. Typically, response to CRT is greater when subjective measures such as symptomatic improvement are used (i.e. NYHA class), relative to more objective, clinical-based measures (i.e. changes in haemodynamic function or LV reverse remodelling) ***(Tomassoni, 2016)***.

Although studies often employ these criteria to dichotomise patients into "responders" and "nonresponders", it is important to recognise that CRT is a complex therapy with patients often exhibiting a wide "spectrum" of responses ***(Foley, 2011)***. In fact, recent evidence suggests that response to CRT should be considered as a dynamic continuum, ranging from negative responders, non-responders, non-progressors, responders, to those that exhibit a super-response to CRT ***(Jafferani and Leal, 2019)*** [Figure 1.5].

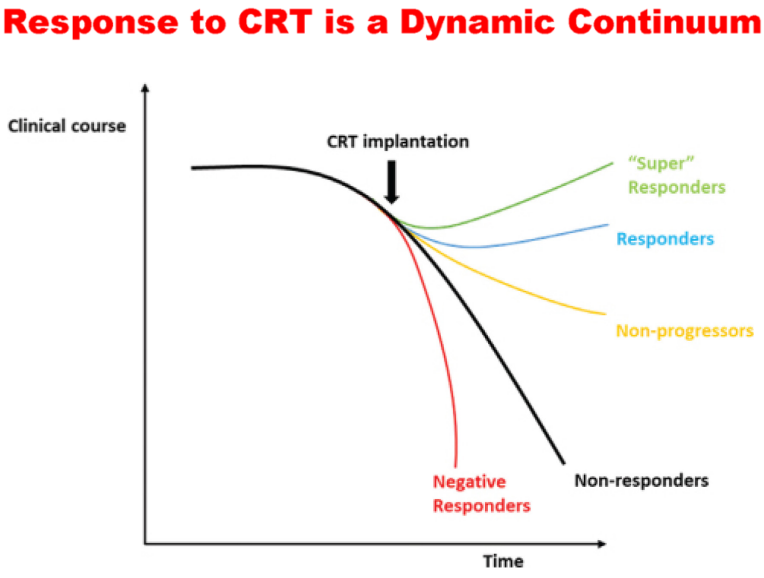

Figure 1.5. Response to CRT is a dynamic continuum.
The clinical course following CRT can be highly variable. At present, patients are considered 'responders' or 'super-responders' to CRT if there is objective improvement in clinical status following CRT. Without CRT, heart failure is normally associated with a progressive deterioration in symptoms, signs and left ventricular systolic function (black line). In this respect, despite the lack of any objective improvement following CRT, non-progressors could also be regarded as 'responders to CRT'. Therefore, the term 'negative responder' or 'non-responder' should be reserved for patients who exhibit worsening clinical status following CRT implantation, in keeping with the natural history of heart failure. Reprinted from (Jafferani and Leal, 2019) *with permissions.*

1.8. Factors influencing response to CRT

1.8.1. Ventricular ectopy

Typically, the best results from CRT are achieved in those with regular, organized and well-timed atrioventricular (AV) activity ***(Healey et al., 2012)***. Even modest increases in the burden of atrial and/or ventricular ectopy have been shown to impair the delivery of biventricular pacing and reduce overall response rates to CRT ***(Ruwald et al., 2018)***. In a recent study evaluating pre-implant ectopic burden on 24-hour Holter monitoring, CRT recipients with an ectopic burden above 0.1% demonstrated a significantly worse outcome following CRT implantation than those with an ectopic burden below 0.1% ***(Mittal et al., 2014; Ruwald et al., 2018)***. This was further corroborated in a sub-study of 698 patients enrolled onto the MADIT-CRT study, where a high ectopic burden on pre-implantation Holter monitoring (defined as a >10 ventricular premature complexes/hour) resulted in a threefold increase in the risk HF or death (HR=2.76, p<0.001) and ventricular tachyarrhythmias (HR=2.79, p<0.001 ***(Ruwald et al., 2018)***. Whether pharmacological or catheter-based suppression of ventricular ectopy improves outcomes following CRT has yet to be established.

1.8.2. Atrial fibrillation

In the setting of AF, there is a higher risk of ineffective CRT delivery due to the loss of atrioventricular synchrony, inherent rhythm irregularity and propensity towards rapid ventricular responses ***(Daubert et al., 2016; Leyva et al., 2014)***. Furthermore, in the absence of atrial synchronous ventricular pacing, interactions can occur between intrinsic (native) conduction and ventricular paced beats, giving rise to the phenomenon of fusion and pseudofusion beats ***(Gasparini et al., 2009)***. To help mitigate against this, AV nodal ablation (AVNA) is often recommended in CRT-treated AF patients who have evidence of incomplete BiV capture. This serves to eliminate intrinsic AV conduction, enabling a high percentage of BiV pacing to be achieved. Even small gains in BiV pacing percentages can significantly enhance the effects of CRT, with the greatest improvements achieved in those able to maintain BiV pacing percentages above 98% ***(Barold and Herweg, 2015)***. In a recent observational study, Gasparani and colleagues presented long-term data in AF patients that were treated with CRT, either in combination with AVNA or rate-slowing medications ***(Gasparini et al., 2013)***. After a median follow-up of 37-months, CRT-treated AF patients that underwent AVNA derived the maximum benefit, with long-term survival rates that were comparable to those in sinus rhythm. In comparison, AF patients treated with rate-limiting medications had significantly higher mortality rates following CRT. However, these benefits must be balanced against the potential risks associated with AVNA. Most notably, it should

be readily apparent that the widespread use of AVNA in CRT-treated AF patients would result in a large subset of patients being rendered pacemaker dependent ***(Gasparini et al., 2009)***. As randomized data is still lacking, further large-scale studies are required to help determine whether AVNA coupled with CRT significantly improves outcomes compared with pharmacological therapy only ***(Gasparini et al., 2009)***.

1.8.3. Patients with a narrow QRS complex

It is widely recognized that LV mechanical dyssynchrony can be present in HF patients with a narrow QRS complex ***(Yu et al., 2003)***. This naturally led some investigators to propose that the benefits of CRT may be extended to this population ***(Leyva et al., 2014; van Bommel et al., 2010)***. However, in two of the most recent, large multicentre RCTS (EchoCRT and LESSER-EARTH), no benefit from CRT was observed in this subgroup of patients ***(Ruschitzka et al., 2013; Thibault et al., 2013b)***. In the EchoCRT (Echocardiography Guided Cardiac Resynchronization Therapy) trial, a total of 809 patients with symptomatic HF (NYHA functional class III-IV), a QRS duration less than 130ms and evidence of mechanical dyssynchrony were studied ***(Ruschitzka et al., 2013)***. All patients underwent CRT-D implantation and were then randomized to receive CRT-ON (n=404) or OFF (n=405). Trial investigators found that the addition of CRT to ICD failed to provide any mortality benefit. In fact, there was a trend towards harm in the CRT-D group, requiring the study to be stopped prematurely on the grounds of futility. Similarly, in the LESSER-EARTH (Evaluation of Resynchronization Therapy for Heart Failure) trial, CRT failed to improve functional status, LV reverse remodeling or clinical outcomes ***(Thibault et al., 2013b)***. This study was also prematurely halted after safety concerns were raised. The excess mortality observed in these studies is of concern and serves as a useful reminder that appropriate selection of eligible CRT recipients is of paramount importance ***(Ruschitzka et al., 2013)***. These publications have been incorporated into the latest European Cardiology Society guidelines of 2021, which now stipulate a minimum QRS cut off value of 130ms for patient selection for CRT ***(Glikson et al., 2021)***. In contrast, older UK-based guidelines (published in 2014) still recommend a lower QRSd cut-off value of 120ms for CRT selection.

1.8.4. LV lead position

Electroanatomical mapping studies have demonstrated that the basal posterolateral LV wall is the most common site for delayed LV activation ***(Auricchio et al., 2004a; Fantoni et al., 2005; Regoli and Auricchio, 2009)***. On this basis, LV lead placement (and consequently the LV pacing site) is directed towards a coronary sinus branch that supplies this region. Unfortunately, this standardized approach to LV lead placement does not account for individual differences in scar location or latest activated segments ***(van Everdingen et al., 2015)***. More recent

evidence suggests that CRT response may be improved by targeting LV pacing to sites that are remote from scar but that lie in close proximity to regions of latest electrical or mechanical activation ***(van Everdingen et al., 2015)***. In fact, studies employing speckle tracking echocardiography (***Khan et al., 2012)***, feature tracking cardiac magnetic resonance ***(Taylor et al., 2016)*** and nuclear scintigraphy ***(Boogers et al., 2011)*** have all shown that individually tailoring LV lead placement towards viable myocardial segments that are late (mechanically) contracting results in better clinical outcomes after CRT. Additionally, in two of the largest multicenter, RCTS: TARGET (Targeted Left Ventricular Lead Placement to Guide Cardiac Resynchronization Therapy) study and STARTER (Speckle Tracking Assisted Resynchronization Therapy for Electrode Region) trials, targeted LV lead placement towards sites of late mechanically activated segments resulted in better outcomes following CRT ***(Khan et al., 2012; Saba Samir et al., 2013)***.

1.8.5. Myocardial scar

Several studies have examined the influence of scar burden, scar location and increasing transmurality on outcomes following CRT implantation ***(Leyva et al., 2011; Wong et al., 2013)***. These studies have shown that myocardial scar burden plays an important role in influencing clinical outcomes following CRT implantation. Indeed, there appears to be an inverse relationship between myocardial scar burden and CRT response ***(Chalil et al., 2007)***. Furthermore, increasing scar transmurality and the presence of posterolateral LV wall scar have been shown to adversely affect clinical outcomes ***(Leyva et al., 2011; Wong et al., 2013)***. Despite this, the relationship between electrical activation and myocardial contraction is still poorly understood and the precise mechanisms by which myocardial scar impairs the delivery of CRT is yet to be fully established. Intuitively, it should be apparent that non-viable tissue is not readily excitable and therefore reduces the amount of myocardium that can be mechanically resynchronized ***(Leyva et al., 2011)***. Additionally, pacing within the vicinity of scarred myocardium has been shown to promote wavefront fragmentation and widening of the QRS complex; factors which are recognized to impair the delivery of CRT ***(Leyva et al., 2011)***.

1.9. Limitations of surface ECG in predicting response to CRT

According to current UK ***(NICE, 2014)***, European ***(Brignole et al., 2013)*** and American guidelines ***(Epstein et al., 2013)***, the 12-lead ECG is the sole diagnostic tool required for the verification of electrical dyssynchrony in CRT recipients. More specifically, selection of patients for CRT is primarily determined by QRS duration (QRSd) and morphology on surface ECG. However, there are important pitfalls to the use of surface ECG-derived criteria that merits further discussion.

QRS Duration

To date, only 5 major RCTs have reported on the association between baseline QRSd and clinical outcomes following CRT, including the COMPANION, CARE-HF, MADIT-CRT, REVERSE (REsynchronization reVErses Remodeling in Systolic left vEntricular dysfunction) and RAFT (Resynchronization-Defibrillation for Ambulatory Heart Failure Trial) trials [Figure 1.6] ***(Sipahi Ilke and Fang James C., 2013)***. In the COMPANION trial, a reduction in the primary endpoint of death or all-cause hospitalization following CRT-P implantation was only observed in those with a QRSd ≥ 148 ms ***(Bristow et al., 2004)***. In fact, there was no benefit from CRT-P in patients with a QRSd < 148ms. Similar findings were also reported following a sub-group analysis of the MADIT-CRT, REVERSE and RAFT trials, which highlighted a lack of benefit for CRT in those with a QRSd < 150 ms ***(Engels et al., 2016)***. In contrast, the CARE-HF trial was the only study to report equivalent clinical benefits in those with a QRSd above (HR 0.60; 95% CI: 0.46-0.79) or below 160 ms (HR 0.74; 95% CI: 0.54-1.02), with respect to all-cause mortality and HF hospitalization ***(Cleland et al., 2005; Poole et al., 2016)***. These conflicting findings may be explained by the unique study design adopted by CARE-HF. Specifically, it required patients with a QRSd between 120-149 ms to have additional echocardiographic evidence of dyssynchrony prior to enrolment onto the study.

Overall, from these studies, one can conclude that QRSd is only a modest predictor of response, with the benefits of CRT primarily restricted to those with a very prolonged QRSd (> 150 ms). Furthermore, in those with moderately prolonged QRSd (between 120-149 ms), measurement of the QRS interval may not be sufficient to accurately identify which patients possess an electrophysiological substrate that is suitable for CRT ***(Strauss et al., 2011)***. In this important subgroup of patients, additional measures of LV electromechanical delay may be required. This is recognised in the latest UK guidelines, which specify the presence of a LBBB morphology in those with a QRSd between 120-149ms, which is used to help distinguish between those who are likely to possess greater electrical dyssynchrony and therefore achieve a better response to CRT.

It is important to note that across the major RCTs, the precise method for measuring QRSd was not stipulated by investigators. This is of relevance, as previous studies have shown that the accuracy of QRSd readings vary depending on

the measurement approach that is employed ***(Pooter et al., 2016)***. In the case of manual QRS measurements, fiducial markers are placed at the beginning and end of the QRS complex after visual inspection the QRS waveform. This can be challenging, as the onset and offset of the QRS complex must be accurately identified across each individual ECG lead. Perhaps unsurprisingly, previous work has shown that this approach is associated with poor reproducibility of QRSd readings and low concordance with automated computer-based measurements ***(Tomlinson et al., 2009)***. In one study, the median inter- and intraobserver variability for manual QRSd measurements was 35ms (range 20-50ms) and 25ms (range 10-50ms), respectively ***(Tomlinson et al., 2009)***. Whilst fully automated (computer-based) approaches offer greater reproducibility in QRSd readings, their accuracy is dependent on the threshold settings used for determining the onset and offset of the QRS complex. These settings vary between different ECG manufacturers and studies have shown small but statistically significant differences in QRSd measurements according to the specific ECG algorithm that is used ***(Kligfield et al., 2018)***.

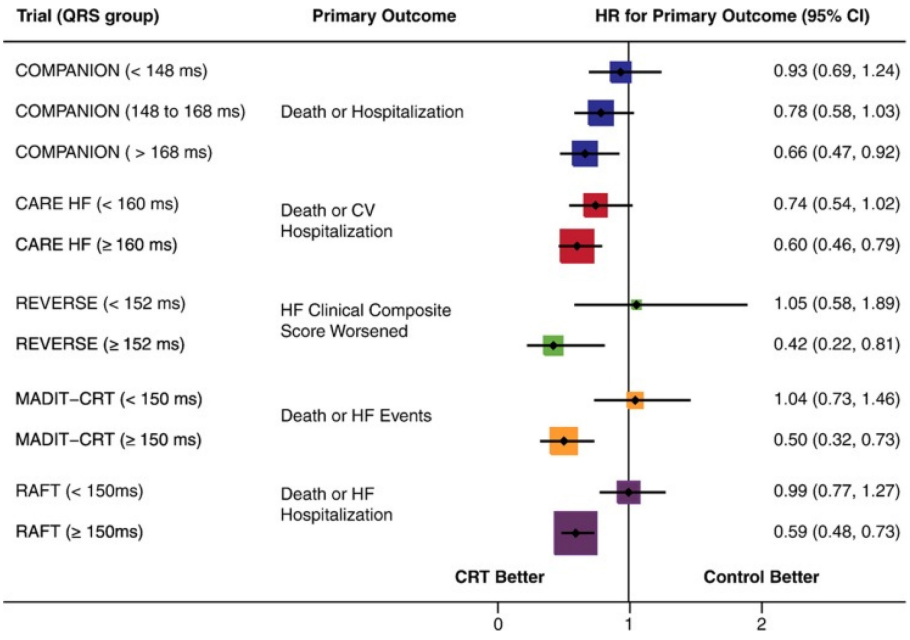

Figure 1.6. Association between QRS duration and clinical outcome after CRT. *The influence of CRT on clinical outcomes in patients enrolled onto the major CRT trials is shown, including those with moderately prolonged (QRS duration 120-150ms) and severely prolonged QRS duration (>150ms). Reprinted from Bryant et al* (Bryant et al., 2013)

QRS Morphology

The presence of a typical LBBB morphology has been shown to be a strong predictor of response, when compared to either RBBB or non-specific intraventricular conduction delay (NICD). In the MADIT-CRT trial, subgroup analysis of the effect of QRS morphology on outcome demonstrated that patients with LBBB who received CRT had a significant decrease in the risk of heart failure hospitalizations or mortality(HR 0.45, $p<0.05$), whilst those who possessed a non-LBBB demonstrated a trend towards an increase in total mortality ***(Strauss et al., 2011; Zareba et al., 2011)***.

Furthermore, in a recent meta-analysis, encompassing some 5000 patients across 4 RCTs, QRS morphology was found to be a strong determinant of response to CRT, with LBBB patients deriving the greatest benefit ***(Sipahi et al., 2012)***. This is reflected in current UK ***(NICE, 2014)***, European ***(Brignole et al., 2013)*** and US guidelines ***(Epstein et al., 2013)***, which emphasise the presence of a LBBB morphology as the only class I indication for CRT ***(Tian et al., 2013)***. Conversely, patients with a non-LBBB morphology and a QRSd between 120-150ms have a lower recommendation level for CRT (class IIb) ***(Auricchio Angelo et al., 2014)***.

Despite widespread agreement that a LBBB configuration is associated with the maximal response to CRT, there is no universal consensus on the electrocardiographic criteria to diagnose LBBB ***(Stipdonk et al., 2019; Tian et al., 2013)***. In fact, as many as 7 different ECG criteria for LBBB have recently been proposed (Table 1.3). As a result, the diagnosis of a LBBB is often open to subjective interpretation. In fact, one study demonstrated significant variability in the probability of classifying LBBB based on these different ECG criteria ***(Stipdonk et al., 2019)***. Even amongst expert cardiologists, the agreement in electrocardiographic identification of LBBB has been shown to be weak ***(Stipdonk et al., 2019)***.

To further complicate the picture, recent electroanatomical mapping studies have shown that up to one-third of patients with ECG criteria for LBBB may not actually possess a true LV activation delay ***(Risum et al., 2015; Strauss et al., 2011)***. Rather, a LBBB-like ECG pattern occurs secondary to a combination of LV hypertrophy (LVH), LV chamber dilatation and/or left anterior fascicular block (LAFB) ***(Strauss et al., 2011)***. Consequently, despite the presence of a LBBB morphology on 12-lead ECG, there is no guarantee that an electrical substrate suitable for CRT is present.

Table 1.3. Variable ECG definitions of left bundle branch block	
Definition	**ECG criteria**
World Health Organization ***(Willems et al., 1985)***	• QRSd ≥ 120ms • Broad and notched or slurred R wave in I, aVL, V_5 and V_6 • Occasional RS pattern in V_5-V_6 • Absent Q wave I, V_5 and V_6 (aVL is a possible exception) • R wave peak time > 60ms in V_5 and V_6 (but normal in leads V_1 and V_2) • rS in leads V_1-V_3 • Wide QS complexes may be present in V_1 and V_2
AHA/ACC/HRS ***(Surawicz et al., 2009)***	• QRSd ≥ 120ms • Notch or slurred R wave in I, aVL, V_5 or V_6 • Occasional RS pattern in V_5-V_6 • Absent Q wave in I, aVL and V_5-V_6 • R wave peak time > 60ms in V_5 and V_6 • Normal R peak time in V_1-V_3 • No negative concordance • Usual discordant ST-T segments
European Society of Cardiology ***(Brignole et al., 2013)***	• QRSd ≥ 120md • QS or rS in lead V_1 • Broad and frequently notched/slurred R-wave in I, aVL, V_5 or V_6 • Absent Q wave in V_5 and V_6
REVERSE ***(Linde et al., 2010)***	• QRSd ≥ 120md • QS or rS in lead V_1 • Broad and frequently notched/slurred R-wave in I, aVL, V_5 or V_6 • Absent Q wave in V_5 and V_6
MADIT (Moss et al., 2009b)	• QRSd ≥ 130ms • QS or rS in V_1 • Broad and notched/slurred R wave in leads I, aVL, V_5 or V_6 • Absent q wave in V_1 and V_2
Strauss ***(Strauss et al., 2011)***	• QRSd ≥ 140ms for men or ≥ 130ms in women • QS or rS in leads V_1 and V_2 • Mid-QRS notching or slurring in ≥ 2 or more contiguous leads, including V_1, V_2, V_5, V_6 and aVL
Adapted from Stipdonk et al (Stipdonk et al., 2019)	

1.10. Strategies to improve response to CRT: towards better characterisation of the LV electrophysiological substrate

Despite over 20-years of experience, the prediction of response to CRT continues to remain a major challenge. In recent years, rather than select patients based on arbitrary values derived from 12-lead ECG analysis, there has been a shift towards delivering a more individualized approach to CRT. This has, in large part, been related to our improved understanding of the complexities of cardiac electrophysiology (Auricchio et al., 2004b; Prinzen et al., 2013). In fact, LBBB is now widely recognized to be a rather complex electrical 'disease', with significant inter- and intraindividual variations in the sequence of LV electromechanical activation. In this respect, the ability to predict who might respond to CRT requires a more complete, 3-dimensional assessment of LV activation patterns, beyond that currently provided by surface (12-lead) ECG.

Left bundle branch block

Studies employing direct mapping of intra-cardiac electrical potentials, including those based on contact (CARTO) or noncontact (EnSite) mapping have provided important insights into the variable activation patterns observed in HF patients with conduction delay (Auricchio et al., 2004b; Fantoni et al., 2005; Rodriguez et al., 2003; Vassallo et al., 1984). These electroanatomical mapping (EAM) studies have shown that, once LBBB ensues, activation of the LV is markedly delayed (Auricchio et al., 2004b; Vassallo et al., 1984). Electrical impulses arriving from the AV node are re-directed via the intact right bundle branch towards the right ventricle. Left ventricular activation then occurs through slow cell-to-cell conduction from the right ventricle ***(Vassallo et al., 1984)***. The time taken from the onset of RV activation (onset of the QRS complex on 12-lead ECG) to the earliest site of LV breakout is referred to as the trans-septal activation time ***(Vassallo et al., 1984)***. Following transseptal conduction, transmission of the activation wavefront to the remaining LV occurs through non-specialized pathways. As left-sided fast conducting Purkinje fibers are not recruited in LBBB patients, LV activation times are usually significantly delayed in LBBB patients. In a recent EAM study, Aurrichio et al identified 2 distinct patterns of LV endocardial activation (Auricchio et al., 2004b).

Type 1 conduction pattern is indicated by the presence of a single, unidirectional wavefront that migrates in an unopposed fashion from the septum to the LV free wall (LVFW). In contrast, type 2 conduction is identified by a "U-shaped" pattern of LV activation and is more commonly found in LBBB patients (Auricchio et al., 2004b; Prinzen et al., 2013; Sohal et al., 2013). A defining feature of type 2 activation patterns is the presence of lines of conduction block, which are commonly located over the anterior LV wall (Figure 1.7). Noncontact mapping has shown that this line of conduction block prevents the direct propagation of wavefronts from the septum to the lateral LV wall. Instead, the depolarizing wavefront reaches the lateral LV wall by rotating or "twisting" around the LV apex and across the inferior wall ***(Sengupta et al., 2013)***.

Although the exact cause of this conduction block has yet to be fully elucidated, recent work has shown that the location of this line of block can be altered through the application of asynchronous pacing, suggesting it possesses a functional nature (Auricchio et al., 2004b; Sengupta et al., 2013). Intuitively, as conduction block imposes a barrier to electrical LV activation, its presence, size and location could be important determinants of the location of late electrically activated segments (LEAS) and therefore, the optimal LV stimulation site.

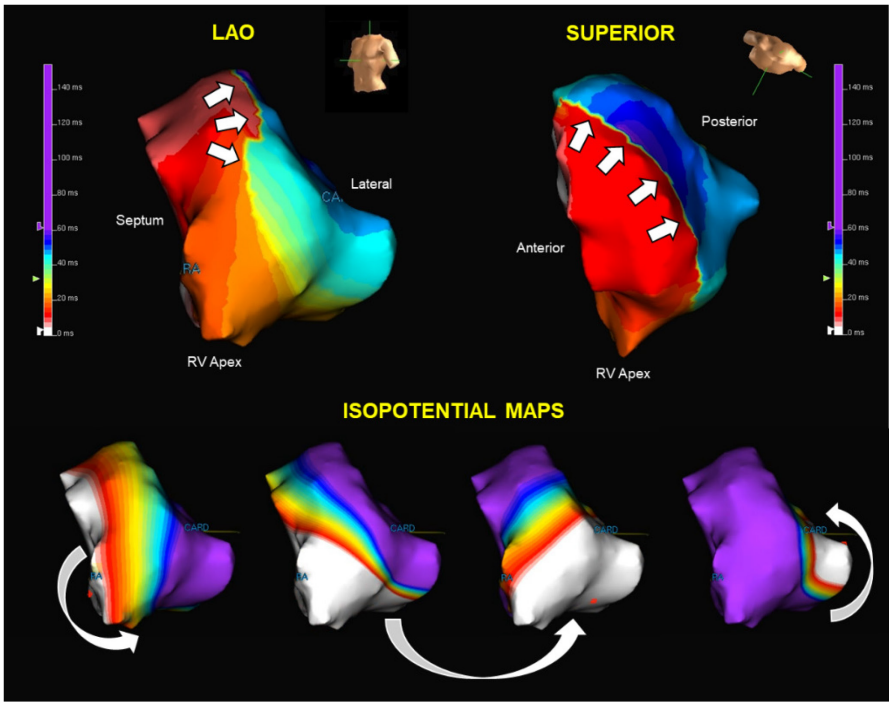

Figure 1.7. Isochronal activation map in LBBB.
(Top) Unipolar isochronal activation maps of LV activation in a left anterior oblique (left) and superior orientation (right) are shown. These maps were obtained using noncontact mapping (EnSite) in a patient with LBBB (chapter 6). There is a line of conduction block (white arrows) which extends from the superior LV wall towards the anterior LV region. (Bottom) The voltage maps display a U-shaped pattern of activation, with the wavefront rotating around the apex to activate the lateral LV wall.

Right bundle branch block

In pure RBBB, left bundle branch conduction and LV activation patterns are typically preserved ***(Jaffe and Morin, 2014)***. Therefore, from a mechanistic viewpoint, the addition of an LV lead to pre-excite the LV free wall would not be expected to result in improved ventricular synchrony ***(Jaffe and Morin, 2014)***. However, utilising detailed three-dimensional EAM techniques, Fantoni et al described the RV and LV endocardial activation sequences in HF patients with RBBB, demonstrating a delay in activation of the anterior and LV lateral wall ***(Fantoni et al., 2005)***. Interestingly, this pattern closely resembled that of LBBB, lending support to the concept that some RBBB patients with coexisting left-sided conduction delay may possess an electrophysiological substrate that is amenable to CRT (Figure 1.8).

This concept of RBBB 'masquerading' as LBBB has been well described previously ***(Richman and Wolff, 1954; Unger et al., 1958)***. Electrocardiographically, this is characterised by the presence of ECG criteria for LBBB in the limb leads, but RBBB criteria in the precordial leads.

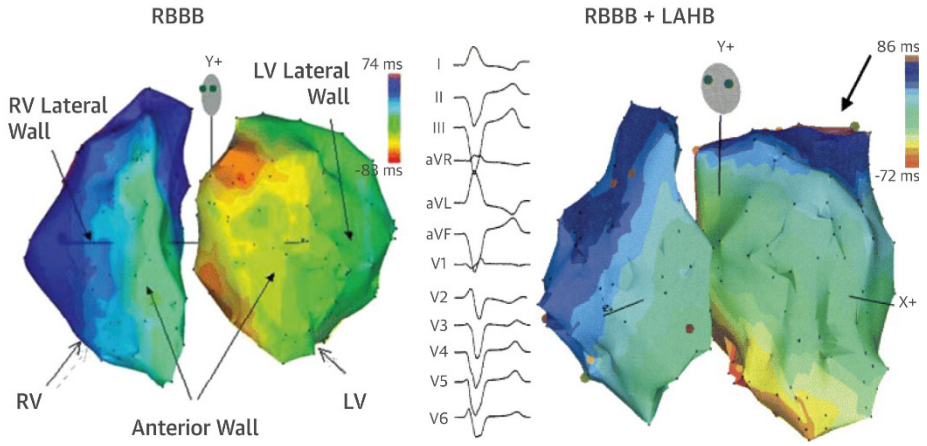

Figure 1.8. Isochronal activation map in RBBB.
(Left) shows the right ventricular and left ventricular isochronal activation map in a patient with pure RBBB, demonstrating early activation of the LV endocardial septum (orange) with rapid spread of activation towards the lateral LV wall (green). There is delayed activation of the RV free wall (blue). (Right) shows the isochronal activation map in a RBBB patient with additional left-sided conduction delay secondary to left anterior hemiblock (LAHB). Adapted with permissions from Poole et al., 2016, Fantoni et al., 2005 and Peichl Pet al., 2004.

1.11. Novel techniques to assess electrical dyssynchrony

During recent years, there has been renewed interest in the development of techniques that enable better characterization of the cardiac substrate and identification of electrical dyssynchrony. This approach would appear logical, given that CRT is primarily an 'electrical therapy', designed to treat an underlying electrical conduction abnormality. Given the complex activation patterns observed in those with dyssynchronous HF, there has been a trend towards utilising novel mapping techniques that can provide a more complete 3-dimensional overview of cardiac activation. Some of these proposed imaging modalities include body surface potential mapping, noninvasive electrocardiographic imaging and vectorcardiography (Figure 1.9).

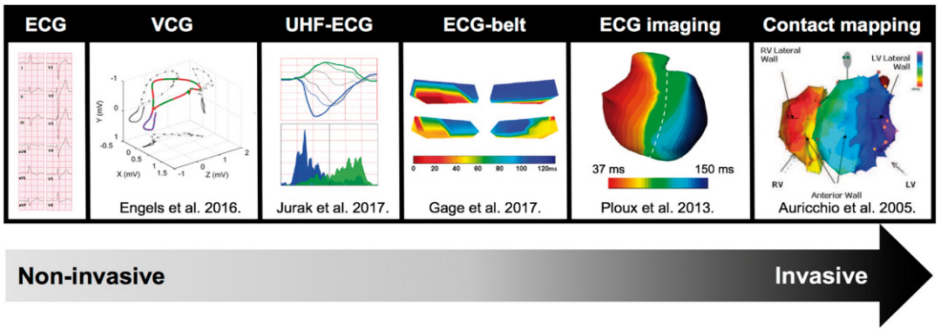

Figure 1.9. Emerging techniques to assess electrical dyssynchrony.
Overview of different techniques available to help quantify LV conduction delay, ranging from noninvasive modalities (12-lead ECG and VCG) to more complex (ECG imaging) and/or invasive approaches (contact mapping). Reprinted from Nguyen et al (Nguyên et al., 2018b).

1.11.1 Body surface potential mapping

Body surface potential mapping (BSPM), which represents an extension of conventional electrocardiography, attempts to overcome the limitations of 12-lead ECG by using additional leads placed on the torso to capture more electrical information. Several different recording systems are available, with the most commonly reported systems using 64 ***(Oostendorp et al., 2011)***, 120 ***(Sapp John L. et al., 2012)*** or 256 surface electrodes ***(Cluitmans, 2016)***.

In its application to CRT, BSPM has been used to help characterise the variable spatial-temporal patterns of ventricular activation **(Gage et al., 2017)**. In two recent studies, Gage et al and Johnson et al used a 53-electrode ECG 'belt' to construct detailed body surface isochronal maps [Figure 1.10] ***(Gage et al., 2017; Johnson et al., 2017)***. As shown in Figure 1.10, LBBB patients had greater delays in posterior electrode activation (representing delayed action of the posterior LV wall) than those with non-LBBB QRS morphologies. Additionally, using body surface isochronal mapping, the authors derived several novel metrics of electrical dyssynchrony, including the standard deviation of activation times (SDAT) and the average left thorax activation time (LTAT). Overall, body surface mapping derived SDAT was found to be a better predictor of CRT response than QRSd. In fact, in those without a class I indication for CRT, only baseline SDAT and the change in SDAT following CRT (ΔSDAT) predicted a favourable response to CRT (defined as ≥5% change in LVEF at 6-months) ***(Gage et al., 2017)***.

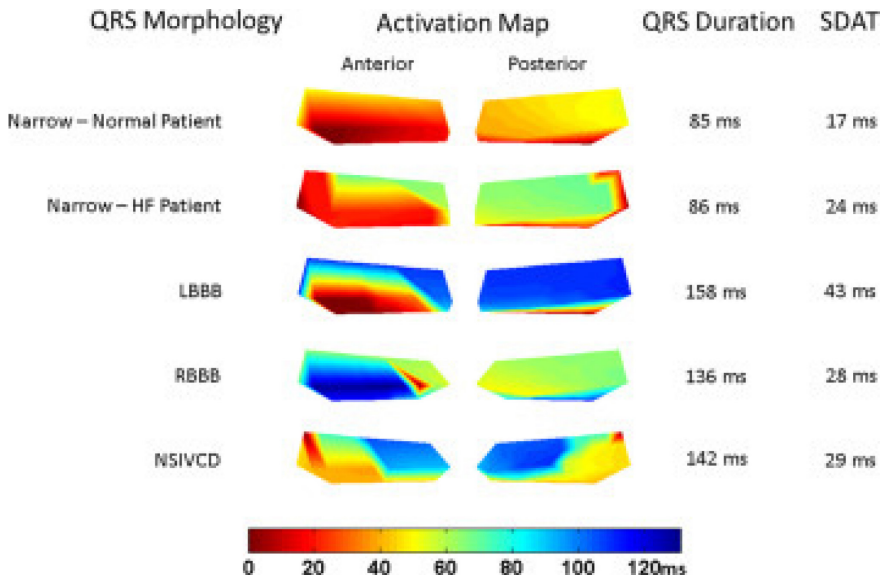

Figure 1.10. ECG belt isochronal maps in patients with different QRS morphologies. *Patient 3D activation maps obtained from anterior and posterior ECG belts in patients with different 12-lead QRS morphologies. As shown, LBBB patients have the greatest delay in activation of posterior ECG electrodes (representing delay in activation of the posterior LV wall) and the largest SDAT values (indicating greater electrical dyssynchrony). Reprinted from Gage et al* (Gage et al., 2017).

Although the larger number of ECG electrodes used in BSPM permits a more accurate and complete picture of the underlying cardiac electrical activity, its use in the clinical setting is limited by the additional procedural complexity, expense and difficulty in consistent interpretation. Additionally, as with traditional 12-lead ECG, the ability to precisely locate electrical events with BSPM is still hindered by electrical interference from intra-thoracic organs. Without the use of cross-sectional imaging to acquire patient-specific anatomical information, it is not possible to project BSPM recordings onto the epicardial surface ***(Gage et al., 2017)***. This limits the ability of BSPM to precisely locate regional cardiac events.

1.11.2. Electrocardiographic imaging

Electrocardiographic imaging (ECGI) is a noninvasive imaging modality that has enjoyed somewhat of a renaissance over recent years. This is in response to the increasing demand for a noninvasive imaging modality that can precisely characterise 3-dimensional LV activation propagation ***(Intini et al., 2005)***.

Fundamentally, all ECGI systems require 2 principal components: (1) electrical data from BSPM and (2) a patient-specific model of 3D heart-torso geometries [Figure 1.11] ***(Rudy Yoram, 2013)***. Typically, computed tomography (CT) imaging is used to construct both the 3D heart model and to determine the precise location of body surface electrodes. By solving the so-called "*inverse problem of electrocardiography*", ECGI systems can noninvasively reconstruct electrical potentials, electrograms and isochronal activation maps on the epicardial surface of the heart **(Ghosh and Rudy, 2005)**. This enables the regional patterns of electrical activity and the variable spatial-temporal relationships between different regions of the heart to be better appreciated. In fact, in a recent validation study, ECGI reliably identified single pacing sites to within 10mm and could distinguish between dual pacing sites that were only 17mm apart ***(Ghanem et al., 2005; Oster Howard S. et al., 1997)***. Similar studies have shown that ECGI can accurately locate LV breakthrough sites, identify lines of conduction block, assess complex patterns of LV activation and reconstruct EGM waveforms ***(Ghanem et al., 2005)***.

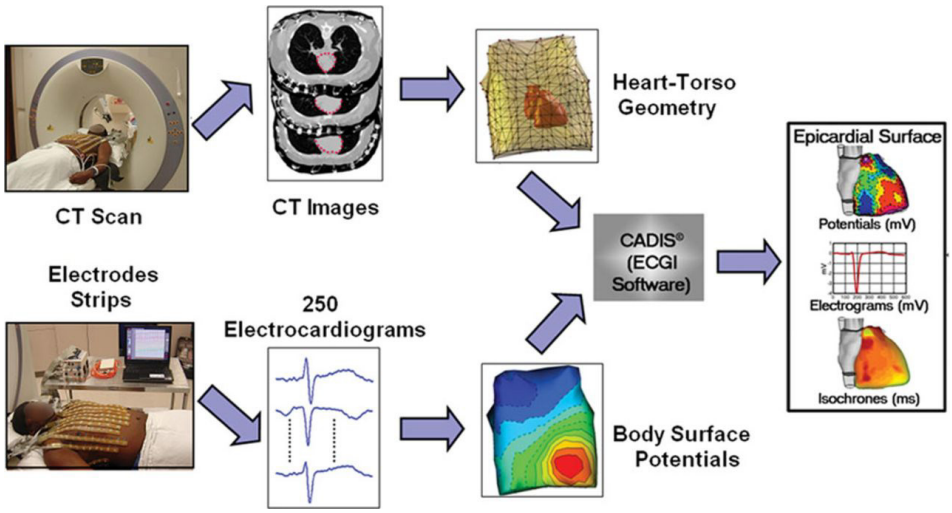

Figure 1.11. Overview of noninvasive ECG imaging.

ECG imaging requires detailed electrical data to be captured from body surface mapping (bottom left). Thereafter, the precise location of body surface electrodes is determined using CT/CMR imaging (top left). The geometry of the heart-torso is also derived from CT, enabling fusion of electrical data with a patient-specific 3D heart model. (Right) An algorithm is used to reconstruct isopotentials, electrograms and colour-encoded isochronal sequences occurring on the epicardial surface of the heart. Reprinted from Rudy et al., 2017 with permissions.

Recently, Ghost et al utilized ECGI to help quantify electrical dyssynchrony in 25 NICM patients undergoing CRT implantation ***(Ghosh et al., 2011)***. The authors devised a novel metric of electrical dyssynchrony, termed the electrical dyssynchrony index (EDI). This was derived by calculating the SDAT across 500 sites located on the LV surface. EDI therefore represented a measure of spatial dispersion of activation across the LV; with larger values denoting greater electrical dyssynchrony. Accordingly, those with larger pre-implant EDI values and lower post-implant values responded better to CRT. Interestingly, there was only a weak correlation between QRSd and EDI. In a similar study, Ploux et al performed ECGI in 33 consecutive CRT recipients using a noninvasive, high-resolution mapping system (ECVUE, CardioInsight Technologies Inc., Cleveland, Ohio) ***(Ploux et al., 2013)***. Using these reconstructed ECGI maps, three separate indices of electrical dyssynchrony were derived: LVAT, RVAT and ventricular electrical uncoupling [VEU] (representing the difference between RV and LV activation times). In contrast to those with NICD (n=15), LBBB patients (n=18) were found to have markedly longer LVATs (91 ± 34ms vs. 115 ± 21ms, p=0.03) and VEU (40 ± 22 vs. 75 ± 12ms, p=0.001) but similar RVATs (58 ± 26ms vs. 62 ± 30ms, p=0.7). The delay in LVAT and VEU was largely due to lines of conduction block that were positioned over anterior, lateral and postero-septal LV surfaces. Overall, VEU was strongly associated with CRT response and proved to a better predictor of than QRSd. In fact, patients with a VEU ≥ 50ms had a 42x fold greater likelihood of meeting the clinical composite endpoint.

1.12. Vectorcardiography

Vectorcardiography (VCG) has recently emerged as a simple tool to help characterise the electrical substrate in patients undergoing CRT implantation. As it reconstructs the electrical heart field in three orthogonal planes, it can provide a more precise 3-dimensional overview of cardiac electric activity. In doing so, it provides more specific geometrical information on the momentary changes in the direction and magnitude of electrical forces in the heart. Indeed, an important advantage of VCG over 12-lead ECG is its ability to resolve QRS wavefront propagation in 3-dimensions.

1.12.1. Fundamental principles

During a normal cardiac cycle, the direction and magnitude of an electrical dipole (an electrical charge with a positive and negative component) changes as the depolarising wavefront propagates through the myocardium. These electrical signals are transmitted to the body surface where they can be recorded using a 12-lead ECG. Fundamentally, the electrocardiogram can be thought of as being composed of a series of vectors ***(Burch, 1985; Keele, 1965)***. These vectors represent the instantaneous strength and direction of the cardiac electrical dipole within a three-dimensional space (i.e. torso) ***(Man et al., 2015)***. As with any vector, the electrical heart vector (EHV) contains information on both the *direction* and *magnitude* of electrical forces acting within the torso. This is in contrast to the scalar 12-lead ECG, which only contains information on the size of electrical forces.

In vectorcardiography, the EHV is projected in the orientation of the body axis (i.e., frontal, transverse and sagittal) and is assumed to arise from a fixed, central position within the torso. Using the typical VCG convention, the X-lead displays activation wavefronts travelling in the right→left direction, whilst the Z-lead and Y-lead display information in the anterior→posterior and superior→inferior direction, respectively ***(Surawicz et al., 2008)***. The final recorded VCG trace is then projected in three orthogonal planes (i.e., frontal, transverse and sagittal) by combining 2 of the recorded VCG leads using a cartesian coordinate system (frontal plane: zy leads, transverse plane: xy leads, sagittal plane: xz leads), as depicted in Figure 1.12. By displaying cardiac electrical activity in this form, vectorcardiography becomes a form of "ECG imaging", wherein the spatial locations of specific ECG waveforms are displayed within a 3-dimensional space ***(Pahlm, 2014)***. To the trained reader, this enables more detailed information on the direction of activation wavefronts to be obtained (relative to the ECG).

Image redacted

Figure 1.12. Schematic representation of 3D vector loops.
(Bottom left) The X, Y and Z VCG planes arise from a fixed, central position with in the torso. The yz leads represents the sagittal plane, xy leads:transverse plane and yz leads: frontal plane. 3D vector loops of atrial (small green line) and ventricular (large green line) depolarisation in the three principle planes are shown. Reprinted from Malmivuo and Plonsey et al (Malmivuo and Plonsey, 1995).

To display the 3D VCG loop, it is customary to sample the changes in vector direction at 2.0 or 2.5-ms intervals ***(Surawicz et al.)***. Using this approach, it is possible to follow the chronologically changes in the bio-electrical forces (momentum vectors) operating within the torso ("3D ECG / Cardiogoniometry (CGM) | enverdis GmbH," n.d.)**.** As all the spatial cardiac vectors are assumed to arise from a single, fixed position, it is then possible to connect the arrow tips of these resultant vectors. As these vector tips are connected, an ansiform line emerges, which is fundamentally how the vectorcardiogram is constructed and displayed ("3D ECG / Cardiogoniometry (CGM) | enverdis GmbH," n.d.). This is schematically shown in Figure 1.13, which depicts the construction of the VCG based on the measurement of successive instantaneous vectors ***(Chou et al., 1974)***.

Image redacted

Figure 1.13. Representation of the 3D vectorcardiogram.
During the normal cardiac cycle, the electrical heart vector changes rapidly in both size and direction. If these vectors are sampled at regular intervals (black arrows), it is possible to join the tips of these vectors to form the QRS loop (blue line) and T loop (small green line). Every colour alteration within these loops represents 10ms intervals. The dashed black line represents the direction of activation. Reprinted from Engels et al (Engels et al., 2016).

At first glance, it may difficult to conceptualise how the electromotive forces generated by different regions within the heart (and at some distance from one another) can be measured separately ***(Grishman et al., 1953)***. This is achieved by replacing the electrical effects of multiple electromotive field forces (generated by different activation wavefronts) by a single spatial cardiac vector, which has both a direction and magnitude ***(Grishman et al., 1953)***. More specifically, when several regions within the heart are depolarising, this spatial cardiac vector is merely the balance of all these forces operating within the 3 orthogonal planes (X, Y and Z) ***(Grishman et al., 1953)***.

1.12.2 Vectorcardiography in CRT

In the field of CRT, the area of the QRS complex (QRS_{area}) on the vectorcardiogram (VCG) has emerged as a promising alternative to 12-lead ECG criteria (i.e. QRSd and morphology) for predicting response ***(Engels et al., 2016; van Deursen et al., 2015a)***. As a 3-dimensional parameter, QRS_{area} yields important information on the dominant axis of cardiac activation and the size of electrical forces that act in the three principle planes ***(Engels et al., 2016)***. Using the 12-lead ECG signal, QRS_{area} is simply derived by calculating the root mean square of the area bound by the QRS complex and the isoelectric baseline, using the following formula: $(X_{area}^2 + Y_{area}^2 + Z_{area}^2)^{1/2}$ [Figure 1.14].

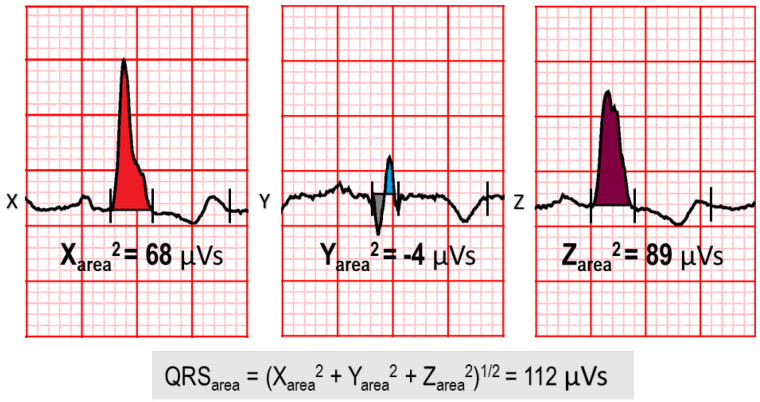

Figure 1.14. Calculating QRS_{area} from the 3D vectorcardiogram.
QRSarea is calculated by determining the area bound by the ventricular deflection curve and the isoelectrical line in each of the three orthogonal planes (X, Y and Z). In this VCG example obtained from a LBBB patient, the largest areas are observed within the X- (right→left direction) and Z-axis (anterior→posterior direction).

QRS_{area} and electrical dyssynchrony

Patients with a LBBB tend to possess greater electrical dyssynchrony and larger QRS_{area} values on the VCG, relative to those with nonspecific interventricular conduction delay (NICD) ***(Engels et al., 2016)***. This has largely been attributed to the fact that LBBB is associated with strong, unidirectional wavefronts that propagate in a dominant anterior→posterior (A→P) and right→left (R→L) direction, resulting in large VCG signals in the X and Z planes, respectively.

In contrast, NICD patients are more likely to have multiple LV breakthrough sites and more rapid, early activation of the LV cavity. Speculatively, the presence of multiple LV activation wavefronts within the LV cavity (with opposing electrical axis) could result in a net "cancellation" of electrical forces and a smaller QRS_{area}. Accordingly, patients with a larger baseline QRS_{area} tend to respond better to CRT than those with a smaller QRS_{area} ***(Maass et al., 2018a; van Deursen et al., 2015a)***. The recent study undertaken by Madi Rad et al provides empirical support for this hypothesis ***(Mafi Rad et al., 2016)***. In 51 consecutive CRT recipients, the authors utilized invasive coronary venous mapping to construct patient-specific, 3-dimensional maps of epicardial LV activation patterns (Figure 1.15). The presence of delayed LV activation, as defined by activation times exceeding 75% of the QRSd, was demonstrated in 38 of 51 patients, including 29/29 with LBBB, 8/15 with IVCD and 1/7 with RBBB. Overall, QRS_{area} outperformed both QRSd and a LBBB morphology in identifying patients with delayed LV activation, with a sensitivity of 87% and a specificity of 92%.

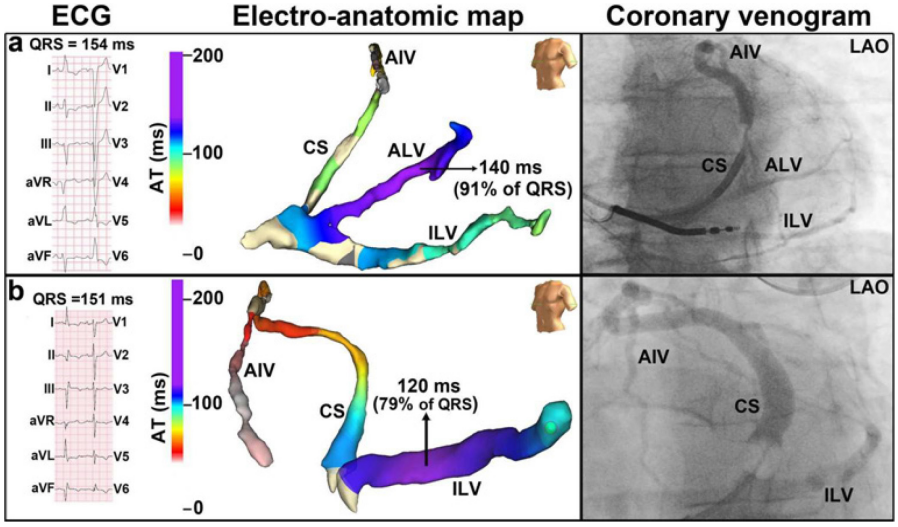

Figure 1.15. Coronary venous EAM in patients with LV activation delay.
Coronary venous EAM in a patient with LBBB (A) and NICD (B), demonstrating the presence of activation delay over the LV free wall (i.e. activation times >75% of QRSd). In both patients, there are suitable coronary sinus venous tributaries that supply these late activated segments. Adapted from Engels et al., 2016 and Mafi Rad et al., 2016 et al with permissions.

QRS_{area} for predicting CRT response

The findings from several recent studies lend support to the use of QRS_{area} as a predictor of CRT response (Table 1.4). These studies have shown that QRS_{area} is a reliable measure of electrical dyssynchrony, with a plethora of evidence now confirming its superiority over conventional 12-lead ECG analysis (QRSd and morphology) ***(Mafi Rad et al., 2016)***. In a small prospective study of 81 CRT candidates, van Deursen et al demonstrated that a larger baseline QRS_{area} >98 μVs predicted a favourable volumetric response to CRT ***(van Deursen et al., 2015a)***. These findings were also corroborated by Maass et al, who found baseline QRS_{area} to be superior to QRSd in the prediction of echocardiographic response following CRT (Maass et al., 2018a). It has recently been suggested that the superior predictive capability of QRS_{area} over conventional ECG criteria is based on its ability to combine information on both QRS and morphology into a single, continuous parameter ***(Maass et al., 2018a; van Deursen et al., 2015a)***.

Based on the promising results obtained from small prospective studies, which have proposed that QRS_{area} is a better predictor of CRT response than QRSd and morphology, more recent work has shifted towards determining if this parameter can predict 'hard' clinical end-points during long-term follow-up ***(Emerek et al., 2019; van Stipdonk et al., 2018)***. In a recent retrospective multicentre study, Stipdonk et al evaluated 1492 CRT patients over a mean follow-up period of 3.4 years ***(van Stipdonk et al., 2018)***. QRS_{area} was superior to QRS morphology and duration (AUC 0.61 versus 0.55 and 0.51, respectively; $p<0.001$) in predicting freedom from the primary endpoint, defined as all-cause mortality, cardiac transplantation or left ventricular assist device (LVAD) implantation. Additionally, a QRS_{area} >109 μVs was found to be an independent predictor of echocardiographic response (ΔLVESV ≥15%). Overall, QRS_{area} was demonstrated to be superior to any single ECG criteria (QRS morphology and duration).

Emerek et al also conducted a retrospective study to evaluate the predictive value of 2 vectorcardiographic parameters, namely QRS_{Area} and SAI QRST, in 705 consecutive patients receiving CRT ***(Emerek et al., 2019)***. The primary endpoint was all-cause mortality, transplantation and LVAD implantation. Based on pre-implant VCG analysis, QRS_{area} was constructed using both the inverse Dower's and Kors method. The authors found that a QRS_{area} obtained using the Kors method was superior to the inverse Dower method in predicting long-term outcome following CRT. Similarly, QRS_{area} was superior to SAI QRST. In keeping with the findings from Stipdonk et al, a small QRS_{area} (< 95 μVs) was independently associated with an increased risk of the primary endpoint (adjusted hazard ratio [aHR]: 1.95, 95% CI: 1.25–2.18, $p<0.001$).

Table 1.4. Summary of clinical trials employing VCG in cardiac resynchronization therapy

Author	Year	Design	Patients, n	VCG parameter	Follow-up	Endpoints	Results
Acute haemodynamic studies							
Pooter et al ***(De Pooter et al., 2017)***	2017	Prospective	25	ΔQRS_{Area}	-	≥10% ΔLV dP/dt_{max}	Changes in the Z axis of the VCG predicted AHR to better than ΔQRSd (AUC 0.81 vs. 0.70, p=0.002)
Ross et al ***(Ross et al., 2018a)***	2018	Prospective	26	ΔQRS_{area} ΔT_{area}	-	≥10% ΔLV dP/dt_{max}	Both ΔQRS_{area} (R^2=0.37 p=0.001) and ΔT_{area} (R_2=0.28, p=0.006) correlated with ΔLV dP/dt_{max} and predicted acute haemodynamic response to CRT (AUC 0.81 and 0.75, both p≤0.03)
LV reverse remodeling							
Van Deursen et al ***(van Deursen et al., 2015a)***	2015	Prospective	81	QRS_{area}	6-months	ΔLVESV ≥15%	QRS_{area} (>98 μVs) predicted response to CRT better than QRSd (AUC 0.78 vs 0.62, p=0.03) and QRS morphology (OR 10.2 versus 5.5)
Engels et al ***(Engels et al., 2015)***	2015	Prospective	244	T_{area} QRS_{area} Sum $QRST_{area}$	6-months	≥5% ΔLVEF	T-wave area predicted CRT-response (OR of 1.172 per 10 μVs increase in T_{area}, p<0.001) better than QRS_{area} (OR = 1.12, 95% CI: 1.05-1.20, p= 0.001)
Tereschenko et al (Tereshchenko et al., 2015)	2015	Retrospective	234	SAI QRST	6-months	ΔLVESV ≥15%	When patients in the top and bottom tertiles were compared, a high SAI QRST value was associated with a higher likelihood of echocardiographic response to CRT (OR 2.5, 95% CI: 1.3-5.0, p=0.01)
Maass et al ***(Maass et al., 2018b)***	2017	Prospective	240	QRS_{area}	6-months	ΔLVESV ≥15%	QRS_{area} was a better predictor of favourable echocardiographic remodelling following CRT than QRS morphology or duration

Nguyên et al (Nguyên et al., 2018a)	2018	Prospective	33	QRS_{area} T_{area} Sum $QRST_{area}$	6-months	ΔLVESV ≥15%	QRS_{area} predicted CRT response with an AUC of 0.74 (p=0.022). All VCG parameters were inversely correlated to myocardial scar burden on CMR imaging
Clinical outcome trials							
Végh et al (Végh et al., 2016)	2015	Retrospective, single centre	335	T_{area} QRS_{area}	3-years	HF hospitalization, cardiac transplantation, LVAD implantation and all-cause mortality	T-wave area was associated with a significantly lower risk of HF hospitalization (HR: 0.53, 95% CI: 0.35–0.83, p< 0.01) and all-cause mortality (HR: 0.57, 95% CI: 0.35–0.96, p =0.03)
Jacobsson et al ***(Jacobsson et al., 2016)***	2016	Retrospective, single centre	496	SAI QRST	2-years	Primary: all-cause mortality Secondary: HF hospitalization, cardiac transplantation and all-cause mortality	Following multivariate adjustment, a low SAI QRST (< 302mV*ms) was associated with an increased risk of the primary (HR 1.8; 95% CI: 1.01–3.2) and secondary endpoints (HR 1.6, 95% CI 1.1–2.2)
Stipdonk et al ***(van Stipdonk et al., 2018)***	2018	Retrospective, multicentre	1492	Pre-CRT QRS_{area}	3.4 years	Primary: all-cause mortality, cardiac transplantation and LVAD implantation Secondary: HF hospitalization (<1 year) and ΔLVESV	A QRS_{area} ≥ 109 μVs was associated with improved event-free survival (HR: 0.49; 95% CI: 0.41-0.59, p<0.001) and a lower likelihood of HF hospitalization (HR: 0.76, 95% CI: 0.60-0.96, p=0.019). Similarly, QRS_{area} was a better predictor of echocardiographic response than either QRS morphology or duration (AUC 0.69 versus 0.58 and 0.58, respectively, p<0.001 for both comparisons)
Emerek et al ***(Emerek et al., 2019)***	2018	Retrospective, single centre	705	Pre-CRT QRS_{area}	3.1 years	Cardiac transplantation, LVAD implantation and all-cause mortality	Pre-implant QRS_{area} ≥ 95 μVs was strongly associated with long-term event-free survival following CRT, including those with LBBB (HR: 2.35; 95% CI: 1.75-3.15, p<0.001) and non-LBBB QRS morphologies (HR: 1.55; 95% CI: 1.07-2.25, p=0.02)
Friedman et al ***(Friedman et al., 2019)***	2019	Retrospective, single centre	527	CRT-induced ΔQRS_{area}		Cardiac transplantation, LVAD implantation and all-cause mortality	Progressive reductions in QRS_{area} following CRT was associated with significantly improved clinical outcomes, independent of QRS morphology and other clinical variables (HR: 0.45, 95% CI: 0.30-0.70, p < 0.001)

1.13. New developments in the delivery of CRT

1.13.1. Multipoint pacing

Given recent developments in quadripolar lead technology, it is now possible to deliver multiple, near simultaneous LV pacing stimuli from within a single coronary sinus branch ***(Rinaldi et al., 2015; van Everdingen et al., 2015)***. This approach, which relies on the use of novel multipoint pacing (MPP) algorithms, delivers multiple single-site pacing vectors across widely spaced electrodes located on the distal tip of multipolar LV leads. By generating multiple LV activation wavefronts, MPP should help to reduce total LV activation times and improve CRT response ***(Kloppe, 2015)***. In support of this, studies have shown that when compared to conventional CRT, MPP results in significantly greater narrowing of the QRS complex ***(Kloppe, 2015)***. Furthermore, when compared to conventional BiV pacing, MPP has been shown to improve cardiac contractility and LV haemodynamics **(Rinaldi et al., 2014, 2013; Thibault et al., 2013a)**, echocardiographic response and long-term clinical outcomes ***(Zanon et al., 2016)***. However, other studies have generated conflicting findings. In the recently published phase I results of the MORE-CRT RCT, the use of MPP did not significantly improve echocardiographic response rates when compared to BiV pacing ***(Leclercq et al., 2019a)***. Notably, post hoc analysis revealed that the optimal results from MPP were primarily achieved in those who were programmed to a wide inter-electrode distance of at least 30mm and with a minimal delay of 5ms ***(Leclercq et al., 2019a; Niazi et al., 2017)***. With these settings, MPP resulted in a significantly higher non-responder conversion rate (relative to conventional MPP programming) and demonstrated a nonsignificant trend towards superiority over conventional BiV pacing (p=0.10). Further research (phase II of the MORE-CRT trial) is currently being undertaken to determine whether these specific MPP settings result in a greater benefit for MPP over standard BiV pacing ***(Leclercq et al., 2019b)***.

1.13.2. Single site left univentricular pacing

Although BiV pacing remains the most common mode of delivery for CRT, studies have recently explored the feasibility and comparative efficacy of left univentricular pacing ***(Burri et al., 2017)***. The success of LV univentricular pacing is dependent on the selection of an appropriate, patient-specific AV delay. This ensures optimal fusion (collision) of wavefronts arising from intrinsic RV activation with those induced by paced pre-excitation of the LV free wall ***(Burri et al., 2017)***. There are several perceived advantages with this approach, including: (i) reduced current drain, (ii) improved battery longevity, and (iii) the ability to preserve physiological conduction to the RV cavity via the native right-sided Purkinje system

(Burri et al., 2017; Thibault et al., 2011).
However, one of the major concerns associated with the use of left univentricular pacing is its ability to widen the QRS complex (relative to BiV pacing) and to potentially increase the degree of electrical dyssynchrony ***(Boriani et al., 2010; Leclercq et al., 2002)***. Despite these concerns, preliminary data arising from animal and clinical studies has largely been promising, demonstrating that single-site, LV-only pacing produces similar energetic and mechanical effects to conventional BiV pacing ***(Leclercq et al., 2002)***. Furthermore, when compared to BiV pacing, LV univentricular pacing has been shown to provide equivalent improvements in symptoms, exercise capacity, quality of life, LV function and reverse remodelling ***(Boriani et al., 2012, 2010; Gasparini et al., 2006)***. Recently, Boriani et al. undertook a meta-analysis of five RCTs comparing the efficacy of LV univentricular pacing vs. BiV pacing in relation to HF hospitalizations and total mortality ***(Boriani et al., 2012)***. The authors concluded that LV-only epicardial pacing was noninferior to BiV pacing, suggesting that this approach may serve as a viable alternative to conventional BiV pacing.

1.13.3. His-bundle pacing

There is significant interest in the use of direct His-bundle pacing (HBP) as an alternative to BiV pacing, primarily due its ability to restore physiological conduction in those with bundle branch block ***(Lewis Andrew J. M. et al., 2019)***. In fact, direct stimulation of the His-bundle has been shown to overcome conduction delay and dramatically reduce or even normalize ventricular activation times ***(El-Sherif et al., 1978)***. Different theories have been proposed to better explain this phenomenon. The simplest theory is based on an understanding that within the His-bundle, there are specific fibres predestined to give rise to the left bundle branch system ***(Narula, 1977)***. Consequently, a focal area of disease or conduction block within this segment could give rise to LBBB. In support of this, studies have shown that the location of conduction block in patients with LBBB is often focal, located at either the level of the His bundle or proximally within the left bundle branch ***(Upadhyay Gaurav A. et al., 2019)***. In these circumstances, it may be possible to overcome or restore normal conduction in the remainder of the Purkinje system by delivering pacing distal to the site of focal disease or conduction block. In fact, studies have reported that up to 70-90% of patients with a bundle branch block exhibit dramatic improvements in QRS duration following HBP ***(Keene et al., 2018)***. In patients with dyssynchronous HF, HBP has also been shown to improve NYHA functional class and LV reverse remodelling. Despite the perceived advantages of HBP, there is a relative paucity of RCTs directly comparing HBP against conventional BiV pacing, with most of the available data obtained from case series or nonrandomized, observational studies. Further work is required to determine whether HBP could serve as a viable, long-term alternative to BiV pacing.

1.13.4. Left bundle branch pacing

Left bundle branch pacing (LBBP) to achieve CRT represents a novel approach for the treatment of patients with dyssynchronous heart failure. Similar to HBP, LBBP is associated with significant QRS narrowing and has been shown to improve electromechanical dyssynchrony ***(Cano and Vijayaraman, 2021)***. However, in contrast to HBP, LBBP is arguably a simpler approach that is associated with higher implant success rates (between 80-97%), more stable lead parameters and lower lead-related complications ***(Cano and Vijayaraman, 2021; Liu et al., 2021; Padala and Ellenbogen, 2020)***. The mechanism by which LBBP corrects LBBB to produce near physiological pacing is similar to that of HBP ***(Liu et al., 2021)***. More specifically, direct stimulation of left bundle branch fibres in a region distal to the area of block can often help to restore normal conduction. Theoretically, LBBP represents the ideal approach to normalize electrical dyssynchrony and to improve haemodynamic physiology ***(Raymond-Paquin, 2021)***. However, very few studies have directly compared LBBP against conventional BiV pacing. In a recent nonrandomized, observational trial, Wu et al demonstrated the feasibility of LBBP in 137 consecutive patients referred for CRT ***(Wu et al., 2021)***. The authors found that, in comparison to BiV pacing, LBBP produced significantly shorter paced QRSd and greater improvements in NYHA functional class and LVEF at 1-year follow-up ***(Wu et al., 2021)***. Although exciting, further large-scale multicentre studies are required to fully determine the role of LBBP in the delivery of CRT.

1.13.5. Endocardial LV pacing

Given recent developments in leadless pacing technologies, there has been significant interest in the use of endocardial LV pacing as an alternative to the epicardial approach ***(Leyva et al., 2014)***. This method affords greater flexibility in LV lead placement, enabling the operator to target endocardial pacing to any site within the LV cavity. Furthermore, it has been suggested that LV endocardial stimulation may result in a faster, more homogenous LV electrical and mechanical activation pattern, and consequently better haemodynamics, than epicardial stimulation from the same epicardial location ***(Strik et al., 2012)***. In keeping with this, recent experimental data has indicated that endocardial LV pacing may actually be superior to epicardial pacing, particularly in non-responders to CRT ***(Hyde et al., 2015)***. However, there is a relative paucity of robust, large-scale RCT data directly comparing the efficacy of endocardial vs. epicardial LV pacing on long-term clinical outcomes ***(Auricchio et al., 2014; Morgan et al., 2016)***. Furthermore, it is important to note that currently available leadless pacing technologies (and transseptal LV lead approaches) remain experimental at the present time ***(Leyva et al., 2014)***.

Moreover, there are important risks associated with endocardial LV lead deployment, including the risk of infection and systemic embolization of vegetation, as well as a risk of cerebrovascular accidents and the requirement for lifelong anticoagulation. Further work is required to establish the precise role and optimal delivery for endocardial LV pacing.

1.14. Objectives

Ultimately, the main objectives of this thesis can be summarised as the *evaluation, validation,* and *clinical application* of novel vectorcardiographic approaches, with the overarching aim of determining whether these approaches can:

1. Improve identification of electrical dyssynchrony.
2. Offer greater insights into the electrophysiological mechanisms underpinning ventricular activation in patients with dyssynchronous HF
3. Provide a simple, noninvasive tool to assess and monitor the response to CRT.
4. Enable construction of patient-specific models of ventricular electrophysiology, potentially allowing identification of sites of latest electrical activation.

A common theme across all the included chapters is to address whether the predictive capability of VCG is superior to conventional 12-lead ECG analysis.

1.15. Structure of the thesis

We have structured the present thesis into the following chapters:

Chapter 1: General introduction. This chapter outlines the main concepts addressed in this thesis. We review current understanding of ventricular electrophysiology in patients with dyssynchronous heart failure. We also review the limitations of 12-lead ECG criteria when selecting suitable candidates for CRT. Thereafter, we provide a description of emerging techniques that can better quantify electrical dyssynchrony, with a particular focus on vectorcardiography. Finally, a summary of the clinical trials employing VCG-derived variables in CRT recipients is included.

Chapter 2: Effect of QRS area reduction and myocardial scar on the haemodynamic response to cardiac resynchronization therapy. The use of pre-

and post-implant QRS_{area} as a novel approach to predict acute CRT response is assessed in this chapter. We also evaluate the role of ΔQRS_{area} as a novel tool to identify the optimal pacing configuration on a quadripolar LV lead.

Chapter 3: Changes in QRS area and QRS duration after cardiac resynchronization therapy predict cardiac mortality, heart failure hospitalizations and ventricular arrhythmias. This chapter describes how pre- and post-implantation QRS_{area} can be used to predict clinical outcomes after CRT.

Chapter 4: Vectorcardiographic direction of ventricular activation as a predictor of long-term outcomes after cardiac resynchronization therapy. In this chapter, we introduce a novel interpretation of the vectorcardiogram termed the temporospatial isochrone (TSI). This novel vector-based approach facilitates the 3D visualization of LV activation wavefronts. Using the principle that LBBB is associated with strong unidirectional wavefronts (from septum→LVFW), we demonstrate that TSI can accurately identify LBBB-like conduction patterns and predict long-term outcomes following CRT.

Chapter 5: Noninvasive mapping of electrical dyssynchrony improves patient selection for cardiac resynchronization therapy: the ElectroCRT study. This chapter evaluates the use of a novel electroanatomical modelling system (ECGSync) to noninvasively map ventricular activation sequences in HF patients undergoing CRT implantation. This approach, based on electrical data obtained from routine 12-lead ECG, facilitates the derivation of novel 3D markers of electrical dyssynchrony. In this chapter, we explore whether these novel dyssynchrony biomarkers predict acute CRT response.

Chapter 6: Electroanatomical modelling for non-invasive QLV mapping in cardia resynchronization therapy: the ECGSync study. In this chapter, isochronal activation maps derived from a novel electroanatomical modelling system (ECGSync) are validated against noncontact mapping (EnSite). More specifically, we investigate whether ECGSync can accurately identify LEAS using a standard 12-lead ECG dataset.

Chapter 8: Discussion and conclusion. In this chapter, we summarise the main findings arising from our research and discuss the clinical implications of each study. Finally, we propose a guideline for future research in this area.

Chapter 7: Contributions. The publications arising from this thesis are listed in this chapter.

PART 1

EVALUATING THE ROLE OF VECTORCARDIOGRAPHY IN CARDIAC RESYNCHRONIZATION THERAPY

Chapter 2

Effect of QRS area reduction and myocardial scar on the haemodynamic response to cardiac resynchronization therapy

Abstract

Aims: Vectorcardiographic QRS area (QRS_{area}) predicts clinical outcomes after CRT. Myocardial scar adversely affects clinical outcomes after CRT.

Objectives: To determine whether, in patients with an ideally deployed quadripolar left ventricular (LV) lead (QUAD), reducing QRS_{area} leads to an acute haemodynamic response (AHR); and, whether scar affects this interaction.

Methods: Patients (n=26, aged 69.2 ± 9.12 years [mean ± SD]) underwent assessment of the maximum rate of change of LV pressure (ΔLV dP/dt_{max}) during CRT using various LV pacing locations (LVPLs). A cardiac magnetic resonance (CMR) scan was used to localize LV myocardial scar.

Results: Interindividually, ΔQRS_{area} (area under the receiver-operating characteristic curve [AUC]: 0.81, $p<0.001$) and change in QRS duration (ΔQRSd) (AUC: 0.76, $p<0.001$) predicted ΔLV dP/dt_{max} after CRT. Scar burden correlated with ΔQRS_{area} ($r=0.35$, $p=0.003$) and ΔQRSd ($r=0.46$, $p<0.001$). A reduction in QRS_{area} was observed with LVPVs remote from scar (-3.28 ± 38.1 µVs) or in LVPVs in patients with no scar at all (-43.8 ± 36.8 µVs), whereas LVPVs over scar increased QRS_{area} (22.2 ± 58.4 µVs) ($p<0.001$ for all comparisons). LVPVs within 1 scarred LV segment were associated with a lower ΔLV dP/dt_{max} (-2.21 ± 11.5%) than LVPVs remote from scar (5.23 ± 10.3%, $p<0.001$) or LVPVs in patients with no scar at all (10.2 ± 7.75%) (both $p<0.001$).

Conclusion: Reducing QRS_{area} improves the AHR to CRT. Myocardial scar adversely affects ΔQRS_{area} and the AHR. These findings support the use of ΔQRS_{area} and CMR in optimizing CRT using QUAD.

Chapter adapted from ***Okafor et al., 2020.***

2.1. Introduction

Cardiac resynchronization therapy (CRT) is an established therapy for patients with impaired left ventricular (LV) systolic function and a wide QRS complex. As well as improving symptoms and quality of life, it also reduces heart failure hospitalizations and improves survival ***(Leyva et al., 2014)***. However, even in guideline-indicated patients, the response to CRT is variable. The 'non-responder' rate range between 9% and 68%, depending on the criteria used to define response ***(Fornwalt et al., 2010)***. Prominent amongst the factors implicated in non-response is suboptimal LV lead deployment ***(Derval et al., 2010; Umar et al., 2016; van Everdingen et al., 2015)***.

Quadripolar LV leads (QUAD) have been no less than a 'game changer' in the field of CRT. The availability of a wide range of LV pacing vectors (LVPVs) not only reduces diaphragmatic stimulation, but also permits LV pacing from widely spaced areas of the myocardium. Several studies have shown that optimizing LVPVs on a QUAD in individual patients improves the acute hemodynamic response (AHR) to CRT ***(Asbach et al., 2013; Osca et al., 2015; Umar et al., 2016)***. Whilst myocardial scar in the vicinity of the LVPV has been shown to be detrimental in studies using bipolar leads, (Kočková et al., 2018; Leyva et al., 2011) no studies have explored whether the same applies to QUAD.

It has recently been shown that vectorcardiographic derived QRS area (QRS_{area}) is superior to QRS duration (QRSd) in predicting total mortality after CRT ***(Emerek et al., 2019; van Stipdonk et al., 2018)***. Moreover, QRS_{area} has been shown to correlate with the maximum rate of rise of LV pressure (LV dP/dt_{max}) (De Pooter et al., 2017; Ross et al., 2018b) and LV reverse remodelling ***(van Deursen et al., 2015a)*** after CRT. This makes sense, insofar as QRS_{area} is a measure of LV electrical dyssynchrony ***(Mafi Rad et al., 2016)***, the natural substrate for CRT. Importantly, a reduction in QRS_{area} has been shown to improve the AHR to CRT in patients with suboptimal LV lead deployment ***(Ross et al., 2018b)***.

In the present study, we explore whether, in patients with an optimally deployed LV lead, assessed by fluoroscopy, the change QRS_{area} (ΔQRS_{area}) after CRT relates to an AHR; whether the AHR in individual patients can be improved by reducing QRS_{area}; and, whether this AHR relates to the position of the LVPV in relation to myocardial scar, assessed using cardiovascular magnetic resonance (CMR).

2.2. Methods

A total of 26 patients referred for CRT implantation at the University Hospital Birmingham, United Kingdom were studied. All patients provided written informed consent. The study was approved by the regional ethics committee and conformed with the Declaration of Helsinki.

2.2.1. Patient population

Inclusion criteria included: sinus rhythm; New York Heart Association (NYHA) classes I-IV; QRSd ≥120 ms; left ventricular ejection fraction (LVEF) ≤ 35%. Exclusion criteria included frequent supraventricular or ventricular ectopy, primary valvular disease; previous mechanical valve replacements; and myocardial infarction, acute coronary syndrome or revascularization in the past 3 months; LV thrombus on CMR.

2.2.2. Device implantation

Device implantation was performed under local anaesthesia and sedation. Standard transvenous techniques were adopted, using a left-sided cephalic and/or axillary venous approach in all patients. A QUAD (Attain Performa, Attain Stability QUAD; Medtronic Plc, Minneapolis) was advanced via the coronary sinus into a lateral or posterolateral LV position, with the implanting physician purposefully directing the LV lead tip towards a distal (apical) position. To achieve bipolar LV pacing from 2 poles in the basal, mid and apical segments, the LV lead was moved in a basal-to-apical direction prior to the pacing protocols. At the outset, a second operator obtained femoral artery access using a 6-French sheath. A multipurpose catheter was advanced retrogradely across the aortic valve into the LV, with a 0.014-inch high-fidelity pressure wire (PressureWire Certus, Abbott, Minnesota) deployed into the mid-LV cavity (Figure 2.1). Heparin was administered and the activated clotting time monitored as per standard practice.

2.2.3. Pacing protocol

All measurements were performed using AAI pacing as reference. Pacing was delivered at 10 bpm above intrinsic heart rate, with the atrioventricular (AV) delay set at 20 ms below the intrinsic AV delay and the interventricular (VV) delay to 0 ms (simultaneous). As this study was not designed to assess the influence of variable AV delays on LV haemodynamics, we elected to programme a single 'physiological' AV delay for all patients. Pacing with an AV delay set to 20ms below the intrinsic AV delay enabled AV synchrony and LV diastolic filling to be maintained

close to a patient's baseline status, whilst avoiding the development of fusion with intrinsic activation. Similarly, to mitigate the variable influence of LV/RV pre-excitation on LV haemodynamics, we elected to deliver simultaneous biventricular pacing (i.e., VV delay = 0ms) for all pacing configurations. Biventricular pacing capture was checked before each pacing protocol. To minimize the impact of sampling error due to respiration, loading conditions and baseline drift, 4 repetitions of a 15 second acquisition was obtained for every LVPV, returning to baseline AAI pacing for another 15 sec after each data acquisition. The following pacing configurations were sequentially assessed: intrinsic rhythm, AAI, right ventricular (RV)-only pacing (VVI); biventricular CRT in basal, mid and apical segments.

2.2.4. Haemodynamics

Patients underwent continuous recording of LV intraventricular pressure with the CardioLab electrophysiology recording system (GE Healthcare, Chicago, US) [Central illustration]. All data was exported prior to offline analysis. The final dataset, which included digital 12-lead ECG signals, intracardiac electrograms, beat-to-beat femoral artery blood pressure and LV pressure were consolidated in the RASCHlab software package (Raphael Schneider, Medtronic, Inc.). The rate of change of LV pressure (ΔLV dP/dt_{max}) was taken as the mean of all beats captured over 15 s, as previously described ***(Umar et al., 2016)***. Atrial and ventricular ectopic beats and the following two beats were excluded from analysis. An AHR was defined as a ≥10% increase in LV dP/dt_{max} in relation to AAI pacing.

2.2.5. Vectorcardiography

A single investigator (O.O.) who was blinded to acute LV haemodynamic data, analysed VCG data using an in-house software package (PEACS, Nieuwerbrug, The Netherlands). The onset and offset of the QRS complexes were manually marked on 12-lead ECGs. Surface ECG-derived QRS complexes were converted to orthogonal X, Y and Z vector signals using the Kors transformation. The area between the ventricular deflection curve and isoelectric baseline was determined for each orthogonal lead (X, Y and Z). Subsequently, QRS_{area} was calculated according to the following formula: $(X_{area}^2 + Y_{area}^2 + Z_{area}^2)^{1/2}$. During biventricular pacing, ΔQRS_{area} was assessed relative to baseline measurements.

2.2.6. Cardiac magnetic resonance

Imaging was performed using a 1.5 Tesla scanner (Avanto, Siemens, Erlangen, Germany) and a phased-array cardiac coil. A short axis (SAX) LV stack was acquired using a steady state in free precession (SSFP) sequence. Left ventricular mass, LV

volumes and LVEF were quantified using CMR42 software analysis (Circle Cardiovascular Imaging Inc., Calgary).

For myocardial scar imaging, a segmented inversion-recovery technique was employed following the intravenous administration of gadobutrol. The location and extent of myocardial scar was assessed using CMR42. To this end, normal myocardium was identified using a region of interest tool, with myocardial scar defined as a signal intensity >2 standard deviations (SD) above normal myocardium. Myocardial scar was then expressed as a percentage of LV mass (% LV scar) and displayed according to a 16-segment American Heart Association model, using CMR42 analysis (Figure 2.1). If pacing was delivered from LVPVs that subtended scarred myocardium (i.e. <1 segment), this was classified as 'within scar'. Similarly, LVPVs 'remote' pacing sites were defined those ≥ 1 AHA segment away from scar. The term 'no scar at all' was applied to LVPVs in patients with no myocardial scar at all.

2.2.7. LV lead position

The location of LV leads was assessed using at 3 orthogonal views, namely the anteroposterior view, the 30° left anterior oblique (LAO) and 30° right anterior oblique (RAO) views, as previously described ***(Leyva et al., 2018b)***. Lead positions were assessed by an investigator who was blinded to all other study data (F.L). For analysis, LVPVs were categorized longitudinally into basal, mid and apical. They were also dichotomised into apical or non-apical, the latter including basal and mid positions. Circumferentially into anterolateral, lateral, posterolateral and posterior.

2.2.8. Statistical analysis

Continuous variables are expressed as mean ± standard deviation (SD). Normality was tested using the Shapiro-Wilk test. The Pearson correlation coefficient was used to assess correlations between continuous variables. Areas under the receiver operating curves (AUC) were used to assess the predictive value of pre- and post-implant variables in relation to AHR. To determine whether combining pre- and post-implant variables improves AHR prediction, logistic regression analysis was used to compute a single output variable for classification using AUCs. Differences between AUCs were assessed using De Long's procedure. Independent t-tests or Mann Whitney U-tests were used to compare variables across LVPVs. Factorial ANOVA or the Kruskal-Wallis test were used to compare variables across the different LVPVs. All statistical analyses were performed using SPSS version 25.0 (IBM. Chicago, Illinois) and MedCalc version 19.1 (MedCalc, Ostend, Belgium). A two-sided $p < 0.05$ was considered statistically significant.

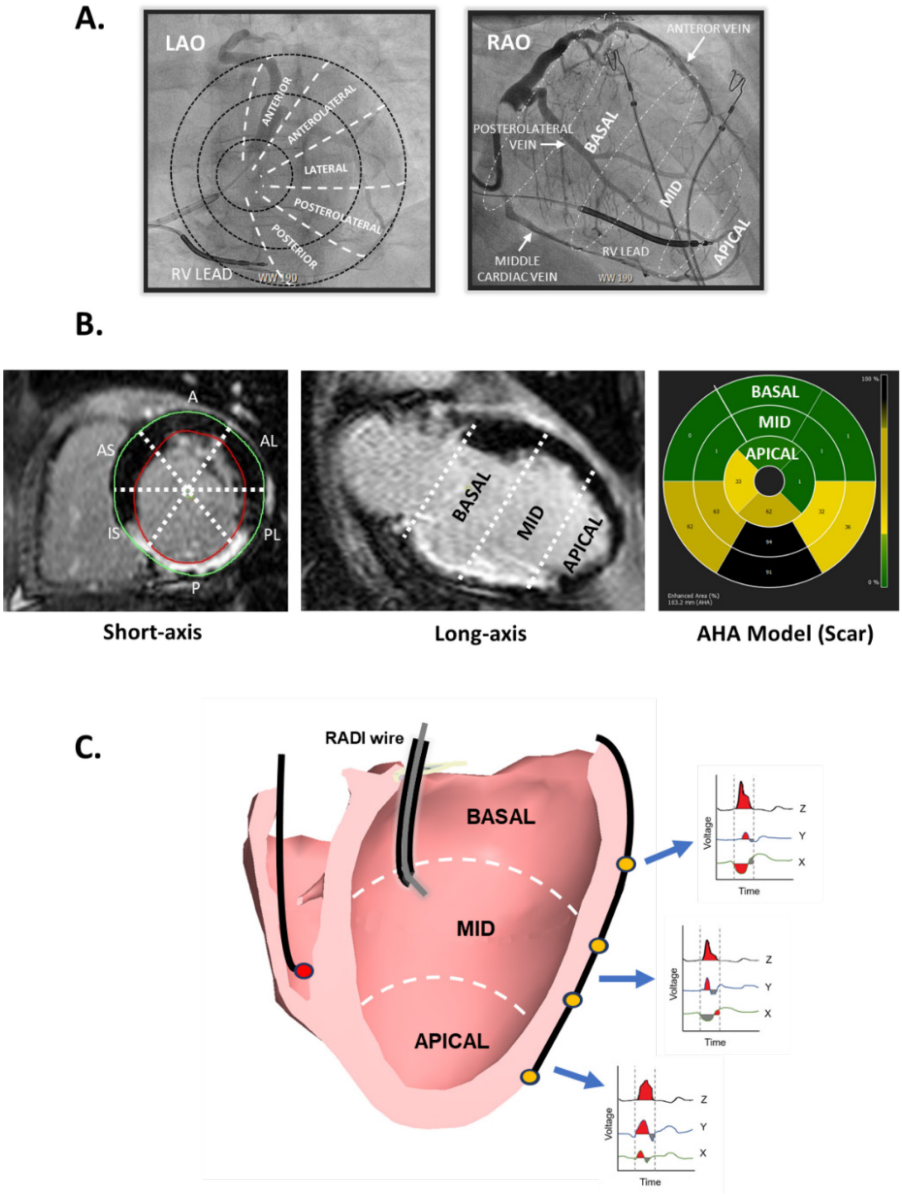

Figure 2.1. Central illustration of study methodology.

Circumferential and longitudinal lead positions were assessed using 30º left anterior oblique (LAO) and right anterior oblique (RAO) fluoroscopic vies of the coronary veins (Panel A). Myocardial scar was quantified using late gadolinium CMR. Panel B shows short axis and long axis views of the left ventricle, in which myocardial scar shows up in white. Scar position is indicated in terms of the American Heart Association segments. Panel C is a diagrammatic representation of the position of the quadripolar lead within a posterolateral vein, in relation to the longitudinal segments. Vectorcardiograms obtained after CRT using various left ventricular pacing configurations are shown (bottom right). Figure adapted from Okafor et al., 2020.

2.3. Results

2.3.1. Baseline characteristics

A total of 4/30 (13.3%) patients enrolled were excluded because of second-degree atrio-ventricular block during atrial (AAI) pacing (n=1); frequent ventricular ectopics (n=1); and the finding of LV thrombus on CMR (n=2). Amongst the 26 patients included (aged 69 ± 9.1 years [mean ± SD], 20/26 [77%] male), the underlying aetiology was ICM in 17/26 (65%) (Table 2.1). A LBBB was present in 20/26 (76.9%) patients and non-LBBB in 6/26 (23.1%) (non-specific intraventricular conduction delay in 5 and right bundle branch block in 1). The QRSd was 156.1 ± 19.76 ms and the LVEF was 24.8 ± 7.87%. A QUAD was deployed in anterolateral (3/26 [12%]), posterolateral (18/26 [69%]) and lateral (5/26 [19%]) positions.

Table 2.1. Baseline Characteristics				
	All	**LBBB**	**Non-LBBB**	**P-value**
N	26	20	6	
Age, yrs	69.2 ± 9.12	67.1 ± 8.85	76.2 ± 6.52	0.019
Sex (male), n (%)	20 (76.9)	15 (75.0)	5 (83.3)	1.00
NYHA class, n (%)				
I	1 (3.8)	1 (5.0)	0 (0)	0.126
II	15 (57.7)	9 (45.0)	6 (100)	
III	9 (34.6)	9 (45.0)	0 (0)	
IV	1 (3.8)	1 (5.0)	0 (0)	
Aetiology, n (%)				
Ischemic	17 (65.4)	12 (60.0)	5 (83.3)	0.380
Non-ischemic	9 (34.6)	8 (40.0)	1 (16.7)	
Co-morbidities, n (%)				
Diabetes mellitus	5 (19.2)	3 (15.0)	2 (33.3)	0.558
Hypertension	7 (26.9)	6 (30.0)	1 (16.7)	1.00
CABG	2 (7.77)	2 (10.0)	0 (0)	1.00
LVEF, (%)	24.8 ± 7.87	23.9 ± 7.92	29.4 ± 5.64	0.614
Medication, n (%)				
ACEI / ARA	26 (100)	20 (100)	6 (100)	
Beta-blocker	23 (88.5)	18 (90.0)	5 (83.3)	1.00
MRA	12 (46.2)	9 (45.0)	3 (50.0)	1.00
ECG variables				
Sinus rhythm, n (%)	25 (96.2)	19 (95.0)	6 (100)	1.00
AF / flutter, n (%)	1 (3.85)	1 (5.0)	0 (0)	
PR interval (ms)	171.3 ± 35.5	179.11 ± 31.9	149.2 ± 43.7	0.325
QRSd (ms)	152.2 ± 19.9	161.3 ± 19.7	142.0 ± 12.2	<0.001
ΔQRSd (ms)	-14.2 ± 20.8	-19.1 ± 18.5	-0.95 ± 21.3	0.001
VCG variables				
QRS area (μVs)	101.1 ± 44.9	110.6 ± 45.1	75.7 ± 28.8	0.009
ΔQRS area (μVs)	-2.71 ± 51.4	-15.7 ± 41.3	36.4 ± 61.2	0.001
Table taken from Okafor et al., 2020.				

2.3.2. Interindividual analyses

As shown in Figure 2.2, QRS_{area} (r=0.43, p<0.001) and QRSd (r=0.38, p=0.001) in the various LVPVs correlated positively with ΔLV dP/dt_{max}. A stronger correlation was observed between ΔQRS_{area} (r=-0.68, p<0.001) and ΔQRSd (r=-0.68, p<0.001) with ΔLV dP/dt_{max}. Apical LVPVs provided a greater increase in LV dP/dt_{max} (6.22 ± 9.37%) than mid (3.20 ± 11.5%) or basal (1.22 ± 12.5%) LVPVs (both p<0.038). There was a close correlation between baseline QRSd and QRS_{area} (r = 0.61, p<0.001) and between ΔQRSd and ΔQRS_{area} (r=-0.71, p<0.001).

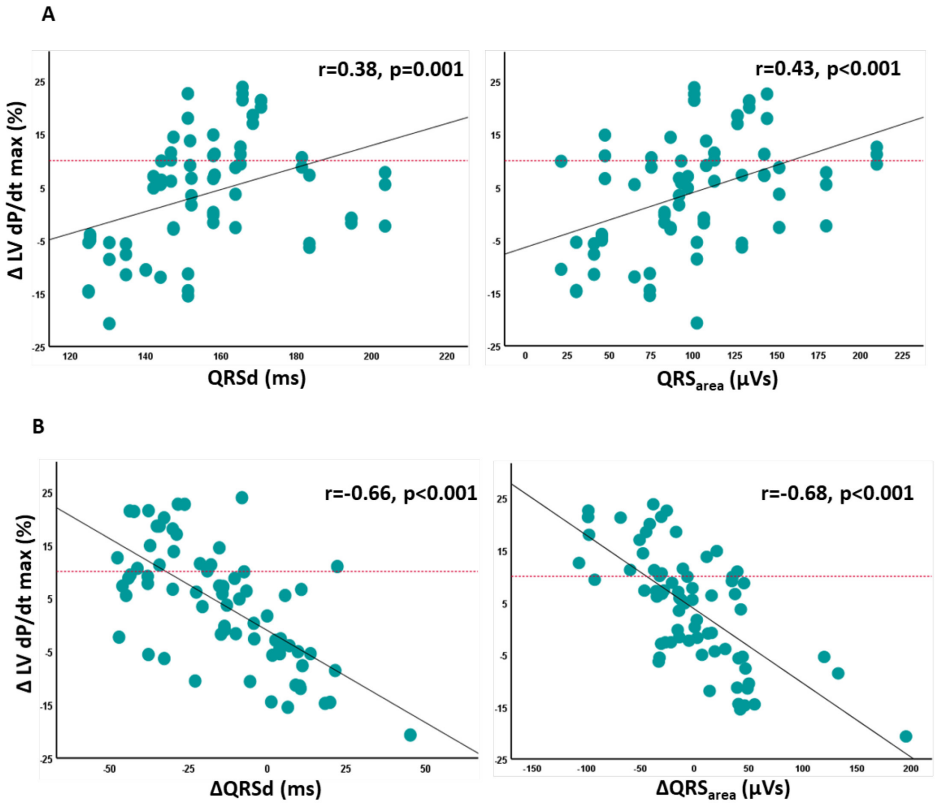

Figure 2.2. Scatterplots of ΔQRS_{area} and ΔQRSd, and AHR.
A) Scatterplots of QRS area (QRS_{area}) and QRS duration (QRSd) against the rate of change in LV pressure (ΔLV dP/dt_{max}) during cardiac resynchronization therapy using different left ventricular pacing vectors; B) Scatterplots of ΔQRS_{area} and ΔQRSd against ΔLV dP/dt_{max} during CRT using different LV pacing vectors. Pearson correlation coefficients (r) are shown. Figure taken from Okafor et al., 2020.

As shown in Figure 2.3, the AUC for AHR was higher for ΔQRS_{area} (AUC: 0.81, 95% confidence interval [CI] 0.70-0.89, p<0.001) and ΔQRSd (AUC: 0.76, 95% CI: 0.65-0.86, p<0.001), than for QRS_{area} (AUC: 0.65, 95% CI: 0.53-0.76, p = 0.032) or QRSd (AUC: 0.67, 95% CI: 0.55-0.77, p = 0.009). The highest AUC for AHR was obtained when ΔQRSd and ΔQRS_{area} were combined into a single continuous variable (AUC: 0.84, 95% CI: 0.73-0.94, p<0.001).

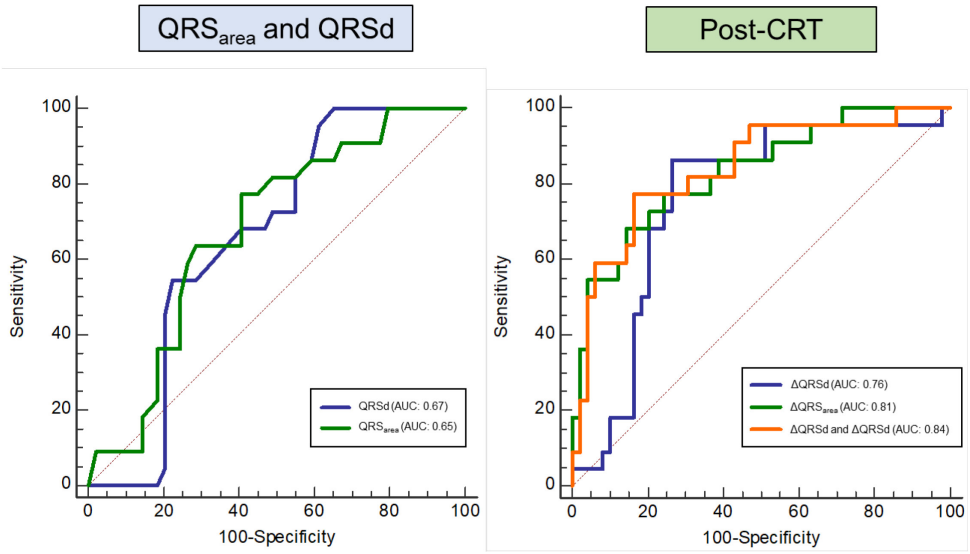

Figure 2.3. Receiver-operating characteristic curves.
Graphs show receiver-operating characteristic curves and corresponding areas under the curve (AUC) for pre-CRT QRS area (QRS_{area}) and QRS duration (QRSd) and post-CRT changes (Δ) thereof. Figure adapted from Okafor et al., 2020.

We determined the optimal ROC-derived cut-off values for QRSd (147ms), QRS_{area} (97μVs), ΔQRSd (-15ms) and ΔQRS_{area} (-30μVs). As shown in Table 2.2, these values were used to determine the sensitivity, specificity, negative and positive predictive values for each parameter. In univariate analysis, QRSd (OR: 3.7; 95% CI: 1.08 – 12.43, p =0.037), QRS_{area} (OR: 4.93; 95% CI: 1.56 – 15.5, p =0.006), ΔQRSd (OR: 17.5; 95% CI: 4.44 – 69.2, p <0.001) and ΔQRS_{area} (OR: 12.9; 95% CI: 3.86 – 42.8, p <0.001) all predicted AHR to CRT (Table 2.2). Left bundle branch block QRS morphology did not predict acute CRT response (p=0.15).

Table 2.2. Diagnostic performance of VCG and ECG-derived parameters								
Predictor variable	**Odds ratio**	**95% C.I.**		**p**	**Sensitivity**	**Specificity**	**PPV**	**NPV**
QRSd ≥ 147 ms	3.7	1.08	12.43	0.037	81.82	44.9	40.0	84.6
QRS_{area} ≥ 97 μVs	4.93	1.56	15.5	0.006	77.3	59.2	46.0	85.3
ΔQRSd ≥ -15 ms	17.5	4.44	69.2	<0.001	86.4	73.5	59.4	92.3
ΔQRS_{area} ≥ -30 μVs	12.9	3.86	42.8	<0.001	68.2	85.7	87.5	87.5

To better assess the interaction between ECG and VCG variables in relation to identifying acute CRT responders, we constructed separate multivariate models using the 2 baseline (QRSd and QRS_{area}) and 2 post-CRT predictors (ΔQRSd and ΔQRS_{area}). As shown in Table 2.3, the addition of vectorcardiographic QRS_{area} rendered QRSd an insignificant predictor of CRT-R (p=0.268) [Table 2.3]. In contrast, both ΔQRSd and ΔQRS_{area} remained independent predictors of CRT-R even after multivariate adjustment (both p<0.018).

Table 2.3. Different multivariate models for predicting AHR to CRT					
	Parameter	**Adjusted Odds Ratio**	**95% C. I**		**P**
MULTIVARIATE MODEL 1 (Pre-implant)	QRSd ≥ 147 ms	2.13	0.56	8.13	0.268
	QRS_{area} ≥ 97 μVs	3.73	1.09	12.82	0.037
MULTIVARIATE MODEL 2 (Post-implant)	ΔQRSd ≥ -15 ms	8.77	1.97	38.46	0.004
	ΔQRS_{area} ≥ -30 μVs	5.15	1.33	20.0	0.018

2.3.3. Intraindividual analyses

As shown in Table 2.4 and Figure 2.4, the optimal and worse ΔLV dP/dt_{max} varied widely between patients (7.08 ± 6.07%; range: 0.1 to 20.5%). Left bundle branch block patients had significantly greater baseline QRS_{area} (110.6 ± 45.1μVs vs75.7 ± 28.8 μVs, p=0.009) and ΔQRS_{area} (-15.7 ± 41.3 vs. 36.4 ± 61.2μVs, p=0.001) than non-LBBB patients. Intraindividually, a wide variation in optimal and worst ΔQRS_{area} was also observed across the various LVPVs (-24.3 ± 21.9%; range: -75.7 to 13.3%).

Table 2.4. A comparison of optimal and worst LVPVs according to ΔLV dP/dt_{max} and ΔQRS_{area}.							
Patient number	**QRS morphology**	**Mean % difference in ΔLV dP/dt_{max}**	**P***	**Optimal LVPV for ΔLV dP/dt_{max}**	**Mean absolute difference in ΔQRS_{area}**	**P***	**Optimal LVPV for ΔQRS_{area}**
1	LBBB	0.10	0.949	Apical	56.9	<0.001	Apical
2	LBBB	20.1	<0.001	Apical	26	<0.001	Apical
3	LBBB	6.78	<0.001	Apical	23.3	0.001	Apical
4	LBBB	4.17	0.220	Apical	2.83	0.491	Apical
5	LBBB	7.16	0.001	Apical	0.65	0.446	Apical
6	LBBB	0.95	0.065	Apical	13.3	0.234	Non-apical
7	LBBB	20.5	<0.001	Apical	15.3	<0.001	Apical
8	LBBB	1.81	0.441	Non-apical	18.8	<0.001	Apical
9	LBBB	5.79	0.096	Non-apical	8.2	<0.001	Apical
10	LBBB	13.6	<0.001	Apical	13.9	0.187	Apical
11	LBBB	1.94	0.798	Apical	33.7	<0.001	Non-apical
12	LBBB	17.3	<0.001	Apical	20.6	<0.001	Apical
13	NICD	2.19	0.802	Apical	17.1	<0.001	Apical
14	LBBB	1.13	0.096	Non-apical	21.4	<0.001	Apical
15	NICD	9.33	<0.001	Apical	11.1	0.022	Apical
16	NICD	15.2	<0.001	Apical	75.7	<0.001	Apical
17	LBBB	10.1	0.001	Non-apical	3.2	0.266	Non-apical
18	LBBB	1.66	0.537	Non-apical	15.8	<0.001	Apical
19	LBBB	11.3	0.031	Non-apical	67.6	<0.001	Apical
20	LBBB	8.10	0.015	Non-apical	69.5	<0.001	Non-apical
21	NICD	5.01	0.007	Apical	32.2	<0.001	Apical
22	LBBB	3.90	0.035	Apical	31.2	0.001	Apical
23	NICD	1.03	0.553	Non-apical	29.6	<0.001	Non-apical
24	LBBB	4.18	0.011	Apical	24.0	<0.001	Apical
25	RBBB	8.23	0.006	Non-apical	18.9	0.034	Apical
26	LBBB	2.41	0.536	Apical	13.1	0.001	Apical

**, P values refer to comparisons between optimal and worst LVPVs.*
Table taken from Okafor et al., 2020.

As shown in Figure 2.4, ΔQRS_{area} mirrored $\Delta LV\ dP/dt_{max}$. As expected, QRS_{area} reduction was greater for optimal (-18.02 ± 61.24 μVs) than for worst (1.43 ± 53 μVs) LVPVs ($p<0.001$). Using ΔQRS_{area} to guide LVPV optimization, 4/26 (15.4%) patients (non-specific intraventricular conduction delay; n=1, LBBB; n=3) could have been 'converted' to haemodynamic responders, improving AHR rates from 31% to 46%. The LVPV associated with the greatest reduction in QRS_{area} was also associated with the optimal AHR to CRT in 19/26 (73.1%) patients (p=0.009). Apical LVPVs provided a greater increase in LV dP/dt_{max} (6.22 ± 9.37%) than mid (3.20 ± 11.5%, p=0.038) or basal (1.22 ± 12.5%LVPVs, $p<0.001$) (non-apical LVPVs: 2.23 ± 12.0%, $p<0.001$). As illustrated in Table 2.2, the wide variation between optimal and worse ΔQRS_{area} and $\Delta LV\ dP/dt_{max}$ was evident in both LBBB and non-LBBB patients, suggesting that ΔQRS_{area} could serve as a novel tool for haemodynamic optimization in both populations.

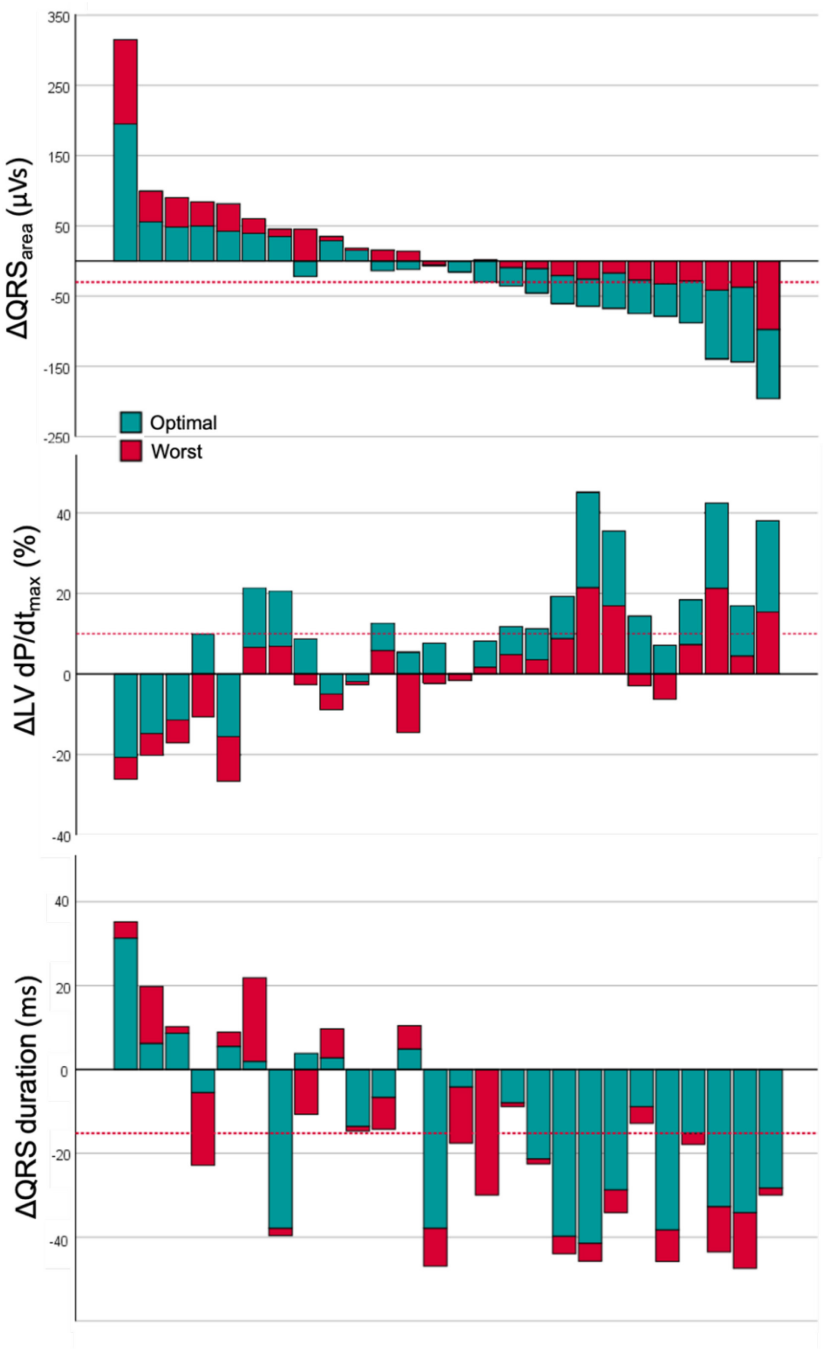

Figure 2.4. Variation in QRS area, QRS duration and AHR across LVPVs. *Graphs show changes in QRS area (ΔQRS_{area}) and QRS duration ($\Delta QRSd$) in optimal and worst left ventricular pacing vectors in individual patients, ordered according to maximum to minimum (ΔQRS_{area}). Figure adapted from Okafor et al., 2020.*

2.3.6. Scar burden

Baseline QRS_{area} was larger in NICM than ICM (132.7 ± 37.1 vs. 81.0 ± 38.1 µVs, p<0.001). In addition, post-implant QRS_{area} reduction was more evident in NICM (-20.5 ± 40.0 µVs) than in ICM (6.20 ± 64.9 µVs) (p<0.001). As shown in Figure 2.4, myocardial scar burden (% LV mass) correlated positively with ΔQRS_{area} (r=0.35, p=0.003).

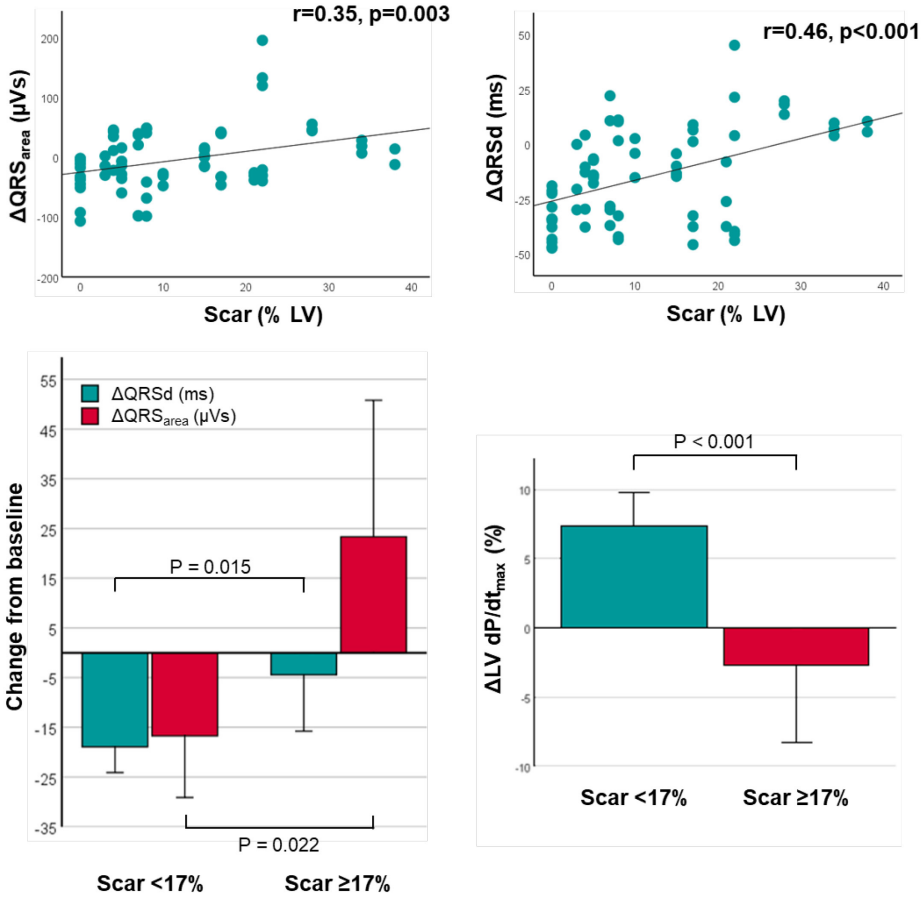

Figure 2.5. Effect of scar burden on ΔQRSarea and ΔQRSd, and AHR.
A) shows scatterplots of scar burden, expressed as % of the total LV mass, against changes in QRS area (ΔQRS_{area}) and QRS duration (ΔQRSd) after CRT using all left ventricular pacing vectors; B) shows a bar graph of scar burden, dichotomized as <17% and ≥17%, in relation ΔQRSarea and ΔQRSd after CRT; C) shows a bar graph of scar burden in relation to acute haemodynamic response, quantified as %ΔLV dP/dt. Figure taken from Okafor et al., 2020.

When all patients were dichotomized into <17% or ≥17% scar burden groups, those with <17% burden had greater reductions in QRS_{area} (-16.7 ± 41.7 vs. 23.3 ± 61.9µVs, p=0.022) and QRSd (-18.9 ± 17.4 vs. -4.43 ± 25.6 ms, p=0.015). In other words, the more scar, the less the reduction in post-CRT QRS_{area}. Similarly, scar burden correlated with ΔQRSd (r=0.46, p<0.001), indicating that the more scar, the lesser the reduction, or increase in QRSd. A scar burden ≥17% was associated with a lower AHR than scar burden<17% (<0.001).

In univariate analyses, myocardial scar (% LV) predicted AHR (AUC: 0.71, 95% CI: 0.59-0.84, p=0.004) (**Figure 4**). In multivariate analyses adjusting for age, myocardial scar was an independent predictor of AHR (odds ratio: 0.93; 95% CI: 0.87-0.99, p=0.017). In contrast, LVEF only correlated with pre-implant QRS_{area} (r=-0.39, p=0.001) and QRSd (-0.33, p=0.005), but not with ΔLV dP/dt_{max}, ΔQRS_{area} or ΔQRSd (all p > 0.2). Moreover, LVEF did not predict AHR (AUC: 0.63; 95% CI: 0.50 – 0.77, p=0.05).

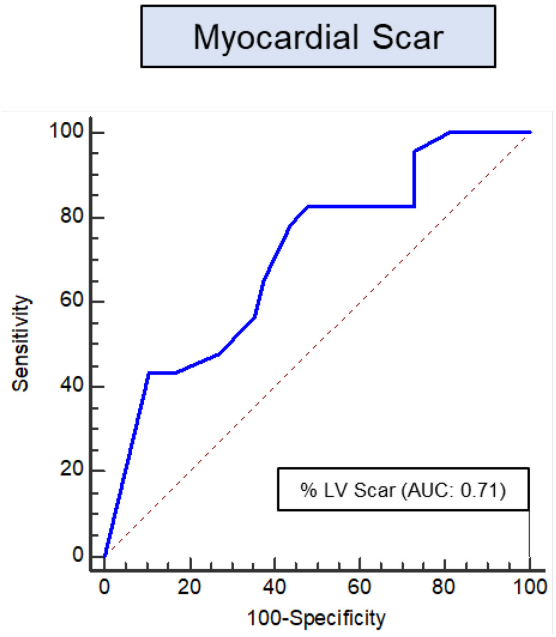

Figure 2.6 . Effect of scar burden on ΔQRS_{area} and ΔQRSd, and AHR.
Receiver-operating characteristic curves of scar burden (%LV mass) in relation to acute haemodynamic response (≥10% ΔLV dP/dt_{max}) is shown. AUC = area under curve. Figure taken from Okafor et al., 2020.

2.3.5. Scar location

A total of 12/7 (71%) ICM patients had a transmural scar involving the LV free wall [inferolateral; n=11, anterolateral n=1]. Compared to patients with no lateral LV wall scar or a subendocardial scar, patients with ICM with transmural scar had lower QRS_{area} reduction (ΔQRS_{area}: -15.5±42.95 vs. 24.3±65.4µVs, p<0.001). As shown in Figure 2.7, a reduction in post-CRT QRS_{area} was only observed LVPVs remote from scar (-3.28 ± 38.1µVs) or in LVPVs in patients with no scar at all (-43.8 ± 36.8 µVs) (both p<0.001). Conversely, LVPVs over scar led to an increase in QRS_{area} (22.2 ± 58.4 µVs, p<0.001 for all comparisons). With respect to AHR, LVPVs within 1 LV segment with scar were associated with a lower ΔLV dP/dt_{max} (-2.21 ± 11.5%) than LVPVs remote from scar (5.23 ± 10.3%, p<0.001) or LVPVs in patients with no scar at all (10.2 ± 7.75%) (both p<0.001).

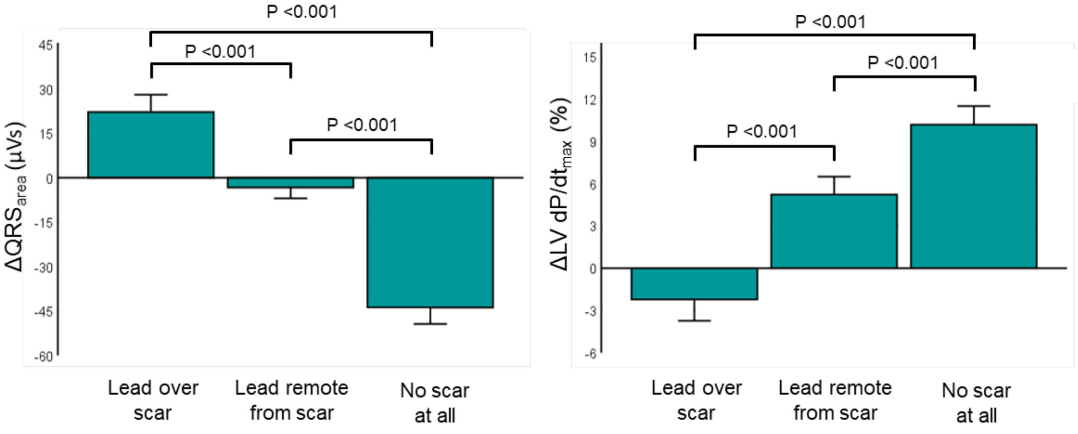

Figure 2.7. Effect of scar on QRS area and AHR.
Bar graphs showing changes in QRS area (ΔQRS_{area}) and rate of change in LV pressure ($\Delta LV\ dP/dt_{max}$) in LVPVs over myocardial scar, remote from scar and in patients with no scar at all. Figure taken from Okafor et al., 2020.

2.3.6. Gender differences

Despite similar QRSd values between men and women (156 ± 23.92 vs. 155.59 ± 18.20 ms, p=0.41), baseline QRS_{area} was significantly larger in females than in males (129.44 ± 50.68 vs 90.78 ± 38.06 µVs, p=0.006). In contrast, post-implant QRS_{area} reduction was similar across both sexes (: -8.66 ± 45.45 vs -1.74 ± 65.51 µVs, p=0.68). There were no observed differences in myocardial scar burden between men and women (%LV scar: 12.15 ± 11.45 vs. 14.5 ± 12.64, p=0.49).

2.4. Discussion

Several findings have emerged in relation to the optimization of LVPVs in CRT recipients who have a fluoroscopically ideal LV lead position. First, altering LVPVs on a QUAD was associated with wide intraindividual variations in LV dP/dt_{max}, QRS_{area}, and QRSd. Second, ΔQRS_{area} correlated with ΔLV dP/dt_{max} across LVPVs. Third, both myocardial scar burden and location of scar in the vicinity of the LVPV had a negative effect on the AHR to CRT.

2.4.1. Haemodynamic effect of altering LVPVs

Early studies suggested that the AHR to CRT varies according to the site of LV pacing, with lateral LV wall pacing generally regarded as superior to non-lateral sites. However, there is conflicting evidence regarding whether LV apical pacing is physiologically superior to nonapical LV pacing ***(Leyva et al., 2018b)***. In the present study, we found that apical LVPLs provided a greater improvement in LV dP/dt_{max} than nonapical LVPLs ($p<0.001$). Although this is at odds with the findings arising from the MADIT-CRT (Multicentre Automatic Defibrillator Implantation Trial - Cardiac Resynchronization Therapy) trial subanalysis, we should consider that in this prospective study, outcomes from CRT were reported between different patients with varying LV lead positions ***(Singh Jagmeet P. et al., 2011)***. Comparatively few studies have explored the effect of varying LV stimulation sites from within a single coronary vein in an individual patient ***(Asbach et al., 2013; Umar et al., 2016)***. In this respect, studies using QUAD have shown marked variations in the AHR across LVPVs within the same coronary vein ***(Asbach et al., 2013; Umar et al., 2016)***. In the present study, intraindividual analysis revealed significant variations in the AHR to CRT in 58% of patients (optimal vs. worst LVPVs). This finding suggests that, even with ideally deployed LV leads, assessed by fluoroscopy, there is 'room' for improving the AHR to CRT.

2.4.2. QRS_{area}

Attention has recently focused on VCG-derived measures of ventricular activation in the field of CRT ***(Mafi Rad et al., 2016)***. Prominent amongst these is QRS_{area}, which appears to reflect LV electrical dyssynchrony. Recently, van Deursen et al have used QRS_{area} to optimise atrioventricular (AV) and interventricular (VV) delays ***(van Deursen et al., 2015b)***. In the present study, we focused on the effect of varying LVPVs, rather than on AV and VV delays. We found that ΔQRS_{area} predicted ΔLV dP/dt_{max} and that varying LVPVs on a QUAD was associated with significant intraindividual variations in ΔQRS_{area} in 77% of patients (optimal vs. worst LVPVs). The LVPV associated with the greatest reduction in QRS_{area} was also associated with the optimal AHR to CRT in 73% patients.

On this basis, we would propose ΔQRS_{area} as a surrogate measure of $\Delta LV\ dP/dt_{max}$ and therefore, as a target for haemodynamic optimization.

2.4.3. Scar burden

Nguyen et al have recently shown a negative correlation between QRS_{area} and myocardial scar burden on CMR (Nguyên et al., 2018a). In the present study, we also found that pre-implant QRS_{area} correlated inversely with myocardial scar burden. Furthermore, scar burden was a negative, independent predictor of AHR. These findings suggest that scar reduces the AHR to CRT, possibly by reducing the volume of myocardium available for contraction and/or interfering with resynchronization.

2.4.4. Scar location

Acute haemodynamic studies using QUAD have not explored the relationship between AHR and myocardial scar ***(Asbach et al., 2013; Umar et al., 2016)***. In the present study, we found that the AHR to CRT depends on the viability of the myocardium in the vicinity of the LVPV. Whilst pacing remote from scar (or no scar at all) led to an AHR, pacing in the vicinity of scar led to a suboptimal AHR. This finding of a negative effect of scar on the AHR to CRT are consistent with pressure-volume loop study of de Roes et al, who found that pacing over myocardial scar was associated with a reduction in cardiac stroke work, whereas pacing from viable myocardium led to an increase ***(de Roest et al., 2014).*** They are also consistent with bipolar LV lead studies showing that CRT with LV pacing over myocardial scar is associated with worse clinical outcomes (Kočková et al., 2018, p.; Leyva et al., 2011). Interestingly, LV pacing over scar was associated with smaller reductions or an increase in QRS_{area}, as well as a suboptimal AHR. Speculatively, it is possible that wavefront fragmentation arising from myocardial scarring permits right ventricular wavefronts to dominate over LV wavefronts, leading to a smaller reduction, or an increase in QRS_{area}, less effective resynchronization and a suboptimal AHR. Potentially, this unique property of ΔQRS_{area} could be exploited to help manipulate the direction (vector) and timing between RV and LV pacing to ensure that the optimal activation sequence is delivered. This could represent a novel strategy to help guide CRT optimization in those implanted with a QUAD.

2.4.5. Clinical implications

In current clinical practice, LVPVs are typically chosen using an arbitrary or iterative (trial-and-error) approach, with the aim of achieving acceptable pacing thresholds whilst avoiding phrenic nerve stimulation. Our findings indicate that even in the context of fluoroscopically ideal LV lead positions, there is 'room' for

haemodynamic optimization.
Moreover, they show that optimal LVPVs can be identified by using ΔQRS_{area} as a surrogate of ΔLV dP/dt_{max}. With regards to myocardial scar, its negative effect on the AHR observed with QUAD is consistent with studies using bipolar leads. Prospective studies are required to determine whether QUAD lead LVPV optimization guided by ΔQRS_{area} and CMR translates to better patient outcomes. Importantly, whilst ΔQRS_{area} can be derived rather simply from pre- and post-implant 12-lead ECGs, we recognise that the use of CMR is not standard practice in all CRT centres. Further work is required to help determine what the overall clinical benefit and cost-effectiveness is of a CMR-guided CRT optimization strategy.

2.4.6. Study limitations

There are several limitations. This was a single-centre study with a relatively small sample size. Given time restrictions, we did not study the effect of atrio-ventricular (AV) and interventricular (VV) delays. Additionally, despite extensive data acquisition across multiple LVPLs, only one coronary vein was assessed in each subject. As we did not explore other available CS tributaries, it remains unclear whether changing the LV lead position according to QRS_{area} reduction and scar location could have further influenced the response to CRT. In this respect, further prospective study is required to explore the practicalities of changing the LV lead position according to these factors. Furthermore, whilst the present study demonstrates that ΔQRS_{area} could serve as a novel tool to help guide CRT optimization, we have not clearly shown it to be superior to ΔQRSd, which is a more commonly used measurement. Finally, we should consider that an acute hemodynamic response does not necessarily relate to a benefit from CRT. In fact, studies have shown that ΔLV dP/dt_{max} represents a poor predictor of long-term CRT response ***(Bogaard et al., 2011; Mullens et al., 2009)***. However, improvements in cardiac contractility occur immediately following CRT and can be measured on a beat-to-beat basis ***(Prinzen and Auricchio, 2012)***. Therefore, it is reasonable to assume that LV dP/dt_{max} improvements following CRT reflect better electrical resynchronization. In contrast, improvements in clinical outcome measures can be more challenging to predict and often reflect the influence of factors unrelated to LV resynchronization ***(Prinzen and Auricchio, 2012)***.

2.4.7. Conclusion

We have shown that, in patients with an ideally deployed LV lead, optimizing LVPVs on a QUAD to achieve the maximum QRS_{area} reduction leads to the best AHR to CRT. Both myocardial scar burden and location of scar the vicinity of the LVPV had a negative effect on the AHR to CRT. These findings have implications for the use of QRS_{area} and CMR in CRT optimization.

Chapter 3

Changes in QRS area and QRS duration after cardiac resynchronization therapy predict cardiac mortality, heart failure hospitalizations and ventricular arrhythmias

Abstract

Background: Predicting clinical outcomes after cardiac resynchronization therapy (CRT) and its optimization remain a challenge. We sought to determine whether pre- and post-implantation QRS area (QRS_{area}) predict clinical outcomes after CRT.

Methods and results: In this retrospective study, QRS_{area}, derived from pre- and post-implantation vectorcardiography, were assessed in relation to the primary endpoint of cardiac mortality after CRT with or without defibrillation. Other endpoints included total mortality, total mortality or heart failure (HF) hospitalization, total mortality or major adverse cardiac events (MACE) and the arrhythmic endpoint of sudden cardiac death or ventricular arrhythmias with or without a shock. In patients (n=380, age 72.0 ± 12.4 years, 68.7% male) undergoing CRT over 7.7 years (median follow-up: 3.8 years [interquartile range 2.3–5.3]), pre-implantation QRS_{area} ≥ 102 μVs predicted cardiac mortality (HR: 0.36; $p < 0.001$), independent of QRS duration (QRSd) and morphology ($p<0.001$). A QRS_{area} reduction ≥ 45 μVs after CRT predicted cardiac mortality (HR: 0.19), total mortality (HR: 0.50), total mortality or HF hospitalization (HR:0.44), total mortality or MACE (HR:0.43) (all $p<0.001$) and the arrhythmic endpoint (HR: 0.26; $p <0.001$). A concomitant reduction in QRS_{area} and QRSd was associated with the lowest risk of cardiac mortality and the arrhythmic endpoint (both HR:0.12, $p<0.001$).

Conclusion: Pre-implantation QRS_{area}, derived from VCG, was superior to QRSd and QRS morphology in predicting cardiac mortality after CRT. A post-implant reduction in both QRS_{area} and QRSd was associated with the best outcomes, including the arrhythmic endpoint.

*Chapter (text and figures) based on **Okafor et al., 2019.***

2.4. Introduction

Cardiac resynchronization therapy (CRT) is an established treatment for patients with heart failure (HF), impaired left ventricular (LV) function and a wide QRS complex ***(Leyva et al., 2014)***. As with any medical therapy, its treatment effect is variable. 'Non-responder' rates range from 9% to 68%, depending on the criteria used to define response ***(Fornwalt et al., 2010)***. Although no medical therapy can be expected to be 100% effective, there is a consensus view that response to CRT can be improved ***(Auricchio and Prinzen, 2017)***.

Manifold imaging studies explored mechanical dyssynchrony in relation to patient selection and optimization but, ultimately, no single measure of mechanical dyssynchrony has been adopted by clinical guidelines ***(Chung et al., 2008)***. In this context, we should consider CRT is an electrical treatment and that its substrate should be electrical rather than mechanical. In this respect, QRS duration (QRSd) has been adopted as a surrogate of electrical dyssynchrony in randomized, controlled trials, and a reduction in QRSd has been shown to predict better long-term outcomes after CRT (Appert et al., 2019; Jastrzębski et al., 2019).

Evidence has recently emerged in support of vectorcardiography (VCG) in the field of CRT. In this respect, QRS area (QRS_{area}) has been shown to correlate with LV lateral wall activation time ***(Mafi Rad et al., 2016)***, the maximum rate of rise of LV pressure ($\Delta LV\ dP/dt_{max}$) ***(De Pooter et al., 2017; Engels et al., 2017)*** and LV reverse remodelling ***(van Deursen et al., 2015a)*** during CRT. Crucially, pre-implantation QRS_{area} has also been shown to be superior to pre-implantation QRSd and QRS morphology in predicting total mortality after CRT ***(Emerek et al., 2019; van Stipdonk et al., 2018)***.

Although QRS_{area} and QRSd duration relate to depolarization in a global sense, QRS_{area} also yields the dominant axis of the activation sequence ***(Lux et al., 1980)***. Given that the objective of CRT is to make depolarization more synchronous, both the pacing location and timing between LV and RV pacing can be used to manipulate activation sequence. In this study, we explored pre- and post-implantation QRS_{area} and QRSd in relation to long-term cardiac mortality, heart failure (HF) hospitalization and major adverse cardiac events (MACEs) after CRT.

3.2. Methods

Patients referred for CRT implantation at the University Hospitals Birmingham, Queen Elizabeth, United Kingdom, were retrospectively evaluated. The study was approved by the local Ethics Committee and local Clinical Audit Department and conforms with the Declaration of Helsinki.

3.2.1. Study population

Patients undergoing CRT implantation from November 2011 to June 2018 were identified. Implantation practice adhered to the United Kingdom's National Institute of Clinical Excellence (NICE) guidelines, which before 2007 recommended CRT with defibrillation (CRT-D) only in the context of secondary prevention. After 2014, NICE recommended CRT-D rather than CRT-pacing (CRT-P) in non-ischaemic cardiomyopathy ***(NICE, 2014)***. Inclusion criteria were: indications for CRT according to NICE guidance and availability of a digitizable 12-lead ECG before and after implantation. Exclusion criteria were: subjects with technically unsuitable ECGs and patients with congenital heart disease.

3.2.2. Device therapy

Device implantation was undertaken using standard transvenous techniques under local anaesthesia and intravenous sedation. Following implantation, patients were followed up in combined cardiac device therapy / HF clinics. Devices were programmed according to physician discretion. Generally, backup atrial pacing was set at 60 beats/min, and the pacing mode was set to DDDR. The atrioventricular delay was set at 90 ms and the inter-ventricular delay to between 0 and -20 ms (LV first). In patients in permanent atrial fibrillation, right ventricular and LV leads were deployed, a CRT generator was implanted and devices were programmed to a ventricular triggered mode. Atrioventricular junction ablation was undertaken according to physicians' discretion. Targeted echocardiographic optimization was only undertaken in symptomatic non-responders.

3.2.3. Lead positions

The anteroposterior, as well as the left anterior and right anterior oblique fluoroscopic views from coronary sinus venography taken at the time of implantation were used retrospectively to assess the LV lead tip position, as previously described ***(Leyva et al., 2018a)***. All LV lead positions were assessed

retrospectively by an experienced implanter (F.L.) who was blinded to clinical outcome data.

3.2.4. ECG

Pre-implantation, standard supine 12-lead ECGs (25mm/s, 10mm/mV) were used for analysis. A LBBB was a QRSd >120ms, rS or QS in lead V1, notched or slurred R-waves in leads I, aVL, V5 or V6, with absent q waves in leads V5 and V6 ***(Linde et al., 2010)***. We used this definition rather than 'strict' Strauss criteria, as the latter is not predictive of clinical outcomes after CRT ***(Emerek et al., 2019)***. Right bundle branch block was defined as a QRS ≥ 120ms, with a wide, positive R-wave deflection in lead V1 and a slurred S wave in leads I and V6. A non-specific intraventricular conduction delay was defined as non-paced QRS >120ms not fitting these criteria. Post-implantation ECGs were undertaken within 3 months after implantation.

3.2.5. Vectorcardiography

Standard 12-lead ECGs were first converted to an Extensible Markup Language (XML) format using ECGScan (AMPS LLC, New York, USA), a commercially available programme approved by the Food and Drugs Administration. A custom-made programme was used for generation of 2 VCGs according to Frank's orthogonal lead system using the Kors transformation matrix. The latter was used given previous evidence that it is superior to other VCG transformations in predicting clinical outcomes after CRT ***(Emerek et al., 2019)***. The start and end of the QRS complex were defined semi-automatically using digital callipers at 200% magnification. For paced rhythms, the onset and end of the QRS complex was measured manually, excluding the pacing spike. Digitization of ECGs and generation of VCGs were undertaken by a single investigator (O.O.) who was blinded to clinical outcomes collected by another investigator (A.Z.). The QRS_{area} was calculated as the integral between the ventricular deflection curve and the isoelectric line in each the 3 orthogonal leads (X, Y and Z), according to the formula: $(X_{area}^2 + Y_{area}^2 + Z_{area}^2)^{1/2}$ (Figure 3.1).

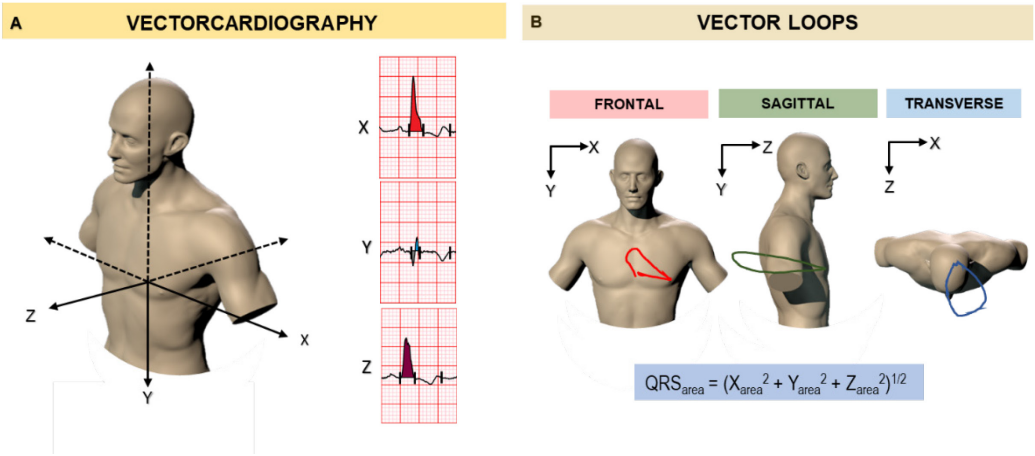

Figure 3.1. Vectorcardiography in Cardiac Resynchronization Therapy.

The VCG displays the various features of the ECG, such as the QRS complex, in the form of "loops", which are determined from vectors representing successive, instantaneous mean electric forces throughout the cardiac cycle. A) shows a representation of the three VCG leads (X, Y and Z), according to Frank's orthogonal lead system. B) shows two-dimensional vector loops in the frontal (X-Y leads), sagittal (Y-Z leads) and transverse (X-Z leads) planes from a patient with a LBBB. As shown, the typical finding in LBBB is a dominant anterior-to-posterior or right ventricular-to left ventricular pattern of activation. The QRS_{area} is calculated as the integral sum of the area bound by the QRS complex and the isoelectric baseline in each VCG lead (X, Y and Z). Figure taken from Okafor et al., 2019.

3.2.6. Endpoints

The primary endpoint was cardiac mortality, which included cardiac transplantation or implantation of a ventricular assist device. The secondary endpoint was total mortality. Ancillary endpoints included total mortality or unplanned HF hospitalization; and total mortality or unplanned hospitalization for major adverse cardiac events (MACE), and the combined endpoint of sudden cardiac death (SCD), ventricular tachycardia, ventricular fibrillation or shock. MACE was comprised of the following endpoints: (i) HF hospitalization, (ii) myocardial infarction, (iii) acute coronary syndrome, (iv) ventricular arrhythmias and (v) atrial fibrillation. Stroke and pulmonary embolism were not regarded as MACE. A HF hospitalization was defined as an unplanned admission related to worsening dyspnoea, in association with peripheral oedema, pulmonary oedema on chest radiography and requirement for intravenous diuretic therapy. Device-treated arrhythmias (appropriately treated with shocks or antitachycardia pacing) not leading to an unplanned hospitalization were not regarded as a hospitalization for MACE. In composite endpoints, the first event was included in statistical analyses. Mortality data was collected through medical record and cross-checked with a

national mortality database. Data was collected retrospectively from medical records and entered into an electronic database every 6 months by investigators who were blinded to clinical and imaging data. Events were adjudicated by blinded investigators on a 6-monthly basis.

3.2.7. Mode of death

Sudden cardiac death was defined as a natural, unexpected death due to cardiac causes, heralded by an abrupt loss of consciousness within one hour of the onset of acute symptoms. Death from pump failure was defined as 'death after a period of clinical deterioration in signs and symptoms of HF despite medical treatment' ***(Rockman et al., 1989)***.

3.2.8. Statistical analysis

Continuous variables are expressed as mean ± standard deviation (SD). Normality was tested using the Shapiro-Wilk test. Comparisons between normally distributed continuous variables were made using the Student's t-test. Categorical variables were analysed using chi-squared tests. Receiver operating characteristic (ROC) curves were created to assess the predicted probabilities of ECG and VCG variables in relation to cardiac mortality. A 10-fold cross-validation was used as the model validation technique for assessing performance, and the average was calculated over 10 repetitions. The measure with largest area under the ROC (AUC) was used for subsequent analyses. The Liu method was also applied to estimate non-parametrically the optimal cut-offs for ECG and VCG measures ***(Liu, 2012)***. Kaplan-Meier curves and the log-rank test were used to assess cumulative survival and Cox proportional hazard models were used to assess relative risks. Proportionality hypotheses were verified by visual examination of log (survival) and Schoenfeld residuals. Variables reaching $p < 0.10$ as univariate predictors of cardiac mortality were entered in multivariate models. The Stata15 (StataCorp, Texas) statistical package was used. The package "cvauroc" was employed for cross-validation of the areas under the ROC curve, and package "cutpt" was used for empirical estimation of optimal cut-offs. A two-sided $p < 0.05$ was considered statistically significant.

3.3. Results

3.3.1. Baseline characteristics

The analytic sample consisted of 380 patients. As shown in Table 3.1, baseline characteristics were typical of a CRT population (age 72.0 ± 12.4 years [mean ± SD], 68.7% male) with a LVEF of 25.8 ± 9.9 % and a QRSd of 153.5 ± 22.7 ms. The cut-off of pre-CRT QRS_{area} derived from Liu method was 102 µVs (86-119 µVs). The QRS_{area} groups were well matched for age, NYHA class, diabetes and hypertension status, upgrade status, LVEF and medication. In the QRS_{area} < 102 µVs group, patients were more likely to be male, to have ischemic cardiomyopathy or a previous coronary artery bypass operation, and a greater proportion received CRT-D rather than CRT-P.

Table 3.1. Characteristics of the study group according to pre-CRT QRS_{area}.

	All	QRS_{area} ≥102 µVs	QRS_{area} <102 µVs	p
N	380	197	183	
Age, yrs	72±12.4	72.2±12.9	71.9±11.7	0.832
Sex (male), n (%)	261 (68.68)	119 (60.41)	142 (77.6)	<0.001
NYHA class, n (%)				
I	26 (7.34)	17 (9.34)	9 (5.23)	0.190
II	87 (24.58)	46 (25.27)	41 (23.84)	
III	225 (63.56)	114 (62.64)	111 (64.53)	
IV	16 (4.52)	5 (2.75)	11 (6.4)	
Aetiology, n (%)				
Ischemic	182 (47.89)	74 (37.56)	108 (59.02)	<0.001
Non-ischemic	198 (52.11)	123 (62.44)	75 (40.98)	
Co-morbidities, n (%)				
Diabetes mellitus	89 (23.42)	41 (20.81)	48 (26.23)	0.213
Hypertension	106 (27.89)	57 (28.93)	49 (26.78)	0.639
CABG	64 (16.84)	23 (11.68)	41 (22.4)	0.005
Device type, n (%)				
CRT-D	209 (55.15)	94 (47.96)	115 (62.84)	0.004
CRT-P	170 (44.85)	102 (52.04)	68 (37.16)	
Upgrades, n (%)				
Pacemaker to CRT-D	39 (47.56)	23 (43.40)	16 (55.17)	0.307
Pacemaker to CRT-P	43 (52.44)	30 (56.60)	13 (44.83)	

CRT-D indication *				
Primary prevention	166 (79.4)	76 (80.9)	90 (78.3)	0.645
Secondary prevention	43 (20.6)	18 (19.1)	25 (21.7)	
LVEF (%)	25.8±9.9	25.5±9.7	26±10.3	0.633
Medication, n (%)				
ACEI / ARA	337 (89.63)	173 (88.72)	164 (90.61)	0.548
Beta-blocker	277 (73.67)	140 (71.79)	137 (75.69)	0.391
MRA	167 (44.41)	80 (41.03)	87 (48.07)	0.170
ECG variables				
Sinus rhythm, n (%)	269 (70.79)	152 (77.16)	117 (63.93)	0.005
AF / flutter, n (%)	111 (29.21)	45 (22.84)	66 (36.07)	
PR interval (ms)	192.5±54.7	181.6±39.8	207.5±67.5	<0.001
QRS (ms)	153.5±22.7	163.9±20.4	142.2±19.5	<0.001
QRS<150 ms, n (%)	169 (44.47)	45 (22.84)	124 (67.76)	<0.001
LBBB, n (%)	239 (62.89)	151 (76.65)	88 (48.09)	<0.001
RBBB, n (%)	33 (8.68)	1 (0.51)	32 (17.49)	<0.001
NICD, n (%)	59 (15.53)	5 (2.54)	54 (29.51)	<0.001
RV-paced, n (%)	49 (12.89)	40 (20.30)	9 (4.92)	<0.001
VCG variable				
QRS area (μVs)	113.4±56.5	156.9±41.7	66.6±22.7	<0.001

3.3.2. Pre-CRT QRS_{area}

Over a median follow-up period of 3.8 years (interquartile range 2.3–5.3), 135/380 (36%) patients died, 70/380 (18%) from cardiac causes and 31/380 (8%) from non-cardiac causes (Table 3.2). The cause of death was unknown in 34/380 (9%).

Table 3.2. Clinical Outcomes.

		Pre-CRT		Post-CRT	
	All	**QRS_{area} ≥102 µVs**	**QRS_{area} <102 µVs**	**QRS_{area} reduction ≥45 µVs**	**QRS_{area} reduction <45 µVs**
N	380	197	183	177	203
Mortality endpoints					
Cardiac mortality	70 (18.4)	21 (10.7)	49 (26.8)	11 (6.21)	59 (29.1)
Sudden cardiac death *	5 (7.14)	1 (4.76)	4 (8.16)	0	5 (8.47)
Death from pump failure *	63 (90.0)	19 (90.5)	44 (89.8)	10 (90.9)	53(89.8)
Total mortality	135 (35.5)	55 (27.9)	80 (43.7)	42 (23.7)	93 (45.8)
Total mortality or HF hospitalization	165 (43.4)	66 (33.5)	99 (54.1)	53 (29.9)	112 (55.2)
Total mortality or hospitalization for MACE	185 (48.7)	74 (37.6)	111 (60.7)	59 (33.3)	126 (62.1)
Ventricular arrhythmic events					
All VT/VF	32 (8.42)	12 (6.09)	20 (10.9)	7 (3.95)	25 (12.3)
VT/VF treated with ATP only	6 (15.8)	4 (2.03)	2 (1.09)	3 (1.69)	3 (1.48)
Appropriate shocks (with or without ATP)	19 (5.0)	7 (3.55)	14 (7.65)	2 (1.13)	17 (8.37)
Inappropriate shocks	1 (0.26)	0	1 (0.5)	0	1 (0.5)

*Clinical outcomes, expressed as n (%), According to pre-CRT QRS_{area} and post-CRT change reduction in QRS_{area}. ATP = anti-tachycardia pacing; VF = ventricular fibrillation; VT = ventricular tachycardia. *, expressed as a percentage of cardiac deaths. Table taken from Okafor et al., 2019.*

The AUC for predicting cardiac mortality was higher for QRS_{area} than for QRSd (0.71 vs. 0.60; p<0.001 for comparison) or QRS morphology (0.71 vs. 0.53; p<0.001 for comparison) (Figure 3.2).

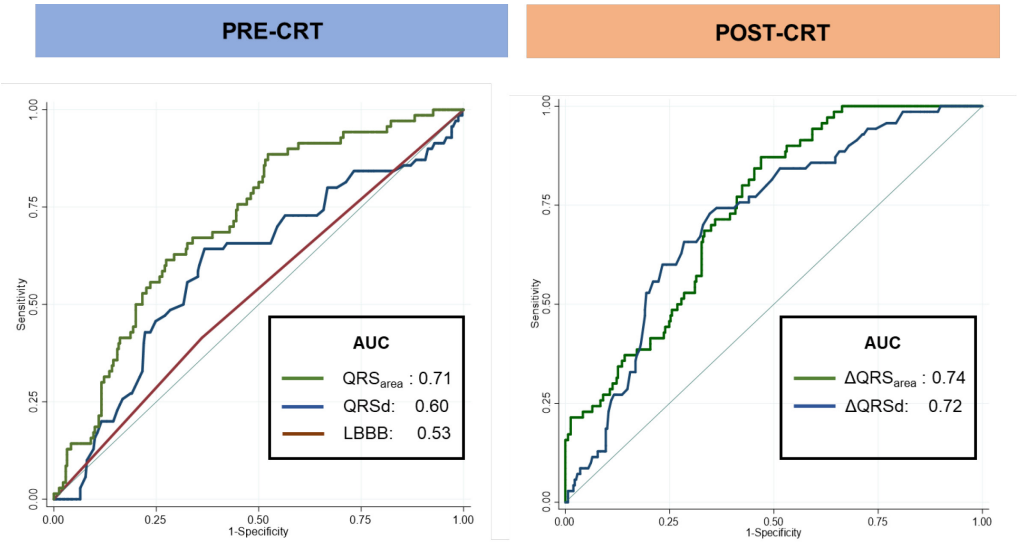

Figure 3.2. Receiver-Operating Characteristics Curves.

Graphs shows areas under the receiver-operator characteristics curves (AUC) for QRSd, QRS_{area} and QRS morphology (LBBB) in the whole cohort. Figure taken from Okafor et al., 2019.

In Kaplan-Meier survival analyses, QRS_{area} ≥ 102 µVs was associated with a lower cardiac mortality (p<0.001), total mortality (p=0.001), total mortality or HF hospitalization and total mortality or MACE (both p<0.001) (Table 3.2 and Figure 3.3).

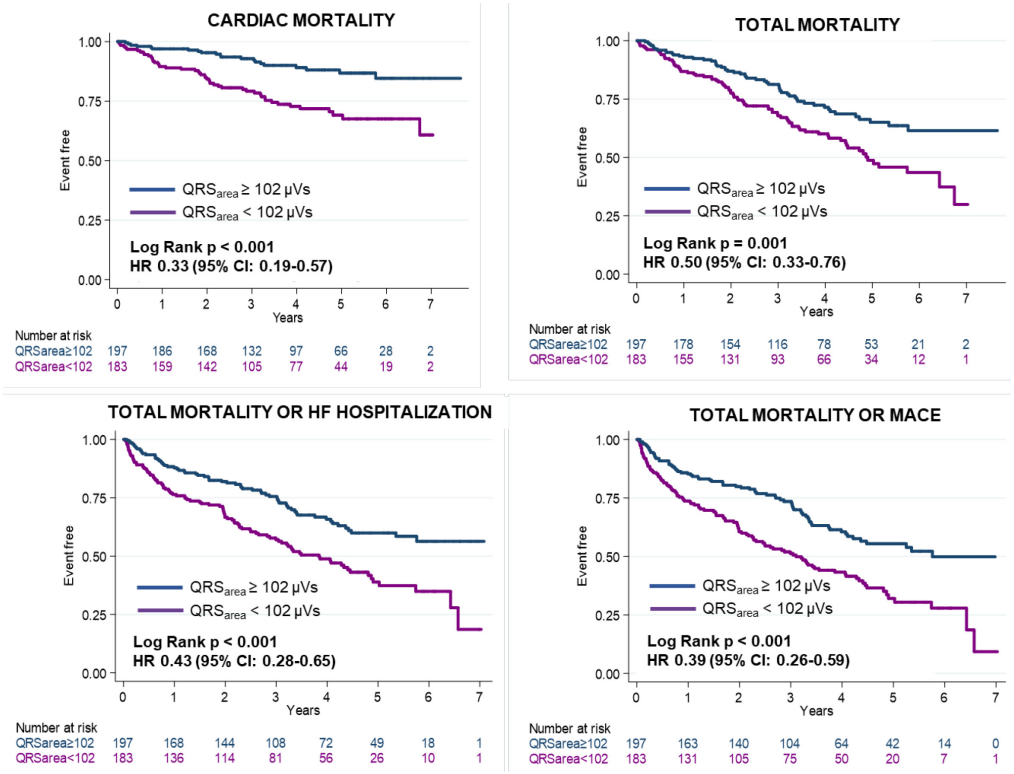

Figure 3.3. Clinical Outcomes According to Pre-CRT QRS_{area}.

Kaplan-Meier survival curves for the various endpoints according to pre-CRT QRS_{area}. Results of univariate Cox proportional hazard models are expressed in terms of HR= hazard ratio (95% C.I.). Figure taken from Okafor et al., 2019.

In univariable Cox proportional hazards analyses, QRS_{area} predicted cardiac mortality, total mortality, total mortality or HF hospitalization and total mortality or MACE (all p<0.001) (Table 3.3).

Table 3.3. Univariable analyses of predictors of clinical outcomes after CRT.																				
	CARDIAC MORTALITY				TOTAL MORTALITY				TOTAL MORTALITY OR HF HOSPITALIZATION				TOTAL MORTALITY OR MACE				SCD, VT/VF OR SHOCK			
	HR	95% C.I.		p	HR	95% C.I.		p	HR	95% C.I.		p	HR	95% C.I.		p	HR	95% C.I.		p
Pre-CRT																				
QRS_{area} (≥102 μVs)	0.33	0.19	0.57	<0.001	0.50	0.33	0.76	<0.001	0.43	0.28	0.65	<0.001	0.39	0.26	0.59	<0.001	0.50	0.25	0.98	0.042
QRSd (≥150 ms)	0.37	0.22	0.64	<0.001	0.60	0.39	0.92	0.018	0.60	0.40	0.91	0.016	0.53	0.35	0.80	0.002	0.38	0.19	0.75	0.006
LBBB	0.80	0.47	1.36	0.408	0.75	0.49	1.15	0.192	0.67	0.44	1.02	0.061	0.82	0.54	1.25	0.355	0.69	0.36	1.31	0.251
Post-CRT																				
ΔQRS_{area} (μVs)	1.02	1.01	1.02	<0.001	1.01	1.01	1.01	<0.001	1.01	1.01	1.01	<0.001	1.01	1.01	1.01	<0.001	1.01	1.01	1.02	0.003
QRS_{area} reduction ≥45 μVs	0.19	0.10	0.36	<0.001	0.45	0.31	0.65	<0.001	0.44	0.32	0.61	<0.001	0.43	0.31	0.58	<0.001	0.26	0.11	0.58	0.001
ΔQRSd (ms)	1.02	1.01	1.03	<0.001	1.01	1.01	1.02	<0.001	1.01	1.01	1.02	<0.001	1.01	1.02	1.02	<0.001	1.01	1.01	1.03	0.003
QRSd reduction *	0.23	0.14	0.39	<0.001	0.48	0.34	0.68	<0.001	0.48	0.35	0.65	<0.001	0.51	0.38	0.68	<0.001	0.33	0.17	0.67	0.018

Results of univariate Cox proportional hazards models, expressed as hazard ratio (HR) and 95% confidence intervals (95% C.I.), for QRS_{area} and QRSd using specified cut-offs (in parentheses), and for QRS morphology (LBBB). Results of analyses using continuous and dichotomous variables are shown., refers to any QRSd reduction below baseline. SCD = sudden cardiac death; VF = ventricular fibrillation; VT = ventricular tachycardia. Table taken from Okafor et al., 2019.*

In multivariate analyses, QRS_{area} (per µVs) predicted cardiac mortality (adjusted HR: 0.99 [95% C.I.]: 0.98-0.99), independent of all baseline variables, including QRSd and QRS morphology (Table 3.4). In comparison, QRSd (per ms) did not predict cardiac mortality following multivariate adjustment for baseline variables and QRS_{area} (aHR: 1.01, 95% C.I: 0.99 – 1.02, p =0.219). When QRS_{area} was removed from the model, QRSd (per ms) remained a non-significant predictor of cardiac mortality (aHR: 1.01; 95% C.I: 1.00 – 1.02, p=0.083) after adjusting for age, sex, HF aetiology, diabetes, medication, baseline rhythm and QRS morphology.

Table 3.4. Univariate and multivariate analysis of pre-implantation variables in relation to cardiac mortality								
	Univariate				Multivariate			
	HR	95% C.I.		p	HR	95% C.I.		p
Age (years)	1.02	1.00	1.04	0.044	1.02	1.00	1.05	0.097
Sex (male)	2.25	1.21	4.19	0.011	1.57	0.80	3.07	0.186
NYHA class (I, II)	0.61	0.32	1.14	0.122				
Ischemic aetiology	1.73	1.07	2.80	0.026	1.07	0.63	1.80	0.813
Co-morbidities								
Diabetes mellitus	2.08	1.28	3.38	0.003	1.56	0.95	2.58	0.081
Hypertension	1.25	0.76	2.08	0.380				
CABG	1.46	0.83	2.54	0.187				
CRT-D	0.79	0.49	1.26	0.327				
Upgrades	1.18	0.67	2.09	0.564				
LVEF (%)	0.98	0.96	1.01	0.141				
Medication								
ACEI / ARA	0.56	0.29	1.10	0.092	0.63	0.31	1.27	0.196
Beta-blocker	0.80	0.48	1.33	0.389				
MRA	1.24	0.78	1.98	0.371				
ECG variables								
AF / flutter	1.62	1.01	2.62	0.047	1.03	0.60	1.76	0.925
PR interval (ms)	1.00	1.00	1.01	0.153				
LBBB	0.79	0.49	1.27	0.331				
RBBB	2.50	1.34	4.65	0.004	0.92	0.42	2.02	0.831
RV-paced	0.56	0.22	1.38	0.207				
NICD	1.08	0.58	2.01	0.806				
QRSd (ms)	0.99	0.98	1.00	0.075	1.01	0.99	1.02	0.219
QRS_{area} (μVs)	0.99	0.98	0.99	<0.001	0.98	0.98	0.99	<0.001

3.3.3. Post-CRT QRS_{area}

The QRS_{area} decreased by 41.0 µVs (interquartile range: -79 to -4) after CRT (Figure 3.4). The cut-off of ΔQRS_{area} derived from Liu method was -45 µVs ([-60] – [-31] µVs).

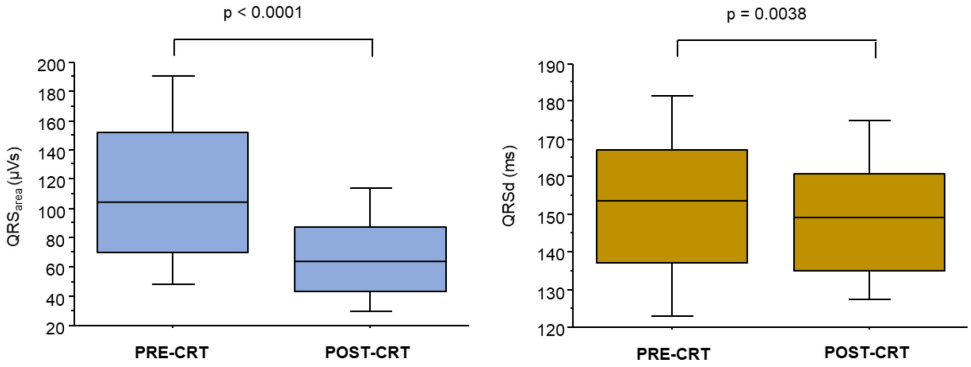

Figure 3.4. Post-CRT changes in QRS_{area} and QRSd.

Box-and-whisker plots of QRS_{area} and QRSd before and after CRT implantation. The horizontal line denotes the median, whereas the inferior and superior limits of the box denote the 1st and 3rd quartiles. The limits of the vertical bar denote maximum and minimum. Figure taken from Okafor et al., 2019.

As shown in Table 3.5, the ΔQRS_{area} groups were well matched for age, NYHA class, hypertension and diabetes status, device type, LVEF and medical therapy**.** A QRS_{area} reduction ≥45µVs group had a lower proportion of men ($p<0.001$), and most had non-ischemic cardiomyopathy ($p<0.001$). Additionally, we found a greater proportion of patients were upgraded to CRT-P in the QRS_{area} reduction ≥45µVs group. As expected from the ΔQRS_{area} grouping, there were significant differences in ECG and VCG variables.

Table 3.5. Characteristics of the study group according to post-CRT ΔQRS_{area}			
	QRSarea reduction ≥45 µVs	**QRSarea reduction <45 µVs**	**p**
N	177	203	
Age, yrs	72.1±13.1	72±11.7	0.979
Sex (male), n (%)	103 (58.19)	158 (77.83)	<0.001
NYHA class, n (%)			
I	14 (8.48)	12 (6.35)	0.322
II	36 (21.82)	51 (26.98)	
III	110 (66.67)	115 (60.85)	
IV	5 (3.03)	11 (5.82)	
Aetiology, n (%)			
Ischemic	67 (37.85)	115 (56.65)	<0.001
Non-ischemic	110 (62.15)	88 (43.35)	
Co-morbidities, n (%)			
Diabetes mellitus	44 (24.86)	45 (22.17)	0.537
Hypertension	50 (28.25)	56 (27.59)	0.886
CABG	17 (9.6)	47 (23.15)	<0.001
Device type, n (%)			
CRT-D	90 (51.14)	119 (58.62)	0.144
CRT-P	86 (48.86)	84 (41.38)	
Upgrades, n (%)			
Pacemaker to CRT-D	14(35)	25 (59.52)	0.026
Pacemaker to CRT-P	26 (65)	17 (40.48)	
LVEF	25.3±9.1	26.2±10.7	0.429
Medication, n (%)			
ACEI / ARA	154(88)	183 (91.04)	0.334
Beta-blocker	125 (71.43)	152 (75.62)	0.357
MRA	82 (46.86)	85 (42.29)	0.374
ECG variables			
Sinus rhythm, n (%)	139 (78.53)	130 (64.04)	0.002
AF / flutter, n (%)	38 (21.47)	73 (35.96)	
PR interval (ms)	178.3±34.5	208.8±67.6	<0.001
QRS (ms)	162.1±20.6	145.9±21.8	<0.001
LBBB, n (%)	134 (75.71)	105 (51.72)	<0.001
RBBB, n (%)	2 (1.13)	31 (15.27)	<0.001
NICD, n (%)	10 (5.65)	49 (24.14)	<0.001

RV-paced, n (%)	31 (17.51)	18 (8.87)	0.012
VCG variable			
QRS area (μVs)	153.9±47.5	78.1±36.3	<0.001
Circumferential Lead Positions			
Anterior	6 (3.39)	8 (3.94)	0.498
Anterolateral	28 (15.8)	37 (18.2)	
Lateral	73 (41.2)	86 (42.3)	
Posterolateral	24 (13.6)	16 (9.03)	
Posterior	46 (26.0)	56 (27.6)	
Longitudinal Lead Positions			
Basal	19 (10.7)	12 (5.91)	0.249
Mid	99 (55.9)	121 (59.6)	
Apical	59 (33.3)	70 (34.5)	

Cardiac mortality was 11/177 (6.21%) in patients with QRS_{area} reduction ≥45 μVs and 59/203 (29.1%) in patients with QRS_{area} reduction <45 μVs. (Table 3.2). The AUC for predicting cardiac mortality for ΔQRS_{area} and ΔQRSd were similar (0.74 vs 0.72; p=0.425 for comparison) (Figure 3.2). In Kaplan-Meier survival analyses, a QRS_{area} reduction ≥45 μVs was associated with a lower cardiac mortality, total mortality, total mortality or HF hospitalization and total mortality or MACE, compared to a QRS_{area} reduction <45 μVs (all p<0.001) (Figures 3.5 and 3.6). In univariate analyses, a QRS_{area} reduction ≥ 45 μVs was a strong predictor of cardiac mortality (HR: 0.19, 95% CI: 0.10-0.36), as well as other endpoints (all p < 0.001) (Table 3.3).

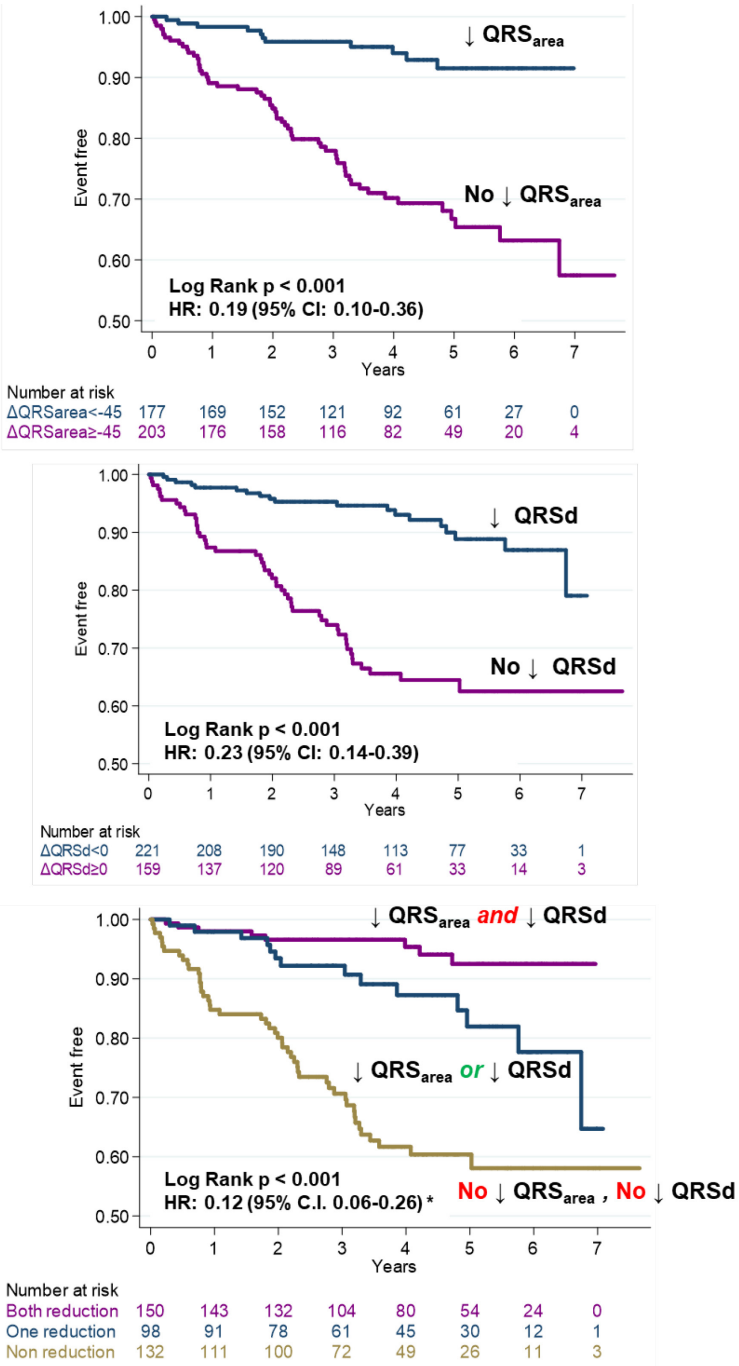

Figure 3.5. QRS_{area} and QRSd in Relation to Cardiac Mortality.

*Kaplan-Meier survival curves and univariate hazard ratios (HR) and (95% confidence intervals [C.I.] for QRS_{area} and QRSd in relation to cardiac mortality. *, refers to the interaction between changes in QRS_{area} and QRSd after CRT. Figure taken from Okafor et al., 2019.*

3.3.4. Interaction of ΔQRS_{area} and $\Delta QRSd$

As shown in Figures 3.2 and 3.5, ΔQRS_{area} and $\Delta QRSd$ were comparable predictors of cardiac mortality. In Cox proportional hazard analyses, a significant interaction between ΔQRS_{area} and $\Delta QRSd$ emerged with respect to cardiac mortality (HR: 0.12, 96% C.I. 0.06-0.26). A similar trend was observed for total mortality, total mortality or HF hospitalization and total mortality or MACE (Figure 3.6).

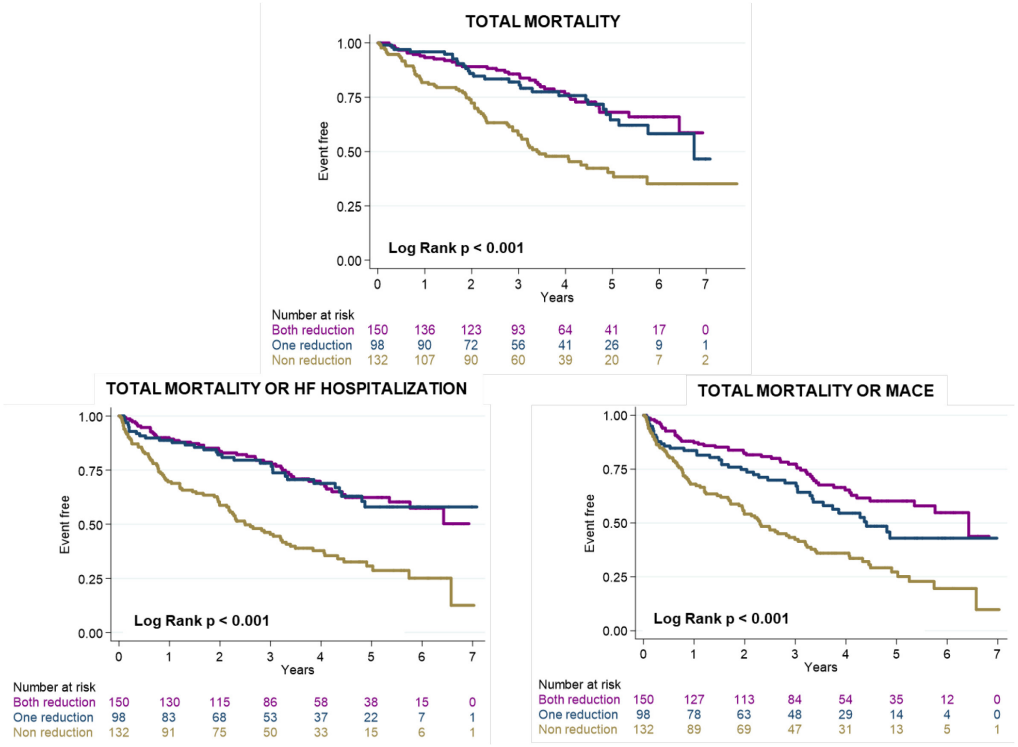

Figure 3.6. Secondary Clinical Endpoints According to Post-CRT Changes in QRS_{area} and QRSd. *Kaplan-Meier survival curves for the various endpoints according to post-CRT reductions in QRS_{area} (≥45μVs) and QRS duration (QRSd to any value below baseline). Figure taken from Okafor et al., 2019.*

3.3.5. Lead positions

Most LV leads were deployed in a lateral or posterolateral position (Table 3.5). As shown in Figure 3.7, there was considerable inter-individual variability in ΔQRS_{area} and ΔQRSd within each LV lead position, but no significant differences emerged in ΔQRS_{area} or ΔQRSd between the different LV lead positions.

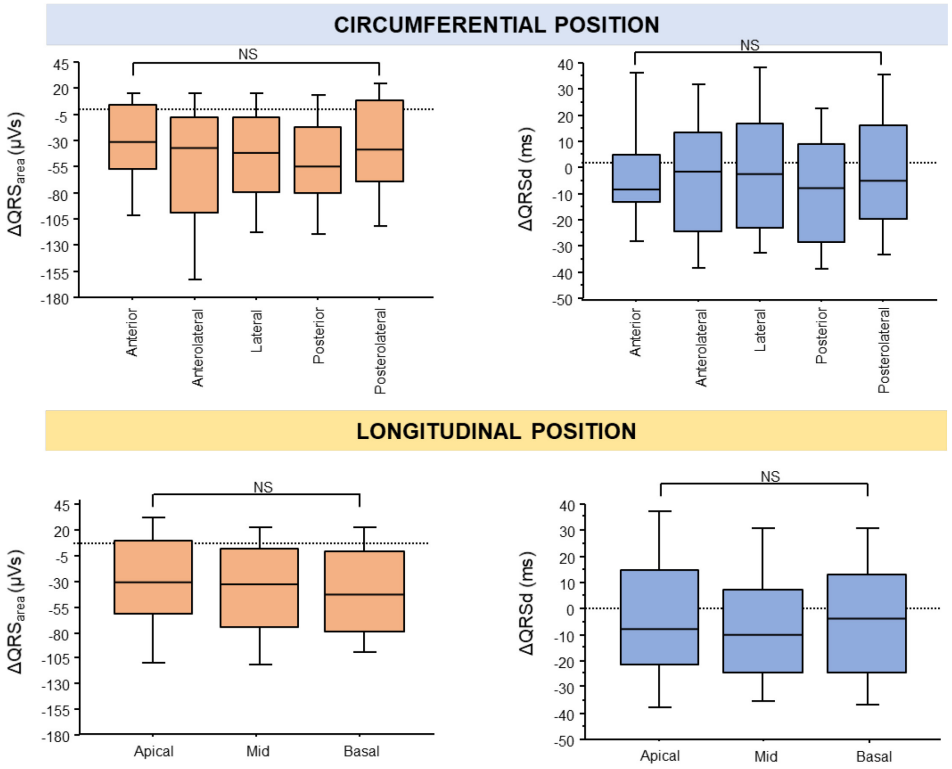

Figure 3.7. QRS_{area} and QRSd According to Left Ventricular Lead Position. *The figure shows post-CRT changes in QRS area (ΔQRS_{area}) and QRS duration (ΔQRSd) according to circumferential (upper panel) and longitudinal (lower panel) left ventricular lead positions. In the box-and-whisker plots, the horizontal line denotes the median, whereas the inferior and superior limits of the box denote the 1st and 3rd quartiles. The limits of the vertical bar denote maximum and minimum. Figure taken from Okafor et al., 2019.*

3.3.6. Arrhythmic events

As shown in Table 3.3 and Figure 3.8, both QRSd and QRS_{area} predicted the combined endpoint of SCD, VT/VF or shock, but no such relationship was observed for QRS morphology. A QRS_{area} reduction ≥45 μVs (HR: 0.26, 95% C.I. 0.11–0.58) and QRSd reduction (HR: 0.33, 95% C.I. 0.17–0.67) predicted this combined endpoint.

Concomitant reductions in QRS_{area} and QRSd were associated with the lowest risk of the arrhythmic endpoint (HR: 0.12, 95% C.I. 0.04 – 0.41).

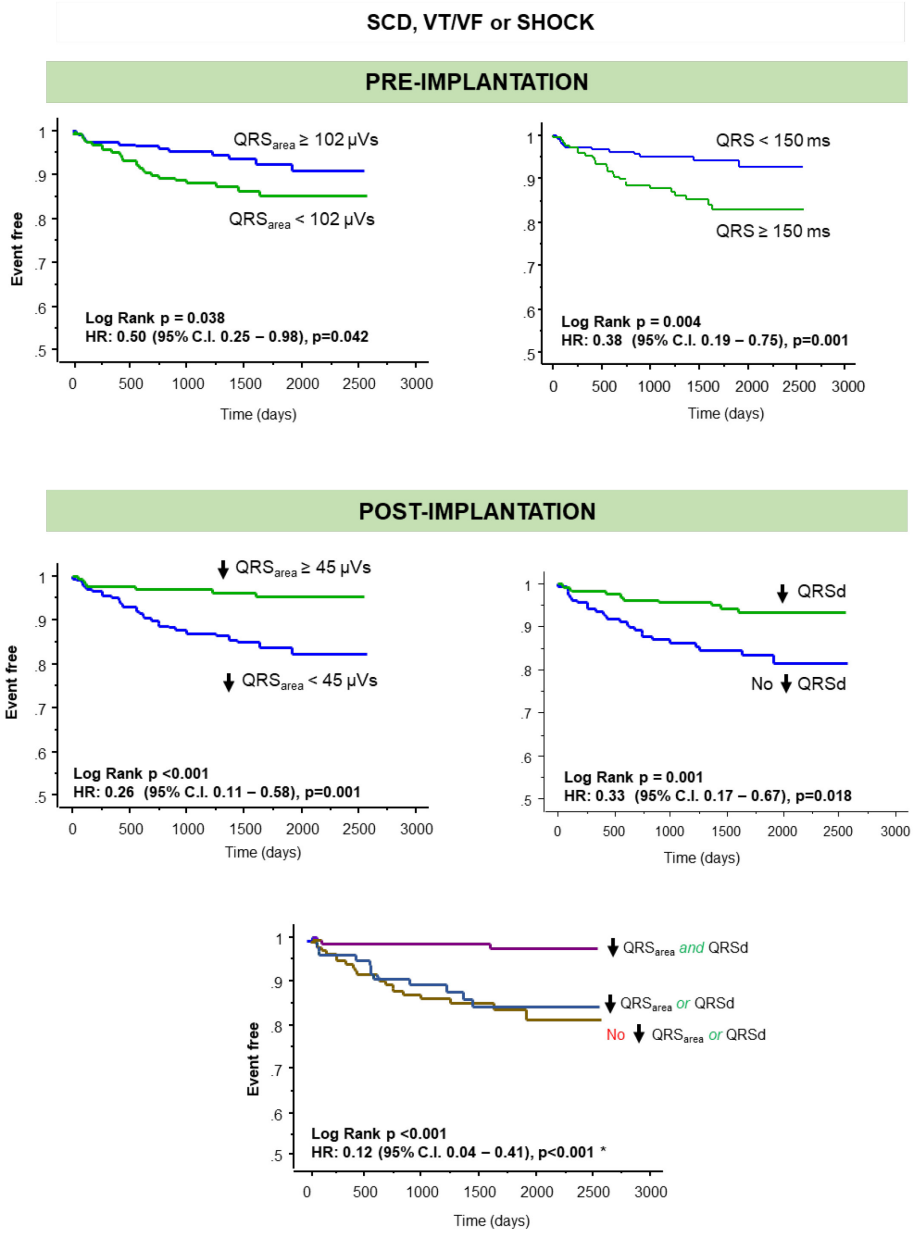

Figure 3.8. Sudden Cardiac Death and Ventricular Arrhythmias According to Post-CRT Changes in QRS_{area} and QRSd. *Kaplan-Meier survival curves for the combined endpoint of sudden cardiac death (SCD), ventricular tachycardia (VT)/ventricular fibrillation (VF) or shock according to post-CRT reductions in QRS_{area} (≥45µVs) QRS duration (QRSd to any value below baseline). *, refers to the comparison of the group with concomitant reductions in QRS_{area} (≥45µVs) and QRSd against the group with no reductions in either variable. Figure taken from Okafor et al., 2019.*

3.4. Discussion

This is the first study to explore both pre- and post-implantation QRS_{area} in relation to long-term, cause-specific mortality, as well as long-term HF hospitalization, MACE and ventricular arrhythmias after CRT. Several findings have emerged. First, pre-implantation QRS_{area} was superior to QRSd and QRS morphology in predicting cardiac mortality after CRT. Second, a QRS_{area} reduction after CRT was associated with favourable outcomes, independent of baseline QRSd or QRS morphology. Third, the best outcomes after CRT were observed in patients exhibiting concomitant reductions in QRS_{area} and QRSd.

3.4.1. Pre-CRT QRS_{area}

This study provides an external validation of the findings of two observational studies showing that QRS_{area} is superior to QRSd and QRS morphology in predicting total mortality after CRT ***(Emerek et al., 2019; van Stipdonk et al., 2018)***. We found that QRS_{area} (<102 μVs) predicted total mortality, with a AUC of 0.71, which is higher than the AUC of 0.61 identified by van Stipdonk et al using a cut-off of 109 μVs ***(van Stipdonk et al., 2018)***. Emerek et al found that a QRS_{area} ≤ 95μVs was associated with a higher total mortality than a QRS_{area} > 95 μVs, with an unadjusted HR of 2.11 (p<0.001) ***(Emerek et al., 2019)***. Using a cut-off of 102 μVs, we have found an unadjusted HR of 1.73 (p=0.002) for total mortality and 2.77 for cardiac mortality (p<0.001).

Previous studies on QRS_{area} ***(Emerek et al., 2019; van Stipdonk et al., 2018)*** did not address cause-specific mortality and only 1 year follow-up data was provided with respect to HF hospitalization ***(van Stipdonk et al., 2018)***. We found that, as well as predicting total mortality, QRS_{area} predicted cardiac mortality, total mortality or HF hospitalization and total mortality or MACE. The relationship between a high QRS_{area} and better clinical outcomes after CRT is not unexpected, as QRS_{area} correlates with electrical dyssynchrony, the natural substrate of CRT ***(De Pooter et al., 2017; Mafi Rad et al., 2016)***.

3.4.2. QRSd

Randomized controlled trials of CRT ***(Bristow et al., 2004; Cleland et al., 2005)*** adopted a QRSd ≥120 ms as an indication for CRT. In COMPANION (Comparison of Medical Therapy, Pacing, and Defibrillation in Heart Failure), patients without LBBB and those with QRSd ≤ 147 ms did not derive a benefit ***(Bristow et al., 2004)***. Similarly, the Multicentre Automatic Defibrillator Implantation Trial–Cardiac Resynchronization Therapy (MADIT-CRT) trial, patients with a QRSd <150 ms derived no survival benefit from CRT (Moss et al., 2009b; Zareba et al., 2011). In the

present study, we found that a QRSd ≥ 150 ms was associated with a lower cardiac mortality, compared to a QRSd < 150 ms. The ability of QRSd to predict cardiac mortality, however, as relatively weak (AUC: 0.60).

Metanalyses of observational studies have shown an inconsistent relationship between post-CRT ΔQRSd ***(Bryant et al., 2013; Kashani and Barold, 2005)*** and 'clinical response'. In these metanalyses, however, 'clinical response' was defined in terms of symptoms, echocardiographic variables and/or hard endpoints, assuming that these are identical, interchangeable measures. On the other hand, studies focusing on hard endpoints do indeed support a relationship between a QRSd reduction and better outcomes after CRT. The Resynchronization Reverses Remodelling in Systolic Left Ventricular Dysfunction (REVERSE) study, the only randomized controlled trial to address ΔQRSd after CRT, explored acute ΔQRSd in the CRT-treated group in relation to the primary endpoint of the clinical composite score, as well as LV reverse remodelling ***(Gold Michael R. et al., 2012)***. Although not designed to address hard endpoints, REVERSE reported an association between ΔQRSd and total mortality or HF hospitalization over a relatively short follow up (12 months in North America and for 24 months in Europe) on univariate analyses, but not in a multivariate model that corrected for baseline QRSd. Importantly, however, the CRT-treated group in REVERSE only had 4 deaths over 24 months, raising the possible play of statistical underpowering. In contrast, an observational study, Appert et al showed that a lack of postoperative QRSd reduction was independently associated with an increased risk of total mortality over a median follow-up period of 48 months ***(Appert et al., 2019)***. In a similar study, Jastrzebski et al showed that a QRSd reduction predicted death from any cause or urgent heart transplantation and death from any cause/urgent heart transplantation or hospital admission for HF over an average follow-up period of 46 months (Jastrzębski et al., 2019). In the present study, in which 135 deaths occurred over a median follow-up of 3.8 years, a QRSd reduction below baseline predicted cardiac mortality, total mortality, total mortality or HF hospitalization and total mortality or MACE.

3.4.3. QRS morphology

Observational studies ***(Sweeney Michael O. et al., 2010; Tian et al., 2013)*** as well as large registries ***(Bilchick et al., 2010)*** and subanalyses of randomized, controlled trials ***(Bristow et al., 2004; Gold Michael R. et al., 2012; Tang et al., 2010; Zareba et al., 2011)*** have shown that patients with a LBBB morphology derive the most benefit from CRT. Whilst some studies have suggested that a LBBB defined using 'strict' criteria, with notching and/or slurring of the QRS complex, is associated with a better LVEF response to *CRT* ***(Tian et al., 2013; van Deursen et al., 2015a)***, this is not a consistent finding ***(Bertaglia et al., 2017; Caputo et al., 2018)***. Moreover, Emerek et al found that 'strict' (Strauss) criteria of LBBB was not predictive of clinical outcomes after CRT ***(Emerek et al., 2019)***. In the present study,

a conventionally defined LBBB did not predict cardiac mortality after CRT (AUC: 0.53).

3.4.4. Lead position

We have observed a considerable inter-individual variability in QRS_{area} at a given LV lead position. In this regard, de Pooter et al also found a similar inter-individual variability in QRS_{area} in CRT recipients with a LBBB ***(De Pooter et al., 2017)***. Crucially, they also found that QRS_{area} and the acute hemodynamic response to CRT in a given patient could be improved by changing the LV lead position. Together, these findings make the case for optimization of QRS_{area} in CRT recipients. To date, however, no studies have prospectively explored this issue.

3.4.5. Arrhythmic events

Several studies have suggested that QRSd predicts SCD ***(Kurl Sudhir et al., 2012; Morin et al., 2009)***. In contrast, no studies have explored QRS_{area} or ΔQRS_{area} in relation to SCD or VT/VF. Although pre-implantation QRS_{area} did not predict this endpoint, its reduction QRS_{area} after CRT was associated with a 74% reduction in the endpoint. Moreover, concomitant QRS_{area} reduction a QRSd reduction was associated with a 88% lower risk of the combined endpoint. This novel finding, which was not anticipated, could speculatively relate to a greater dispersion of depolarization in relation to arrhythmic events. The physiological basis for this empirical finding requires further study.

3.4.6. Clinical perspective

Attention has recently focused on ECG imaging using body surface mapping as a tool for identifying electrical dyssynchrony and to predict response to CRT ***(Gage et al., 2017; Ploux et al., 2013)***. Whilst there is a proof-of-principle and encouraging clinical data to support the use of this technique in CRT, it requires specialised acquisition. Importantly, data on body surface mapping in relation to long-term outcomes after CRT are lacking. In contrast, QRS_{area} can be readily derived from the standard 12-lead ECG and crucially, is now known to predict long-term clinical outcomes. The role of QRS_{area} in patient selection and CRT optimization requires further investigation.

3.4.7. Limitations

This study has all the limitations of an observational study. Although we have corrected for potential confounders using statistical means, unobserved variables may have contributed to outcomes. Importantly, VCGs were derived retrospectively from 12-lead ECGs undertaken prior to implantation.

Inconsistencies in electrode position could conceivably influence VCG analysis ***(Tomlinson et al., 2009)***.

Notwithstanding, all ECGs were acquired by trained cardiac technicians using standardized operating procedure in routine clinical practice. Consequently, our results should be generalizable to a 'real-world' environment. Unfortunately, we did not systematically collect data on device programming. In this respect, variable programming at implantation and follow-up could account for variations in ECG and VCG variables, as well as outcomes.

3.4.8. Conclusions

Pre-implantation QRS_{area} was superior to QRSd and QRS morphology in predicting clinical outcomes after CRT. A concomitant reduction in QRSd and QRS_{area} after CRT was associated with the lowest risk of cardiac and total mortality, as well as ventricular arrhythmias. These findings add support for the use of QRS_{area} and QRSd in the risk stratification and optimization of CRT recipients.

PART 2

TRANSITIONING TOWARDS A PERSONALIZED, MODEL-BASED VECTORCARDIOGRAPHIC APPROACH

Chapter 4

Vectorcardiographic direction of ventricular activation as a predictor of long-term outcomes after cardiac resynchronization therapy

Abstract

Background: Although QRS duration and a LBBB morphology are crucial as an indication for CRT, these 12-lead ECG-derived parameters are poor predictors of clinical outcomes.

Objectives: To determine whether the sequence of ventricular activation, measured using the temporospatial isochrone ratio (TSI_{ratio}) on vectorcardiography (VCG) predicts clinical outcomes after CRT.

Methods: In this retrospective study, TSI_{ratio}, QRS_{area}, QRS duration (QRSd) and QRS morphology (LBBB), derived from pre-implantation ECGs, were assessed in relation to the primary endpoint of cardiac mortality after CRT.

Results: In patients (n=720, age 72.8±11.8 years, 71.3% male) undergoing CRT over 7.7 years (median follow-up period of 3.7 [interquartile range 2.3 – 5.1] years), TSI_{ratio} < 92% predicted cardiac mortality (adjusted hazard ratio [aHR]: 2.21, 95% C.I. 1.54-3.17; p<0.001), independent of known confounders. A TSI_{ratio} < 92% predicted cardiac mortality in the strata of QRSd (< or ≥150 ms) and QRS morphology (LBBB or non-LBBB) (all p<0.0001). Both TSI_{ratio} < 92% and a QRS_{area} <102 ms also predicted total mortality or heart failure hospitalization.

Conclusion: Vectorcardiographic TSI_{ratio} is superior to QRSd and QRS morphology in predicting cardiac mortality after CRT. These findings support the use of pre-implantation VCG in predicting clinical outcomes after CRT.

4.1. Introduction

Current guidelines recommend the use of 12-lead ECG criteria (QRS duration [QRSd] and morphology) to help guide patient selection for ***CRT (Brignole et al., 2013; NICE, 2014)***. However, even in carefully selected patients, the response to CRT is variable and often unpredictable, with up to one-third of patients failing to derive any benefit ***(Risum et al., 2015; Taylor et al., 2016)***. Whilst this nonresponse is multifactorial, it is likely that incomplete characterisation of the LV electrophysiologic substrate plays an important role.

Recent observations from landmark CRT trials (REVERSE, MADIT-CRT and RAFT) has suggested that patients with a LBBB morphology appear to derive the greatest benefit from CRT, in contrast to those with non-specific interventricular conduction delay or RBBB ***(Engels et al., 2016)***. Accordingly, these patients attract a class I recommendation for CRT, whilst those with a non-LBBB QRS morphology achieve a class IIa or IIb recommendation only ***(Stipdonk et al., 2019)***. However, not all patients with a LBBB morphology respond to CRT, reflecting the limitations of 12-lead ECG to identify true LBBB. In fact, studies employing LV endocardial mapping have recently demonstrated that up to one-third of patients with ECG criteria for LBBB are actually misdiagnosed ***(Risum et al., 2015)***. In these patients, similar ECG appearances may arise secondary to a combination of left ventricular hypertrophy, LV dilatation and/or left anterior fascicular block ***(Risum et al., 2015)***.

Vectorcardiography (VCG), which was first described in 1920, offers an alternative interpretation of the 12-lead ECG. It can be used to noninvasively characterise the three-dimensional (3D) sequence of ventricular activation and to help improve identification of electrical dyssynchrony ***(Mafi Rad et al., 2016)***. Intuitively, VCG measures that reflect late left ventricular (LV) free wall activation could help identify patients who are most likely to benefit from CRT. In the present study, we hypothesized that quantifying the direction of LV activation using a novel representation of the vectorcardiogram, termed the temporospatial isochrone ratio (TSI_{ratio}), may help to predict long-term, event-free survival following CRT.

4.2. Methods

The study population comprised of 998 patients who underwent CRT implantation at the Queen Elizabeth Hospital (Birmingham, UK) between August 2011 to June 2018. Patients were included in the study if they met the inclusion criteria for CRT-pacing (CRT-P) or CRT-defibrillator implantation according to the National Institute of Clinical Excellence (NICE) guidelines ***(NICE, 2014)***. In all patients, pre-procedural 12-lead ECGs were performed within 6 months of CRT implantation, with surface ECG data uploaded onto hospital servers in PDF file format. Exclusion criteria included subjects with technically insufficient and/or

absent 12-lead ECG data (n=241), those who underwent CRT implantation for high-degree AV block or following AV nodal ablation (n=22) and patients with uncorrected congenital heart disease (n=15). In total, 278 patients were excluded from this study (Figure 4.1).

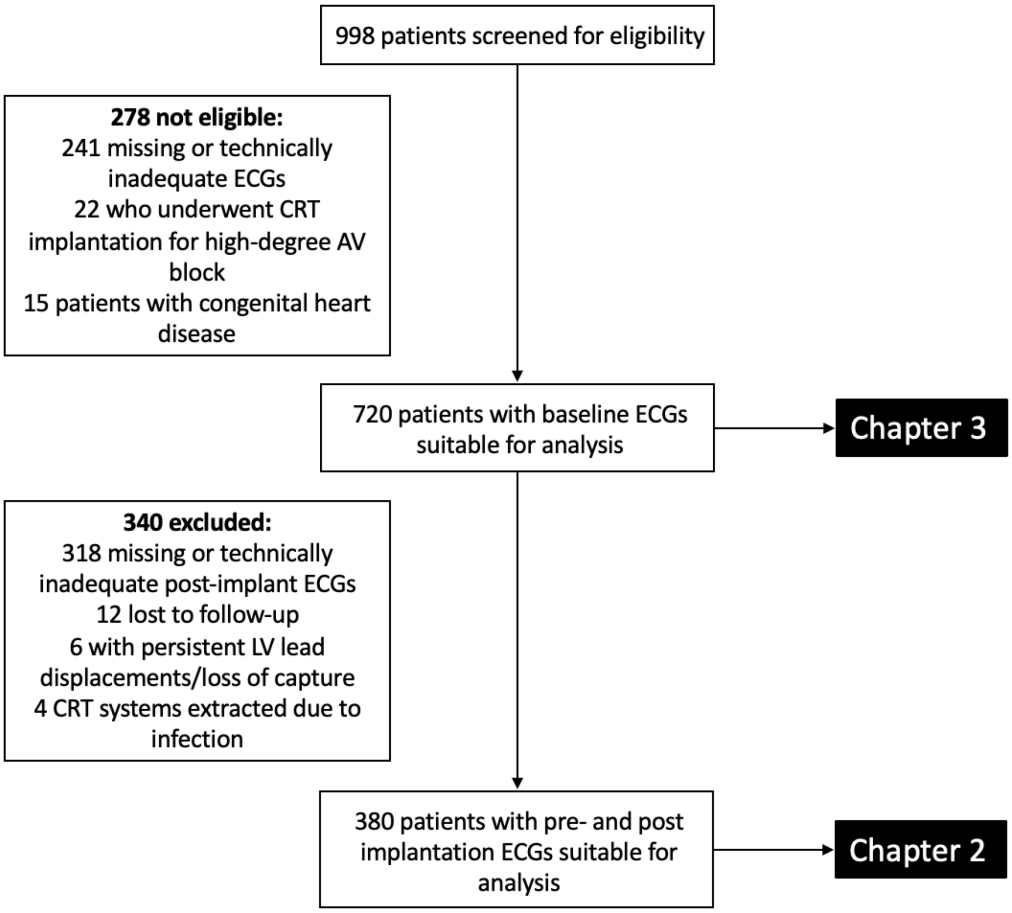

Figure 4.1. Study population for Chapters 2 and 3. *A total of 998 patients underwent CRT implantation at Queen Elizabeth Hospital, Birmingham, UK, between August 2011 to June 2018. For the present study, a total of 720 patients who met all the inclusion and none of the exclusion criteria and with baseline 12-lead ECGs suitable for digitization were studied. In Chapter 2, where pre-and post-implantation ECGs were both required, a total of 380 patients were deemed suitable for analysis.*

4.2.1. Electro-vectorcardiography analysis

Standard 12-lead ECGs were acquired at a paper speed of 25mm/s and with an amplitude of 10mm/mV. As previously defined in **Chapter 2** (section 2.3.5), the presence of a LBBB QRS morphology was determined by the following electrocardiographic criteria: a QRSd >120ms, rS or QS in lead V1, notched or slurred R-waves in leads I, aVL, V_5 or V_6, with absent q waves in leads V_5 and V_6. Conversely, RBBB was defined as a QRSd ≥ 120ms, with a wide, positive R-wave deflection in lead V_1 and a slurred S wave in leads I and V_6. To enable construction of VCGs via the Kors transformation method ***(Kors et al., 1990)***, surface ECGs were first converted to a digitized format using ECGScan (AMPS LLC, New York, USA). ECGScan is a validated, commercially available programme that permits the retrospective conversion of paper or electronically ECGs into a digitized format ***(Badilini et al., 2005)***. Following digitization, a custom-made programme was used to construct 3-lead VCGs. Thereafter, QRS_{area} was calculated as the integral between the ventricular deflection curve and baseline in each the 3 orthogonal leads (x, y and z), with the final 3-dimensional value derived using the following formula: $(X_{area}^2 + Y_{area}^2 + Z_{area}^2)^{1/2}$.

4.2.2. Mean temporal spatial isochrone signal

In this study, we introduce a novel VCG-based methodology termed the mean temporal spatial isochrone (TSI). The meanTSI method computes the 3D vectorcardiogram (x,y and z signals) from a routine 12-lead ECG, but also incorporates a standard heart-torso model with standard ECG electrode positions (Figure 4.2). The vector between electrode and heart is used to weigh the independent ECG leads in the x, y, and z direction, i.e. the extremity leads Vr, Vl, and Vf and the precordial lead V1-V6. The summation of each of these 9 vector signals gives an electrode specific VCG signal over time, VCGel(t) in mV.

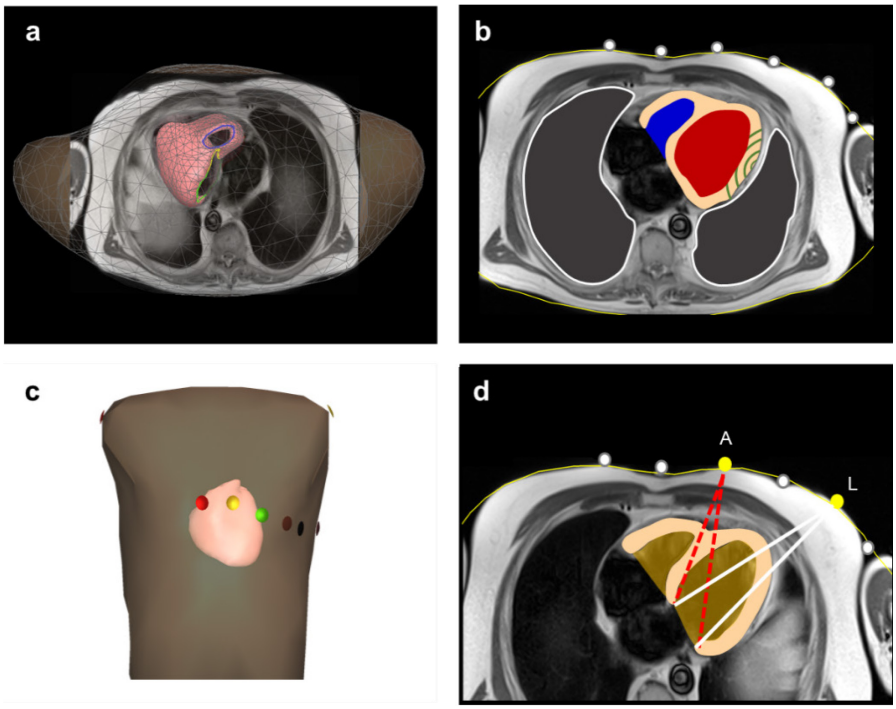

Figure 4.2. Major components of the meanTSI method. *Panel a) A standard heart-torso model was used for all patients. Panel b) The relevant tissues used in the volume conductor model are shown, including the segmented thorax, ventricles, lungs and blood cavities. The position of precordial ECG electrodes relative to the torso and the heart is shown in (c) and (d), respectively. Panel (d) The vector between ECG electrodes and the heart is used to weigh the independent ECG leads in the x, y and z direction. The final electrical potential measured by any specific ECG lead is determined by the distance of the electrode from the heart, as well as the strength and direction of the cardiac electrical dipole (Man et al.). The combined influence of these factors gives rise to the concept of 'lead vector', which describes the portion of the heart vector that is "seen" by the different ECG leads (Man et al.). In this example, electrical potentials recorded by anterior (A) electrodes and lateral (L) electrodes would be determined by the angle subtended by an activation wavefront and the surface ECG electrode. Significantly adapted from van Dam et al., 2013 with permission.*

From this VCGel(t) the mean QRS axis can be computed, as well as the mean direction of all VCG samples. The mean QRS axis thus represents the dominant activation direction within the heart. As the heart position is known within the torso-heart models used, the mean QRS axis is positioned at the centre of the ventricular mass (Figure 4.3a).

The meanTSI estimates the position of the mean activation in the heart from the same VCG. The VCGel(t) represents the mean direction of activation at time t. Assuming a constant propagation velocity v in the heart, the (mean TSI) position in the heart over time is:

$$\overrightarrow{mean\ TSI}(t+1) = \overrightarrow{mean\ TSI}(t) + v \cdot \frac{\overrightarrow{VCG}(t)}{\left\|\overrightarrow{VCG}(t)\right\|}$$

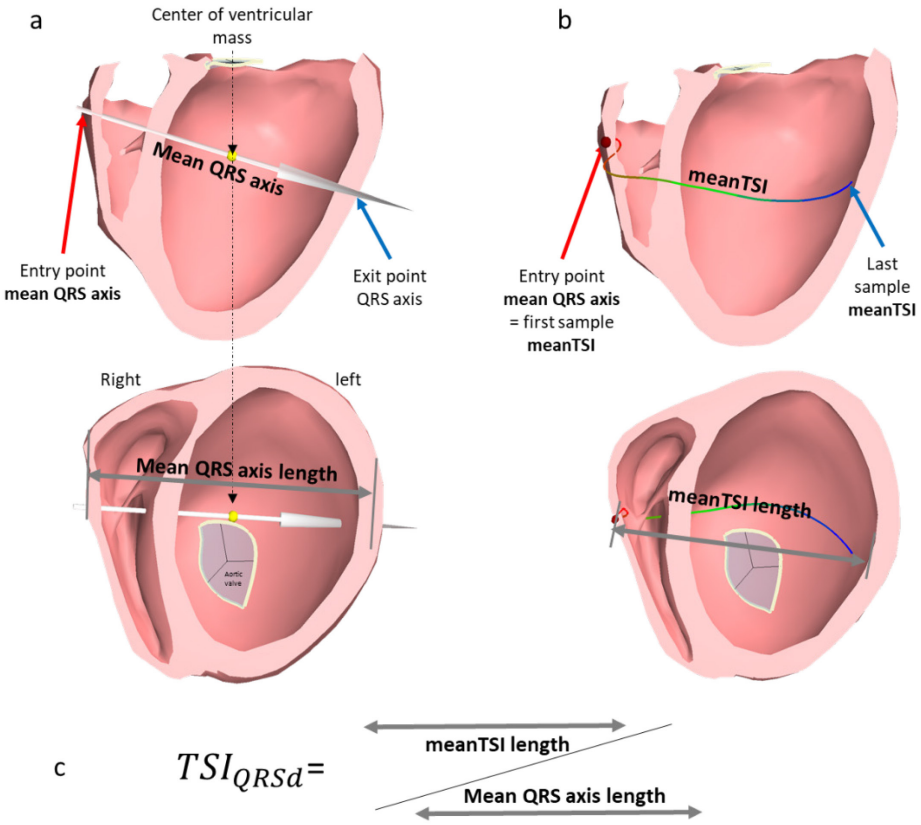

Figure 4.3. Illustration of the 3D QRS axis and the mean TSI path. *(a) The mean QRS axis enters the heart (red arrow panel: top left) and exits the heart (blue arrow panel: top left), this results in the mean QRS axis length.(b) The meanTSI is started at the entry point of the mean QRS axis. The distance between the last and first sample of the meanTSI is the meanTSI length (c) The mean TSI ratio is now defined as: meanTSI length / mean QRS axis length.*

4.2.3. Temporal spatial isochrone ratio: novel marker of LV dyssynchrony

Using the 3D QRS axis and the meanTSI signal computed from the VCG, it is possible to quantify the mean path of cardiac activation by expressing it as a ratio between the two signals. This is termed the TSI_{ratio} and represents a novel measure of the dispersion of cardiac activation. For this study, the point where the mean QRS axis enters the ventricular wall is taken as the initial point for the mean TSI (Figure 4.2). The spatial distance between the first and last point on the mean TSI path corresponds to the onset and end of the activation. This distance depends on the direction of the mean QRS axis, from left to right and from anterior-to-posterior, i.e. the. Therefore, we defined TSI_{QRSd} as:

$$TSI_{QRSd} = \frac{meanTSI_{last} - meanTSI_{first}}{mean\ QRS\ axis_{entry} - mean\ QRS\ axis_{exit}} \times 100\%$$

When the TSI_{ratio} value is 100%, the mean TSI follows exactly the QRS mean axis, i.e. the ventricular activation dispersion is significant, for instance in a typical LBBB pattern, consistent with unidirectional LV activation towards the LV basal segments. Low values for TSI_{ratio} indicate multiple wave fronts, i.e. His-Purkinje system activations. Accordingly, we hypothesized that a high TSI_{ratio} should distinguish between patients with LBBB and non-LBBB conduction pattern.

4.2.4. Endpoints

Clinical outcome data was collected retrospectively and obtained from a computerised search of electronic medical records, including discharge summaries, death certificates or coroner referral information. The primary endpoint was cardiac mortality and the secondary endpoint was a composite of total mortality and heart failure (HF) hospitalization. Cardiac mortality was defined as pump-failure related, when death occurred "*after a period of clinical deterioration in signs and symptoms of HF despite medical treatment*" ***(Leyva et al., 2018b)***. Heart failure hospitalization was defined as an unplanned admission related to worsening shortness of breath, signs of peripheral oedema, evidence of pulmonary congestion on chest radiography and/or requirement for intravenous diuretics. Total mortality included all non-cardiovascular causes and when the following major adverse cardiovascular events (MACE) resulted in death: stroke, pulmonary embolus and acute coronary syndromes. All events were collected at 6-monthly intervals by two experienced investigators and adjudicated by a final investigator who was blinded to all clinical and electrocardiographic data.

4.2.5. Statistical analysis

Continuous variables are expressed as mean ± standard deviation (SD) and were tested using the Student t-test. Normality was tested using the Shapiro-Wilk test. Categorical variables were analysed using chi-squared tests. Receiver operating characteristic (ROC) curves were created to assess the predicted probabilities of 2 ECG measures (QRS duration and LBBB) and 2 vectorcardiographic measures (TSI_{ratio} and QRS_{area}). Ten-fold cross-validation was used as the model validation technique for assessing the performance, and the average was calculated over 10 repetitions. To assess the relationship between VCG parameters and reaching the primary or secondary endpoint, Kaplan-Meier analysis of survival and log-rank testing was performed. Cox proportional-hazards regression models were fitted with covariates ($p \leq 0.1$) and used to determine hazard ratios using a stepwise selection approach (Wald method). Statistical analyses were performed using SPSS V25.0 (SPSS Inc. Chicago, Illinois), MedCalc version 19.2.1 (MedCalc Software bvba, Ostend, Belgium) and with Stata15 (StataCorp, Texas). A two-sided P-value ≤ 0.05 was considered statistically significant.

4.3. Results

4.3.1. Baseline characteristics

A total of 998 patients underwent CRT implantation from January 2011 to April 2018. Of these, 720 patients had digitizable pre-implantation ECGs. As shown in Table 1, the baseline characteristics of the analytic sample were typical of a CRT population (age 72.8 ± 11.8 years [mean ± SD], 71.3% male) with a LVEF of 25.5±9.9 % and a QRSd of 153.4 ± 24 ms. The TSI_{ratio} <92% and TSI_{ratio} ≥92% groups were well matched for age, NYHA class, comorbidities, device type (CRT-P or CRT-D), upgrade status, LVEF and medical therapy. The TSI_{ratio} ≥92% group had a higher proportion of men ($p<0.001$), and most had ischemic cardiomyopathy ($p=0.038$) (Table 4.1). As expected from the TSI_{ratio} grouping, there were significant differences in ECG and VCG variables. In particular, TSI_{ratio} ≥92% was strongly associated with LBBB ($p<0.001$). Typical examples of TSI_{ratio} in patients diagnosed with LBBB and NICD QRS morphologies is shown in Figure 4.4a and 4.4b, respectively.

Table 4.1. Characteristics of the study group according to TSI_{ratio}				
	All	**TSI:QRS≥92**	**TSI:QRS<92**	**P**
N	720	406	314	
Age, yrs	72.8±11.8	72.5±12.1	73.2±11.5	0.462
Sex (male), n (%)	513(71.25)	270(66.5)	243(77.39)	0.001
NYHA class, n (%)				
I	70(10.59)	45(12.06)	25(8.68)	0.423
II	192(29.05)	111(29.76)	81(28.13)	
III	373(56.43)	204(54.69)	169(58.68)	
IV	26(3.93)	13(3.49)	13(4.51)	
Aetiology, n (%)				
Ischemic	366(51.19)	192(47.76)	174(55.59)	0.038
Non-ischemic	349(48.81)	210(52.24)	139(44.41)	
Co-morbidities, n (%)				
Diabetes mellitus	187(26.08)	108(26.8)	79(25.16)	0.620
Hypertension	224(31.24)	134(33.25)	90(28.66)	0.188
CABG	125(17.43)	71(17.62)	54(17.2)	0.883
Device type, n (%)				
CRT-D	386(53.76)	218(53.69)	168(53.85)	0.968
CRT-P	332(46.24)	188(46.31)	144(46.15)	
Upgrades, n (%)	145 (20.1)	80 (19.7)	65 (20.7)	0.879
Pacemaker to CRT-D	73(12.54)	43(13.19)	30(11.72)	0.642
Pacemaker to CRT-P	72(12.37)	37(11.35)	35(13.67)	
LVEF (%)	25.5±9.9	25.7±9.8	25.2±10.1	0.460
Medication, n (%)				
ACEIs / ARA	620(87.57)	350(87.94)	270(87.1)	0.736
Beta-blockers	538(75.99)	309(77.64)	229(73.87)	0.244
MRAs	308(43.50)	182(45.73)	126(40.65)	0.176
ECG variables				
Sinus rhythm, n (%)	510(70.83)	304(74.88)	206(65.61)	0.007
Atrial fibrillation/flutter, n (%)	210(29.17)	102(25.12)	108(34.39)	
QRSd (ms)	153.4±24	159.6±19.4	145.3±26.9	<0.001
QRSd<150 ms, n (%)	317 (44.03)	128(31.53)	189(60.19)	<0.001
LBBB, n (%)	432(60.0)	282(69.46)	150(47.77)	<0.001
VCG variables				
QRS_{area} (μVs)	111.5±57.1	130±58.2	87.5±45.7	<0.001
TSI_{ratio} (%)	85.9±19.1	98.1±2.5	70.2±19.7	<0.001

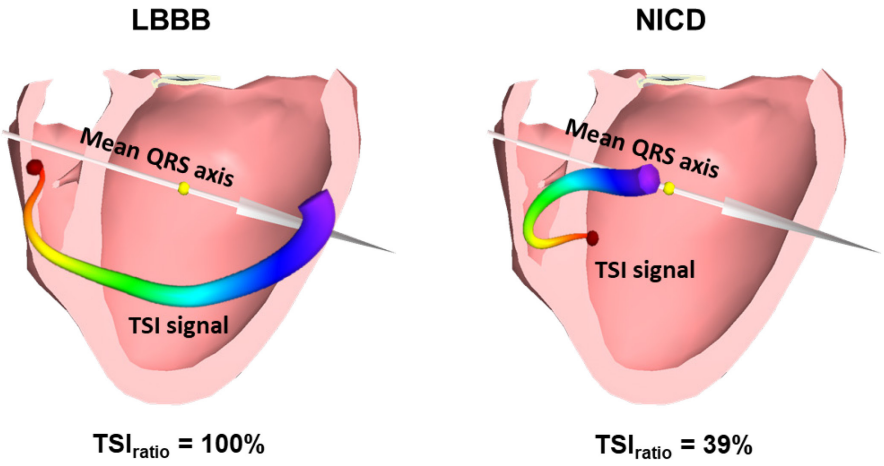

Figure 4.4. Different LV activation patterns as displayed by TSI.
(Left) A characteristic LBBB activation pattern is shown, with the mean TSI signal identifying early RV free wall activation, a right-to-left trans-septal vector and a strong, unidirectional wavefront propogating towards the basal LV wall. (Right) The contrasting LV activation sequence in a patient with NICD is shown. There is an initial left-to-right septal vector, after which the TSI signal remains relatively static in the mid-LV cavity (indicating opposing right and left activation wavefronts).

4.3.2. TSI_{ratio}

Over a median follow-up period of 3.7 years (interquartile range 2.3 – 5.1) years, 259 out of 720 (36%) patients died, 151/720 (21%) from cardiac causes and 60/720 (8.3%) from non-cardiac causes. The cause of death was unknown in 48/720 (6.7%). Using ROC analysis, the AUC for predicting cardiac mortality was higher for TSI_{ratio} than QRSd (0.68 vs 0.59, $p<0.001$) and QRS morphology (0.68 vs. 0.57, $p<0.001$) [Figure 4.5]. There were no significant differences in the AUC between TSI_{ratio} and QRS_{area} (0.68 vs 0.63, p=0.056).

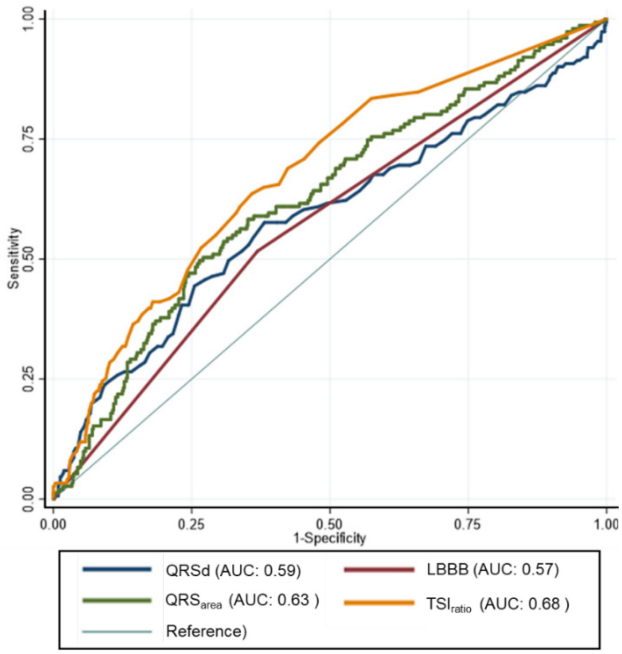

Figure 4.5. Receiver operating characteristics (ROC) curves for predicting cardiac mortality. *The ROC curves for QRSd, QRS_{area}, LBBB and TSI_{ratio} are shown, with the area under the curve signifying the performance of each variable in relation to cardiac mortality.*

As shown in Table 4.2, the results from 10-fold cross-validation were slightly lower but confirms that the largest area under the curve (AUC) was higher for TSI_{ratio} (AUC: 0.67; 95% confidence intervals [C.I.]: 0.62-0.72) than for QRS_{area} (AUC: 0.62), QRSd (AUC: 0.58) and LBBB QRS morphology (AUC: 0.54).

Table 4.2. Cross-validation analyses of ECG and VCG parameters in relation to cardiac mortality

Parameter	c-statistics	95% CI	P
TSI_{ratio}	0.67	0.62 – 0.72	<0.001
QRS_{area}	0.62	0.57 – 0.67	<0.001
QRSd	0.58	0.52 – 0.63	0.005
LBBB	0.54	0.48 – 0.59	0.001

As shown in Figure 4.6, the presence of a LBBB conduction pattern ($TSI_{ratio} \geq$ 92%) was strongly associated with a lower cardiac mortality and total mortality or HF hospitalization and total mortality or MACE (all p<0.0001). In univariable Cox proportional hazards analyses (Table 4.3), TSI_{ratio} predicted cardiac mortality (HR: 0.33, 95% C.I: 0.23-0.48) and total mortality or HF hospitalization (HR: 0.51, 95% CI: 0.38-0.69, both p<0.0001).

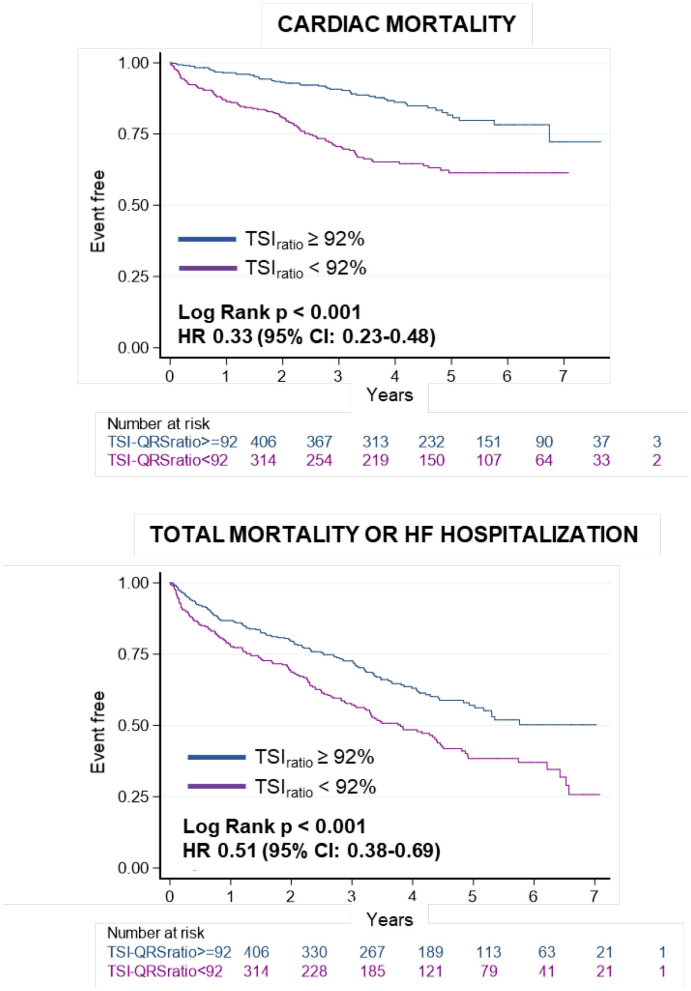

Figure 4.6. Kaplan Meier estimates of survival free from the primary and secondary endpoints. *Kaplan-Meier survival curves and univariate hazard ratios (HR) and 95% confidence intervals [C.I.] for TSI_{ratio} in relation to cardiac mortality and total mortality of HF hospitalization are shown..*

Table 4.3. Univariable analyses of ECG and VCG predictors of clinical outcomes after CRT								
	Cardiac mortality				Total mortality or HF hospitalization			
	HR	95% C.I.		p	HR	95% C.I.		p
TSI_{ratio}	0.33	0.23	0.48	<0.001	0.51	0.38	0.69	<0.001
QRS_{area}	0.52	0.36	0.75	0.001	0.52	0.38	0.70	<0.001
LBBB	0.55	0.38	0.79	0.001	0.60	0.44	0.81	0.001
QRSd	0.50	0.35	0.72	<0.001	0.54	0.40	0.73	<0.001

Differences in cardiac mortality between the TSI_{ratio} groups were observed in the different strata of QRSd (< or ≥150 ms) and QRS morphology (LBBB or non-LBBB) (Figure 4.7).

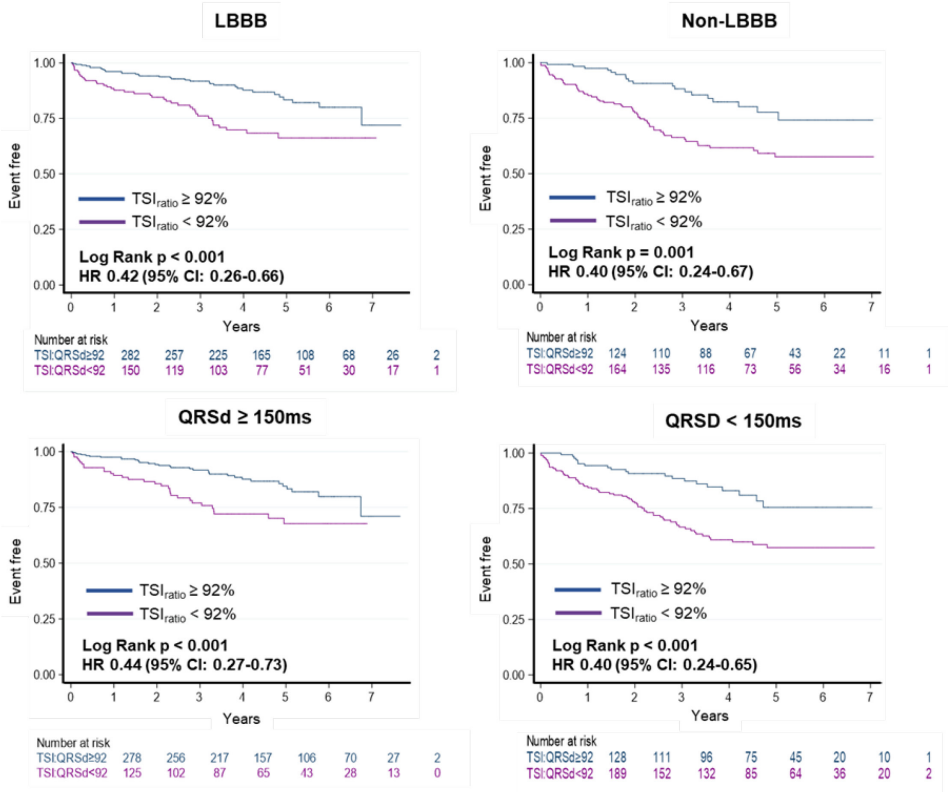

Figure 4.7. Kaplan-Meier estimates of survival following CRT implantation. *Kaplan-Meier plots of survival free from cardiac mortality are shown for LBBB and non-LBBB groups (top panel),as well as those with a QRSd ≥ 150ms and <150ms (bottom panel). The different curves relate to a TSI_{ratio} ≥ and <92%.*

In multivariable analyses, a TSI_{ratio} < 92% predicted cardiac mortality (adjusted HR [aHR]: 2.21, 95% C.I. 1.54-3.17, p<0.001), after adjustment for age, sex, HF aetiology, comorbidities, device type, upgrade status, medication, QRS morphology, QRS duration and LVEF (Table 4.4).

Table 4.4. Univariate and multivariate analysis of pre-implantation variables in relation to cardiac mortality

	Univariate				Multivariate			
	HR	**95% C.I.**		**p**	**HR**	**95% C.I.**		**p**
Age (years)	1.02	1.00	1.03	0.0013	1.02	1.00	1.04	0.020
Sex (male)	1.92	1.28	2.90	0.002	1.58	1.00	2.50	0.050
NYHA class (I, II)	0.64	0.43	0.96	0.029	0.73	0.49	1.11	0.142
Ischemic aetiology	1.25	0.91	1.73	0.169				
Co-morbidities								
Diabetes mellitus	1.48	1.05	2.09	0.024	1.40	0.97	2.02	0.076
Hypertension	0.99	0.69	1.40	0.935				
CABG	1.03	0.68	1.56	0.890				
CRT-D	0.72	0.52	1.00	0.048	0.79	0.53	1.17	0.244
Upgrades	1.38	0.95	2.01	0.094				
LVEF (%)	0.99	0.97	1.01	0.117				
Medication								
ACEI / ARA	0.43	0.29	0.64	<0.001	0.55	0.35	0.88	0.013
Beta-blocker	0.92	0.64	1.33	0.672				
MRA	0.94	0.68	1.30	0.715				
ECG variables								
AF / flutter	1.67	1.20	2.31	0.002	1.17	0.80	1.70	0.424
PR interval (ms)	1.00	1.00	1.01	0.304				
QRSd<150 (ms)	1.83	1.33	2.53	<0.001	1.37	0.97	1.93	0.071
LBBB	0.59	0.43	0.81	0.001	0.77	0.55	1.07	0.117
RBBB	1.47	0.89	2.44	0.132				
RV-paced	1.04	0.64	1.71	0.868				
NICD	1.63	1.14	2.33	0.007				
QRS_{area} < 102 (μVs)	1.79	1.29	2.48	0.001	1.56	1.07	2.27	0.02
TSI_{ratio} < 92 (%)	2.64	1.89	3.68	<0.001	2.21	1.54	3.17	<0.001

4.3.3. TSI_{ratio} vs QRSd and morphology in the prediction of clinical outcomes

In linear regression analysis, a positive correlation was observed between TSI_{ratio} and QRSd (r=0.50, p<0.001). We also observed correlations between TSI_{ratio} > 92% and QRS morphology (p=0.002). To draw firmer conclusions regarding the predictive role of TSI_{ratio}, we constructed 3 successive multivariate models: 1 evaluating ECG parameters only (i.e., QRSd < 150ms and LBBB QRS morphology), 1 evaluating TSI_{ratio} < 92% and the final model evaluating the combination of TSI_{ratio} < 92%, QRSd < 150ms and a LBBB QRS morphology (Table 4.5). We adjusted for age, sex, HF aetiology, comorbidities, device type, upgrade status, and medication in each multivariate model. Vectorcardiographic QRS_{area} was excluded from multivariate analyses. In the first multivariate model, QRSd < 150ms (aHR: 1.70, 95% C.I. 1.23 - 2.34, p=0.001), but not LBBB QRS morphology (p=0.076), predicted cardiac mortality (Table 4.5). In the second multivariate model, TSI_{ratio} was a strong predictor of cardiac mortality (aHR: 2.65; 95% CI. 1.89 - 3.69, p < 0.001) [Table 4.5]. However, after inclusion of TSI_{ratio} < 92% into the final multivariate model, QRSd < 150ms was no longer a significant predictor of outcomes (aHR: 1.37, 95% CI. 0.93 – 2.02, p=0.108). As shown in Table 4.5, TSI_{ratio} ≤ 92% remained a significant predictor of cardiac mortality (aHR: 2.65, 95% CI: 1.89 - 3.69, p<0.001), independent of baseline QRSd and morphology. In fact, neither QRSd or QRS morphology had any measurable influence on the association between TSI_{ratio} < 92% and occurrence of the primary endpoint.

Table 4.5. Various multivariate regression models for ECG and VCG-derived parameters in relation to cardiac mortality

	Parameter	aHR (95% C.I.)	p
MODEL 1 (ECG only):	LBBB	0.72 (0.49 – 1.17)	0.076
	QRSd < 150ms	1.70 (1.23 – 2.34)	0.001
MODEL 2 (VCG only)	TSI_{ratio} < 92%	2.65 (1.89 – 3.69)	<0.001
MODEL 3 (ECG and VCG):	LBBB	0.84 (0.58 – 1.23)	0.377
	QRSd < 150ms	1.37 (0.93 – 2.02)	0.108
	TSI_{ratio} < 92%	2.65 (1.89 – 3.69)	<0.001

4.3.4. QRS_{area}

As shown in Figure 4.8, patients with LBBB had significantly larger QRS_{area} values (120.5 ± 72.7 μVs), relative to those with NICD (59.3 ± 37.7 μVs) and RBBB (45.2 ± 34.6 μVs) [p<0.001 for LBBB vs. non-LBBB comparison]. The largest QRS_{area} values were observed in patients with RV-paced rhythms (141.9 ± 76.3 μVs). In Kaplan-Meier survival analyses, QRS_{area} ≥ 102 μVs was associated with lower cardiac mortality and total mortality or HF hospitalization (all p<0.001). In univariable Cox proportional hazards analyses, QRS_{area} predicted cardiac mortality (HR: 0.52, 95% C.I. 0.36-0.75) and total mortality or HF hospitalization (HR: 0.52, 95% C.I. 0.38-0.70) [both p<0.0001]. In multivariate analyses, QRS_{area} ≤ 102 μVs emerged as a significant predictor of cardiac mortality (adjusted HR [aHR]: 1.56, 95% CI: 1.07-2.27, p=0.02), independent of QRSd and morphology.

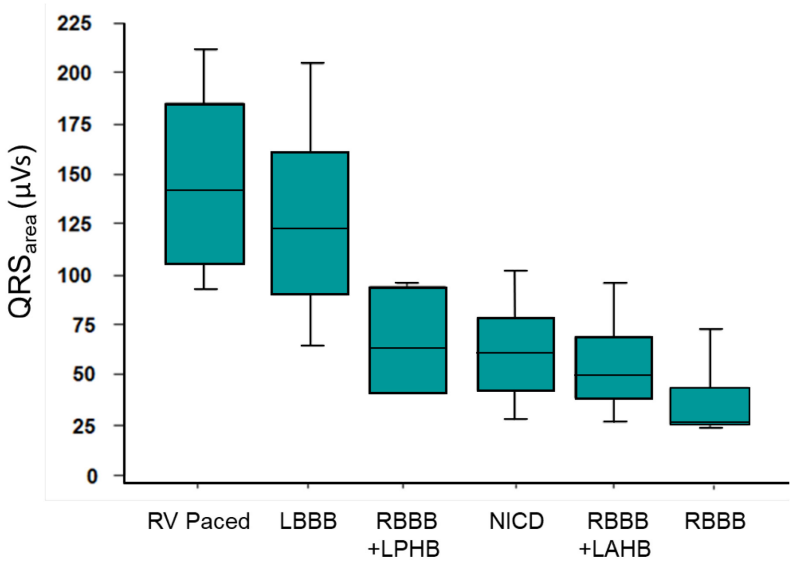

Figure 4.8. Relationship between vectorcardiographic QRS_{area} and QRS morphology. *Boxplots showing the relationship between QRS_{area} and different QRS morphologies are shown. The horizontal line denotes the median, whereas the inferior and superior limits of the box denote the 1st and 3rd quartiles. The limits of the vertical bar denote maximum and minimum. LAHB = left anterior hemiblock; LPHB = left posterior hemiblock; RV = right ventricular*

4.3.5. QRS duration

In univariable Cox proportional hazards analyses, QRSd predicted cardiac mortality (HR: 0.50, 95% C.I. 0.35-0.72) and total mortality or HF hospitalization (HR: 0.54, 95% C.I. 0.40-0.73) [both p=0.001]. In univariable Cox proportional hazards analyses, a QRSd <150ms also predicted cardiac mortality (HR: 1.83, 95% C.I. 1.33-2.53, p<0.001) and total mortality or HF hospitalization (HR: 1.37, 95% C.I. 0.97-1.93, p<0.001).

4.3.6. QRS morphology

In Kaplan-Meier survival analyses, LBBB was associated with a lower cardiac mortality, total mortality or HF hospitalization and total mortality or MACE (all p<0.001). In univariable Cox proportional hazards analyses, LBBB predicted cardiac mortality (HR: 0.55, 95% C.I. 0.38-0.79) and total mortality or HF hospitalization (HR: 0.60, 95% C.I. 0.44-0.81) (all p=0.001).

4.4. Discussion

This study presents a novel 12-lead ECG-based technique for identifying and visualizing LV activation wavefronts. Several findings have emerged. First, TSI_{ratio} was superior to QRSd and QRS morphology in predicting cardiac mortality after CRT. Second, this relationship was observed in subgroups with a QRSd< or ≥150 ms and in both LBBB and non-LBBB subgroups. Third, QRS_{area} also emerged as a strong, albeit weaker predictor of cardiac mortality, but was comparable to TSI_{ratio} with respect to other endpoints.

4.4.1. TSI_{ratio}

To our knowledge, this is the first study to evaluate TSI_{ratio} as a predictor of clinical outcomes in CRT recipients. TSI_{rato} is a very physiological parameter, as it considers several aspects of cardiac activation. First it accounts for the heart orientation, and the direction of activation, i.e. the mean QRS axis. But most importantly it estimates the dispersion in distance within the ventricles between the onset of activation and the latest activated site. In contrast, QRSd only gives information on how long the activation takes, not how disperse the activation is. Whilst vectorcardiographic QRS_{area} is a better measure of LV activation dispersion, it is not directly related to cardiac anatomy. In the present study, we used a high TSI_{ratio} value to denote the presence of a unidirectional activation wavefront with late LV free wall (LVFW) activation (Figure 4.3). Logically, patients with a high TSI_{ratio} should benefit the most from CRT.

Overall, a total of 406 patients (56%) had a typical LBBB conduction pattern, as evidenced by a high TSI_{ratio} on VCG. Of these, 282 patients (69%) had a LBBB QRS morphology, and 124 patients (30.5%) had a non-LBBB morphology on 12-lead ECG. We found that a $TSI_{ratio} \geq 92$ ms was associated with 67% lower cardiac mortality than a $TSI_{ratio} < 92$ ms. When considered together with QRSd and QRS morphology, it emerged as the strongest predictor of cardiac mortality. Importantly, TSI_{ratio} remained a significant predictor of cardiac mortality in the QRS < 150 ms and the QRS morphology subgroups. Patients with non-LBBB and $TSI_{ratio} \geq 92\%$ had a 60% lower cardiac mortality than patients with non-LBBB and $TSI_{ratio} < 92\%$. On the other hand, a QRS < 150ms and $TSI_{ratio} \geq 92\%$ was associated with a 60% lower cardiac mortality compared with a QRS < 150ms and $TSI_{ratio} < 92\%$. These findings suggest that TSI_{ratio} identifies patients with class I and non-class I indications who may derive a greater benefit from CRT. Finally, we constructed several multivariate models to better illustrate the relationship between TSI_{ratio}, QRSd and QRS morphology in relation to the prediction of clinical outcomes. Our results show that TSI_{ratio} predicts clinical outcomes independent of QRSd and QRS morphology and helps improve prognostication beyond conventional 12-lead ECG analysis.

4.4.2. Identifying LBBB activation patterns

The defining feature of true LBBB is a significant delay in activation between the septum and the LVFW ***(Strauss et al., 2011)***. These patients usually have larger LV activation delays and logically, are more likely to possess an electrical substrate that is amenable to CRT ***(Varma et al., 2015)***. In this study, a high TSI_{ratio} (>92%) was used to identify those with typical LBBB conduction pattern. Conversely, low TSI_{ratio} values denote the presence of multiple activation wavefronts with opposing electrical axes, resulting in a TSI signal that remains relatively static within the LV cavity. Using this approach, we found that nearly one third of LBBB patients (31%) and 80% of those with a NICD QRS morphology did not possess a true LBBB-like activation pattern. Patients without a typical LBBB activation sequence had a 2.6-fold increased risk of an adverse outcome following CRT. This is in keeping with the findings reported by Risum et al, who found that up to one third (37%) of LBBB patients did not possess a characteristic LBBB contraction pattern on 2-dimensional strain echocardiography analysis ***(Risum et al., 2015)***. Similar to our study, the authors demonstrated that the absence of a typical LBBB contraction pattern was independently associated with poor clinical outcomes following CRT implantation [aHR: 3.1, 95% CI: 1.64-5.88; p<0.005] ***(Risum et al., 2015)***.

4.4.3. Clinical Implications

Despite the close correlation between LBBB and CRT response, the use of conventional ECG criteria to define LBBB lacks specificity, with up to one-third of patients with LBBB misdiagnosed (Auricchio et al., 2004b; Risum et al., 2015; Vassallo et al., 1984). As a result, there is a need for a more robust marker to identify those with true LBBB activation patterns ***(Risum et al., 2015)***. In this respect, TSI_{ratio} may be ideally suited, as it noninvasively characterises the 3-dimensional sequence of ventricular activation and can easily discriminate between LBBB and non-LBBB conduction patterns. In contrast to other mapping approaches, including body surface potential mapping and electrocardiographic imaging, measurement of TSI_{ratio} can be undertaken rapidly and inexpensively using simple 12-lead ECG data.

4.4.4. Limitations

The current analysis is based on a retrospective study. Our findings should be interpreted in the context of the limitations inherent to this type of study design. Further prospective research is required to help confirm the findings arising from this study. Additionally, it is important to note that TSI assumes a uniform propagation velocity and therefore, this parameter does not consider the potential

impact of myocardial scar on wavefront propagation. Finally, the validity of our TSI method has been tested in a patient non-specific 3D heart-torso model. We believe that the extension of this method to a patient-specific model is likely to further improve its predictive value, although this remains to be proven.

4.4.5. Conclusion

We have shown that TSI_{ratio} is a better predictor of clinical outcomes after CRT than QRSd and QRS morphology. These findings add increasing support for VCG in the prediction of outcomes after CRT. A notable advantage of the techniques described herein is that these variables can be derived from a routine 12-lead ECG, which is available in all patients undergoing CRT.

Chapter 5

Noninvasive mapping of electrical dyssynchrony improves patient selection for cardiac resynchronization therapy: the ElectroCRT study

Abstract

Background: Poor quantification of baseline electrical dyssynchrony is felt to be an important factor contributing to the high non-responder rates to cardiac resynchronization therapy (CRT).

Objectives: These were several fold: 1) to investigate the feasibility of using a 12-lead ECG-based electroanatomical imaging system (ECGSync) to noninvasively map 3-dimensional (3D) ventricular activation sequences; and 2) to determine whether a novel measure of electrical dyssynchrony (electrical dyssynchrony index [EDI]) predicts the acute haemodynamic response (AHR) to CRT.

Methods: Thirty-two consecutive CRT patients (aged 69 ± 9.1 years [mean ± SD], 74.1% male, QRS: 150.8 ± 22.0ms, LBBB in 19 [79.2%]) underwent pre-procedural electroanatomical modelling using ECGSync. AHR was assessed using the change in the rate of rise of LV pressure (≥ 10% ΔLV dP/dt_{max}), in relation to AAI pacing. EDI was computed by determining the standard deviation of activation times across 1500 mesh nodes located on a patient-specific 3D heart model.

Results: Baseline EDI emerged as a better predictor of AHR to CRT (area under the receiver-operating characteristic curve [AUC]: 0.81; 95% confidence intervals [CI]: 0.59-1.00, p=0.005) than QRSd (p=0.29). Using a 31ms cut-off value, EDI identified acute CRT responders (≥ 10% ΔLV dP/dt) with a sensitivity of 70% and a specificity of 86.4%. In logistic regression analysis, EDI values ≥ 31ms were associated with a 14.8-fold greater likelihood of an AHR to CRT (odds ratio [OR]: 14.8; 95% CI: 2.40–91.2, p=0.004).

Conclusion: ECGSync-derived EDI predicts AHR to CRT response better than QRSd and a LBBB morphology. These findings support the use of ECGSync to help guide patient selection for CRT.

5.1. Introduction

Cardiac resynchronization therapy (CRT) has been shown to improve morbidity and mortality in patients with left ventricular (LV) systolic dysfunction and conduction delay ***(Cleland et al.)***. Recent guidelines put forth by European and International cardiology societies recommend the use of 12-lead ECG criteria (QRS duration and morphology) to help guide patient selection for CRT ***(Brignole et al., 2013; NICE, 2014)***. It is well accepted, however, that surface ECG provides only a limited overview of ventricular electrical activity ***(Ploux et al., 2013)***. In fact, ECG-derived surrogates of electrical dyssynchrony, including the duration and morphology of the QRS complex, have been shown to be poor predictors of CRT response ***(Poole et al., 2016)***. Given these limitations, there has been renewed interest in the development of novel mapping technologies that can better characterise the electrophysiologic substrate.

Electrocardiographic imaging (ECGI) is a recently developed, noninvasive, three-dimensional (3D) mapping technology, which combines body surface potential mapping (BSPM) [using up to 250 surface electrodes] with patient-specific heart-torso anatomy derived from computed tomography (CT) to provide high-resolution images of epicardial activation ***(Bear et al., 2018)***. Although ECGI has been proposed as novel strategy to better characterise LV activation sequences and help improve patient selection for CRT, this imaging modality has yet to be widely adopted into routine clinical practice ***(Potyagaylo et al., 2018)***. Arguably, this may be due to the high costs associated with current ECGI systems, the requirement for additional radiation exposure from CT imaging and the relative lack of robust clinical validation studies ***(Bear et al., 2018; Potyagaylo et al., 2018)***.

In the present study, we introduce a novel 3-dimensional (3D) mapping system (ECGSync) that overcomes many of these limitations. In contrast to existing ECGI systems, ECGSync utilizes routinely available clinical data, including 12-lead ECG and cardiac magnetic resonance (CMR) to provide high-resolution reconstructions of ventricular excitation (cardiac isochrones). The aims of this study were several-fold: (1) to explore the specific characteristics of LV activation in patients with left bundle branch block (LBBB) and non-LBBB QRS morphologies; and (2) to determine whether a novel ECGSync-derived measure of electrical dyssynchrony predicts acute CRT response.

5.2. Methods

The ECG-based ELECTROanatomical mapping of electrical dyssynchrony in Cardiac Resynchronization Therapy (Electro-CRT) study is a prospective, single-centre, interventional trial.

5.2.1. Study population

Patients with a LV ejection fraction (LVEF) ≤ 35%, QRS duration ≥ 120ms, New York Heart Association (NYHA) class: I-IV and on optimal pharmacological therapy, who were referred for CRT implantation at the Queen Elizabeth Hospital (Birmingham, UK) were prospectively enrolled. Exclusion criteria included the following: unstable baseline rhythms, recent acute coronary syndromes (<3 months), contraindications to CMR and patients with clinically significant valvular abnormalities and/or mechanical vale prosthesis. The study was approved by the regional ethics committee, with all patients providing written consent to participate in the study. The study conformed with the principles of the Declaration of Helsinki.

5.2.2. Clinical study

All patients underwent standard implantation of a biventricular pacing system (CRT-P or CRT-D). Chronic implantable right atrial and right ventricular leads were placed in the right atrium and the right ventricular apex, respectively. A quadripolar (QUAD) LV pacing lead (Attain Performa, Attain Stability QUAD; Medtronic Plc, Minneapolis) was positioned in a lateral or posterolateral branch of the coronary sinus (CS). The location of QUAD leads was assessed by means of standard fluoroscopic images in at least 2 orthogonal views: left anterior oblique (LAO) 30° and right anterior oblique (RAO) 30°. Using implanted LV leads, QLV was measured according to the methodology described by Gold et al ***(Gold et al., 2016)***. During CRT implantation, continuous 12-lead ECG recording was performed using the CardioLab Electrophysiology recording system (GE Healthcare, USA). A sampling gain of 1000Hz, with a high-pass filter of 0.05 Hz and low-pass filter of 100 Hz was applied to all recorded ECG signals. Surface ECGs were exported for offline analysis and a 3D vectorcardiogram synthesized according to the method proposed by Kors et al ***(Kors et al., 1990)***.

The pacing protocol was performed with atrial pacing (AAI) delivered at 10 bpm above the intrinsic heart rate (baseline reference). Biventricular pacing was delivered with simultaneous right ventricular and LV pacing (interventricular delay = 0ms). A short atrioventricular (AV) delay was programmed (20ms below intrinsic AV delay) to avoid fusion with intrinsic activation. We performed a total of 4 repetitions for every experimental pacing configuration (lasting 15 seconds each), returning to the baseline pacing settings (AAI pacing) in between each recording to ensure a stable haemodynamic status.

To assess CRT response, we undertook continuous recording of beat-to-beat LV (intraventricular) pressure measurements using a 0.014-inch high-fidelity pressure wire (PressureWire Certus, St Jude Medical, Minnesota) deployed within the mid-LV cavity. The contractile ability of LV was characterised by measuring the maximum rate of rise of LV pressure (LV dP/dt_{max}) of LV. This is a measure of the

initial velocity of myocardial contraction and is a derivative of the LV-pressure. Measurements were obtained at baseline and during biventricular pacing, with repeated measurements undertaken (4 repetitions at 15 second intervals) to minimize the impact of sampling error. Relative to baseline AAI pacing, a ≥10% change in LV dP/dt_{max} (ΔLV dP/dt_{max}) was used to identify acute haemodynamic responders (AHR) to CRT. We selected this cut-off value as previous studies have shown that this accounts for intrinsic drift in baseline LV dP/dt_{max} measurements (typically < 10%) and correlates well with long-term LV remodelling following CRT ***(Duckett et al., 2011)***.

5.2.3. Electroanatomical modelling

Patient-specific models of ventricular electrophysiology were constructed using ECGSync (PEACS, Arnheim, The Netherlands). The methodology adopted by ECGSync can be better understood by considering its 4 major components ***(van Dam et al., 2013)***:

1) Cardiac source model
2) Volume conductor model
3) ECG electrode localization
4) Fastest route algorithm

Cardiac source model

In the first component, the generation of ECG surface potentials using ECGSync requires the specification of the current sources originating from biophysical processes at the level of the cell membrane: the source model. We used the equivalent dipole layer surface model (EDL) as the cardiac source model. In this model the equivalent dipole layer is located at the closed surface S_h bounding the ventricular myocardium, comprising epicardium and endocardium. The double layer may be viewed as a sheet of current dipoles directed along the local surface normal of cardiac bounding surface S_h. This source model has a direct link with cardiac electrophysiology and has previously been shown to be very effective in the simulation of the potentials during depolarization and repolarization of the ventricles ***(van Oosterom, 2002, 2001)***. The time course of the local strength of the double layer represents a generic version of the transmembrane potential (TMP) of a healthy myocytes ***(van Dam et al., 2010; van Oosterom and Oostendorp, 2004)***.

The transmembrane potential of a node n is described by the magnitude a_n of the upstroke of the TMP, and the timing of the onset of local depolarization δ_n. In this study the magnitude is set to a fixed value a_n, representing healthy myocardial tissue. Accordingly, the source strength at node n at time instant t with depolarization onset δ_n can be denoted as $S(t, \delta_n, a_n)$.

Volume conductor model

In the second component, the specification of the thorax (geometry and conductivity) is required, in which the potential field is generated: the volume conductor model. In this study, the relevant geometry of heart and the thorax were derived from CMR images. Cardiac magnetic resonance (CMR) was performed using a 1.5 tesla scanner (Avanto, Siemens, Erlangen, Germany) and a phased-array cardiac coil. A patient-specific heart-torso model was constructed by manually segmenting the endocardial and epicardial envelopes of the ventricular myocardium using GeomPEACS (PEACS, The Netherlands) ***(van Dam et al., 2015)***. All contour delineations were performed in the diastolic (i.e. resting) phase of the cardiac cycle. Mitral, tricuspid and aortic valves were incorporated into the cardiac model for co-localization. The envelopes of the thorax hull were also delineated and appropriately meshed. The transfer matrix, describing the potential transfer form the current source to the 12 lead ECG electrode locations, was constructed for up to 1500 cardiac meshes nodes and the mesh location of the 12 lead ECG electrodes on the thorax hull. Based on the above source model and the transfer matrix $A(\ell, n)$ of the thorax volume model, the ECG signals at lead ℓ on the surface of the thorax is calculated as:

$$ECG_{\ell}(t) = \sum_{n=1}^{N} A(\ell, n)\, S(t, \delta_n), \quad \text{Eqn.(1)}$$

Electrode localization and fastest route algorithim

In the third component, the location of body surface ECG electrodes needs to be specified. This was determined using body surface 3D photo-imaging (Kinect camera, Microsoft). An in-house software package was used to analyse all sensory input obtained from the 3D camera. Previous work using this approach has shown that the measurement error for localizing precordial ECG electrodes is <5mm ***(van Dam et al., 2009b)***. Once the position of ECG electrodes relative to the heart orientation is known, ECGsync uses the fastest route algorithm to simulate the ventricular activation sequence for all ventricular nodes based on a given point of origin for the ventricular activation ***(van Dam et al., 2009b)***. Using this activation sequence (Equ 1) will generate the ECG sequence for the given point of origin as described by van Dam et al ***(van Dam et al., 2009a)***.

In the ECGsync algorithm, ECGs are generated for all possible points of origin from the right ventricle. All correlations between these generated ECGs and the true measured ECG are calculated. Finally, the point of origin generating the ECG with the highest correlation with the true ECG is taken as the most likely point of origin for the observed intrinsic LBBB activation of the ventricles. Estimates of cardiac activation, activation isochrones and other synchronicity measures are obtained from this node activation sequence ***(van Dam et al., 2009b)***. A 3D reconstruction of cardiac electric activity (cardiac isochrones) can then be derived by minimizing the difference between the measured body surface potentials and

those based on the source description ***(van Dam et al., 2013)***.

5.2.4. Dyssynchrony

The following metrics of regional and global LV dyssynchrony were derived from intrinsic activation maps (ECGSync):

- **Electrical dyssynchrony index (EDI):** This was derived by computing the standard deviation of activation times (SDAT) across 1500 mesh nodes located on a patient-specific heart model (including endocardial, mid-myocardial and epicardial surfaces) [Figure 5.1].

- **Transseptal activation times (TSAT):** defined as the time interval from the onset of the QRS complex to the earliest LV breakout site from which activation consistently spread away. In LBBB patients, this represents the time difference between the onset of RV activation and the earliest LV (septal) breakout focus.

5.2.5. Statistical analysis

Continuous variables are presented as mean ± standard deviation (SD). Normality was visually assessed using P-P and Q-Q plots and objectively tested using the Shapiro-Wilk test. Categorical variables are expressed as counts with percentages, with comparative analysis undertaken using chi-square tests. To assess the correlation between two continuous variables, the Pearson correlation coefficient (r) was used. All statistical analysis was performed using IBM SPSS V25.0 (SPSS Inc. Chicago, Illinois) and MedCalc version 19.2.1 (MedCalc Software bvba, Ostend, Belgium). A two-sided P-value ≤ 0.05 was considered statistically

significant.

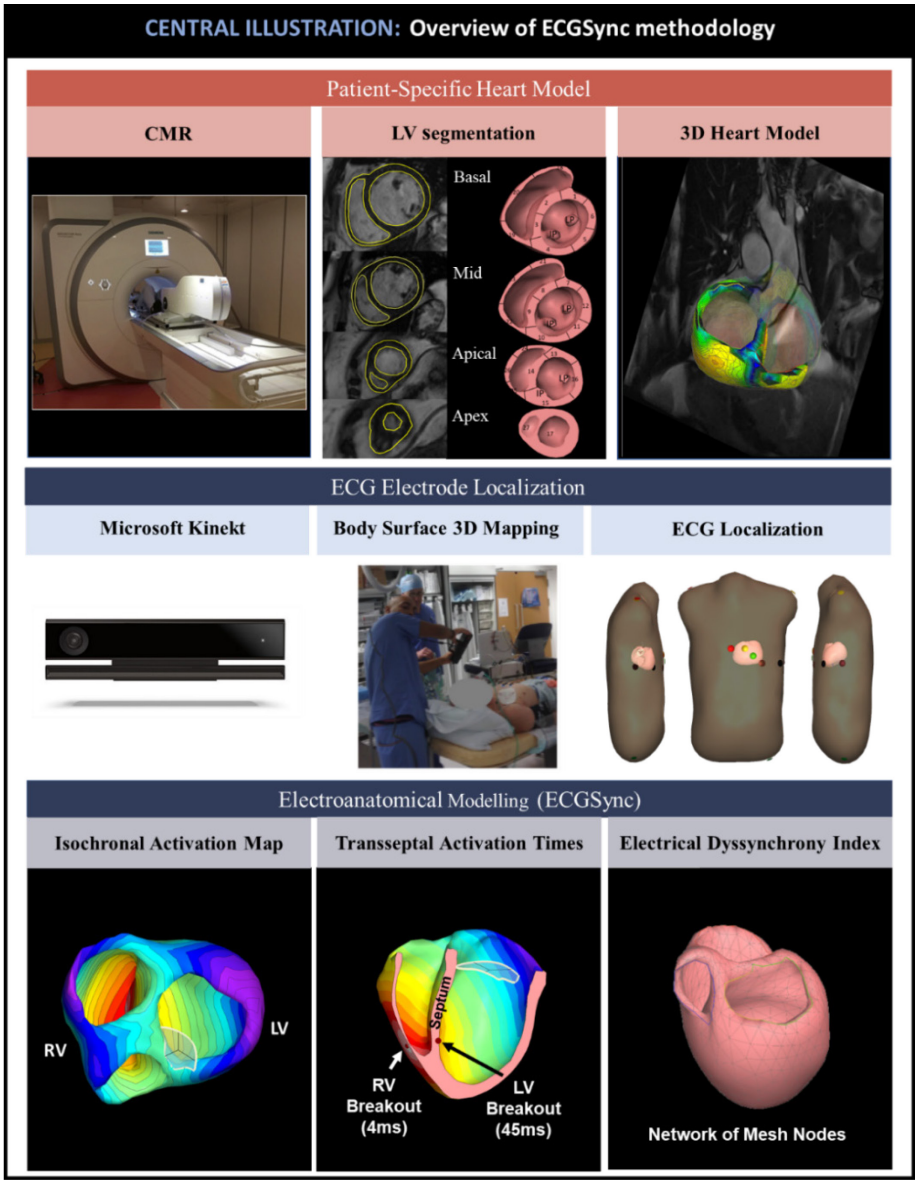

Figure 5.1. Overview of ECGSync. *The major components of the ECGSync algorithm are shown in panels A-C. (A): A 3D heart-torso model is reconstructed from cross-sectional CMR images using GeomPEACS. (B): The location of precordial ECG electrodes is determined using body surface 3D photoimaging (Kinect camera, Microsoft). (C): ECGSync integrates information obtained from 12-lead ECG, CMR and body surface 3D imaging to compute the precise sequence of ventricular activation (cardiac isochrones). From these activation maps, TSAT and EDI are derived by determining the activation timings across a network of 1500 mesh nodes (bottom right).*

5.3. Results

5.3.1. Baseline characteristics

Thirty-two consecutive CRT recipients (aged 69.6 ± 9.15 years [mean ± SD]) were included in this study. The baseline characteristics for this cohort are presented in Table 5.1. Most patients were male (23/32 [71.9%]), in NYHA class II or III (30/32 [93.8%]), with a baseline LVEF of 25.3 ± 7.90 %. Additionally, over half of patients had a nonischaemic HF aetiology (18/32 [56.3%]). A LBBB QRS morphology was present in 71.9% of patients (23/32), with a mean QRSd of 153.5 ± 18.6ms. Electroanatomical maps were successfully acquired in all patients prior to CRT implantation. The time taken to generate the 3D CMR models and the ECGSync maps were 22.2 ± 2.68min and 4.02 ± 0.46min, respectively, totalling 26.2 ± 2.37min (using a sample of 12 studies).

Table 5.1. Baseline characteristics

	All
N	32
Age, yrs	69.6±9.15
Sex (male), n (%)	23 (71.9)
NYHA class, n (%)	
I	1 (3.13)
II	20 (62.5)
III	10 (31.3)
IV	1 (3.13)
Aetiology, n (%)	
Ischemic	14 (43.8)
Non-ischemic	18 (56.3)
LVEF	25.3±7.90
ECG variables	
Sinus rhythm, n (%)	31 (96.9)
AF / flutter, n (%)	1 (3.13)
PR interval (ms)	176.9±39.9
QRSd (ms)	153.5±18.6
LBBB, n (%)	23 (71.9)
RBBB, n (%)	1 (3.13)
NICD, n (%)	8 (25.0)

5.3.2. Activation maps

Native rhythm was imaged in all patients during AAI pacing. Representative maps for LBBB, non-specific intraventricular conduction delay (NICD) and right bundle branch block (RBBB) are illustrated in Figure 5.2. As shown in Table 5.2, there was significant interindividual variability in the location of early and late electrically activated LV segments (LEAS). All LBBB patients exhibited a single breakout focus arising from the RV apex (7/23 [30.4%]), RV septum (7/23 [30.4%]) or RV free wall (9/23 [39.1%]). No spontaneous LV breakthrough sites were observed in any LBBB patient. Following initial RV activation, the wavefront proceeded towards the LV endocardial septum (basal, *n = 2* [8.7%]; mid, *n = 10* [43.5%]; apical, *n = 11* [47.8%]). Thereafter, a single wavefront emerged from the septum and proceeded towards the LV free wall (LVFW). In LBBB patients (n=23), LEAS was located anterior/anterolaterally in 39.1% of cases (basal, n = 9) and lateral/posterolaterally in 60.9% (basal, n = 13; mid, n = 1). Within the LBBB cohort, we observed a wide range of EDI values (range: 21-39 ms), indicating that the amount of electrical dyssynchrony varied considerably in these patients [Table 5.2].

In contrast, the mapped 3D ventricular activation sequences in non-LBBB patients (NICD; *n = 8*; RBBB, *n = 1*) exhibited a more variable pattern. All NICD patients demonstrated a single RV breakout focus. Additionally, 6 out of 8 NICD patients (75%) had further spontaneous LV breakout foci. In most instances, these LV breakthrough sites were clustered around the septum (indicating preserved proximal His-Purkinje activation). In 3 NICD patients, the LV breakthrough site occurred in the vicinity of the left posterior fascicle (mid inferoseptal region). Overall, the onset of LV activation occurred much earlier in NICD patients than in LBBB (TSAT: 9.88 ± 13.9ms vs. 35.3 ± 13.0ms, p =0.02). Due to the presence of early LV breakthrough sites and multiple wavefronts (with opposing directions), EDI values were significantly lower in NICD than in LBBB patients (27.3 ± 4.15ms vs. 26.1 ± 5.27ms, p=0.021) [based on 5 consecutive beats]. The basal anterior/ anterolateral LV wall (5/8 [62.5%]) was the most common site of latest LV activation in NICD patients, followed by the lateral (2/8 [25%]) and posterolateral LV regions (1/8 [12.5%]).

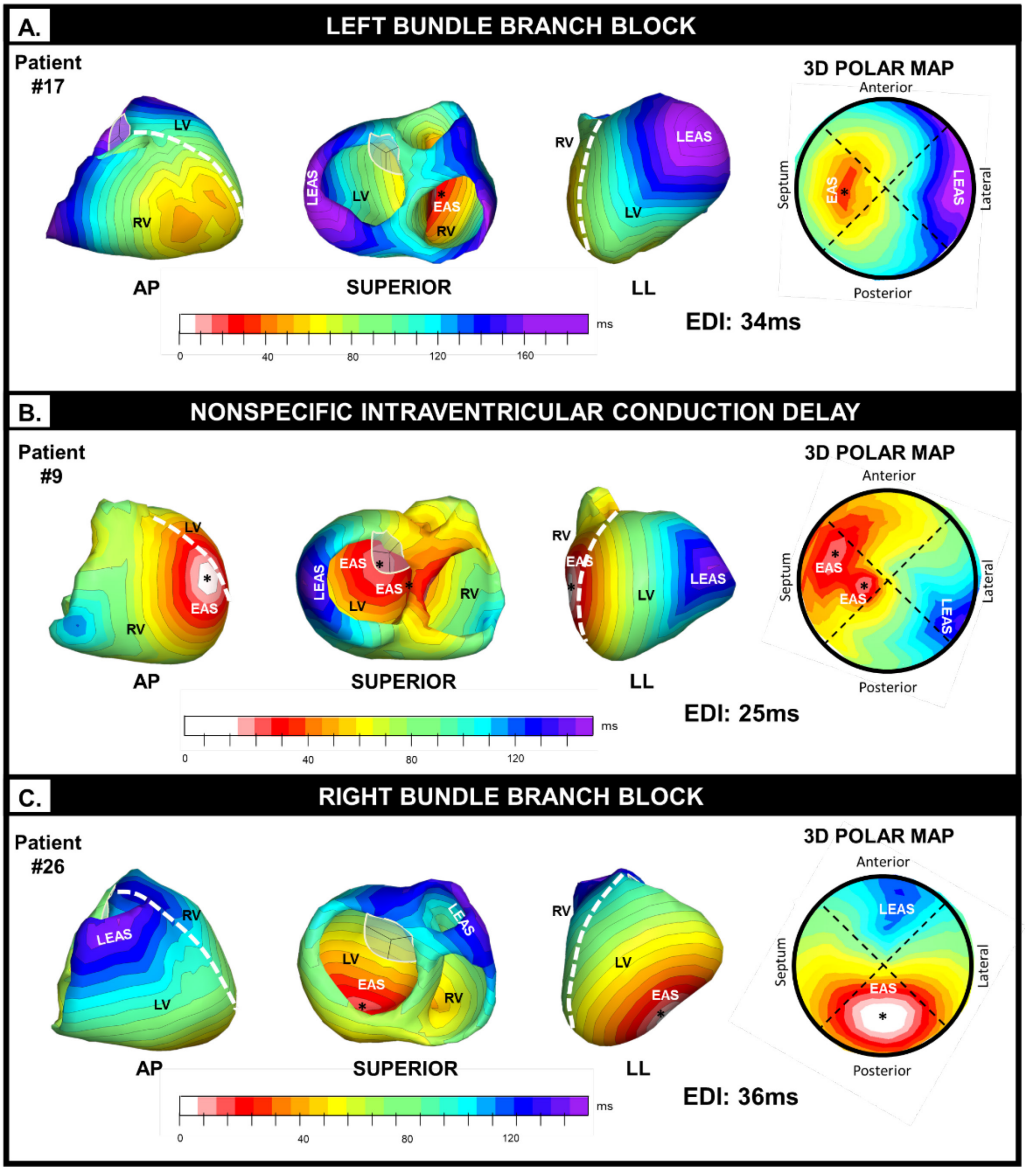

Figure 5.2. ECGSync-derived 3D activation maps.

Isochronal (activation) maps of the right and left ventricle in patients with (A) LBBB, (B) NICD and (C) RBBB are shown. These maps are displayed in three views: anteroposterior (AP), superior and left lateral (LL). 3D polar maps of LV activation are also shown (far right). Early ventricular activation sites (white) are indicated by the asterisk. The location of LEAS (purple) is annotated on the activation maps. All activation times (milliseconds) are relative to the onset of the QRS complex. EAS = earliest activated segment

Table 5.2. Comparison of LV activation patterns in LBBB and non-LBBB patients								
Patient no.	**Age/ Gender**	**QRS morphology**	**Aetiology**	**Earliest BO site**	**LV BO site**	**TSAT (ms)**	**LEAS**	**EDI (ms)**
1	70/M	LBBB	ICM	RV apex	Apicoseptum	28	B-L	39
2	65/F	LBBB	ICM	RVFW	Mid septum	25	M-L	28
3	75/F	LBBB	ICM	RVFW	Basal septum	58	B-AL	39
4	67/M	LBBB	ICM	RV apex	Mid septum	28	B-AL	27
5	57/M	LBBB	NICM	RV septum	Mid septum	19	B-L	37
6	62/M	LBBB	NICM	RV apex	Basal septum	28	B-PL	37
7	75/M	NICD	ICM	RV posterior wall	Apicoseptum	32	B-AL	30
8	57/M	LBBB	ICM	RV apex	Apicoseptum	30	B-AL	32
9	63/M	NICD	ICM	LV septum	Mid septum	0	B-L	25
10	78/M	LBBB	ICM	RV septum	Mid septum	30	B-L	29
11	55/M	LBBB	NICM	RVFW	Apicoseptum	48	B-L	33
12	81/M	LBBB	ICM	RV apex	Apicoseptum	28	B-L	27
13	75/M	NICD	ICM	RV septum	Basal septum	21	B-AL	28
14	72/M	NICD	ICM	LV septum	Mid septum	0	B-PL	28
15	63/M	NICD	ICM	LV septum	Basal septum	0	B-L	27
16	79/F	NICD	ICM	LV posterior wall	LV posterior wall	26	B-A	29
17	83/M	LBBB	NICM	RVFW	Apicoseptum	70	B-L	34
18	53/F	LBBB	NICM	RV septum	Mid septum	23	B-A	27
19	79/M	LBBB	ICM	RV septum	Mid septum	28	B-L	25
20	66/M	LBBB	NICM	RV apex	Apicoseptum	37	B-AL	28
21	76/F	LBBB	NICM	RV septum	Mid septum	28	B-AL	30
22	80/M	NICD	NICM	LV mid-inferoseptum	LV mid-inferoseptum	0	B-AL	28
23	70/M	LBBB	NICM	RVFW	Apicoseptum	46	B-PL	31
24	82/M	NICD	NICM	LV mid-inferoseptum	LV mid-inferoseptum	0	B-AL	25

25	56/F	LBBB	NICM	RVFW	Mid septum	45	B-PL	31
26	76/M	RBBB	ICM	LV mid-posterior wall	LV mid-posterior wall	19	B-A/RVOT	36
27	57/M	LBBB	ICM	RV apex	Apicoseptum	52	B-L	22
28	64/M	LBBB	NICM	RV septum	Apicoseptum	45	B-AL	25
29	56/F	LBBB	NICM	RVFW	Apicoseptum	25	B-AL	21
30	79/F	LBBB	NICM	RVFW	Apicoseptum	35	B-L	27
31	71/F	LBBB	NICM	RVFW	Mid septum	35	B-AL	27
32	72/M	LBBB	NICM	RV septum	Mid septum	20	B-L	27

*A = anterior; AHR = acute haemodynamic responder; AL = anterolateral; B = basal; F = female; L = lateral LV wall; M = male; N = No; PL = posterolateral; RVFW = right ventricular free wall; RVOT = right ventricular outflow tract; Y = Yes. *, refers to the mean ΔLV dP/dt_{max} value across basal, mid and apical positions on a QUAD.*

5.3.3. LV activation delay and electrical dyssynchrony

With respect to invasive measures of LV electrical delay (QLV), there was a better correlation with EDI (r=0.35, p=0.04) than for QRSd (p=0.10). Overall, LBBB patients had greater amounts of electrical dyssynchrony and LV activation delay than non-LBBB patients, as evidenced by the larger QRSd (160.1 ± 16.7ms vs. 134.3 ± 9.65ms, p=0.002), EDI (27.3 ± 4.15ms vs. 26.1 ± 5.27ms, p=0.021) and QLV values (120.8 ± 41.6ms vs. 77.7 ± 26.1ms, p=0.011).

5.3.4. Correlation between electrical parameters and acute haemodynamics

As shown in Figure 5.3A, baseline EDI values were significantly larger in CRT-responders [CRT-R] (>10% ΔLV dP/dt_{max}) then CRT-nonresponders [CRT-NR] (32.9 ± 5.43 ms vs. 27.8 ± 3.08 ms, p=0.022). In contrast, baseline QRSd values did not significantly differ between CRT-R and CRT-NR [156.3 ± 12.3 ms vs. 151.4 ± 22.8 ms, p=0.35]. When using ΔLV dP/dt_{max} as a continuous variable, we observed a significant correlation with EDI (r=0.34, p=0.044) but not QRSd (r=0.31, p=0.084) [Figure 5.3B).

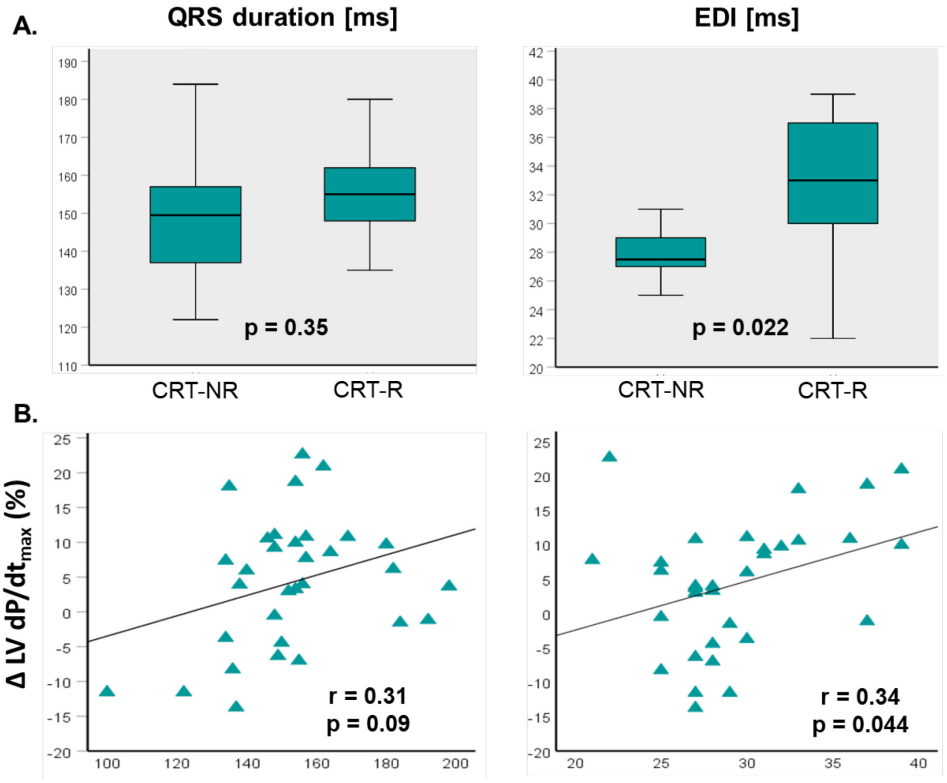

Figure 5.3. Relationship between QRS duration, EDI and AHR to CRT response. *(A) Boxplots showing the difference in QRS duration and EDI values in CRT-responders (CRT-R) and CRT-nonresponders (CRT-NR). The horizontal line denotes the median, whereas the inferior and superior limits of the box denote the 1st and 3rd quartiles. (B) Scatter plots of QRSd and EDI against ΔLV dP/dt_{max}.*

5.3.5. Response to CRT

In total, 10 out of 32 (31.3%) patients (LBBB, *n* = 9; RBBB, *n* = 1) were acute CRT-R. As shown in Figure 5.4, the area under the curve (AUC) for predicting acute CRT response was higher for VCG-derived parameters, including EDI (AUC: 0.81; 95% confidence intervals [CI]: 0.59-1.00, p=0.005), TSI_{ratio} (AUC: 0.82; 95% confidence intervals [CI]: 0.65-0.93, p<0.001) and QRS_{area} (AUC: 0.77; 95% confidence intervals [CI]: 0.59-0.90, p=0.01) than for QRSd (AUC: 0.61, 95% CI: 0.41-0.81, p=0.29) or QRS morphology (AUC: 0.54; 95% CI: 0.36 – 0.72, p=0.53).

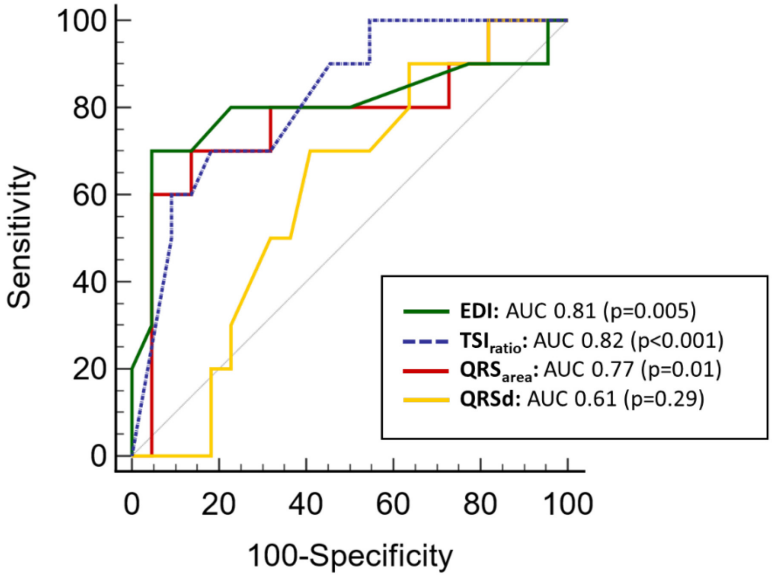

Figure 5.4. Receiver operating characteristic curves.

The receiver-operating characteristic (ROC) curves for EDI, TSI_{ratio}, QRS_{area} and QRSd are shown. The area under the curve (AUC) is used to compare the ability of each parameter to identify acute CRT responders.

The optimal ROC-derived cut-off value for EDI was 31ms. As shown in Table 5.3, high EDI values (≥ 31ms) identified AHR to CRT with a sensitivity of 70% and a specificity of 95.5%. The positive and negative predictive values for EDI were 87.5% and 87.5%, respectively. In contrast, QRSd values ≥ 150ms had a relatively lower specificity (54.6%) and low positive predictive values (41.2%). Overall, 70% of patients with baseline EDI values ≥ 31ms were correctly identified as CRT-R. In comparison, only 38.9% of patients with a baseline QRSd value ≥ 150 ms were correctly identified as CRT-R. The presence of a LBBB QRS morphology was associated with the lowest specificity (18.2%) and positive predictive values (33.3%).

Table 5.3. Diagnostic performance of VCG and ECG-derived parameters								
Predictor variable	**Odds ratio**	**95% C.I.**		**p**	**Sensitivity**	**Specificity**	**PPV**	**NPV**
LBBB QRS morphology	2	0.19	20.6	0.56	90	18.2	33.3	80
QRSd > 150ms	2.33	0.48	11.49	0.30	70	54.6	41.2	80.0
QRS_{area} > 142	10.5	1.86	58.8	0.008	70	86.4	70.0	86.4
TSI_{ratio} > 95%	7.9	1.48	43.5	0.016	70	81.8	63.6	85.7
EDI > 31ms	14.8	2.40	91.2	0.004	70	95.5	87.5	87.5

In univariate analysis, when comparing EDI against conventional surface ECG parameters (i.e., QRSd > 150ms or a LBBB QRS morphology), only EDI emerged as a significant predictor of CRT-R (p=0.004) [Table 5.3]. In fact, EDI values ≥ 31ms were associated with a 14.8-fold increased likelihood of an AHR to CRT (p=0.004), whilst neither QRSd nor LBBB morphology emerged as significant predictors of CRT response (both p>0.29).

5.3.6. Relationship between 12-lead ECG parameters, ECGSync-derived EDI and CRT response

Figure 5.5 shows plots of QRSd and EDI according to QRS morphology. As illustrated, low EDI values (< 31 ms) were observed in nearly all non-LBBB patients (8/9, [88.9%]), indicating a relative lack of baseline dyssynchrony in this group. In LBBB patients, a wide range of EDI values were observed (range: 21 – 39).

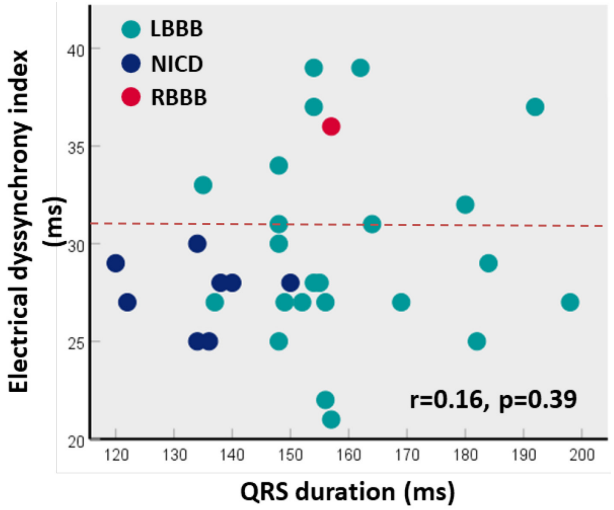

Figure 5.5. Scatter plot of EDI against QRSd.

Scatter plot demonstrating the relationship between ECGSync-derived EDI (x-axis) and QRSd (y-axis). The different colours represent the QRS morphology for each patient, including LBBB (turquoise), NICD (blue) and RBBB (red). The dotted red line represents the cut-off between high (≥ 31ms) and low (<31ms) EDI values.

As shown in Figure 5.6, we compared differences in ΔLV dP/dt_{max} and CRT response rates in LBBB and non-LBBB subgroups according to high vs. low EDI values. In our LBBB cohort, low EDI values were present in 14 out of 23 patients (60.9%), with this cohort also experiencing a low CRT response rate (16.7%). In contrast, the CRT responder rate was 66.7% when both a LBBB QRS morphology and high EDI value were present. There were no CRT-R in the subgroup of patients with a non-LBBB QRS morphology and a low EDI value (n=8 patients). When comparing patients with high versus low EDI values, we observed significantly greater increases in LV dP/dt_{max} in patients with a LBBB QRS morphology (11.58 ± 6.74 vs. 3.05 ± 8.97%, p=0.03), but not for those with a non-LBBB QRS morphology (p=0.075) [Figure 5.6]. Notably, robust statistical analysis in the non-LBBB cohort was limited by the relatively small number of patients (n=9) and the presence of only 1 CRT-R.

We also observed significantly greater LV dP/dt_{max} increases in the QRSd subgroups of ≥ 150 ms (11.04 ± 2.73 vs. 4.36 ± 2.40%, p<0.001) and < 150 ms (12.58 ± 2.73 vs. -2.52 ± 2.59%, p=0.003) when those with a high versus low EDI values were compared.

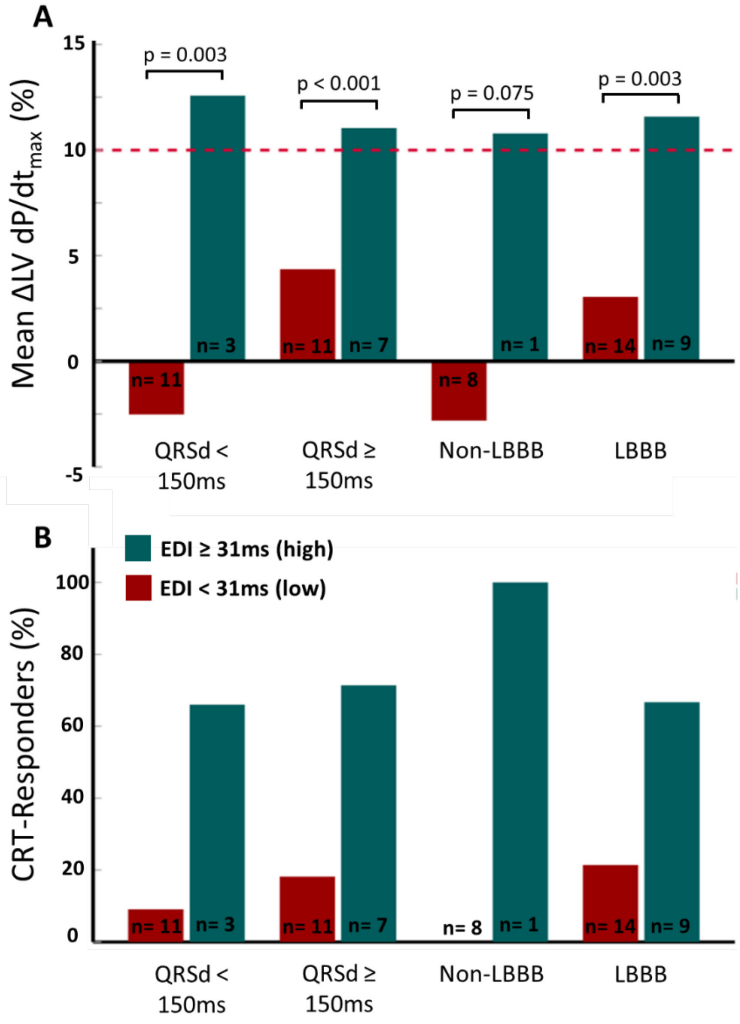

Figure 5.6. Influence of EDI on LV haemodynamics and CRT response.
Bar graph demonstrating the influence of high ( ) and low (< 31ms) EDI values (x-axis) and QRSd (y-axis). The different colours represent the QRS morphology for each patient, including LBBB (turquoise), NICD (blue) and RBBB (red).

5.4. Discussion

The present study demonstrates the feasibility of using a noninvasive 12-lead ECG-based electroanatomical modelling (ECGMod) system to undertake detailed 3D mapping of ventricular activation. Several important findings have emerged from this study. First, ECGSync-derived EDI, which is easily obtained from routine 12-lead ECG analysis, is a good surrogate measure of LV electrical delay (QLV). Second, EDI predicts acute CRT response more reliably than conventional 12-lead ECG criteria (i.e., QRSd and LBBB morphology). Third, there are distinct differences in the LV activation characteristics between patients with LBBB and non-LBBB QRS morphologies.

5.4.1. Electrical dyssynchrony and CRT response

There is increasing evidence to support the use of ECGI as a novel tool to help guide patient selection for CRT ***(Bear et al., 2018; Jia et al., 2006; Ploux et al., 2013; Varma et al., 2007)***. In fact, recent work has shown that ECGI-derived markers of dyssynchrony can predict CRT response more reliably than 12-lead ECG ***(Bear et al., 2018; Ploux et al., 2013)***. In the present study, we used a novel ECG mapping system (ECGSync) to derive a 3D metric of electrical dyssynchrony (EDI). In contrast to QRSd, which provides only a global estimate of ventricular activation delay, EDI is a more specific measure of the spatial dispersion of ventricular activation ***(Ghosh et al., 2011)***. When EDI has a high value, the dispersion is significant, for instance in a typical LBBB pattern. Accordingly, we hypothesized that a high EDI should translate to a greater benefit from CRT. In support of this notion, our findings confirm that EDI is a strong predictor of acute CRT response (AUC: 0.81, p=005). Overall, EDI outperformed both QRSd and a LBBB morphology in identifying AHR to CRT, with a sensitivity of 70% and a specificity of 95.5%. In logistic regression analysis, EDI values ≥ 31ms were associated with a 14.8-fold increased likelihood of an AHR to CRT (p=0.004), whilst neither QRSd nor LBBB morphology emerged as significant predictors of CRT response (both p>0.29).

5.4.2. Differences in LV activation patterns amongst LBBB and non-LBBB patients

Data comparing the LV electrical activation patterns in LBBB and non-LBBB patients is limited and largely restricted to studies employing EAM (Auricchio et al., 2004b; Derval Nicolas et al., 2017; Fantoni et al., 2005; Rodriguez et al., 2003; Vassallo et al., 1984) or noninvasive ECGI ***(Ghosh et al., 2011; Jia et al., 2006; Ploux et al., 2013)***. In the present study, we found that the sequence of ventricular excitation differed markedly between CRT recipients. In our LBBB cohort, visual

inspection of isochronal activation maps confirmed that LV activation nearly always (22/23 [95.7%]) proceeded from an early RV breakout focus. There was slow propagation of RV wavefronts with a right-to-left transseptal vector. This resulted in large delays in transseptal conduction times (≥ 20ms), with the earliest breakout focus occurring on LV (endocardial) septum. Thereafter, the wavefront propagated from the septum towards the LVFW, with LEAS frequently located over the basal lateral or posterolateral LV wall (61% of LBBB patients). These findings are consistent with those reported by Auricchio et al using EAM (Auricchio et al., 2004b) and those of Ploux et al, who used a 252-electrode ECGI system ***(Ploux et al., 2013)***. In contrast, non-LBBB patients (6 out of 9 [66.7%]) frequently displayed normal or near normal transseptal times (< 20ms), indicating that conduction proceeded normally through the proximal segments of the His-Purkinje system ***(Upadhyay Gaurav A. et al., 2019)***. These patients also frequently possessed multiple LV breakthrough sites. Due to the presence of multiple wavefronts, there was less heterogeneity of activation and consequently, less electrical dyssynchrony.

5.4.3. Clinical implications for CRT

In current clinical practice, patient selection for CRT is primarily dictated by the duration and morphology of the QRS complex on 12-lead ECG. However, several studies have shown that baseline QRSd is not helpful when assessing electrical dyssynchrony prior to CRT implantation ***(Dupont et al., 2012; Tereshchenko et al., 2015)***. In fact, subgroup analyses of the large CRT trials have suggested that a LBBB QRS morphology is a better predictor of CRT response than QRSd ***(Sipahi et al., 2012)***. Unfortunately, the use of surface ECG to identify patients with true LBBB is fraught with difficulty, with recent EAM studies suggesting that up to one-third of patients may be incorrectly diagnosed (Auricchio et al., 2004b; Risum et al., 2015; Vassallo et al., 1984). These studies have also shown that a LBBB QRS morphology is not always predictive of a suitable electrical substrate for CRT (Auricchio et al., 2004b; Thomas et al., 2019). Based on our own observations, we found that a typical LBBB QRS morphology was a poor predictor of electrical dyssynchrony on noninvasive 3D ECG mapping. In fact, most of our LBBB patients (14 out of 23 [60.9%]) did not possess a dyssynchronous LV activation pattern (i.e., EDI values < 31ms); with this cohort also experiencing a low response rate to CRT (3/18 [16.7%]). In contrast, the majority of LBBB patients with high EDI values (≥ 31ms) were found to be acute CRT responders (6/9 [66.7%]). This highlights the incremental value of ECGSync over LBBB morphology in the prediction of CRT response. Clearly, surface ECG was unable to define the complex changes in ventricular conduction that occur in patients with LBBB and non-LBBB. This underscores the need for a novel 3D mapping technology to better characterize the electrical substrate prior to CRT implantation. The potential to derive detailed 3D information on ventricular electrical activity from routine 12-lead ECG has important clinical implications.

6.4.4. Study limitations

This study describes our single-centre experience with a novel ECGSync system. There were several important limitations. Most notably, our study comprised of a relatively small sample size. This is consistent with other studies employing invasive haemodynamic monitoring to assess acute CRT response. Additionally, as we have not validated ECGSync against traditional ECG mapping approaches (ECVUE, CardioInsight Technologies Inc., Cleveland, Ohio), we cannot convincingly conclude that the isochrone maps generated by ECGSync are a true reflection of events occurring *in vivo*. Therefore, the accuracy of our novel 3D mapping approach remains unproven. Finally, our ECGSync model assumes a homogenous conduction velocity. It is therefore opaque to conduction inhomogeneities arising from myocardial scar or functional blocks. This is important, as ECGSync cannot identify regions of fixed or functional block, which have been well characterised by other ECGI systems ***(Ghosh et al., 2011; Jia et al., 2006; Ploux et al., 2013)***.

6.4.5. Conclusions

In this acute haemodynamic study, we have shown that novel indices of dyssynchrony derived from a 12-lead ECG-based electroanatomic modelling system predict acute CRT response better than QRSd or LBBB morphology. Additionally, ECGSync identified several activation characteristics that can help distinguish between those with a LBBB and non-LBBB QRS morphology. On this basis, ECGSync may provide a simple, noninvasive tool to help improve patient selection for CRT.

Chapter 6

Electroanatomical Modelling for Noninvasive QLV Mapping in Cardiac Resynchronization Therapy: The ECGSync Study

Abstract

Background: Left ventricular (LV) pacing over late electrically activated myocardial segments (LEAS), identified by a long QLV interval, is associated with better clinical outcomes after cardiac resynchronization therapy (CRT).

Objective: To validate a novel, non-invasive electroanatomic modelling system based on the 12-lead ECG (ECGMod) against non-contact electroanatomic mapping (EnSite) and intraoperative LV lead-derived QLVs in CRT recipients.

Methods: In this acute study, ECGMod and EnSite were used to derive isochronal maps and QLV during intrinsic rhythm and right ventricular (RV) pacing. ECGMod-derived maps were merged with three-dimensional ventricular envelopes derived from a pre-implantation cardiovascular magnetic resonance scan.

Results: According to expert assessment of isochronal maps using Ensite as reference, ECGMod was reliable in identifying LEAS during intrinsic rhythm in 13/16 (81.3%) patients (Fleiss' K: 0.88, 95% confidence interval [CI] 0.73-1.00, p<0.001) and RV-pacing (K: 0.96 [95% C.I. 0.86-1.00], p<0.001). In a sample of 192 electrograms recorded during intrinsic rhythm and RV pacing, ECGMod-QLV agreed with EnSite-QLV (r=0.59, p<0.001; mean bias: -3.97 ± 28.9 ms). In 32 electrograms, ECGMod-QLV agreed with LV lead-derived QLV (r=0.53, p=0.002, mean bias: -2.03 ± 29.8 ms). There was excellent interobserver agreement for ECGMod-derived QLV (r=0.94, p<0.001; mean bias: -0.42 ± 10.3ms).

Conclusion: ECGMod was reliable for identifying LEAS, using EnSite isochronal maps and LV lead derived QLV as reference. ECGMod-derived QLV was highly reproducible. These findings support the use of a 12-lead ECG-based QLV map using ECGMod for targeting LV lead deployment prior to CRT implantation.

6.1. Introduction

Cardiac resynchronization therapy (CRT) is an electrical treatment in which electrical dyssynchrony is pre-requisite for a therapeutic response. In the background of this paradigm, a QRS > 120 ms was adopted as a simple, arbitrary measure of electrical dyssynchrony by the core randomized, controlled clinical trials of CRT ***(Leyva et al., 2014)***. It has since emerged that some guideline-indicated patients do not derive a benefit from CRT ***(Fornwalt et al., 2010)***. There is evidence to suggest that targeted left ventricular (LV) lead deployment may improve response ***(Leyva et al., 2014)***.

In line with the central paradigm of CRT, a notion has arisen according to which pacing late electrically activated myocardial segments (LEAS) should achieve the most effective cardiac resynchronization. In this respect, LV pacing in sites with the longest time delay from the onset of the surface QRS complex to the local intrinsic activation at the left ventricular (LV) pacing site (QLV) is associated with a better acute hemodynamic response ***(Everdingen et al., 2018; Gold et al., 2014; Singh et al., 2006)*** and LV reverse remodelling ***(Gold et al., 2011; Polasek et al., 2012)***. In addition, CRT using LV pacing in sites with a long QLV has been shown to improve quality of life ***(Gold et al., 2016)*** and long-term clinical outcomes ***(Roubicek Tomas et al., 2015)***. In these studies, QLV was acquired at the time of implantation, from an already deployed LV lead ***(Gold et al., 2011)***. As proposed by some authors ***(Gold et al., 2011; Singh et al., 2006)***, LEAS should ideally be identified by intra-operative 'mapping' of QLV from all accessible coronary veins. In this regard, invasive electroanatomical mapping (EAM), such as CARTO ***(Kittnar et al., 2018; Kiuchi et al., 2007; Peichl et al., 2004)*** and Ensite NavX ***(Del Greco et al., 2012; Fujiwara et al., 2014; Niazi et al., 2015)*** has shown promise in its ability to provide an endocardial 'QLV map' at the time of implantation. Coronary venous EAM has also been used to provide an epicardial QLV map ***(Mafi Rad et al., 2016)***. These techniques, however, are invasive, lengthen implantation time and are not without risks. A non-invasive technique that permits a 'QLV map' prior to implantation, without intraprocedural complexity or additional radiation exposure and procedure times, is desirable.

Various electrocardiographic imaging (ECGI) techniques have emerged as non-invasive tools for visualising and quantifying LV activation. Prominent amongst these is CardioInsight, which combines body surface potentials from a 252-electrode vest with patient-specific anatomy, derived from computed tomography. Two studies have provided proof of concept that CardioInsight can provide useful measures of electrical dyssynchrony in CRT recipients ***(Ploux et al., 2013; Sieniewicz et al., 2019)***. The ECG 'belt, which is a simplification of CardioInsight, has been applied in a similar fashion ***(Johnson et al., 2017)***.

In the present study, we compared a novel, non-invasive electroanatomic modelling (ECGMod) system based on the standard 12-lead ECG (ECGSync) to a non-contact EAM system (EnSite), in identifying LEAS.

6.2. Methods

The ECGSync study is an acute study comparing ECGSync to non-contact EAM, namely Ensite, in the non-invasive identification of LEAS and quantification of QLV. The study was approved by the local Ethics Committee and complied with the Declaration of Helsinki. All patients provided written informed consent.

6.2.1. Patients

Inclusion criteria were: indications for CRT, according to current European Society of Cardiology guidelines; NYHA class II-IV, LVEF ≤35%, a QRS ≥120ms; receiving optimal pharmacologic therapy. Exclusion criteria were: frequent atrial or ventricular ectopics, atrial fibrillation or atrial flutter, mechanical aortic valve or significant valvular disease and significant peripheral vascular disease; recent acute coronary syndrome (<3 months); contraindications to CMR.

The aetiology of heart failure was confirmed on basis of clinical history, the finding of impaired LV function on echocardiography. The diagnosis of ischemic cardiomyopathy with transmural or subendocardial myocardial scar was defined by late-gadolinium enhancement cardiac magnetic resonance (CMR) ***(McCrohon et al., 2003)***.

6.2.2. Electrophysiology study

During CRT implantation, a left cephalic and/or single-puncture axillary/subclavian access was used as access for all leads. Right atrial leads were deployed in the right atrial appendage and right ventricular (RV) lead in the RV apex. After coronary sinus cannulation, an occlusive, retrograde venogram was obtained and a quadripolar LV lead (Attain Performa, Attain Stability; Medtronic, Minneapolis, US) or a temporary, multipolar LV lead (Pathfinder, Cardima Inc., Duluth, Georgia) was deployed in a lateral or posterolateral vein. The position of the LV lead was adjusted during the procedure to sense QLV in the various myocardial segments. Simultaneously, a second operator introduced a 64-electrode Ensite Array balloon (Abbott, city, country) via the right femoral artery access (9-French sheath), with retrograde advancement into the LV through the aortic valve. Systemic anticoagulation was achieved with intravenous heparin, titrated to achieve activated clotting time of 350 s during the procedure.

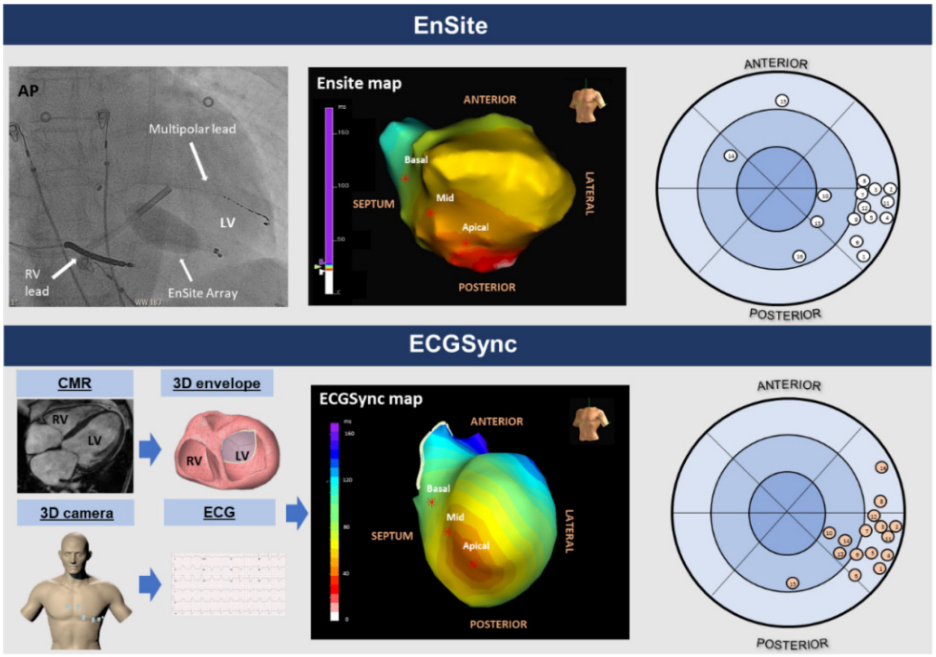

Figure 6.1. Validation of ECGMod Against Non-Contact Mapping.
In this validation of a novel electroanatomical model of cardiac activation based on the 12-lead ECG (ECGMod) against non-contact mapping (EnSite), patients underwent an electrophysiological study in which an Ensite Array balloon was inserted into the LV retrogradely, across the aortic valve. A pre-implantation cardiovascular magnetic resonance scan was undertaken and short-axis cine images were used to reconstruct endocardial and epicardial envelopes (left sided panel). The digitized 12-lead ECG was used to construct isochronal maps (middle panels). The Ensite- and ECGMod-derived isochronal maps were assessed for agreement by electrophysiologists, using a polar map (representative map). Agreement between Ensite- and ECGMod-derived QLV was also assessed.

6.2.3. Pacing protocol

ECG acquisitions and EnSite mapping was undertaken during intrinsic rhythm and RV pacing. For analysis, a sampling period of 10 beats prior and 10 beats immediately after each rhythm assessment was used, in order to minimize sampling error and the effects of respiration and variations in loading conditions. The RV pacing protocol consisted of DDD pacing delivered at 10 beats per minute (bpm) above intrinsic heart rate, with a short atrioventricular (AV) delay (intrinsic AV delay minus 20 ms) to avoid fusion with intrinsic activation.

6.2.4. Electroanatomical mapping

A non-contact mapping system (EnSite Precision Cardiac Mapping System (Model EE300, Endocardial Solutions, St. Paul, MN, USA) was used to obtain beat-to-beat LV activation maps. For analysis, we used reconstructed isopotential (voltage) maps with virtual electrodes placed in septal, anterior, lateral and posterior LV wall positions (basal, mid and apical). Unipolar EGMs were acquired at 1200Hz, with a high-pass filter setting of 8Hz.

6.2.5. ECGSync

Non-invasive, ECG mapping of LV endocardial and epicardial activation was performed using a novel ECGMod system (ECGSync; PEACS, The Netherlands), which yields ventricular isochronal maps from a standard 12-lead ECG ***(van Dam et al., 2015)***. ECGSync has been specifically designed to identify patterns of ventricular propagation and late ventricular activation. To this end, digital, standard 12-lead ECGs were acquired at the time of implantation using the Prucka system (General Electric, Connecticut). In order to generate patient-specific models, cardiovascular magnetic resonance (CMR) DICOM images of ECG-gated, short-axis, steady-state in free precession LV cines obtained prior to the electrophysiological study were manually segmented and used to construct three-dimensional endocardial and epicardial envelopes in end-diastole, using GEOM-PEACS [PEACS, The Netherlands] ***(van Dam et al., 2015)***. For each heart model, we constructed a transfer matrix comprising of up to 1500 mesh nodes imbedded onto triangulated, ventricular endocardial and epicardial envelopes, incorporating the mitral, tricuspid and aortic valves for co-localization.

Single-beat, LV activation maps were constructed from surface 12-lead ECGs using ECGSync. A detailed description of the methodological details for ECGSync is included in **Chapter 5** (Section 5.2.3). Briefly, ECGSync has 4 components: First, a cardiac current source model, is the equivalent double layer model, which represent currents generated during the depolarization. Second, the spatial relation of the ECG electrodes to the heart. Third, the electrical volume conductor effect dominated by tissues with electrical conductivity values that differ from those of the surrounding tissues.

Last, the patient-specific geometry of the heart, lungs and thorax derived from CMR, was delineated using manual contouring of the epicardium and endocardium, lungs, and thorax to yield patient-specific geometries. The fastest route-based algorithm was used to estimate the activation isochrones, using anatomical landmarks as the starting points of the investigated activations ***(van Dam et al., 2009a)***. These anatomical landmarks are related to areas where the Purkinje

system is known to activate the heart, i.e., papillary muscles, moderator band and the left and right septum.

6.2.6. LV activation times

In line with accepted definitions ***(Derval Nicolas et al., 2017)***, timing variables on both EnSite and ECGSync were defined as follows:

- **Transseptal activation time (TSAT):** from the onset of the QRS complex to the earliest detected LV endocardial breakthrough.
- **LV breakthrough:** as the LV site activated within 10ms of LV activation. In EnSite, the timing of this event was within the initial 10% decrease in amplitude during the rapid downstroke of the associated virtual electrogram.
- **LV activation time (LVAT):** from the earliest to the latest LV endocardial activation on both EnSite and ECGSync.
- **QLV**: as the time from the onset of the QRS complex on the surface ECG (lead V2) to the latest LV activation. On EnSite, the QLV interval was measured from the beginning of the QRS complex on the surface lead V_2 to the latest peak negative rate of voltage change (-dV/dt) on reconstructed unipolar EGMs. On the LV leads, this was the time from the beginning of the QRS complex on the surface lead V2 to the peak of the sensed QRS on the lead electrode.

6.2.7. Segmental positions

The convention of Singh et al was used to identify the segmental localization of QLV on both EnSite and ECGSync, and LV lead electrodes (Figure 6.2) ***(Singh Jagmeet P. et al., 2011)***.

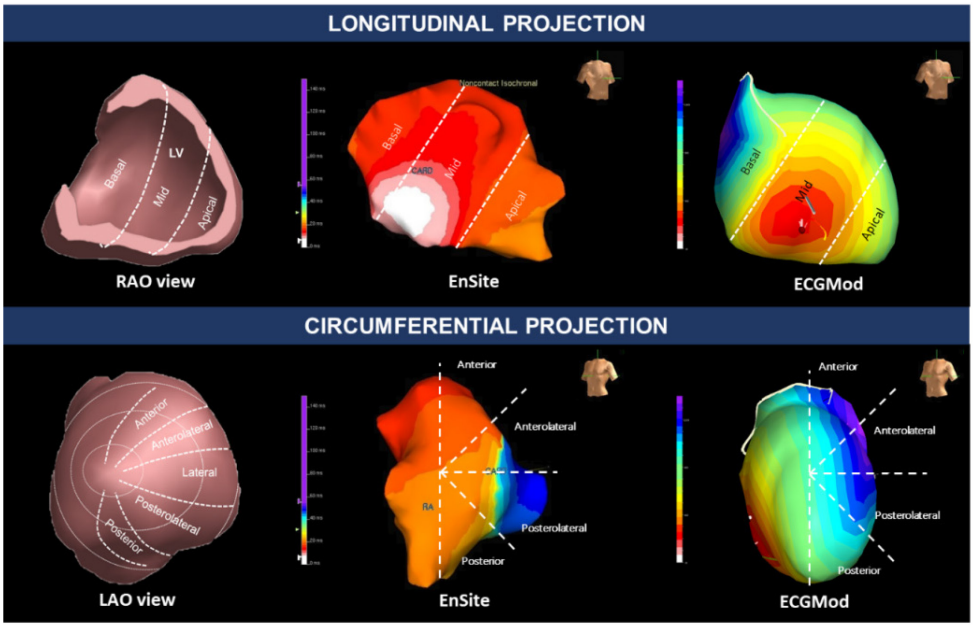

Figure 6.2. Left Ventricular Segmentation

The convention of Singh et al was used for the localization of LV activation and lead positions (Singh Jagmeet P. et al., 2011). *Accordingly, longitudinal positions were assigned using the 30º right anterior oblique (RAO) in both Ensite and ECGMod (A) and classified into basal, mid and apical sectors. Circumferential positions were assigned using the 30º left anterior oblique (LAO) fluoroscopic view and classified into anterior, anterolateral, lateral, posterolateral and posterior sectors, running from the great cardiac vein to the inferior cardiac vein (assumed to run along the inferior interventricular groove). For comparison with fluoroscopy, the RAO fluoroscopic view of the LV was divided into basal, mid and apical, assuming that the great cardiac vein (anterior interventricular vein) runs along the interventricular groove and that the coronary sinus runs along the atrioventricular groove.*

6.2.8. Interobserver agreement

For the comparison of ECGSync- and Ensite-derived QLV, a single observer (O.O.) quantified QLVs on separate occasions, blinded to the results of each technique in turn. Interobserver agreement analyses of ECGSync-QLV were based on the QLVs quantified by an experienced (O.O.) and an inexperienced observer (A.Z.). Ensite- and ECGMod-derived isochronal maps were assessed for agreement by 3-independent consultant electrophysiologists (M. L, M. K and J.dB) according to the location of LV breakthrough sites and LEAS. To help facilitate comparisons, activation maps were displayed in identical RAO, LAO, anterior and posterior projections (Appendix A). The level of agreement between ECGMod and Ensite-derived activation maps was quantified using a 5-point scoring system (1: no

agreement, 2: poor agreement, 3: satisfactory agreement, 4: good agreement and 5: excellent agreement). For the purposes of inter-rater reliability analyses, overall scores of ≥ 3 were used to define agreement between ECGMod and Ensite, whilst scores of < 3 indicated no agreement. To help minimize bias, experts were blinded to the methodological approach adopted by ECGMod.

6.2.9. Statistical analysis

Continuous variables are expressed as mean ± standard deviation (SD) and compared using the t-test or the Mann-Whitney U test. Categorical variables are expressed as counts with percentages. Normality was tested using the Shapiro-Wilk test. To assess the correlation between two continuous variables, the Pearson correlation coefficient (r) was used. Inter-rater reliability analyses for isochronal maps was undertaken using Fleiss' K statistic ***(Fleiss, 1971)*** with bootstrapped 95% confidence intervals (C.I.). Bland-Altman analyses were used to assess the agreement between ECGSync- and EnSite-derived QLV and the interobserver agreement for ECGSync QLV. All statistical analyses were undertaken using Stata, SPSS (SPSS Inc., Chicago, Illinois) and MedCalc (MedCalc, Ostend, Belgium). A two-sided $p < 0.05$ was considered statistically significant.

6.3. Results

6.3.1. Baseline characteristics

Sixteen patients (aged 68.9 ± 8.32 years [mean ± SD]) were recruited. As shown in Table 1, 10 [62.5%] had a LBBB), the QRSd was 150.4 ± 21.1ms and the LVEF was 25.1 ± 8.37%. The underlying aetiology was ischemic in 13/16 (81.3%) and non-ischemic in 3/16 (18.8%). Isochronal maps were successfully acquired in all patients during sinus rhythm and in 14/15 (93.3%) patients during RV-paced rhythm. The complete datasets (isochronal maps) can be found in Appendix A.

Table 6.1. Characteristics of the study group.

Variable	
N	16
Age, yrs	68.9±8.32
Sex (male), n (%)	13 (81.3)
NYHA class, n (%)	
I	1 (6.25)
II	5 (31.3)
III	9 (56.3)
IV	1 (6.25)
Aetiology, n (%)	
Ischemic	13 (81.3)
Non-ischemic	3 (18.8)
LVEF (%)	25.1±8.37
ECG variables	
Sinus rhythm, n (%)	15 (93.8)
AF / flutter, n (%)	1 (6.25)
PR interval (ms)	172.3±30.9
QRSd (ms)	150.4±21.1
LBBB, n (%)	10 (62.5)
NICD, n (%)	5 (37.5)

6.3.2. Activation intervals

According to EAM, patients with LBBB had a longer TSAT (43.6 ± 18.4 vs. 12.7 ± 15.1ms, p=0.003) and LVAT (114.7 ± 18.1 vs. 66.5 ± 22.8ms, p=0.001) than NICD patients (Figure 6.3 and Table 6.2). Transseptal activation times were similar during intrinsic and RV paced rhythms (32.0 ± 22.7 vs. 31.4 ± 8.74ms, p=0.89). There was a correlation between TSAT and baseline QRSd during sinus rhythm (r=0.81, p<0.001), but not during RV pacing (r=0.13, p=0.66). In fact, TSAT remained relatively constant between patients during RV pacing (irrespective of baseline QRSd), with an associated narrow distribution of TSAT values (SD: 8.74ms). Relative to intrinsic conduction, RV pacing increased LVAT (150.8 ± 19.6 vs. 96.6 ± 30.8ms, p<0.001).

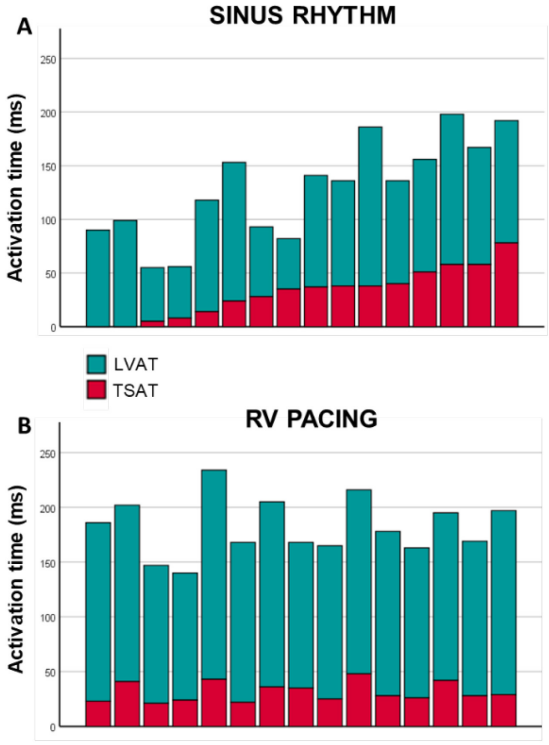

Figure 6.3. Left ventricular activation times according to EnSite.
Bar graphs showing EnSite-derived LV activation times (LVAT) and transseptal activation times (TSAT; red) during native (intrinsic) conduction (Panel A) and right ventricular pacing (Panel B) for each patient.

Table 6.2. Comparison of LV activation times during intrinsic and RV-paced rhythms											
Patient no.	Aetiology	QRS morphology	QRSd (ms)	INTRINSIC RHTYHM				RV PACED RHYTHM			
				TSAT (ENSITE)	TSAT (ECGMod)	LVAT (ENSITE)	LVAT (ECGMod)	TSAT (ENSITE)	TSAT (ECGMod)	LVAT (ENSITE)	LVAT (ECGMod)
1	ICM	LBBB	162	40	28	96	158	26	31	137	144
2	ICM	LBBB	155	14	25	104	134	43	21	191	126
3	ICM	LBBB	154	24	49	129	135	22	38	146	108
4	ICM	LBBB	137	51	28	105	102	42	20	153	144
5	NICM	LBBB	154	38	19	98	123	48	26	168	114
6	NICM	LBBB	192	78	28	114	187	29	17	168	148
7	ICM	NICD	134	35	32	47	132	35	30	133	119
8	ICM	LBBB	180	38	30	148	137	28	35	150	125
9	ICM	NICD	136	0	0	99	96	41	29	161	130
10	ICM	LBBB	184	58	30	140	128	-	-	-	-
11	NICM	LBBB	135	58	48	109	155	28	25	141	127
12	ICM	LBBB	152	37	28	104	158	25	24	140	117
13	ICM	NICD	140	0	21	90	132	23	22	163	147
14	ICM	NICD	150	5	0	50	128	21	21	126	135
15	ICM	NICD	122	8	0	48	110	24	28	116	109
16	ICM	NICD	120	28	26	65	135	36	22	169	128

6.3.3. ECGSync and EnSite isochronal maps

According to expert adjudication, ECGMod correctly identified LV breakthroughs in 14/16 (87.5%) patients (Fleiss' K: 0.92; 95% confidence intervals [C.I.]: 0.80 to 1.00, p<0.001) and LEAS in 13/16 (81.3%) patients (K: 0.88; 95% CI: 0.73 to 1.00, p<0.001) during intrinsic rhythm, using EnSite as reference. In RV-pacing, ECGMod correctly identified LV breakthroughs in 14/15 (93.3%) (K: 0.91; 95% CI: 0.78 to 1.00, p<0.001) and LEAS in 14/15 (93.3%) patients (K = 0.96; 95% 0.86 to 1.00, p<0.001). Representative maps are shown in Figure 6.4.

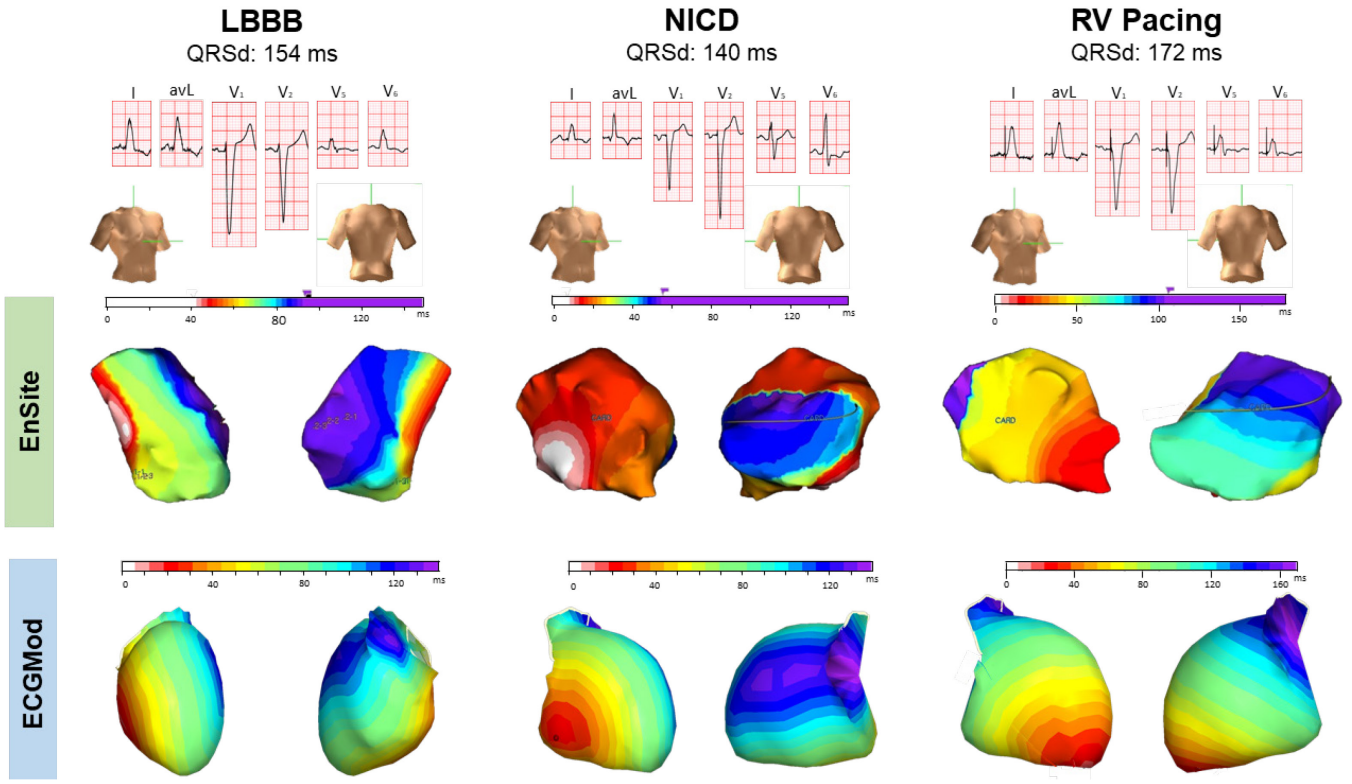

Figure 6.4. Isochronal Maps. *Typical LV isochronal maps using ECGMod and non-contact EnSite mapping. A) shows isochronal maps of a patient with a LBBB, in whom there is a single LV breakthrough in the septum and thereafter, a homogeneous propagation within the LV cavity, with the latest activation in the basal lateral LV wall. B) shows isochronal maps from a patient with a non-specific intraventricular conduction delay (NICD), in which there is single septal breakthrough and a large area of late activation over the left ventricular free wall. C) shows isochronal maps of a patient undergoing right ventricular (RV) pacing, in which pattern of depolarization was similar to a native LBBB, with a single LV breakout in the septum and thereafter, late activation over the basal anterolateral wall.*

The location of LV breakthroughs and LEAS was allocated using a polar map, using the convention of Singh et al ***(Singh Jagmeet P. et al., 2011)***. As shown in Figure 6.5, the location of LEAS during intrinsic conduction varied between patients, being located anterior/anterolaterally in 2/16 (12.5%) patients and inferior/inferolaterally in 13/16 (81.3%) patients [basal, n = 10; mid, n = 3]. In one patient, LEAS occurred at the junction of the posterior and inferoseptal LV wall. The LEAS during RV pacing was located on the basal anterior/anterolateral LV wall in 3/15 (20%) patients and inferior/inferolaterally in 12/15 (80%) patients [basal, n = 11; mid, n = 1].

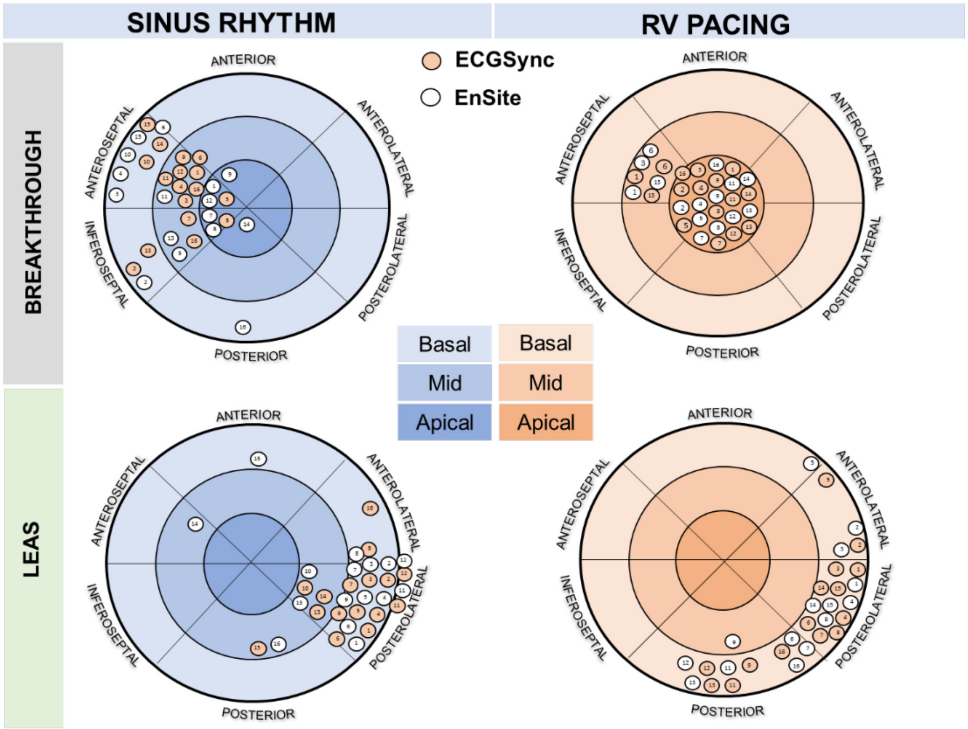

Figure 6.5. Agreement Between EnSite and ECGMod Isochronal Maps.
Representative polar maps for the assessment of breakthrough and late electrically activated segments (LEAS) for one observer. The upper panel shows the adjudicated left ventricular breakthrough sites in sinus rhythm and right ventricular (RV) pacing. The lower panels show the adjudicated LEAS in sinus rhythm and RV pacing. The convention of Singh et al was used for the localization of LV segments (Singh Jagmeet P. et al., 2011).

6.3.4. ECGSync- and EnSite-derived QLV times

Using Ensite, 192 unipolar (virtual) EGMs were recorded during sinus rhythm. The QLV interval was measured at 48 points in each LV position (septal, anterior, posterior and lateral). Across all sampled LV sites (n=192), the corresponding ECGSync-derived QLV correlated with EnSite-derived QLV ($r=0.59$, $p<0.001$) [Figure 6.6]. With respect to myocardial segments in which the longest QLV was located, the correlation was highest for anterior ($r=0.52$, $p>0.001$), lateral and posterior LV wall sites ($r=0.48$, $p=0.001$ for both), followed by the septum ($r=0.34$, $p=0.018$). Overall, the mean bias across all ECGMod QLV measurements was -3.97 ± 28.9ms (95% limits of agreement [LOA]: -60.7 to 52.7), compared to EnSite (Figure 6.6). Across individual LV positions, the mean bias was 5.0 ± 23.9 ms (95% LOA: -41.9 to 51.9) for the septum, 6.29 ± 23.0 ms (95% LOA: -51.4 to 38.8) for anterior segments, -6.40ms ±32.8 ms 9ms (95% LOA: -70.7 to 57.9) for posterior segments and 8.2 ± 33.3 ms (95% LOA: -73.5 to 57.1) for the lateral segments.

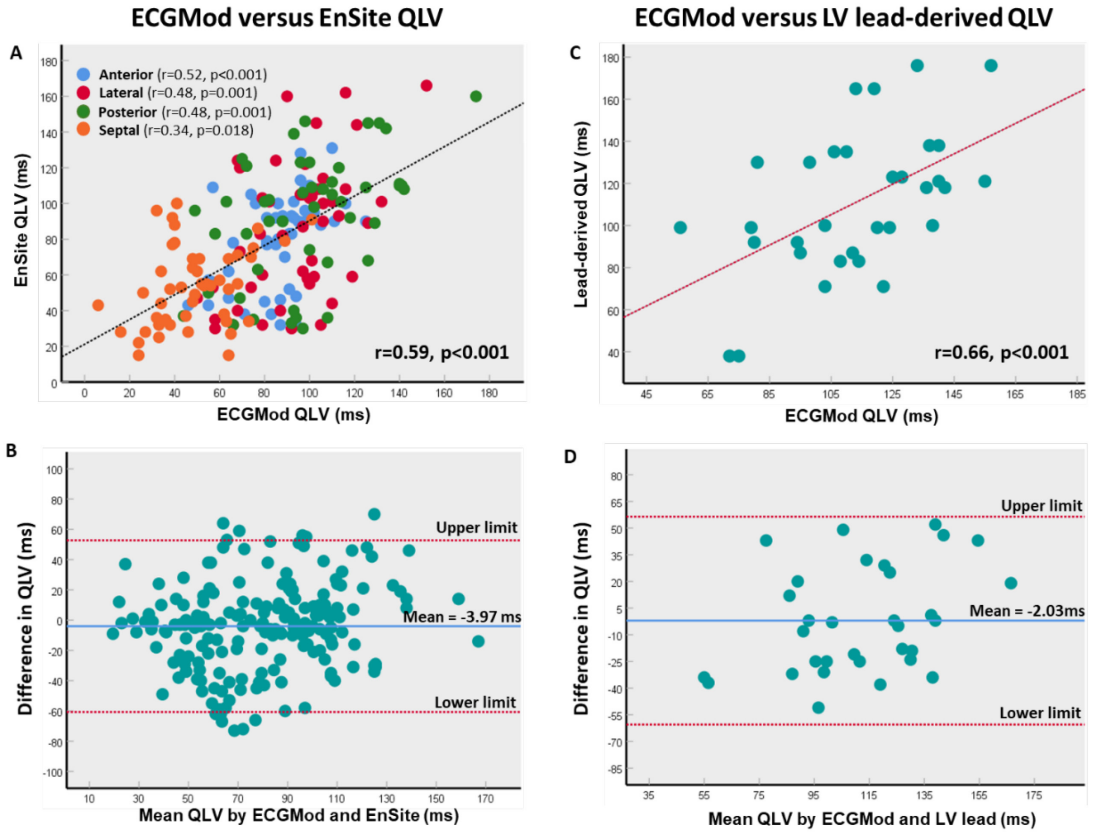

Figure 6.6. Agreement Between ECGMod- and EnSite-Derived QLV. *A) Shows scatterplot for ECGMod- EnSite-derived QLV. A total of 3 points in anterior, lateral, posterior and septal sectors were sampled in 16 patients using both techniques. B) shows Bland-Altman plots for agreement between ECGMod- and EnSite-derived QLV. C) shows scatterplot for scatterplot for ECGMod-derived QLV and left ventricular lead-derived QLV. D) shows Bland-Altman plots for agreement between ECGMod-derived QLV and left ventricular lead-derived QLV.*

6.3.5. Agreement between ECGSync and LV lead-derived QLV

Using the sensed LV electrograms, QLV intervals were obtained from implanted multipolar LV leads. A total of 32 QLV measurements were recorded by adjusting the position of the lead to subtend basal (n = 16) and mid (n = 16) LV segments. The segment subtended by the relevant LV pacing poles was used to determine the appropriate anatomical segment on reconstructed 3-dimensional activation maps (ECGSync). Overall, ECGSync-QLV correlated with LV lead-derived QLV ($r=0.53$, $p<0.002$). As shown in Figure 6.6, the mean bias between ECGSync and lead derived QLV was -2.03 ± 29.8ms (95% LOA: -60.5 to 56.4).

6.3.6. Interobserver agreement for ECGSync-derived QLV

To determine interobserver agreement of ECGSync QLV, 2 investigators (O.O and A.Z) undertook QLV measurements separately. As shown in Figure 6.7 there was excellent correlation in ECGSync-derived QLV values between the two 2 investigators ($r=0.94$, $p<0.001$). Additionally, Bland-Altman analysis revealed a mean bias of -0.42ms ± 10.3ms (95% LOA: -20.5 to 19.7), with no significant difference in the QLV values obtained from either observer ($p=0.57$).

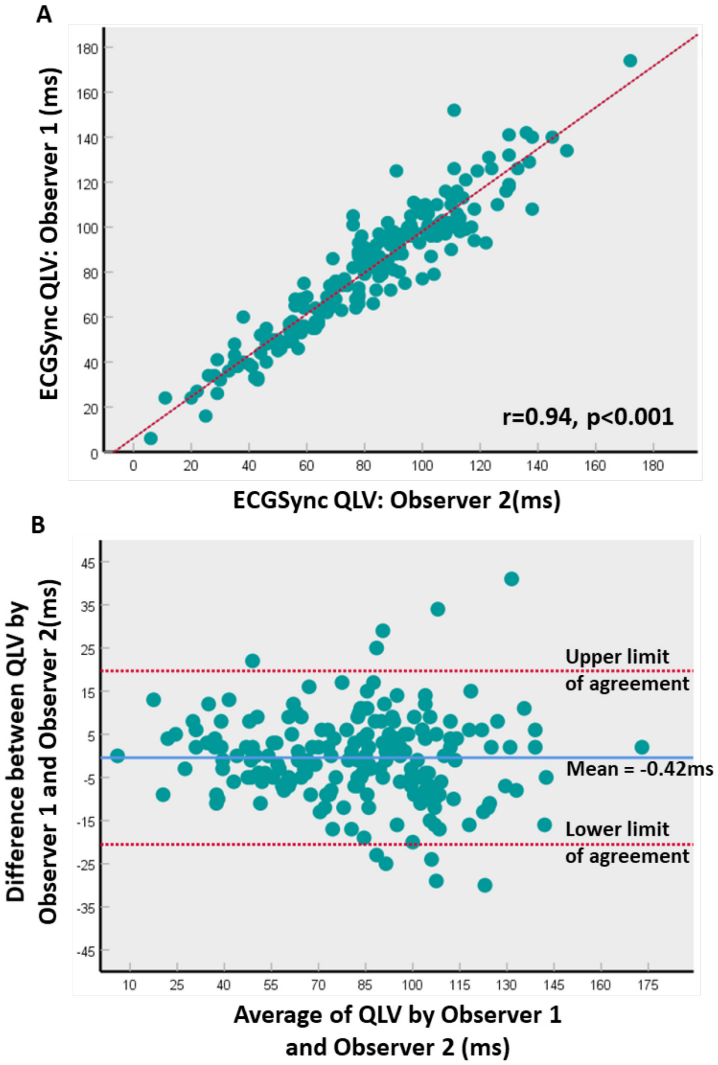

Figure 6.7. Interobserver Agreement for ECGMod-derived QLV.
A) Shows scatterplot for ECGMod-derived QLV for 2 observers. A total of 3 points in anterior, lateral, posterior, and septal sectors were sampled in 16 patients by two observers. B) shows Bland-Altman plots for agreement between ECGMod-derived QLV for the two observers.

6.4. Discussion

This study has emerged in the context of increasing demand for a non-invasive technique that allows mapping of LEAS in advance of CRT implantation. We have validated a novel, 12-lead ECGMod system (ECGSync) against invasive, non-contact mapping (EnSite) in potential CRT recipients. Several findings have emerged. First, there was excellent inter-rater reliability amongst electrophysiologists with respect to the location of LEAS from ECGSync isochronal maps, using EnSite as reference. Second, there was excellent agreement between ECGSync-QLV and EnSite-QLV. Third, there was excellent agreement between ECGSync- and LV lead-derived QLV. Last, there was excellent interobserver agreement with respect to ECGSync QLV.

6.4.1. QLV

Whilst a randomized, controlled clinical outcome trial on the use of QLV to target LV pacing sites is yet to emerge ***(Singh et al., 2018)***, there is compelling evidence from observational studies in its favour. In 71 patients undergoing CRT implantation, Singh et al. showed that a longer QLV was associated with a better acute LV hemodynamic response and a lower risk of total mortality or heart failure hospitalization ***(Singh et al., 2006)***. In a subanalysis of the SmartDelay Determined AV Optimization (SMART-AV) trial, Gold et al showed that patients in the highest quartile of QLV had a 3.21-fold better reverse LV remodelling response after CRT ***(Gold et al., 2011)***.

Whilst acquisition of a single QLV in a chosen coronary vein is simple, the method and complexity of targeting the longest QLV was not addressed by the core studies of QLV, as these were retrospective subanalyses in which implanters did not target QLV ***(Gold et al., 2011; Singh et al., 2006)***. In practice, QLV is measured at the chosen vein and the implanter decides whether the QLV is acceptable. Importantly, however, this approach excludes the possibility that other unmapped sites may actually have a longer QLV and therefore be superior to the chosen site. This issue was addressed by Zanon et al, who systematically screened all anatomically suitable coronary veins in order to identify the longest QLV ***(Zanon Francesco et al., 2014)***. In this hemodynamic study, concordance between the optimum hemodynamic response and a long QLV (>95 ms) was observed in 96.8% of patients. To determine the optimal QLV, however, implanters surveyed an average of 2.9 coronary veins and 6.4 pacing sites.

Whilst procedure times were not quantified, it is likely that intraoperative QLV mapping was time-consuming. In an EnSite mapping study of coronary veins, Mafi-Rad et al mapped an average of 3 veins per patient and mapping time added 19 ± 7 min to the implantation procedure, extending the fluoroscopy time to 21 ± 4 min. ***(Mafi Rad et al., 2015)***. In a sample of 416 de novo CRT-D/CRT-P implants from our centre, mean procedure time ('skin-to-skin') was 77.6 min and fluoroscopy time was 13.0 min (previously unpublished data). Coronary vein mapping, as described by Mafi-Rad et al, would have added 25% to our implantation procedure times and nearly doubled fluoroscopy times. In the present study, we have shown that ECGSync can be used to obtain an entire, patient specific QLV map non-invasively in 26.2 min, obviating intraoperative QLV measurements, invasive EAM and/or additional radiation exposure.

6.4.2. Patterns of LV activation

It is important to appreciate that ECGSync is a ECGMod technique, whereas ECGI is based on the inverse solution. Accordingly, ECGMod takes into account the whole cardiac cycle, whereas most ECGI techniques only determine epicardial activation. Notwithstanding the limitations of ECGI, promising validation data for various techniques have emerged from animal experiments ***(Burnes et al., 2000; Cluitmans et al., 2017)*** and open-chest human studies ***(Ghanem et al., 2005)***. However, Duchateau et al showed a poor correlation between CardioInsight against high-resolution, epicardial contact mapping (CARTO 3 or Rhythmia) in locating the origin of ventricular arrhythmias ***(Duchateau et al., 2019)***. In a comparison of CardioInsight and CARTO in 8 patients, Graham et al showed moderate spatial accuracy of CardioInsight in locating breakthroughs ***(Graham Adam J. et al., 2019)***. Whilst these studies focused on locating breakthroughs, others have explored LEAS. In a comparison of another 123-electrode body surface mapping system (BioSemi), concordance of LEAS with CARTO was poor ***(Kittnar et al., 2018)***.

In this study, we depart from the notion that identification of late activation, rather than breakthroughs, is paramount in CRT. We found that, according to expert adjudication, ECGSync was able to accurately identify LEAS during both sinus rhythm and RV-pacing, using EnSite as reference. Moreover, there was excellent quantitative agreement between ECGSync- and EnSite-derived QLV. In LBBB patients, LEAS were consistently located in the basal lateral wall, with both Ensite and ECGSync. These findings are consistent with those of Derval et al who used CARTO (contact mapping) ***(Derval Nicolas et al., 2017)*** and those of Jia et al, who used a 224-electrode vest (ECGI) ***(Jia et al., 2006)***.

6.4.3. Clinical implications

In this study, we have shown that isochronal maps obtained using ECGSync are similar to those obtained using EnSite, enabling identification of LEAS, according to experienced electrophysiologists. As a notable advantage of ECGSync, it is based on the standard 12-lead ECG, which is universally available. Accordingly, ECGSync can be undertaken prior to CRT device implantation, obviating the need for multiple intraoperative measurements of QLV, invasive EAM or the application of multielectrode ECG vests. Speculatively, ECGSync modelling could also be undertaken in the process of CRT optimization.

With respect to patient selection, it is noteworthy that that QRS duration performs poorly in identifying LEAS ***(Mafi Rad et al., 2016)*** and that selecting patients on QRS duration alone may include those who do not benefit from CRT using conventional LV positions and exclude patients who could benefit from targeted LV lead deployment over LEAS. A pre-implantation QLV map could inform implanters on the potential target site with the longest QLV, regardless of the pre-implant QRS duration. Whether or not QLV mapping could extend current CRT indications beyond a QRS>120ms, remains to be explored.

6.4.4. Study limitations

There are several limitations. First, this study involves a small sample size, as it applies to all studies using invasive EAM. Notwithstanding, we were able to generate 62 LV activation maps using both EAM and ECGSync and have shown meaningful ECGSync maps, as judged by highly experienced electrophysiologists. Second, we have only validated ECGSync using LV endocardial activation maps, as EnSite does not address epicardial activation. Finally, whilst Ensite was used as the 'gold- standard', it is noteworthy that its accuracy reduces as the LV chamber size increases ***(Schilling Richard J. et al., 1998)***.

6.4.5. Conclusions

ECGSync, a ECGMod technique based on a standard 12-lead ECG, provides a QLV map that closely mirrors that obtained using EnSite. We have shown that late LV activation, assessed using ECGSync, -derived QLV map is reproducible and compares well with EnSite. This may have implications for targeting LV lead deployment and the optimization of CRT.

Chapter 7

Discussion and conclusion

This chapter provides the reader with a general discussion and overview of the results presented in this thesis. Ultimately, the aim of this thesis was to utilize vectorcardiography to help improve response rates to CRT. In this respect, we should consider the clinical relevance of the main findings arising from our research and whether this improves upon (i) patient selection for CRT, (ii) prediction of response or (iii) the ability to individually optimize the delivery of CRT. Finally, we discuss and explore potential avenues for future research in this area.

7.1. Improving patient selection for CRT

The 12-lead ECG remains an important clinical tool to help determine patient eligibility for CRT. In **chapter 2**, we explored the use of VCG to help improve patient selection for CRT. Our study demonstrates that baseline QRS_{area} is larger in patients that possess greater electrical dyssynchrony (i.e. LBBB vs. non-LBBB patients) and accordingly, is larger in CRT responders versus non-responders. In keeping with previous studies, we show that QRS_{area} is a significant predictor of acute CRT response ***(De Pooter et al., 2017; Ross et al., 2018b; van Deursen et al., 2015a)***. Another key finding arising from **chapter 2** is the demonstration of a close relationship between QRS_{area} and myocardial scar, which is widely recognised to play an important role in mediating CRT response (Mafi Rad et al., 2016; Nguyên et al., 2018a). Patients with large myocardial scar burdens had significantly lower

QRS_{area} values. This is perhaps unsurprising, given that QRS_{area} is a measure of the strength of unopposed electrical forces propagating through the myocardium ***(van Deursen et al., 2015a)***. Logically, in the presence of scarred (non-conductive) myocardium, there is reduced recruitment

of electrically active tissue and consequently a smaller QRS_{area} (Nguyên et al., 2018a; van Deursen et al., 2015a). We also found that when pacing is delivered over myocardial scar, there is actually an increase in QRS_{area} (but not QRSd) values. This unexpected finding may be particularly relevant in patients with LVFW scar (target area for LV lead implantation), where there is often a delicate balance between ensuring pacing is delivered to regions that are free from scar but within late electrically activated segments (LEAS) ***(Bisson Arnaud et al., 2018)***.

Chapter 3 describes the retrospective evaluation of pre- and post-implant QRSarea, QRSd and QRS morphology in 380 HF patients undergoing CRT implantation. At the time that this study was first conceived, no published data on the role of QRS_{area} was available with respect to predicting clinical outcomes after CRT. However, Emerek et al and Stipdonk et al soon reported that baseline QRS_{area} represented a strong, independent predictor of clinical outcomes following CRT ***(Emerek et al., 2019; van Stipdonk et al., 2018)***. Notably, the clinical endpoints adopted by these studies were restricted to HF hospitalizations and all-cause mortality. Our research group were the first to report on the association between pre-implant QRS_{area} and cause-specific mortality, as well as the risk of MACE and arrhythmic endpoints (sudden cardiac death, ventricular tachycardia/ventricular fibrillation, or shock). We found that QRS_{area} represented a powerful predictor of long-term clinical outcomes after CRT. Notably, baseline QRS_{area} was superior to both QRSd and QRS morphology in predicting the primary (cardiac mortality) and secondary endpoints (total mortality, heart failure hospitalization and MACE) after CRT. In comparison, a conventionally defined LBBB morphology did not predict outcomes following CRT. Despite this, current UK and international guidelines still emphasise the importance of a LBBB QRS morphology as the primary selection criteria for CRT. In fact, based on the latest NICE guidelines, CRT is only indicated in non-LBBB patients that possess one of the following: (i) a significantly prolonged QRSd (≥150ms) or (ii) advanced and refractory heart failure symptoms (NYHA IV). Although this serves to minimize the proportion of patients who are unlikely to benefit from CRT, it may also exclude a proportion of non-LBBB patients that possess an electrophysiological substrate that is still amenable for CRT.

Based on the findings arising from **chapters 2** and **3**, it is conceivable that vectorcardiographic QRS_{area} could be used alongside QRSd and QRS morphology to help guide patient selection for CRT. For example, in borderline cases for CRT (i.e. non-LBBB patients with a QRSd < 150ms), QRS_{area} may be used to help identify a subgroup of these patients that possess sufficient amounts of electrical dyssynchrony to justify the early use of CRT. However, further prospective study is required to validate this hypothesis.

7.2. Novel predictors of CRT response

Studies have shown that whilst CRT helps to reduce the regional and global abnormalities induced by LBBB, it rarely normalises or 'cures' dyssynchronopathy ***(Ploux et al., 2015)***. Consequently, to help predict response on an individual level, the degree of improvement in LV resynchronization following CRT should also be assessed. On this basis, in **chapter 2**, we explored whether ΔQRS_{area} could be used to noninvasively quantify LV resynchronization and help serve as a novel predictor of CRT response. Our results confirm that ΔQRS_{area} is a strong predictor of acute CRT response. In **chapter 3**, we evaluated the use of ΔQRS_{area} as a novel predictor of long-term clinical outcomes following CRT. We found that in patients undergoing CRT, a substantial post-implant reduction in QRS_{area} predicted long-term event-free survival clinical endpoints (with respect to cause-specific mortality). Although ΔQRS_{area} and ΔQRSd were comparable predictors of cardiac mortality following CRT, we demonstrated an important interaction between these two parameters. Namely, the best clinical outcomes were achieved in those who exhibited a concomitant reduction in both QRS_{area} and QRSd.

In **chapter 4**, we introduce a novel interpretation of the vectorcardiogram termed the TSI. In contrast to conventional VCG approaches, TSI plots the x, y and z signals of the vectorcardiogram relative to the major orthogonal planes of the heart (i.e. left anterior oblique, right anterior oblique and 4 chamber view) ***(van Dam, 2017)***. This enables the relationship between the mean TSI signal (i.e. the mean path of cardiac activation) and cardiac anatomy to be better appreciated ***(van Dam, 2017)***. We quantified this relationship using the TSI_{ratio} and demonstrated that this novel VCG-derived parameter was superior to QRSd and LBBB in the prediction of clinical outcomes following CRT.

In **chapter 5**, we introduce a novel ECGI-derived measure of electrical dyssynchrony, termed the electrical dyssynchrony index (EDI). This parameter takes into consideration the spatial dispersion of activation times across the whole of LV cavity. It is therefore a more specific 3D index of electrical dyssynchrony. We found that the degree of electrical dyssynchrony varied widely amongst CRT recipients, including those with a typical LBBB morphology and significantly prolonged QRSd (>150ms). Interestingly, neither QRSd nor LBBB predicted AHR to CRT, which highlights the limitations of 12-lead ECG to guide patient selection for CRT. In contrast, EDI emerged as a powerful predictor of acute CRT response, with patients possessing a large EDI value (≥31ms) having a 14.8x fold greater likelihood of response to CRT.

7.3. Optimizing the delivery of CRT

Although current guidelines recommend the use of QRSd and morphology on the 12-lead ECG to help guide patient selection for CRT, these parameters do not provide any information on the nature or location of late electrically activated segments (LEAS). Alternative approaches to help individualize LV lead placement towards LEAS include the use of ECGI and invasive EAM techniques. In this respect, evidence from recent studies employing these techniques has shown that directing LV pacing over LEAS can provide a superior response to CRT ***(Raja et al., 2019)***. However, these mapping techniques are time-consuming, expensive, and highly invasive, thereby limiting their widespread application in the clinical setting.

On this basis, in **chapter 6**, we explored whether a novel 12-lead ECG-based mapping system (ECGSync) could be used to noninvasively identify the location of LEAS. When validated against invasive, catheter-based mapping techniques (Ensite), we demonstrated that ECGSync could accurately locate the site of maximal LV (electrical) delay from routine 12-lead ECG data. This represents a very important validation study. In fact, despite the availability of different ECGI modalities for well over 10 years, no study has previously validated ECGI against noncontact mapping with respect to its ability to noninvasively identify LEAS.

Another method that has recently been proposed to help optimize LV lead placement is through the invasive measurement of Q-LV intervals. At present, however, QLV can only be obtained from the LV lead at the time of CRT implantation. In **chapter 6**, we also explored whether ECGSync can accurately and noninvasively 'map' QLV times prior to CRT implantation. We observed a good correlation between ECGSync-derived QLV times and those obtained invasively from reconstructed virtual LV EGMs (Ensite). Similarly, there was a good association between ECGSync-derived and epicardial LV lead-derived QLV times.

7.4. Guidelines for future research

To achieve a more complete understanding of the role of QRS_{area} as a predictor of CRT response, including its incremental value to currently available 12-lead ECG parameters, further large-scale, multicentre prospective studies are required. Ideally, this type of study would collect data on 12-lead ECG, echocardiography and clinical outcomes ***(Engels, 2016)***. However, as CRT is now an established therapy for HF patients, it is unlikely that this type of study, which is both expensive and time-consuming to perform, will be conducted in the very near future. However, the methodologies presented in **chapters 2** and **3** demonstrate that vectorcardiograms can be derived rather simply from retrospective analysis of stored 12-lead ECGs. This approach lends itself to further study to provide external validation to the findings presented in this thesis. Notably, one could revisit the

landmark CRT trials and retrospectively assess the predictive value for QRS_{area}. This could help to provide further confirmation as to whether TSI_{ratio} and QRS_{area} are better than QRS duration and QRS morphology in predicting the benefit from CRT.

Second, the results presented in **chapters 5** and **6** may represent the beginning of a new type of ECGI system. This approach could offer the benefits of conventional ECGI systems, but without the major financial and logistically impediments associated with the need for complex body-surface potential mapping (BSPM) systems ***(Cluitmans, 2016)***. As ECGSync is based on routinely available MRI and 12-lead ECG datasets, it naturally lends itself to a far simpler transition into the working clinical environment. However, whilst the data presented in **chapters 5** and **6** is encouraging, it is important to note that the studies undertaken in this thesis represent preliminary validation work. Consequently, only a small cohort of recipients were enrolled into these studies. Further work is required to validate the accuracy of ECGMod.

As a logical continuation to the work presented in **chapter 6,** it would be useful to prospectively evaluate whether LV lead deployment in LEAS (as determined by ECGSync) results in a better response to CRT. Logically, if BiV pacing is delivered from a LV lead positioned over late electrically activated segments (which are free from scar), there is likely to be greater electrical resynchronization and a better response to CRT than pacing from a nonoptimal LV pacing sites.

Finally, as we have already shown that ECGSync can be utilized in the context of paced rhythms, it would be interesting to evaluate the spatial accuracy ECGSync in locating a pacing lead stimulus. Our department is currently evaluating whether, in HF patients who have already undergone CRT implantation, we can utilize computed tomography to precisely locate the position of RV and LV leads on reconstructed patient-specific heart-torso models.

7.5. Conclusion

Throughout this thesis, we have explored the use VCG as a simple, noninvasive tool to help improve CRT response rates. Based on the body of work presented herein, we propose that VCG is superior to conventional 12-lead ECG analysis (QRSd and morphology) in the prediction of response to CRT. Furthermore, we have shown that VCG-derived parameters provide supplementary information that enhances (rather than replaces) the predictive role of 12-lead electrocardiography. Based on work presented in this thesis, it is likely that improvements in patient selection could be achieved by combining 12-lead ECG analysis alongside VCG.

Chapter 8

Contributions

8.1. Main contributions related to this thesis

8.1.1. Journal papers

- **Okafor, O.,** Zegard, A., Van Dam, P., Stegemann, B., Qiu, T., Marshall, H. and Leyva, F., 2019. Changes in QRS Area and QRS Duration After Cardiac Resynchronization Therapy Predict Cardiac Mortality, Heart Failure Hospitalizations, and Ventricular Arrhythmias. Journal of the American Heart Association, 8(21), p.e013539.
- **Okafor, O,** 2019**.** Post-implantation QRS area is a better predictor of cardiac mortality after CRT than QRS duration and LBBB. Cardiac Rhythm News.
- **Okafor, O**., De Bono, J., McNulty, D., Ahmed, A., Marshall, H., Ray, D. and Qiu, T., 2019. Effect of QRS area reduction and myocardial scar on the haemodynamic response to cardiac resynchronization therapy. Submitted to Heart Rhythm.
- Leyva, F., Zegard, A., **Okafor, O**., De Bono, J., McNulty, D., Ahmed, A., Marshall,

H., Ray, D. and Qiu, T., 2019. Survival after cardiac resynchronization therapy: results from 50 084 implantations. *EP Europace,* 21(5), pp.754-762.

8.1.2. International conferences

European Heart Rhythm Association (EHRA) 2020

- **Okafor, O.,** Umar, F., Zegard, A., Stegemann, B., Marshall, H., Lencioni, M., de Bono, J., van Dam, P. and Leyva, F., 2020. Targeting left ventricular lead position in cardiac resynchronization therapy using a novel, 12-lead ECG-based electrocardiographic imaging system. *EP Europace* – In print
- Zegard, A., Qiu, T., McNulty, D., Evison, F., **Okafor, O**., Marshall, H., Gasparini, M. and Leyva, F., 2020. Pacemaker therapy after cardiac valve replacement surgery: implant on heart failure hospitalizations. *EP Europace* – In print

European Heart Rhythm Association (EHRA) 2019

- **Okafor, O.,** Umar, F., Zegard, A., Marshall, H., Flannigan, S., Lencioni, M., de Bono, J., Griffith, M. and Leyva, F., 2019. Electrical activation versus mechanical contraction in cardiac resynchronization therapy recipients: comparison between electroanatomical mapping and feature-tracking cardiovascular magnetic resonance. *EP Europace* Volume 21, Issue Supplement_2, Pages ii1072–ii1092 (921).
- **Okafor, O.,** Van Dam, P., Zegard, A., Stegemann, and Leyva, F., 2019. Post-implantation changes in vectorcardiographic QRS area as a marker of long-term clinical outcomes after cardiac resynchronization therapy. *EP Europace* Volume 21, Issue Supplement_2, Pages ii1072–ii1092 (P541).
- Zegard, A., **Okafor, O**., De Bono, J., McNulty, D., Ahmed, A., Marshall, H., Ray, D., Qiu, T. and Leyva, F., 2019. Survival after cardiac resynchronization therapy: results from 50,084 implantations. *EP Europace* Volume 21, Issue Supplement_2, Pages ii1072–ii1092, (918).
- Zegard, A., **Okafor, O**., De Bono, J., Lencioni, M., Chalil, S., Marshall, H., Hudsmith, L. and Qiu, T. and Leyva, F., 2019. Myocardial phenotype of patients with indications for secondary prevention implantable cardioverter defibrillator therapy: insights from cardiovascular magnetic resonance. *EP Europace* Volume 21, Issue Supplement_2, Pages ii1072–ii1092, (P528).
- Zegard, A., **Okafor, O**., Qiu, T., De Bono, J., Thorne, S., Clif, P., Marshall, H., Hudsmith, L. and Leyva, F., 2019. Long-term outcomes of cardiac resynchronization therapy in adult congenital heart disease. *EP Europace* Volume 21, Issue Supplement_2, Pages ii1072–ii1092, (P542).

8.1.3. National conferences

Heart Rhythm Congress (HRC) 2019

- **Okafor, O.,** Zegard, A., Van Dam, P., Stegemann, B., Qiu, T., Marshall, H. and Leyva, F. Reductions in QRS area predict long-term clinical outcomes after cardiac resynchronization therapy. *European Journal of Arrhythmia & Electrophysiology*. 2019;5(Suppl. 1):abstr20
- **Okafor, O.,** Umar, F., Walton, J., Stegemann, B., Zegard, A., de Bono, J., Lencioni, M., Marshall, H. and Leyva, F. Left ventricular pacing vector optimisation in an ideally deployed quadripolar lead in cardiac resynchronization therapy: effect of optimising QRS area. *European Journal of Arrhythmia & Electrophysiology*. 2019;5(Suppl. 1):abstr33
- **Okafor, O.,** Umar, F., Van Dam, P., Walton, J., Stegemann, B., Zegard, A., Lencioni, M., de Bono, J., Marshall, H., Qiu, T. and Leyva. Three-dimensional 12-lead ECG-based electrocardiographic imaging in cardiac resynchronization therapy recipients – validation against non-contact electroanatomical mapping. *European Journal of Arrhythmia & Electrophysiology*. 2019;5(Suppl. 1):abstr40
- **Okafor, O.,** Van Dam, P., Zegard, A., Stegemann, B., Qiu, T., Marshall, H. and Leyva, F. Vectorcardiographic direction of ventricular activation as a predictor of long-term outcomes after cardiac resynchronization therapy. *European Journal of Arrhythmia & Electrophysiology*. 2019;5(Suppl. 1):abstr100
- Zegard, A., **Okafor, O**., De Bono, J., Steeds, R., Hudsmith, L., Stegemann, B., Jani, A., Marshall, H., Holloway, B., Ray, D. and Qiu, T., Leyva, F. Prognosis of incidental left bundle branch block. *European Journal of Arrhythmia & Electrophysiology*. 2019;5(Suppl. 1):abstr55

References

3D ECG / Cardiogoniometry (CGM) | enverdis GmbH, n.d. URL http://www.enverdis.com/cardiogoniometry.

Abraham William T., Hayes David L., 2003. Cardiac Resynchronization Therapy for Heart Failure. Circulation 108, 2596–2603.

Abraham, W.T., Fisher, W.G., Smith, A.L., Delurgio, D.B., Leon, A.R., Loh, E., Kocovic, D.Z., Packer, M., Clavell, A.L., Hayes, D.L., Ellestad, M., Trupp, R.J., Underwood, J., Pickering, F., Truex, C., McAtee, P., Messenger, J., MIRACLE Study Group. Multicenter InSync Randomized Clinical Evaluation, 2002. Cardiac resynchronization in chronic heart failure. N. Engl. J. Med. 346, 1845–1853.

Abraham, W.T., Young, J.B., León, A.R., Adler, S., Bank, A.J., Hall, S.A., Lieberman, R., Liem, L.B., O'Connell, J.B., Schroeder, J.S., Wheelan, K.R., 2004. Effects of Cardiac Resynchronization on Disease Progression in Patients With Left Ventricular Systolic Dysfunction, an Indication for an Implantable Cardioverter-Defibrillator, and Mildly Symptomatic Chronic Heart Failure. Circulation 110, 2864–2868.

Appert, L., Menet, A., Altes, A., Ennezat, P.V., Bardet-Bouchery, H., Binda, C., Guyomar, Y., Delelis, F., Castel, A.-L., Le Goffic, C., Guerbaai, R.-A., Graux, P., Tribouilloy, C., Maréchaux, S., 2019. Clinical Significance of Electromechanical Dyssynchrony and QRS Narrowing in Patients With Heart Failure Receiving Cardiac Resynchronization Therapy. Can J Cardiol 35, 27–34.

Asbach, S., Hartmann, M., Wengenmayer, T., Graf, E., Bode, C., Biermann, J., 2013. Vector Selection of a Quadripolar Left Ventricular Pacing Lead Affects Acute Hemodynamic Response to Cardiac Resynchronization Therapy: A Randomized Cross-Over Trial. PLoS One 8.

Auricchio, A., Delnoy, P.-P., Butter, C., Brachmann, J., Van Erven, L., Spitzer, S., Moccetti, T., Seifert, M., Markou, T., Laszo, K., Regoli, F., for the Collaborative Study Group, Ramos, Marta Aceña, Pasotti, E., Scopigni, F., Ramos, Marta Acenã, Hagne, C., Siclari, F., Demertzis, S., Sinha, A., Schalji, M., Wellens, H.J.J., Padeletti, L., Van Hemel, N., 2014. Feasibility, safety, and short-term outcome of leadless ultrasound-based endocardial left ventricular resynchronization in heart failure patients: results of the Wireless Stimulation Endocardially for CRT (WiSE-CRT) study. EP Europace 16, 681–688.

Auricchio, A., Faletra, F.F., 2020. Use of Contemporary Imaging Techniques for Electrophysiological and Device Implantation Procedures. JACC Cardiovasc Imaging 13, 851–865.

Auricchio, A., Fantoni, C., Regoli, F., Carbucicchio, C., Goette, A., Geller, C., Kloss, M., Klein, H., 2004a. Characterization of left ventricular activation in patients with heart failure and left bundle-branch block. Circulation 109, 1133–1139.

Auricchio, A., Fantoni, C., Regoli, F., Carbucicchio, C., Goette, A., Geller, C., Kloss, M., Klein, H., 2004b. Characterization of left ventricular activation in patients with heart failure and left bundle-branch block. Circulation 109, 1133–1139.

Auricchio, A., Prinzen, F.W., 2017. Enhancing Response in the Cardiac Resynchronization Therapy Patient: The 3B Perspective—Bench, Bits, and Bedside. JACC: Clinical Electrophysiology 3, 1203–1219.

Auricchio, A., Stellbrink, C., Sack, S., Block, M., Vogt, J., Bakker, P., Huth, C., Schöndube, F., Wolfhard, U., Böcker, D., Krahnefeld, O., Kirkels, H., Pacing Therapies in Congestive Heart Failure (PATH-CHF) Study Group, 2002. Long-term clinical effect of hemodynamically optimized cardiac resynchronization therapy in patients with heart failure and ventricular conduction delay. J. Am. Coll. Cardiol. 39, 2026–2033.

Auricchio Angelo, Lumens Joost, Prinzen Frits W., 2014. Does Cardiac Resynchronization Therapy Benefit Patients With Right Bundle Branch Block. Circulation: Arrhythmia and Electrophysiology 7, 532–542.

Badilini, F., Erdem, T., Zareba, W., Moss, A.J., 2005. ECGScan: a method for conversion of paper electrocardiographic printouts to digital electrocardiographic files. J Electrocardiol 38, 310–318.

Barold, S.S., Herweg, B., 2015. Cardiac Resynchronization in Patients with Atrial Fibrillation. J Atr Fibrillation 8, 1383.

Bear, L.R., Huntjens, P.R., Walton, R.D., Bernus, O., Coronel, R., Dubois, R., 2018. Cardiac electrical dyssynchrony is accurately detected by noninvasive electrocardiographic imaging. Heart Rhythm 15, 1058–1069.

Bertaglia, E., Migliore, F., Baritussio, A., De Simone, A., Reggiani, A., Pecora, D., D'Onofrio, A., Rapacciuolo, A., Savarese, G., Pierantozzi, A., Marenna, B., Ruffa, F., Campari, M., Malacrida, M., Stabile, G., 2017. Stricter criteria for left bundle branch block diagnosis do not improve response to CRT. Pacing Clin Electrophysiol 40, 850–856.

Bilchick, K.C., Kamath, S., DiMarco, J.P., Stukenborg, G.J., 2010. Bundle-branch block morphology and other predictors of outcome after cardiac resynchronization therapy in Medicare patients. Circulation 122, 2022–2030.

Bisson Arnaud, Pucheux Julien, Andre Clémentine, Bernard Anne, Pierre Bertrand, Babuty Dominique, Fauchier Laurent, Clementy Nicolas, 2018. Localization of Left Ventricular Lead Electrodes in Relation to Myocardial Scar in Patients Undergoing Cardiac Resynchronization Therapy. Journal of the American Heart Association 7,

Bogaard, M.D., Houthuizen, P., Bracke, F.A., Doevendans, P.A., Prinzen, F.W., Meine, M., van Gelder, B.M., 2011. Baseline left ventricular dP/dtmax rather than the acute improvement in dP/dtmax predicts clinical outcome in patients with cardiac resynchronization therapy. Eur J Heart Fail 13, 1126–1132.

Boogers, M.J., Chen, J., van Bommel, R.J., Borleffs, C.J.W., Dibbets-Schneider, P., van der Hiel, B., Al Younis, I., Schalij, M.J., van der Wall, E.E., Garcia, E.V., Bax, J.J., 2011. Optimal left ventricular lead position assessed with phase analysis on gated myocardial perfusion SPECT. Eur J Nucl Med Mol Imaging 38, 230–238.

Boriani, G., Gardini, B., Diemberger, I., Reggiani, M.L.B., Biffi, M., Martignani, C., Ziacchi, M., Valzania, C., Gasparini, M., Padeletti, L., Branzi, A., 2012. Meta-analysis of randomized controlled trials evaluating left ventricular vs. biventricular pacing in heart failure: effect on all-cause mortality and hospitalizations. European Journal of Heart Failure 14, 652–660.

Boriani, G., Kranig, W., Donal, E., Calo, L., Casella, M., Delarche, N., Lozano, I.F., Ansalone, G., Biffi, M., Boulogne, E., Leclercq, C., 2010. A randomized double-blind comparison of biventricular versus left ventricular stimulation for cardiac resynchronization therapy: The Biventricular versus Left Univentricular Pacing with ICD Back-up in Heart Failure Patients (B-LEFT HF) trial. American Heart Journal 159, 1052-1058.e1.

Breithardt, O.A., Sinha, A.M., Schwammenthal, E., Bidaoui, N., Markus, K.U., Franke, A., Stellbrink, C., 2003. Acute effects of cardiac resynchronization therapy on functional mitral regurgitation in advanced systolic heart failure. J. Am. Coll. Cardiol. 41, 765–770.

Brignole, M., Auricchio, A., Baron-Esquivias, G., Bordachar, P., Boriani, G., Breithardt, O.-A., Cleland, J., Deharo, J.-C., Delgado, V., Elliott, P.M., Gorenek, B., Israel, C.W., Leclercq, C., Linde, C., Mont, L., Padeletti, L., Sutton, R., Vardas, P.E., Zamorano, J.L., Achenbach, S., Baumgartner, H., Bax, J.J., Bueno, H., Dean, V., Deaton, C., Erol, C., Fagard, R., Ferrari, R., Hasdai, D., Hoes, A.W., Kirchhof, P., Knuuti, J., Kolh, P., Lancellotti, P., Linhart, A., Nihoyannopoulos, P., Piepoli, M.F., Ponikowski, P., Sirnes, P.A., Tamargo, J.L., Tendera, M., Torbicki, A., Wijns, W., Windecker, S., Kirchhof, P., Blomstrom-Lundqvist, C., Badano, L.P., Aliyev, F., Bänsch, D., Baumgartner, H., Bsata, W., Buser, P., Charron, P., Daubert, J.-C., Dobreanu, D., Faerestrand, S., Hasdai, D., Hoes, A.W., Le Heuzey, J.-Y., Mavrakis, H., McDonagh, T., Merino, J.L., Nawar, M.M., Nielsen, J.C., Pieske, B., Poposka, L., Ruschitzka, F., Tendera, M., Van Gelder, I.C., Wilson, C.M., 2013. 2013 ESC Guidelines on cardiac pacing and cardiac resynchronization therapyThe Task Force on cardiac pacing and resynchronization therapy of the European Society of Cardiology (ESC). Developed in collaboration with the European Heart Rhythm Association (EHRA). Europace 15, 1070–1118.

Bristow, M.R., Saxon, L.A., Boehmer, J., Krueger, S., Kass, D.A., De Marco, T., Carson, P., DiCarlo, L., DeMets, D., White, B.G., DeVries, D.W., Feldman, A.M., 2004. Cardiac-Resynchronization Therapy with or without an Implantable Defibrillator in Advanced Chronic Heart Failure. New England Journal of Medicine 350, 2140–2150.

Bryant, A.R., Wilton, S.B., Lai, M.P., Exner, D.V., 2013. Association between QRS duration and outcome with cardiac resynchronization therapy: a systematic review and meta-analysis. J Electrocardiol 46, 147–155.

Burch, G.E., 1985. The history of vectorcardiography. Medical History 29, 103–131.

Burnes, J.E., Taccardi, B., Rudy, Y., 2000. A Noninvasive Imaging Modality for Cardiac Arrhythmias. Circulation 102, 2152–2158.

Burri, H., Prinzen, F.W., Gasparini, M., Leclercq, C., 2017. Left univentricular pacing for cardiac resynchronization therapy. EP Europace 19, 912–919.

Cano, Ó., Vijayaraman, P., 2021. LBB Area Pacing for Cardiac Resynchronization Therapy. American College of Cardiology.

Caputo, M.L., van Stipdonk, A., Illner, A., D'Ambrosio, G., Regoli, F., Conte, G., Moccetti, T., Klersy, C., Prinzen, F.W., Vernooy, K., Auricchio, A., 2018. The definition of left bundle branch block influences the response to cardiac resynchronization therapy. Int. J. Cardiol. 269, 165–169.

Cazeau, S., Leclercq, C., Lavergne, T., Walker, S., Varma, C., Linde, C., Garrigue, S., Kappenberger, L., Haywood, G.A., Santini, M., Bailleul, C., Daubert, J.C., Multisite Stimulation in Cardiomyopathies (MUSTIC) Study Investigators, 2001. Effects of multisite biventricular pacing in patients with heart failure and intraventricular conduction delay. N. Engl. J. Med. 344, 873–880.

Chalil, S., Foley, P.W.X., Muyhaldeen, S.A., Patel, K.C.R., Yousef, Z.R., Smith, R.E.A., Frenneaux, M.P., Leyva, F., 2007. Late gadolinium enhancement-cardiovascular magnetic resonance as a predictor of response to cardiac resynchronization therapy in patients with ischaemic cardiomyopathy. Europace 9, 1031–1037.

Cheng, A., Helm, R.H., Abraham, T.P., 2009. Pathophysiological mechanisms underlying ventricular dyssynchrony. Europace 11, v10–v14.

Chou, T.-C., Helm, R.A., Kaplan, S., 1974. Clinical vectorcardiography, 2d ed. ed. Grune & Stratton, New York.

Chung, E.S., Leon, A.R., Tavazzi, L., Sun, J.-P., Nihoyannopoulos, P., Merlino, J., Abraham, W.T., Ghio, S., Leclercq, C., Bax, J.J., Yu, C.-M., Gorcsan, J., St John Sutton, M., De Sutter, J., Murillo, J., 2008. Results of the Predictors of Response to CRT (PROSPECT) trial. Circulation 117, 2608–2616.

Cleland, J.G.F., Daubert, J.-C., Erdmann, E., Freemantle, N., Gras, D., Kappenberger, L., Tavazzi, L., 2005. The Effect of Cardiac Resynchronization on Morbidity and Mortality in Heart Failure. New England Journal of Medicine 352, 1539–1549.

Cluitmans, M., 2016. Noninvasive reconstruction of cardiac electrical activity: Mathematical innovation, in vivo validation and human application. University of Maastricht.

Cluitmans, M.J.M., Bonizzi, P., Karel, J.M.H., Das, M., Kietselaer, B.L.J.H., de Jong, M.M.J.,

Prinzen, F.W., Peeters, R.L.M., Westra, R.L., Volders, P.G.A., 2017. In Vivo Validation of Electrocardiographic Imaging. JACC: Clinical Electrophysiology 3, 232–242.

Daubert, C., Behar, N., Martins, R.P., Mabo, P., Leclercq, C., 2016. Avoiding non-responders to cardiac resynchronization therapy: a practical guide. Eur Heart J ehw270.

De Pooter, J., El Haddad, M., De Buyzere, M., Aranda, H.A., Cornelussen, R., Stegemann, B., Rinaldi, C.A., Sterlinski, M., Sokal, A., Francis, D.P., Jordaens, L., Stroobandt, R.X., Van Heuverswyn, F., Timmermans, F., 2017. Biventricular Paced QRS Area Predicts Acute Hemodynamic CRT Response Better Than QRS Duration or QRS Amplitudes: Paced QRS Area Predicts CRT Response. Journal of Cardiovascular Electrophysiology 28, 192–200.

de Roest, G.J., Wu, L., de Cock, C.C., Hendriks, M.L., Delnoy, P.P.H.M., van Rossum, A.C., Allaart, C.P., 2014. Scar tissue-guided left ventricular lead placement for cardiac resynchronization therapy in patients with ischemic cardiomyopathy: an acute pressure-volume loop study. Am. Heart J. 167, 537–545.

Del Greco, M., Marini, M., Bonmassari, R., 2012. Implantation of a biventricular implantable cardioverter-defibrillator guided by an electroanatomic mapping system. Europace 14, 107–111.

Del Negro, A., n.d. Combined CRT/ICD Devices Show Promise: MIRACLE ICD Trial [WWW Document]. Medscape. URL http://www.medscape.com/viewarticle/456492 (accessed 4.19.19).

Derval, N., Steendijk, P., Gula, L.J., Deplagne, A., Laborderie, J., Sacher, F., Knecht, S., Wright, M., Nault, I., Ploux, S., Ritter, P., Bordachar, P., Lafitte, S., Réant, P., Klein, G.J., Narayan, S.M., Garrigue, S., Hocini, M., Haissaguerre, M., Clementy, J., Jaïs, P., 2010. Optimizing Hemodynamics in Heart Failure Patients by Systematic Screening of Left Ventricular Pacing Sites: The Lateral Left Ventricular Wall and the Coronary Sinus Are Rarely the Best Sites. Journal of the American College of Cardiology 55, 566–575.

Derval Nicolas, Duchateau Josselin, Mahida Saagar, Eschalier Romain, Sacher Frederic, Lumens Joost, Cochet Hubert, Denis Arnaud, Pillois Xavier, Yamashita Seigo, Komatsu Yuki, Ploux Sylvain, Amraoui Sana, Zemmoura Adlane, Ritter Philippe, Hocini Mélèze, Haissaguerre Michel, Jaïs Pierre, Bordachar Pierre, 2017. Distinctive Left Ventricular Activations Associated With ECG Pattern in Heart Failure Patients. Circulation: Arrhythmia and Electrophysiology 10, e005073.

Duchateau, J., Sacher, F., Pambrun, T., Derval, N., Chamorro-Servent, J., Denis, A., Ploux, S., Hocini, M., Jaïs, P., Bernus, O., Haïssaguerre, M., Dubois, R., 2019. Performance and limitations of noninvasive cardiac activation mapping. Heart Rhythm 16, 435–442.

Duckett, S.G., Ginks, M., Shetty, A.K., Bostock, J., Gill, J.S., Hamid, S., Kapetanakis, S.,

Cunliffe, E., Razavi, R., Carr-White, G., Rinaldi, C.A., 2011. Invasive Acute Hemodynamic Response to Guide Left Ventricular Lead Implantation Predicts Chronic Remodeling in Patients Undergoing Cardiac Resynchronization Therapy. Journal of the American College of Cardiology 58, 1128–1136.

Dupont, M., Rickard, J., Baranowski, B., Varma, N., Dresing, T., Gabi, A., Finucan, M., Mullens, W., Wilkoff, B.L., Tang, W.H.W., 2012. Differential response to cardiac resynchronization therapy and clinical outcomes according to QRS morphology and QRS duration. J. Am. Coll. Cardiol. 60, 592–598.

Duraes, A.R., Passos, L.C.S., Falcon, H.C. de S., Marques, V.R., Fern, M., Medeiros, es da S., Martins, J. de C.S., 2016. Bundle Branch Block: Right and Left Prognosis Implications. Interventional Cardiology Journal 2.

Easy Notecards [WWW Document], n.d. . Print Cardiac Electrocardiogram flashcards | Easy Notecards. URL https://www.easynotecards.com/print_list/77278 (accessed 4.3.20).

Ellery, S., Williams, L., Frenneaux, M., 2006. Role of resynchronisation therapy and implantable cardioverter defibrillators in heart failure. Postgrad Med J 82, 16–23.

El-Sherif, N., Amay-Y-Leon, F., Schonfield, C., Scherlag, B.J., Rosen, K., Lazzara, R., Wyndham, C., 1978. Normalization of bundle branch block patterns by distal His bundle pacing. Clinical and experimental evidence of longitudinal dissociation in the pathologic his bundle. Circulation 57, 473–483.

Emerek, K., Friedman, D.J., Sørensen, P.L., Hansen, S.M., Larsen, J.M., Risum, N., Thøgersen, A.M., Graff, C., Kisslo, J., Søgaard, P., Atwater, B.D., 2019. Vectorcardiographic QRS area is associated with long-term outcome after cardiac resynchronization therapy. Heart Rhythm 16, 213–219.

Engels, E.B., 2016. Something old, something new: vectorcardiographic loop size and response to cardiac resynchronization therapy. Maastricht University.

Engels, E.B., Mafi-Rad, M., van Stipdonk, A.M.W., Vernooy, K., Prinzen, F.W., 2016. Why QRS Duration Should Be Replaced by Better Measures of Electrical Activation to Improve Patient Selection for Cardiac Resynchronization Therapy. Journal of Cardiovascular Translational Research 9, 257–265.

Engels, E.B., Strik, M., van Middendorp, L.B., Kuiper, M., Vernooy, K., Prinzen, F.W., 2017. Prediction of optimal cardiac resynchronization by vectors extracted from electrograms in dyssynchronous canine hearts: ENGELS ET AL . Journal of Cardiovascular Electrophysiology 28, 944–951.

Engels, E.B., Végh, E.M., Van Deursen, C.J.M., Vernooy, K., Singh, J.P., Prinzen, F.W., 2015. T-wave area predicts response to cardiac resynchronization therapy in patients with left bundle branch block. J. Cardiovasc. Electrophysiol. 26, 176–183.

Epstein, A.E., DiMarco, J.P., Ellenbogen, K.A., Estes, N.A.M., Freedman, R.A., Gettes, L.S., Gillinov, A.M., Gregoratos, G., Hammill, S.C., Hayes, D.L., Hlatky, M.A., Newby, L.K., Page, R.L., Schoenfeld, M.H., Silka, M.J., Stevenson, L.W., Sweeney, M.O., American College of Cardiology Foundation, American Heart Association Task Force on Practice Guidelines, Heart Rhythm Society, 2013. 2012 ACCF/AHA/HRS focused update incorporated into the ACCF/AHA/HRS 2008 guidelines for device-based therapy of cardiac rhythm abnormalities: a report of the American College of Cardiology Foundation/American Heart Association Task Force on Practice Guidelines and the Heart Rhythm Society. Circulation 127, e283-352.

Everdingen, W. van, Zweerink, A., Cramer, M.J., Doevendans, P., Nguyen, U.C., Rossum, A. van, Prinzen, F., Vernooy, K., Allaart, C., Meine, M., 2018. Can We Use the Intrinsic Left Ventricular Delay (qlv) to Optimize the Pacing Configuration for Cardiac Resynchronization Therapy with a Quadripolar Left Ventricular Lead? J Am Coll Cardiol 71, A945.

Fantoni, C., Kawabata, M., Massaro, R., Regoli, F., Raffa, S., Arora, V., Salerno-Uriarte, J.A., Klein, H.U., Auricchio, A., 2005. Right and left ventricular activation sequence in patients with heart failure and right bundle branch block: a detailed analysis using three-dimensional non-fluoroscopic electroanatomic mapping system. J. Cardiovasc. Electrophysiol. 16, 112–119; discussion 120-121.

Fleiss, J.L., 1971. Measuring nominal scale agreement among many raters. Psychological Bulletin.

Foley, P., 2011. CARDIOVASCULAR MAGNETIC RESONANCE IN THE PREDICTION OF OUTCOME AFTER CARDIAC RESYNCHRONISATION THERAPY 275.

Fornwalt, B.K., Sprague, W.W., BeDell, P., Suever, J.D., Gerritse, B., Merlino, J.D., Fyfe, D.A., León, A.R., Oshinski, J.N., 2010. Agreement is poor among current criteria used to define response to cardiac resynchronization therapy. Circulation 121, 1985–1991.

Friedman, D.J., Emerek, K., Hansen, S.M., Polcwiartek, C., Sørensen, P.L., Loring, Z., Sutter, J., Søgaard, P., Kisslo, J., Graff, C., Atwater, B.D., 2019. Non-invasively quantified changes in left ventricular activation predict outcomes in patients undergoing cardiac resynchronization therapy. Journal of Cardiovascular Electrophysiology 30, 2475–2483.

Fujiwara, R., Yoshida, A., Fukuzawa, K., Takei, A., Kiuchi, K., Itoh, M., Imamura, K., Suzuki, A., Nakanishi, T., Yamashita, S., Matsumoto, A., Tanaka, H., Hirata, K.-I., 2014. Discrepancy between electrical and mechanical dyssynchrony in patients with heart failure and an electrical disturbance. Pacing Clin Electrophysiol 37, 576–584.

Gage, R.M., Curtin, A.E., Burns, K.V., Ghosh, S., Gillberg, J.M., Bank, A.J., 2017. Changes in electrical dyssynchrony by body surface mapping predict left ventricular remodeling in patients with cardiac resynchronization therapy. Heart Rhythm 14, 392–399.

Gasparini, M., Bocchiardo, M., Lunati, M., Antonio Ravazzi, P., Santini, M., Zardini, M., Signorelli, S., Passardi, M., Klersy, C., 2006. Comparison of 1-year effects of left ventricular and biventricular pacing in patients with heart failure who have ventricular arrhythmias and left bundle-branch block: The Bi vs Left Ventricular Pacing: An International Pilot Evaluation on Heart Failure Patients with Ventricular Arrhythmias (BELIEVE) multicenter prospective randomized pilot study. American Heart Journal 152, 155.e1-155.e7.

Gasparini, M., Leclercq, C., Lunati, M., Landolina, M., Auricchio, A., Santini, M., Boriani, G., Lamp, B., Proclemer, A., Curnis, A., Klersy, C., Leyva, F., 2013. Cardiac Resynchronization Therapy in Patients With Atrial Fibrillation. JACC: Heart Failure 1, 500–507.

Gasparini, M., Regoli, F., Galimberti, P., Ceriotti, C., Cappelleri, A., 2009. Cardiac resynchronization therapy in heart failure patients with atrial fibrillation. EP Europace 11, v82–v86.

Ghanem, R.N., Jia, P., Ramanathan, C., Ryu, K., Markowitz, A., Rudy, Y., 2005. Noninvasive Electrocardiographic Imaging (ECGI): Comparison to intraoperative mapping in patients. Heart Rhythm 2, 339–354.

Ghosh, S., Rudy, Y., 2005. Accuracy of Quadratic Versus Linear Interpolation in Noninvasive Electrocardiographic Imaging (ECGI). Ann Biomed Eng 33, 1187–1201.

Ghosh, S., Silva, J.N.A., Canham, R.M., Bowman, T.M., Zhang, J., Rhee, E.K., Woodard, P.K., Rudy, Y., 2011. Electrophysiologic substrate and intraventricular left ventricular dyssynchrony in nonischemic heart failure patients undergoing cardiac resynchronization therapy. Heart Rhythm 8, 692–699.

Glikson, M., Nielsen, J.C., Kronborg, M.B., Michowitz, Y., Auricchio, A., Barbash, I.M., Barrabés, J.A., Boriani, G., Braunschweig, F., Brignole, M., Burri, H., Coats, A.J.S., Deharo, J.-C., Delgado, V., Diller, G.-P., Israel, C.W., Keren, A., Knops, R.E., Kotecha, D., Leclercq, C., Merkely, B., Starck, C., Thylén, I., Tolosana, J.M., ESC Scientific Document Group, Leyva, F., Linde, C., Abdelhamid, M., Aboyans, V., Arbelo, E., Asteggiano, R., Barón-Esquivias, G., Bauersachs, J., Biffi, M., Birgersdotter-Green, U., Bongiorni, M.G., Borger, M.A., Čelutkienė, J., Cikes, M., Daubert, J.-C., Drossart, I., Ellenbogen, K., Elliott, P.M., Fabritz, L., Falk, V., Fauchier, L., Fernández-Avilés, F., Foldager, D., Gadler, F., De Vinuesa, P.G.G., Gorenek, B., Guerra, J.M., Hermann Haugaa, K., Hendriks, J., Kahan, T., Katus, H.A., Konradi, A., Koskinas, K.C., Law, H., Lewis, B.S., Linker, N.J., Løchen, M.-L., Lumens, J., Mascherbauer, J., Mullens, W., Nagy, K.V., Prescott, E., Raatikainen, P., Rakisheva, A., Reichlin, T., Ricci, R.P., Shlyakhto, E., Sitges, M., Sousa-Uva, M., Sutton, R., Suwalski, P., Svendsen, J.H., Touyz, R.M., Van Gelder, I.C., Vernooy, K., Waltenberger, J., Whinnett, Z., Witte, K.K., Kronborg, M.B., Michowitz, Y., Auricchio, A., Barbash, I.M., Barrabés, J.A., Boriani, G., Braunschweig, F., Brignole, M., Burri, H., Coats, A.J.S., Deharo, J.-C., Delgado, V., Diller, G.-P., Israel, C.W., Keren, A., Knops, R.E., Kotecha, D., Leclercq, C., Merkely, B., Starck, C., Thylén, I., Tolosana, J.M., 2021. 2021 ESC Guidelines on

cardiac pacing and cardiac resynchronization therapy. European Heart Journal 42, 3427–3520.

Gnani, S., Ellis, C., Majeed, A., 2001. Co-existing conditions of health services associated with heart failure: general practice based study. Health Statistics Quarterly 12, 27–33.

Gold Michael R., Thébault Christophe, Linde Cecilia, Abraham William T., Gerritse Bart, Ghio Stefano, St. John Sutton Martin, Daubert Jean-Claude, 2012. Effect of QRS Duration and Morphology on Cardiac Resynchronization Therapy Outcomes in Mild Heart Failure. Circulation 126, 822–829.

Gold, M.R., Birgersdotter-Green, U., Singh, J.P., Ellenbogen, K.A., Yu, Y., Meyer, T.E., Seth, M., Tchou, P.J., 2011. The relationship between ventricular electrical delay and left ventricular remodelling with cardiac resynchronization therapy. Eur Heart J 32, 2516–2524.

Gold, M.R., Leman, R.B., Wold, N., Sturdivant, J.L., Yu, Y., 2014. The effect of left ventricular electrical delay on the acute hemodynamic response with cardiac resynchronization therapy. J. Cardiovasc. Electrophysiol. 25, 624–630.

Gold, M.R., Singh, J.P., Ellenbogen, K.A., Yu, Y., Wold, N., Meyer, T.E., Birgersdoter-Green, U., 2016. Interventricular Electrical Delay Is Predictive of Response to Cardiac Resynchronization Therapy. JACC: Clinical Electrophysiology 2, 438–447.

Graham Adam J., Orini Michele, Zacur Ernesto, Dhillon Gurpreet, Daw Holly, Srinivasan Niel T., Lane Jem D., Cambridge Alex, Garcia Jason, O'Reilly Nanci J., Whittaker-Axon Sarah, Taggart Peter, Lowe Martin, Finlay Malcolm, Earley Mark J., Chow Antony, Sporton Simon, Dhinoja Mehul, Schilling Richard J., Hunter Ross J., Lambiase Pier D., 2019. Simultaneous Comparison of Electrocardiographic Imaging and Epicardial Contact Mapping in Structural Heart Disease. Circulation: Arrhythmia and Electrophysiology 12, e007120.

Grishman, A., Scherlis, L., Lasser, R.P., 1953. Spatial vectorcardiography. Am. J. Med. 14, 184–200.

Healey, J.S., Hohnloser, S.H., Exner, D.V., Birnie, D.H., Parkash, R., Connolly, S.J., Krahn, A.D., Simpson, C.S., Thibault, B., Basta, M., Philippon, F., Dorian, P., Nair, G.M., Sivakumaran, S., Yetisir, E., Wells, G.A., Tang, A.S.L., 2012. Cardiac Resynchronization Therapy in Patients With Permanent Atrial Fibrillation: Results From the Resynchronization for Ambulatory Heart Failure Trial (RAFT). Circ Heart Fail 5, 566–570.

Higgins, S.L., Hummel, J.D., Niazi, I.K., Giudici, M.C., Worley, S.J., Saxon, L.A., Boehmer, J.P., Higginbotham, M.B., De Marco, T., Foster, E., Yong, P.G., 2003. Cardiac resynchronization therapy for the treatment of heart failure in patients with intraventricular conduction delay and malignant ventricular tachyarrhythmias. Journal of the American College of Cardiology 42, 1454–1459.

Higgins, S.L., Yong, P., Sheck, D., McDaniel, M., Bollinger, F., Vadecha, M., Desai, S., Meyer, D.B., 2000. Biventricular pacing diminishes the need for implantable cardioverter defibrillator therapy. Ventak CHF Investigators. J. Am. Coll. Cardiol. 36, 824–827.

Hyde, E.R., Behar, J.M., Claridge, S., Jackson, T., Lee, A.W.C., Remme, E.W., Sohal, M., Plank, G., Razavi, R., Rinaldi, C.A., Niederer, S.A., 2015. Beneficial Effect on Cardiac Resynchronization From Left Ventricular Endocardial Pacing Is Mediated by Early Access to High Conduction Velocity Tissue. Circulation: Arrhythmia and Electrophysiology 8, 1164–1172.

Intini, A., Goldstein, R.N., Jia, P., Ramanathan, C., Ryu, K., Giannattasio, B., Gilkeson, R., Stambler, B.S., Brugada, P., Stevenson, W.G., Rudy, Y., Waldo, A.L., 2005. Electrocardiographic imaging (ECGI), a novel diagnostic modality used for mapping of focal left ventricular tachycardia in a young athlete. Heart Rhythm 2, 1250–1252.

Jacobsson, J., Borgquist, R., Reitan, C., Ghafoori, E., Chatterjee, N.A., Kabir, M., Platonov, P.G., Carlson, J., Singh, J.P., Tereshchenko, L.G., 2016. Usefulness of the Sum Absolute QRST Integral to Predict Outcomes in Patients Receiving Cardiac Resynchronization Therapy. Am. J. Cardiol. 118, 389–395.

Jaffe, L.M., Morin, D.P., 2014. Cardiac Resynchronization Therapy: History, Present Status, and Future Directions. Ochsner J 14, 596–607.

Jafferani, A., Leal, M., 2019. Advances in Cardiac Resynchronization Therapy. J Innov Cardiac Rhythm Manage. 10, 3681–3693.

Jastrzębski, M., Baranchuk, A., Fijorek, K., Kisiel, R., Kukla, P., Sondej, T., Czarnecka, D., 2019. Cardiac resynchronization therapy-induced acute shortening of QRS duration predicts long-term mortality only in patients with left bundle branch block. Europace 21, 281–289.

Jia, P., Ramanathan, C., Ghanem, R.N., Ryu, K., Varma, N., Rudy, Y., 2006. Electrocardiographic imaging of cardiac resynchronization therapy in heart failure: Observation of variable electrophysiologic responses. Heart Rhythm 3, 296–310.

Johnson, W.B., Vatterott, P.J., Peterson, M.A., Bagwe, S., Underwood, R.D., Bank, A.J., Gage, R.M., Ramza, B., Foreman, B.W., Splett, V., Haddad, T., Gillberg, J.M., Ghosh, S., 2017. Body surface mapping using an ECG belt to characterize electrical heterogeneity for different left ventricular pacing sites during cardiac resynchronization: Relationship with acute hemodynamic improvement. Heart Rhythm 14, 385–391.

Kashani, A., Barold, S.S., 2005. Significance of QRS complex duration in patients with heart failure. J. Am. Coll. Cardiol. 46, 2183–2192.

Keele, K.D., 1965. A History of Electrocardiography. Med Hist 9, 193–194.

Khan, F.Z., Virdee, M.S., Palmer, C.R., Pugh, P.J., O'Halloran, D., Elsik, M., Read, P.A., Begley, D., Fynn, S.P., Dutka, D.P., 2012. Targeted left ventricular lead placement to guide cardiac resynchronization therapy: the TARGET study: a randomized, controlled trial. J. Am. Coll. Cardiol. 59, 1509–1518.

Kittnar, O., Riedlbauchová, L., Adla, T., Suchánek, V., Tomis, J., Ložek, M., Valeriánová, A., Hrachovina, M., Popková, M., Veselka, J., Janoušek, J., Lhotská, L., 2018. Outcome of resynchronization therapy on superficial and endocardial electrophysiological findings. Physiol Res 67, S601–S610.

Kiuchi, K., Yoshida, A., Fukuzawa, K., Takano, T., Kanda, G., Takami, K., Hirata, K., 2007. Identification of the right ventricular pacing site for cardiac resynchronization therapy (CRT) guided by electroanatomical mapping (CARTO). Circ. J. 71, 1599–1605.

Kligfield, P., Badilini, F., Denjoy, I., Babaeizadeh, S., Clark, E., De Bie, J., ... & Green, C. L. (2018). Comparison of automated interval measurements by widely used algorithms in digital electrocardiographs. American heart journal, 200, 1-10.

Kloppe, A., 2015. Clinical Evidence Demonstrating the Benefit of MultiPoint Pacing Cardiac Resynchronisation Therapy.

Kočková, R., Sedláček, K., Wichterle, D., Šikula, V., Tintěra, J., Jansová, H., Pravečková, A., Langová, R., Krýže, L., El-Husseini, W., Segeťová, M., Kautzner, J., 2018. Cardiac resynchronization therapy guided by cardiac magnetic resonance imaging: A prospective, single-centre randomized study (CMR-CRT). Int. J. Cardiol. 270, 325–330.

Kors, J.A., Van Herpen, G., Sittig, A.C., Van Bemmel, J.H., 1990. Reconstruction of the Frank vectorcardiogram from standard electrocardiographic leads: diagnostic comparison of different methods. Eur Heart J 11, 1083–1092.

Krumholz, H.M., Parent, E.M., Tu, N., Vaccarino, V., Wang, Y., Radford, M.J., Hennen, J., 1997. Readmission After Hospitalization for Congestive Heart Failure Among Medicare Beneficiaries. Arch Intern Med 157, 99–104.

Kurl Sudhir, Mäkikallio Timo H., Rautaharju Pentti, Kiviniemi Vesa, Laukkanen Jari A., 2012. Duration of QRS Complex in Resting Electrocardiogram Is a Predictor of Sudden Cardiac Death in Men. Circulation 125, 2588–2594.

Leclercq, C., Burri, H., Curnis, A., Delnoy, P.P., Rinaldi, C.A., Sperzel, J., Lee, K., Calò, L., Vicentini, A., Concha, J.F., Thibault, B., 2019a. Cardiac resynchronization therapy non-responder to responder conversion rate in the more response to cardiac resynchronization therapy with MultiPoint Pacing (MORE-CRT MPP) study: results from Phase I. European Heart Journal 40, 2979–2987.

Leclercq, C., Burri, H., Curnis, A., Delnoy, P.P., Rinaldi, C.A., Sperzel, J., Lee, K., Cohorn, C.,

Thibault, B., 2019b. Rationale and design of a randomized clinical trial to assess the safety and efficacy of multipoint pacing therapy: MOre REsponse on Cardiac Resynchronization Therapy with MultiPoint Pacing (MORE-CRT MPP–PHASE II). American Heart Journal 209, 1–8.

Leclercq, C., Faris, O., Tunin, R., Johnson, J., Kato, R., Evans, F., Spinelli, J., Halperin, H., McVeigh, E., Kass, D.A., 2002. Systolic Improvement and Mechanical Resynchronization Does Not Require Electrical Synchrony in the Dilated Failing Heart With Left Bundle-Branch Block. Circulation 106, 1760–1763.

Lewis Andrew J. M., Foley Paul, Whinnett Zachary, Keene Daniel, Chandrasekaran Badrinathan, 2019. His Bundle Pacing: A New Strategy for Physiological Ventricular Activation. Journal of the American Heart Association 8, e010972.

Leyva, F., Foley, P.W., Chalil, S., Ratib, K., Smith, R.E., Prinzen, F., Auricchio, A., 2011. Cardiac resynchronization therapy guided by late gadolinium-enhancement cardiovascular magnetic resonance. Journal of Cardiovascular Magnetic Resonance 13, 29.

Leyva, F., Nisam, S., Auricchio, A., 2014. 20 Years of Cardiac Resynchronization Therapy. Journal of the American College of Cardiology 64, 1047–1058.

Leyva, F., Zegard, A., Okafor, O., de Bono, J., McNulty, D., Ahmed, A., Marshall, H., Ray, D., Qiu, T., 2019. Survival after cardiac resynchronization therapy: results from 50 084 implantations. Europace 21, 754–762. h

Leyva, F., Zegard, A., Taylor, R.J., Foley, P.W.X., Umar, F., Patel, K., Panting, J., van Dam, P., Prinzen, F.W., Marshall, H., Qiu, T., 2018a. Long-Term Outcomes of Cardiac Resynchronization Therapy Using Apical Versus Nonapical Left Ventricular Pacing. J Am Heart Assoc 7.

Leyva, F., Zegard, A., Umar, F., Taylor, R.J., Acquaye, E., Gubran, C., Chalil, S., Patel, K., Panting, J., Marshall, H., Qiu, T., 2018b. Long-term clinical outcomes of cardiac resynchronization therapy with or without defibrillation: impact of the aetiology of cardiomyopathy. Europace 20, 1804–1812.

Lim, S.H., Lip, G.Y.H., Sanderson, J.E., 2008. Ventricular optimization of biventricular pacing: a systematic review. Europace 10, 901–906.

Linde, C., Abraham, W.T., Gold, M.R., Daubert, C., REVERSE Study Group, 2010. Cardiac resynchronization therapy in asymptomatic or mildly symptomatic heart failure patients in relation to etiology: results from the REVERSE (REsynchronization reVErses Remodeling in Systolic Left vEntricular Dysfunction) study. J. Am. Coll. Cardiol. 56, 1826–1831.

Liu, P., Wang, Q., Sun, H., Qin, X., Zheng, Q., 2021. Left Bundle Branch Pacing: Current Knowledge and Future Prospects. Front Cardiovasc Med 8, 630399.

Liu, X., 2012. Classification accuracy and cut point selection. Stat Med 31, 2676–2686.

Lux, R.L., Urie, P.M., Burgess, M.J., Abildskov, J.A., 1980. Variability of the body surface distributions of QRS, ST-T and QRST deflection areas with varied activation sequence in dogs. Cardiovasc. Res. 14, 607–612.

Maass, A.H., Vernooy, K., Wijers, S.C., van 't Sant, J., Cramer, M.J., Meine, M., Allaart, C.P., De Lange, F.J., Prinzen, F.W., Gerritse, B., Erdtsieck, E., Scheerder, C.O.S., Hill, M.R.S., Scholten, M., Kloosterman, M., Ter Horst, I.A.H., Voors, A.A., Vos, M.A., Rienstra, M., Van Gelder, I.C., 2018a. Refining success of cardiac resynchronization therapy using a simple score predicting the amount of reverse ventricular remodelling: results from the Markers and Response to CRT (MARC) study. Europace 20, e1–e10.

Maass, A.H., Vernooy, K., Wijers, S.C., van 't Sant, J., Cramer, M.J., Meine, M., Allaart, C.P., De Lange, F.J., Prinzen, F.W., Gerritse, B., Erdtsieck, E., Scheerder, C.O.S., Hill, M.R.S., Scholten, M., Kloosterman, M., ter Horst, I.A.H., Voors, A.A., Vos, M.A., Rienstra, M., Van Gelder, I.C., 2018b. Refining success of cardiac resynchronization therapy using a simple score predicting the amount of reverse ventricular remodelling: results from the Markers and Response to CRT (MARC) study. Europace 20, e1–e10.

Mafi Rad, M., Blaauw, Y., Dinh, T., Pison, L., Crijns, H.J., Prinzen, F.W., Vernooy, K., 2015. Left ventricular lead placement in the latest activated region guided by coronary venous electroanatomic mapping. Europace 17, 84–93.

Mafi Rad, M., Wijntjens, G.W.M., Engels, E.B., Blaauw, Y., Luermans, J.G.L.M., Pison, L., Crijns, H.J., Prinzen, F.W., Vernooy, K., 2016. Vectorcardiographic QRS area identifies delayed left ventricular lateral wall activation determined by electroanatomic mapping in candidates for cardiac resynchronization therapy. Heart Rhythm 13, 217–225.

Mahmood, S.S., Levy, D., Vasan, R.S., Wang, T.J., 2014. The Framingham Heart Study and the Epidemiology of Cardiovascular Diseases: A Historical Perspective. Lancet 383, 999–1008.

Malmivuo, J., Plonsey, R., 1995. BioelectromagnetismPrinciples and Applications of Bioelectric and Biomagnetic Fields. Oxford University Press.

Man, S., Maan, A.C., Schalij, M.J., Swenne, C.A., 2015. Vectorcardiographic diagnostic & prognostic information derived from the 12-lead electrocardiogram: Historical review and clinical perspective. Journal of Electrocardiology 48, 463–475.

McCrohon, J.A., Moon, J.C.C., Prasad, S.K., McKenna, W.J., Lorenz, C.H., Coats, A.J.S., Pennell, D.J., 2003. Differentiation of Heart Failure Related to Dilated Cardiomyopathy and Coronary Artery Disease Using Gadolinium-Enhanced Cardiovascular Magnetic Resonance. Circulation 108, 54–59.

Mills Robert W., Cornelussen Richard N., Mulligan Lawrence J., Strik Marc, Rademakers Leonard M., Skadsberg Nicholas D., van Hunnik Arne, Kuiper Marion, Lampert Anniek, Delhaas Tammo, Prinzen Frits W., 2009. Left Ventricular Septal and Left Ventricular Apical Pacing Chronically Maintain Cardiac Contractile Coordination, Pump Function and Efficiency. Circulation: Arrhythmia and Electrophysiology 2, 571–579.

Mittal, S., 2017. Maximizing outcomes in patients receiving cardiac resynchronization therapy. Supplement to EP Lab Digest 4, 4–11.

Mittal, S., Aktas, M.K., Moss, A.J., Mcnitt, S., Kutyifa, V., Steinberg, J.S., Zareba, W., 2014. The Impact of Nonsustained Ventricular Tachycardia on Reverse Remodeling, Heart Failure, and Treated Ventricular Tachyarrhythmias in MADIT-CRT. Journal of Cardiovascular Electrophysiology 25, 1082–1087.

Morgan, J.M., Biffi, Mauro, Gellér, László, Leclercq, Christophe, Ruffa, Franco, Tung, Stanley, Defaye, Pascal, Yang, Z., Gerritse, B., van Ginneken, M., Yee, Raymond, Jais, Pierre, on behalf of the ALSYNC Investigators, Böcker, D., Lacroix, D., Lawo, T., Pietersen, A., Pürerfellner, H., Rosenqvist, M., Thijs, V., Fisher, J., Altafullah, I., Bank, A., Mugglin, A., Biffi, M., Connelly, D., Defaye, P., Gellér, L., Gras, D., Herzet, J.M., Jais, P., Lau, E., Leclercq, C., Morgan, J., Poty, H., Ruffa, F., Santini, M., Segal, O., Tavernier, R., Tung, S., Vernooy, K., Yee, R., the ALSYNC Investigators, 2016. ALternate Site Cardiac ResYNChronization (ALSYNC): a prospective and multicentre study of left ventricular endocardial pacing for cardiac resynchronization therapy. European Heart Journal 37, 2118–2127.

Morin, D.P., Oikarinen, L., Viitasalo, M., Toivonen, L., Nieminen, M.S., Kjeldsen, S.E., Dahlöf, B., John, M., Devereux, R.B., Okin, P.M., 2009. QRS duration predicts sudden cardiac death in hypertensive patients undergoing intensive medical therapy: the LIFE study. Eur. Heart J. 30, 2908–2914.

Moss, A.J., Hall, W.J., Cannom, D.S., Klein, H., Brown, M.W., Daubert, J.P., Estes, N.A.M., Foster, E., Greenberg, H., Higgins, S.L., Pfeffer, M.A., Solomon, S.D., Wilber, D., Zareba, W., MADIT-CRT Trial Investigators, 2009a. Cardiac-resynchronization therapy for the prevention of heart-failure events. N. Engl. J. Med. 361, 1329–1338.

Moss, A.J., Hall, W.J., Cannom, D.S., Klein, H., Brown, M.W., Daubert, J.P., Estes, N.A.M., Foster, E., Greenberg, H., Higgins, S.L., Pfeffer, M.A., Solomon, S.D., Wilber, D., Zareba, W., MADIT-CRT Trial Investigators, 2009b. Cardiac-resynchronization therapy for the prevention of heart-failure events. N. Engl. J. Med. 361, 1329–1338.

Mullens, W., Verga, T., Grimm, R.A., Starling, R.C., Wilkoff, B.L., Tang, W.H.W., 2009. Persistent Hemodynamic Benefits of Cardiac Resynchronization Therapy With Disease Progression in Advanced Heart Failure. Journal of the American College of Cardiology 53, 600–607.

Murray-Thomas, T., Cowie, M.R., 2003. Epidemiology and clinical aspects of congestive heart failure. J Renin Angiotensin Aldosterone Syst 4, 131–136.

Narula, O.S., 1977. Longitudinal dissociation in the His bundle. Bundle branch block due to asynchronous conduction within the His bundle in man. Circulation 56, 996–1006.

Nguyên, U.C., Claridge, S., Vernooy, K., Engels, E.B., Razavi, R., Rinaldi, C.A., Chen, Z., Prinzen, F.W., 2018a. Relationship between vectorcardiographic QRS area , myocardial scar quantification, and response to cardiac resynchronization therapy. Journal of Electrocardiology 51, 457–463.

Nguyên, U.C., Verzaal, N.J., van Nieuwenhoven, F.A., Vernooy, K., Prinzen, F.W., 2018b. Pathobiology of cardiac dyssynchrony and resynchronization therapy. Europace 20, 1898–1909.

Niazi, I., Baker, J., Corbisiero, R., Love, C., Martin, D., Sheppard, R., Worley, S.J., Varma, N., Lee, K., Tomassoni, G., 2017. Safety and Efficacy of Multipoint Pacing in Cardiac Resynchronization Therapy: The MultiPoint Pacing Trial. JACC: Clinical Electrophysiology 3, 1510–1518.

Niazi, I.K., Sperzel, J., Heist, E.K., Rosenberg, S.P., Ryu, K., Yang, M., D'Avila, A., Singh, J.P., 2015. Three-Dimensional Cardiac Mapping Characterizes Ventricular Contractile Patterns during Cardiac Resynchronization Therapy Implant: A Feasibility Study. Pacing Clin Electrophysiol 38, 1091–1098.

NICE, 2014. Overview | Implantable cardioverter defibrillators and cardiac resynchronisation therapy for arrhythmias and heart failure | Guidance | NICE TA314.

Okafor O, Zegard A, van Dam P, Stegemann B, Qiu T, Marshall H, Leyva F. Changes in QRS Area and QRS Duration After Cardiac Resynchronization Therapy Predict Cardiac Mortality, Heart Failure Hospitalizations, and Ventricular Arrhythmias. J Am Heart Assoc. 2019 Nov 5;8(21):e013539. doi: 10.1161/JAHA.119.013539.

Okafor O, Umar F, Zegard A, van Dam P, Walton J, Stegemann B, Marshall H, Leyva F. Effect of QRS area reduction and myocardial scar on the hemodynamic response to cardiac resynchronization therapy. Heart Rhythm. 2020 Dec;17(12):2046-2055. doi: 10.1016/j.hrthm.2020.07.025.

Oostendorp, T.F., van Dessel, P.F.H.M., Coronel, R., Belterman, C., Linnenbank, A.C., van Schie, I.H., van Oosterom, A., Oosterhoff, P., van Dam, P.M., de Bakker, J.M.T., 2011. Noninvasive detection of epicardial and endocardial activity of the heart. Neth Heart J 19, 488–491.

Osca, J., Alonso, P., Cano, Ó., Sánchez, J.M., Tejada, D., Andrés, A., Sancho Tello, M.J., Olagüe, J., 2015. The use of quadripolar left ventricular leads improves the hemodynamic response to cardiac resynchronization therapy. Pacing Clin Electrophysiol 38, 326–333.

Oster Howard S., Taccardi Bruno, Lux Robert L., Ershler Philip R., Rudy Yoram, 1997. Noninvasive Electrocardiographic Imaging. Circulation 96, 1012–1024.

Padala, S.K., Ellenbogen, K.A., 2020. Left bundle branch pacing is the best approach to physiological pacing. Heart Rhythm O2 1, 59–67.

Pahlm, O., 2014. Cardiac Electrophysiology: From Cell to Bedside.

Peichl, P., Kautzner, J., Čihák, R., Bytešník, J., 2004. The Spectrum of Inter- and Intraventricular Conduction Abnormalities in Patients Eligible for Cardiac Resynchronization Therapy. Pacing and Clinical Electrophysiology 27, 1105–1112.

Ploux, S., Eschalier, R., Whinnett, Z.I., Lumens, J., Derval, N., Sacher, F., Hocini, M., Jaïs, P., Dubois, R., Ritter, P., Haïssaguerre, M., Wilkoff, B.L., Francis, D.P., Bordachar, P., 2015. Electrical dyssynchrony induced by biventricular pacing: implications for patient selection and therapy improvement. Heart Rhythm 12, 782–791.

Ploux, S., Lumens, J., Whinnett, Z., Montaudon, M., Strom, M., Ramanathan, C., Derval, N., Zemmoura, A., Denis, A., De Guillebon, M., Shah, A., Hocini, M., Jaïs, P., Ritter, P., Haïssaguerre, M., Wilkoff, B.L., Bordachar, P., 2013. Noninvasive Electrocardiographic Mapping to Improve Patient Selection for Cardiac Resynchronization Therapy: Beyond QRS Duration and Left Bundle Branch Block Morphology. Journal of the American College of Cardiology 61, 2435–2443.

Polasek, R., Kucera, P., Nedbal, P., Roubicek, T., Belza, T., Hanuliakova, J., Horak, D., Wichterle, D., Kautzner, J., 2012. Local electrogram delay recorded from left ventricular lead at implant predicts response to cardiac resynchronization therapy: Retrospective study with 1 year follow up. BMC Cardiovasc Disord 12, 34.

Ponikowski, P., Anker, S.D., AlHabib, K.F., Cowie, M.R., Force, T.L., Hu, S., Jaarsma, T., Krum, H., Rastogi, V., Rohde, L.E., Samal, U.C., Shimokawa, H., Budi Siswanto, B., Sliwa, K., Filippatos, G., 2014. Heart failure: preventing disease and death worldwide. ESC Heart Fail 1, 4–25.

Poole, J.E., Singh, J.P., Birgersdotter-Green, U., 2016. QRS Duration or QRS Morphology: What Really Matters in Cardiac Resynchronization Therapy? Journal of the American College of Cardiology 67, 1104–1117.

Pooter, J., Haddad, M., Stroobandt, R., 2016. Different Methods to Measure QRS Duration in CRT Patients: Impact on the Predictive Value of QRS Duration Parameters. Ann Noninvasive Electrocardiol, 21, 305-315

Potyagaylo, D., Chmelevsky, M., Zubarev, S., Budanova, M., Kalinin, V., Kalinin, A., Lebedev, D., 2018. Evaluation of ECGI Localization Accuracy for Single Pacings in CRT Patients.

Prinzen, F.W., Auricchio, A., 2012. The “Missing” Link Between Acute Hemodynamic Effect

and Clinical Response. J Cardiovasc Transl Res 5, 188–195.

Prinzen, F.W., Kroon, W., Auricchio, A., 2013. U-Shaped Mechanical Activation 4 U?∗. JACC: Cardiovascular Imaging 6, 874–876.

Raja, D., Pandurangi, U., Pathak, R., 2019. 3-D Electro-Anatomical Mapping Guided Lead Placement in CRT. Heart, Lung and Circulation 28, S144.

Ramanathan, C., Ghanem, R.N., Jia, P., Ryu, K., Rudy, Y., 2004. Noninvasive electrocardiographic imaging for cardiac electrophysiology and arrhythmia. Nat Med 10, 422–428.

Raymond-Paquin, A., 2021. Left Bundle Branch Pacing: A Perfect Compromise?

Regoli, F., Auricchio, A., 2009. The role of invasive mapping in the electrophysiology laboratory. Europace 11, v40–v45.

Richman, J.L., Wolff, L., 1954. Left bundle branch block masquerading as right bundle branch block. American Heart Journal 47, 383–393.

Rinaldi, C.A., Burri, H., Thibault, B., Curnis, A., Rao, A., Gras, D., Sperzel, J., Singh, J.P., Biffi, M., Bordachar, P., Leclercq, C., 2015. A review of multisite pacing to achieve cardiac resynchronization therapy. Europace 17, 7–17.

Rinaldi, C.A., Kranig, W., Leclercq, C., Kacet, S., Betts, T., Bordachar, P., Gutleben, K.-J., Shetty, A., Keel, A., Ryu, K., Farazi, T.G., Simon, M., Naqvi, T.Z., 2013. Acute effects of multisite left ventricular pacing on mechanical dyssynchrony in patients receiving cardiac resynchronization therapy. J Card Fail 19, 731–738.

Rinaldi, C.A., Leclercq, C., Kranig, W., Kacet, S., Betts, T., Bordachar, P., Gutleben, K.-J., Shetty, A., Donal, E., Keel, A., Ryu, K., Farazi, T.G., Simon, M., Naqvi, T.Z., 2014. Improvement in acute contractility and hemodynamics with multipoint pacing via a left ventricular quadripolar pacing lead. J Interv Card Electrophysiol 40, 75–80.

Risum, N., Tayal, B., Hansen, T.F., Bruun, N.E., Jensen, M.T., Lauridsen, T.K., Saba, S., Kisslo, J., Gorcsan, J., Sogaard, P., 2015. Identification of Typical Left Bundle Branch Block Contraction by Strain Echocardiography Is Additive to Electrocardiography in Prediction of Long-Term Outcome After Cardiac Resynchronization Therapy. Journal of the American College of Cardiology 66, 631–641.

Rockman, H.A., Juneau, C., Chatterjee, K., Rouleau, J.L., 1989. Long-term predictors of sudden and low output death in chronic congestive heart failure secondary to coronary artery disease. Am. J. Cardiol. 64, 1344–1348.

Rodriguez, L.-M., Timmermans, C., Nabar, A., Beatty, G., Wellens, H.J.J., 2003. Variable patterns of septal activation in patients with left bundle branch block and heart failure. J. Cardiovasc. Electrophysiol. 14, 135–141.

Ross, S., Odland, H.H., Aranda, A., Edvardsen, T., Gammelsrud, L.O., Haland, T.F.,

Cornelussen, R., Hopp, E., Kongsgaard, E., 2018a. Cardiac resynchronization therapy when no lateral pacing option exists: vectorcardiographic guided non-lateral left ventricular lead placement predicts acute hemodynamic response. Europace 20, 1294–1302.

Ross, S., Odland, H.H., Aranda, A., Edvardsen, T., Gammelsrud, L.O., Haland, T.F., Cornelussen, R., Hopp, E., Kongsgaard, E., 2018b. Cardiac resynchronization therapy when no lateral pacing option exists: vectorcardiographic guided non-lateral left ventricular lead placement predicts acute hemodynamic response. Europace 20, 1294–1302.

Roubicek Tomas, Wichterle Dan, Kucera Pavel, Nedbal Pavel, Kupec Jindrich, Sedlakova Jana, Cerny Jan, Stros Jan, Kautzner Josef, Polasek Rostislav, 2015. Left Ventricular Lead Electrical Delay Is a Predictor of Mortality in Patients With Cardiac Resynchronization Therapy. Circulation: Arrhythmia and Electrophysiology 8, 1113–1121.

Rudy Yoram, 2013. Noninvasive Electrocardiographic Imaging of Arrhythmogenic Substrates in Humans. Circulation Research 112, 863–874.

Rudy Yoram, 2017. Noninvasive ECG imaging (ECGI): Mapping the arrhythmic substrate of the human heart. International Journal of Cardiology 237, P13–14. DOI:https://doi.org/10.1016/j.ijcard.2017.02.104

Ruschitzka, F., Abraham, W.T., Singh, J.P., Bax, J.J., Borer, J.S., Brugada, J., Dickstein, K., Ford, I., Gorcsan, J., Gras, D., Krum, H., Sogaard, P., Holzmeister, J., EchoCRT Study Group, 2013. Cardiac-resynchronization therapy in heart failure with a narrow QRS complex. N. Engl. J. Med. 369, 1395–1405.

Ruwald, A.-C., Aktas, M.K., Ruwald, M.H., Kutyifa, V., McNitt, S., Jons, C., Mittal, S., Steinberg, J.S., Daubert, J.P., Moss, A.J., Zareba, W., 2018. Postimplantation ventricular ectopic burden and clinical outcomes in cardiac resynchronization therapy-defibrillator patients: a MADIT-CRT substudy. Ann Noninvasive Electrocardiol 23, e12491.

Saba Samir, Marek Josef, Schwartzman David, Jain Sandeep, Adelstein Evan, White Pamela, Oyenuga Olusegun A., Onishi Tetsuari, Soman Prem, Gorcsan John, 2013. Echocardiography-Guided Left Ventricular Lead Placement for Cardiac Resynchronization Therapy. Circulation: Heart Failure 6, 427–434.

Sapp John L., Dawoud Fady, Clements John C., Horáček B. Milan, 2012. Inverse Solution Mapping of Epicardial Potentials. Circulation: Arrhythmia and Electrophysiology 5, 1001–1009.

Schilling Richard J., Peters Nicholas S., Davies D. Wyn, 1998. Simultaneous Endocardial Mapping in the Human Left Ventricle Using a Noncontact Catheter. Circulation 98, 887–898.

Sengupta, P.P., Kramer, C.M., Narula, J., 2013. Cardiac Resynchronization: The Flow of Activation Sequence. J Am Coll Cardiol Img 6, 924–926.

Sieniewicz, B.J., Jackson, T., Claridge, S., Pereira, H., Gould, J., Sidhu, B., Porter, B., Niederer, S., Yao, C., Rinaldi, C.A., 2019. Optimization of CRT programming using non-invasive electrocardiographic imaging to assess the acute electrical effects of multipoint pacing. J Arrhythm 35, 267–275.

Singh Jagmeet P., Klein Helmut U., Huang David T., Reek Sven, Kuniss Malte, Quesada Aurelio, Barsheshet Alon, Cannom David, Goldenberg Ilan, McNitt Scott, Daubert James P., Zareba Wojciech, Moss Arthur J., 2011. Left Ventricular Lead Position and Clinical Outcome in the Multicenter Automatic Defibrillator Implantation Trial–Cardiac Resynchronization Therapy (MADIT-CRT) Trial. Circulation 123, 1159–1166.

Singh, J.P., Berger, R.D., Doshi, R.N., Lloyd, M., Moore, D., Daoud, E.G., 2018. Rationale and design for ENHANCE CRT: QLV implant strategy for non-left bundle branch block patients. ESC Heart Fail 5, 1184–1190.

Singh, J.P., Fan, D., Heist, E.K., Alabiad, C.R., Taub, C., Reddy, V., Mansour, M., Picard, M.H., Ruskin, J.N., Mela, T., 2006. Left ventricular lead electrical delay predicts response to cardiac resynchronization therapy. Heart Rhythm 3, 1285–1292.

Sipahi, I., Chou, J.C., Hyden, M., Rowland, D.Y., Simon, D.I., Fang, J.C., 2012. Effect of QRS morphology on clinical event reduction with cardiac resynchronization therapy: meta-analysis of randomized controlled trials. Am. Heart J. 163, 260-267.e3.

Sipahi Ilke, Fang James C., 2013. QRS Duration Criteria to Select Patients for Cardiac Resynchronization Therapy. Circulation: Arrhythmia and Electrophysiology 6, 436–442.

Sohal, M., Shetty, A., Duckett, S., Chen, Z., Sammut, E., Amraoui, S., Carr-White, G., Razavi, R., Rinaldi, C.A., 2013. Noninvasive Assessment of LV Contraction Patterns Using CMR to Identify Responders to CRT. JACC: Cardiovascular Imaging 6, 864–873.

Stipdonk, A.M.W. van, Vanbelle, S., Horst, I.A.H. ter, Luermans, J.G., Meine, M., Maass, A.H., Auricchio, A., Prinzen, F.W., Vernooy, K., 2019. Large variability in clinical judgement and definitions of left bundle branch block to identify candidates for cardiac resynchronisation therapy. International Journal of Cardiology 286, 61–65.

Strauss, D.G., Selvester, R.H., Wagner, G.S., 2011. Defining left bundle branch block in the era of cardiac resynchronization therapy. Am. J. Cardiol. 107, 927–934.

Strik, M., Rademakers, L.M., van Deursen, C.J.M., van Hunnik, A., Kuiper, M., Klersy, C., Auricchio, A., Prinzen, F.W., 2012. Endocardial Left Ventricular Pacing Improves Cardiac Resynchronization Therapy in Chronic Asynchronous Infarction and Heart Failure Models. Circulation: Arrhythmia and Electrophysiology 5, 191–200.

Surawicz, B., Childers, R., Deal, B.J., Gettes, L.S., Bailey, J.J., Gorgels, A., Hancock, E.W., Josephson, M., Kligfield, P., Kors, J.A., Macfarlane, P., Mason, J.W., Mirvis, D.M., Okin, P., Pahlm, O., Rautaharju, P.M., van Herpen, G., Wagner, G.S., Wellens, H., American Heart Association Electrocardiography and Arrhythmias Committee, Council on Clinical Cardiology, American College of Cardiology Foundation, Heart Rhythm Society, 2009. AHA/ACCF/HRS recommendations for the standardization and interpretation of the electrocardiogram: part III: intraventricular conduction disturbances: a scientific statement from the American Heart Association Electrocardiography and Arrhythmias Committee, Council on Clinical Cardiology; the American College of Cardiology Foundation; and the Heart Rhythm Society. Endorsed by the International Society for Computerized Electrocardiology. J. Am. Coll. Cardiol. 53, 976–981.

Surawicz, B., Knilans, T.K., Chou, T.-C., Surawicz-Knilans (Eds.), 2008. Chou's electrocardiography in clinical practice: adult and pediatric, 6. ed. ed. Elsevier, Saunders, Philadelphia, Pa.

Sutherland, K., 2010. Bridging the quality gap: heart failure. Health Foundation, London.

Sweeney Michael O., van Bommel Rutger J., Schalij Martin J., Borleffs C. Jan Willem, Hellkamp Anne S., Bax Jeroen J., 2010. Analysis of Ventricular Activation Using Surface Electrocardiography to Predict Left Ventricular Reverse Volumetric Remodeling During Cardiac Resynchronization Therapy. Circulation 121, 626–634.

Tang, A.S.L., Wells, G.A., Talajic, M., Arnold, M.O., Sheldon, R., Connolly, S., Hohnloser, S.H., Nichol, G., Birnie, D.H., Sapp, J.L., Yee, R., Healey, J.S., Rouleau, J.L., Resynchronization-Defibrillation for Ambulatory Heart Failure Trial Investigators, 2010. Cardiac-resynchronization therapy for mild-to-moderate heart failure. N. Engl. J. Med. 363, 2385–2395.

Taylor, R.J., Umar, F., Panting, J.R., Stegemann, B., Leyva, F., 2016. Left ventricular lead position, mechanical activation, and myocardial scar in relation to left ventricular reverse remodeling and clinical outcomes after cardiac resynchronization therapy: A feature-tracking and contrast-enhanced cardiovascular magnetic resonance study. Heart Rhythm 13, 481–489.

Tereshchenko, L.G., Cheng, A., Park, J., Wold, N., Meyer, T.E., Gold, M.R., Mittal, S., Singh, J., Stein, K.M., Ellenbogen, K.A., SMART-AV Trial Investigators, 2015. Novel measure of electrical dyssynchrony predicts response in cardiac resynchronization therapy: Results from the SMART-AV Trial. Heart Rhythm 12, 2402–2410.

Thibault, B., Dubuc, M., Khairy, P., Guerra, P.G., Macle, L., Rivard, L., Roy, D., Talajic, M., Karst, E., Ryu, K., Paiement, P., Farazi, T.G., 2013a. Acute haemodynamic comparison of multisite and biventricular pacing with a quadripolar left ventricular lead. Europace 15, 984–991.

Thibault, B., Ducharme, A., Harel, F., White, M., O'Meara, E., Guertin, M.-C., Lavoie, J., Frasure-Smith, N., Dubuc, M., Guerra, P., Macle, L., Rivard, L., Roy, D., Talajic, M., Khairy, P., Evaluation of Resynchronization Therapy for Heart Failure (GREATER-

EARTH) Investigators, 2011. Left ventricular versus simultaneous biventricular pacing in patients with heart failure and a QRS complex ≥120 milliseconds. Circulation 124, 2874–2881.

Thibault, B., Harel, F., Ducharme, A., White, M., Ellenbogen, K.A., Frasure-Smith, N., Roy, D., Philippon, F., Dorian, P., Talajic, M., Dubuc, M., Guerra, P.G., Macle, L., Rivard, L., Andrade, J., Khairy, P., LESSER-EARTH Investigators, 2013b. Cardiac resynchronization therapy in patients with heart failure and a QRS complex <120 milliseconds: the Evaluation of Resynchronization Therapy for Heart Failure (LESSER-EARTH) trial. Circulation 127, 873–881.

Thomas, G., Kim, J., Lerman, B.B., 2019. Improving Cardiac Resynchronisation Therapy. Arrhythm Electrophysiol Rev 8, 220–227.

Tian, Y., Zhang, P., Li, X., Gao, Y., Zhu, T., Wang, L., Li, D., Wang, J., Yuan, C., Guo, J., 2013. True complete left bundle branch block morphology strongly predicts good response to cardiac resynchronization therapy. Europace 15, 1499–1506.

Tomassoni, G., 2016. How to Define Cardiac Resynchronization Therapy Response. Journal of Innovations in Cardiac Rhythm Management 7, S1–S7.

Tomlinson, D.R., Bashir, Y., Betts, T.R., Rajappan, K., 2009. Accuracy of manual QRS duration assessment: its importance in patient selection for cardiac resynchronization and implantable cardioverter defibrillator therapy. Europace 11, 638–642.

Umar, F., Taylor, R.J., Stegemann, B., Marshall, H., Flannigan, S., Lencioni, M., De Bono, J., Griffith, M., Leyva, F., 2016. Haemodynamic effects of cardiac resynchronization therapy using single-vein, three-pole, multipoint left ventricular pacing in patients with ischaemic cardiomyopathy and a left ventricular free wall scar: the MAESTRO study. Europace 18, 1227–1234.

Unger, P.N., Lesser, M.E., Kugel, V.H., Lev, M., 1958. The concept of masquerading bundle-branch block; an electrocardiographic-pathologic correlation. Circulation 17, 397–409.

Upadhyay Gaurav A., Cherian Tharian, Shatz Dalise Y., Beaser Andrew D., Aziz Zaid, Ozcan Cevher, Broman Michael T., Nayak Hemal M., Tung Roderick, 2019. Intracardiac Delineation of Septal Conduction in Left Bundle-Branch Block Patterns. Circulation 139, 1876–1888.

van Bommel, R.J., Tanaka, H., Delgado, V., Bertini, M., Borleffs, C.J.W., Ajmone Marsan, N., Holzmeister, J., Ruschitzka, F., Schalij, M.J., Bax, J.J., Gorcsan, J., 2010. Association of intraventricular mechanical dyssynchrony with response to cardiac resynchronization therapy in heart failure patients with a narrow QRS complex. Eur Heart J 31, 3054–3062.

van Dam, P.M., 2017. A new anatomical view on the vector cardiogram: The mean temporal-spatial isochrones. Journal of Electrocardiology 50, 732–738.

van Dam, P.M., Gordon, J.P., Laks, M.M., Boyle, N.G., 2015. Development of new anatomy reconstruction software to localize cardiac isochrones to the cardiac surface from the 12 lead ECG. J Electrocardiol 48, 959–965.

van Dam, P.M., Oostendorp, T.F., Linnenbank, A.C., van Oosterom, A., 2009a. Non-Invasive Imaging of Cardiac Activation and Recovery. Ann Biomed Eng 37, 1739–1756.

van Dam, P.M., Oostendorp, T.F., van Oosterom, A., 2010. ECGSIM: Interactive simulation of the ECG for teaching and research purposes, in: 2010 Computing in Cardiology. pp. 841–844.

van Dam, P.M., Oostendorp, T.F., van Oosterom, A., 2009b. Application of the fastest route algorithm in the interactive simulation of the effect of local ischemia on the ECG. Med Biol Eng Comput 47, 11–20.

van Dam, P.M., Tung, R., Shivkumar, K., Laks, M., 2013. Quantitative localization of premature ventricular contractions using myocardial activation ECGI from the standard 12-lead electrocardiogram. Journal of Electrocardiology 46, 574–579.

van Deursen, C.J.M., Vernooy, K., Dudink, E., Bergfeldt, L., Crijns, H.J.G.M., Prinzen, F.W., Wecke, L., 2015a. Vectorcardiographic QRS area as a novel predictor of response to cardiac resynchronization therapy. Journal of Electrocardiology 48, 45–52.

van Deursen, C.J.M., Wecke, L., van Everdingen, W.M., Ståhlberg, M., Janssen, M.H.G., Braunschweig, F., Bergfeldt, L., Crijns, H.J.G.M., Vernooy, K., Prinzen, F.W., 2015b. Vectorcardiography for Optimization of Stimulation Intervals in Cardiac Resynchronization Therapy. J Cardiovasc Transl Res 8, 128–137.

van Everdingen, W.M., Cramer, M.J., Doevendans, P.A., Meine, M., 2015. Quadripolar Leads in Cardiac Resynchronization Therapy. JACC: Clinical Electrophysiology 1, 225–237.

van Oosterom, A., 2002. Solidifying the solid angle. J Electrocardiol 35 Suppl, 181–192.

van Oosterom, A., 2001. Genesis of the T wave as based on an equivalent surface source model. J Electrocardiol 34 Suppl, 217–227.

van Oosterom, A., Oostendorp, T.F., 2004. ECGSIM: an interactive tool for studying the genesis of QRST waveforms. Heart 90, 165–168.

van Stipdonk, A.M.W., ter Horst, I., Kloosterman, M., Engels, E.B., Rienstra, M., Crijns, H.J.G.M., Vos, M.A., van Gelder, I.C., Prinzen, F.W., Meine, M., Maass, A.H., Vernooy, K., 2018. QRS Area Is a Strong Determinant of Outcome in Cardiac Resynchronization Therapy. Circulation: Arrhythmia and Electrophysiology 11.

Varma, N., Jia, P., Rudy, Y., 2007. Electrocardiographic imaging of patients with heart failure with left bundle branch block and response to cardiac resynchronization therapy.

Journal of Electrocardiology 40, S174–S178.

Varma, N., Ploux, S., Ritter, P., Wilkoff, B., Eschalier, R., Bordachar, P., 2015. Noninvasive Mapping of Electrical Dyssynchrony in Heart Failure and Cardiac Resynchronization Therapy. Cardiac Electrophysiology Clinics 7, 125–134.

Vassallo, J.A., Cassidy, D.M., Marchlinski, F.E., Buxton, A.E., Waxman, H.L., Doherty, J.U., Josephson, M.E., 1984. Endocardial activation of left bundle branch block. Circulation 69, 914–923.

Végh, E.M., Engels, E.B., van Deursen, C.J.M., Merkely, B., Vernooy, K., Singh, J.P., Prinzen, F.W., 2016. T-wave area as biomarker of clinical response to cardiac resynchronization therapy. Europace 18, 1077–1085.

Vinereanu, D., 2008. Mitral regurgitation and cardiac resynchronization therapy. Echocardiography 25, 1155–1166.

Willems, J.L., Robles de Medina, E.O., Bernard, R., Coumel, P., Fisch, C., Krikler, D., Mazur, N.A., Meijler, F.L., Mogensen, L., Moret, P., 1985. Criteria for intraventricular conduction disturbances and pre-excitation. World Health Organizational/International Society and Federation for Cardiology Task Force Ad Hoc. J. Am. Coll. Cardiol. 5, 1261–1275.

Wong, J.A., Yee, R., Stirrat, J., Scholl, D., Krahn, A.D., Gula, L.J., Skanes, A.C., Leong-Sit, P., Klein, G.J., McCarty, D., Fine, N., Goela, A., Islam, A., Thompson, T., Drangova, M., White, J.A., 2013. Influence of Pacing Site Characteristics on Response to Cardiac Resynchronization Therapy. Circulation: Cardiovascular Imaging 6, 542–550.

Wu, S., Su, L., Vijayaraman, P., Zheng, R., Cai, M., Xu, L., Shi, R., Huang, Z., Whinnett, Z.I., Huang, W., 2021. Left Bundle Branch Pacing for Cardiac Resynchronization Therapy: Nonrandomized On-Treatment Comparison With His Bundle Pacing and Biventricular Pacing. Canadian Journal of Cardiology 37, 319–328.

Young, J.B., Abraham, W.T., Smith, A.L., Leon, A.R., Lieberman, R., Wilkoff, B., Canby, R.C., Schroeder, J.S., Liem, L.B., Hall, S., Wheelan, K., Multicenter InSync ICD Randomized Clinical Evaluation (MIRACLE ICD) Trial Investigators, 2003. Combined cardiac resynchronization and implantable cardioversion defibrillation in advanced chronic heart failure: the MIRACLE ICD Trial. JAMA 289, 2685–2694.

Yu, C.-M., Lin, H., Zhang, Q., Sanderson, J.E., 2003. High prevalence of left ventricular systolic and diastolic asynchrony in patients with congestive heart failure and normal QRS duration. Heart 89, 54–60.

Zannad, F., Huvelle, E., Dickstein, K., Veldhuisen, D.J. van, Stellbrink, C., Køber, L., Cazeau, S., Ritter, P., Maggioni, A.P., Ferrari, R., Lechat, P., 2007. Left bundle branch block as a risk factor for progression to heart failure. European Journal of Heart Failure 9, 7–14.

Zanon, F., Marcantoni, L., Baracca, E., Pastore, G., Lanza, D., Fraccaro, C., Picariello, C., Conte, L., Aggio, S., Roncon, L., Pacetta, D., Badie, N., Noventa, F., Prinzen, F.W., 2016. Optimization of left ventricular pacing site plus multipoint pacing improves remodeling and clinical response to cardiac resynchronization therapy at 1 year. Heart Rhythm 13, 1644–1651.

Zanon Francesco, Baracca Enrico, Pastore Gianni, Fraccaro Chiara, Roncon Loris, Aggio Silvio, Noventa Franco, Mazza Alberto, Prinzen Frits, 2014. Determination of the Longest Intrapatient Left Ventricular Electrical Delay May Predict Acute Hemodynamic Improvement in Patients After Cardiac Resynchronization Therapy. Circulation: Arrhythmia and Electrophysiology 7, 377–383.

Zareba, W., Klein, H., Cygankiewicz, I., Hall, W.J., McNitt, S., Brown, M., Cannom, D., Daubert, J.P., Eldar, M., Gold, M.R., Goldberger, J.J., Goldenberg, I., Lichstein, E., Pitschner, H., Rashtian, M., Solomon, S., Viskin, S., Wang, P., Moss, A.J., MADIT-CRT Investigators, 2011. Effectiveness of Cardiac Resynchronization Therapy by QRS Morphology in the Multicenter Automatic Defibrillator Implantation Trial-Cardiac Resynchronization Therapy (MADIT-CRT). Circulation 123, 1061–1072.

APPENDIX A

Patient 1 – Intrinsic

LBBB

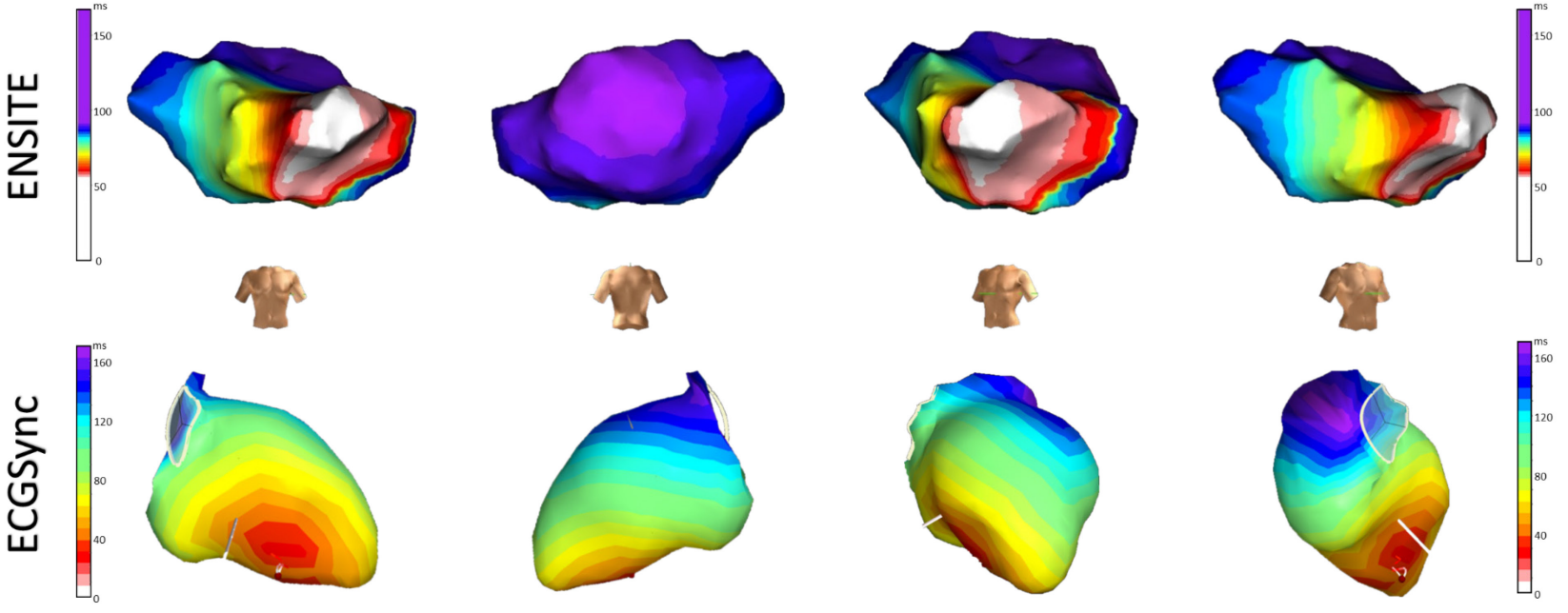

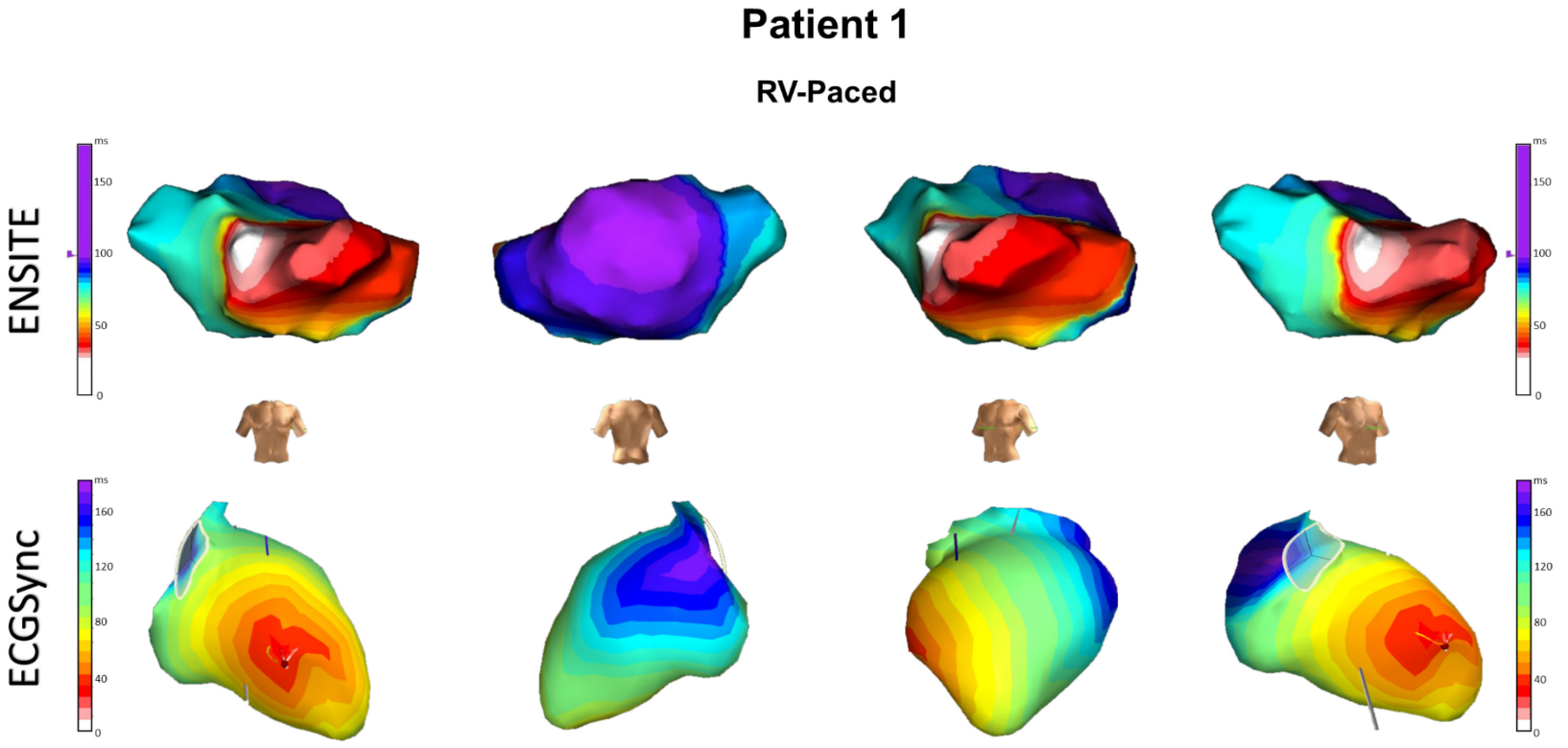
Patient 1
RV-Paced
ENSITE
ECGSync
ms
150
100
50
0
160
120
80
40

Patient 2 – Intrinsic

LBBB

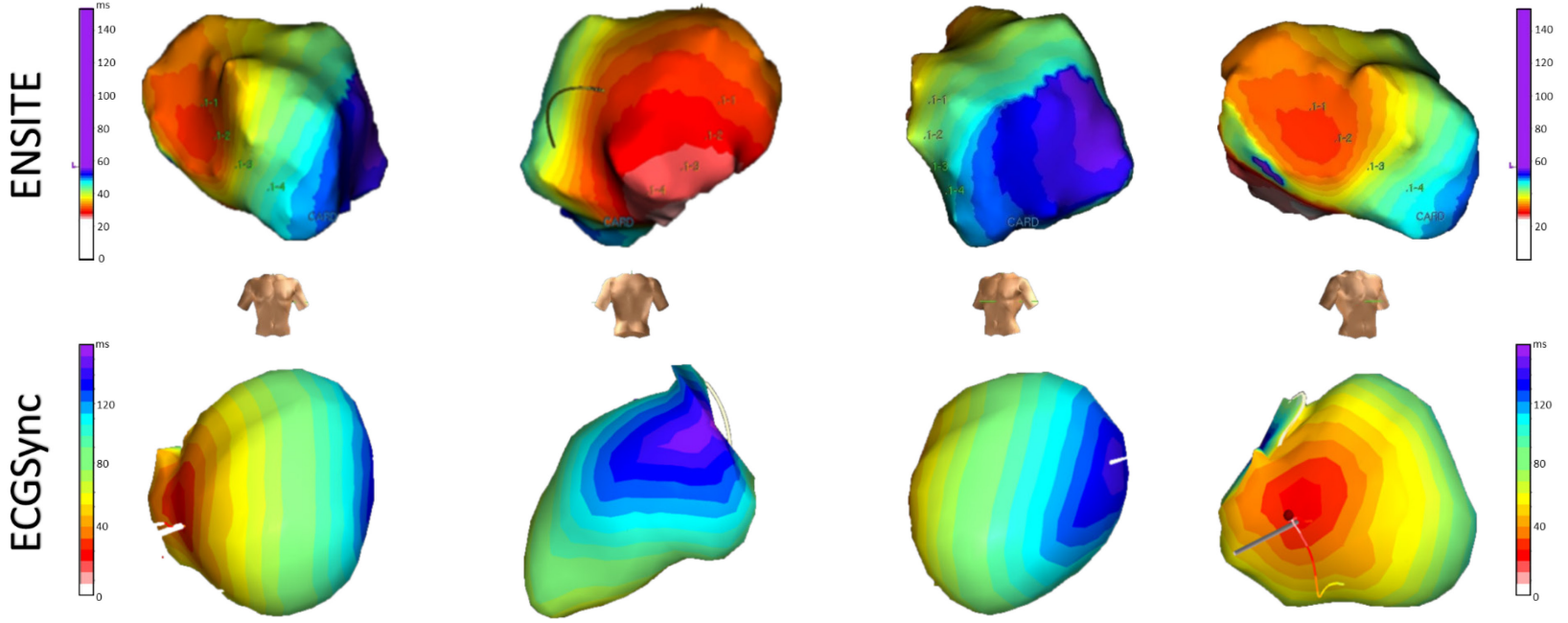

Patient 2

RV-Paced

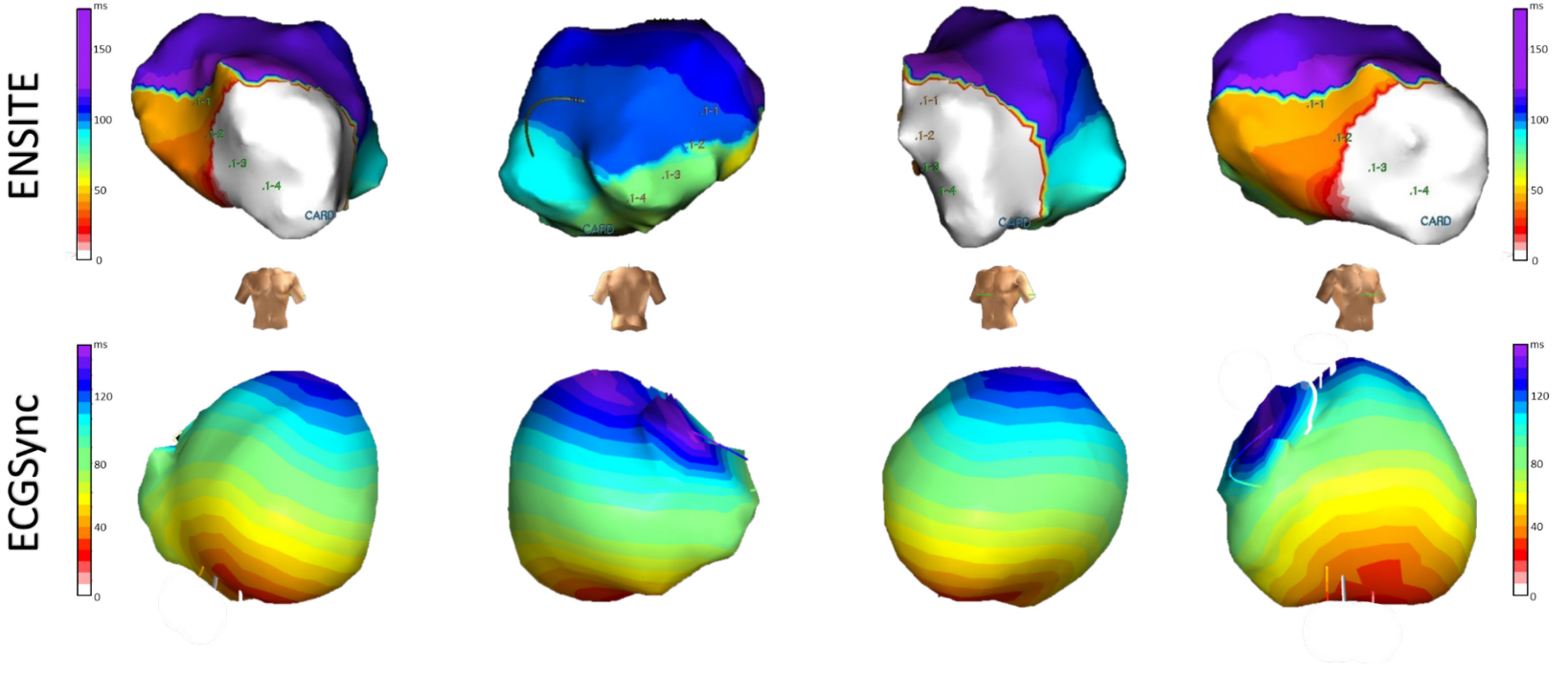

Patient 3 – Intrinsic

LBBB

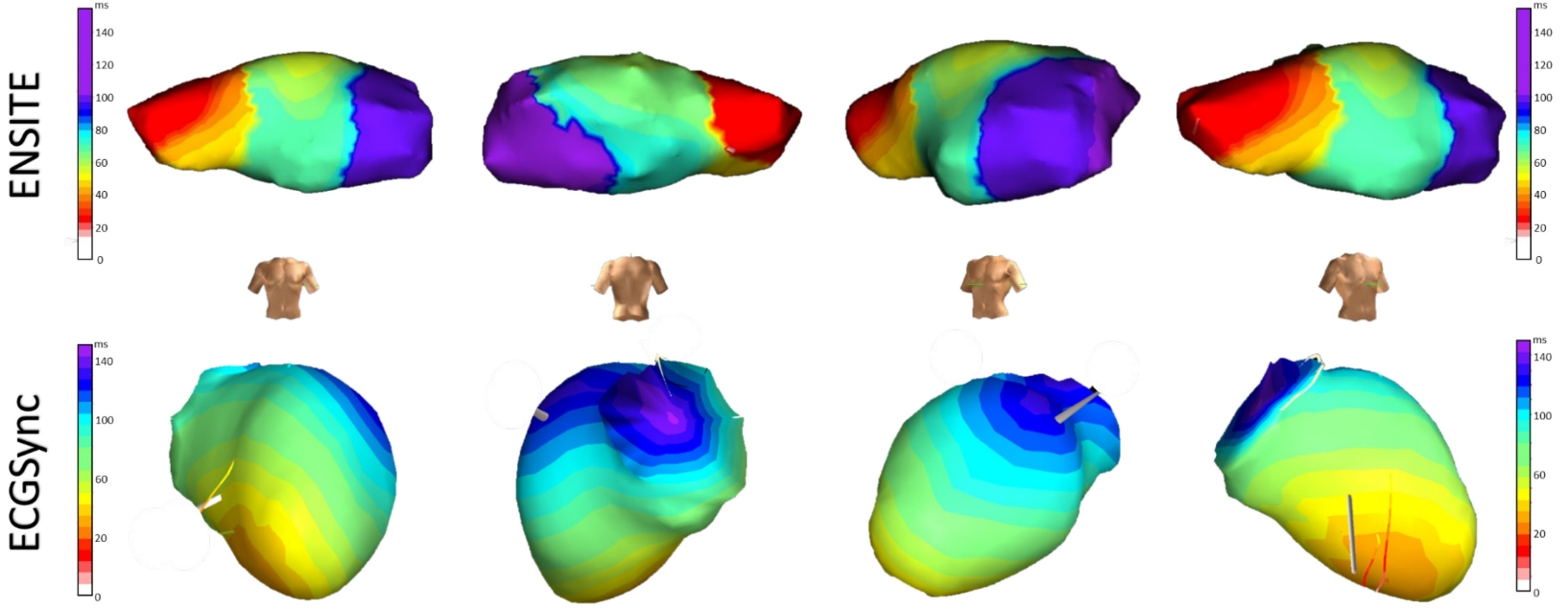

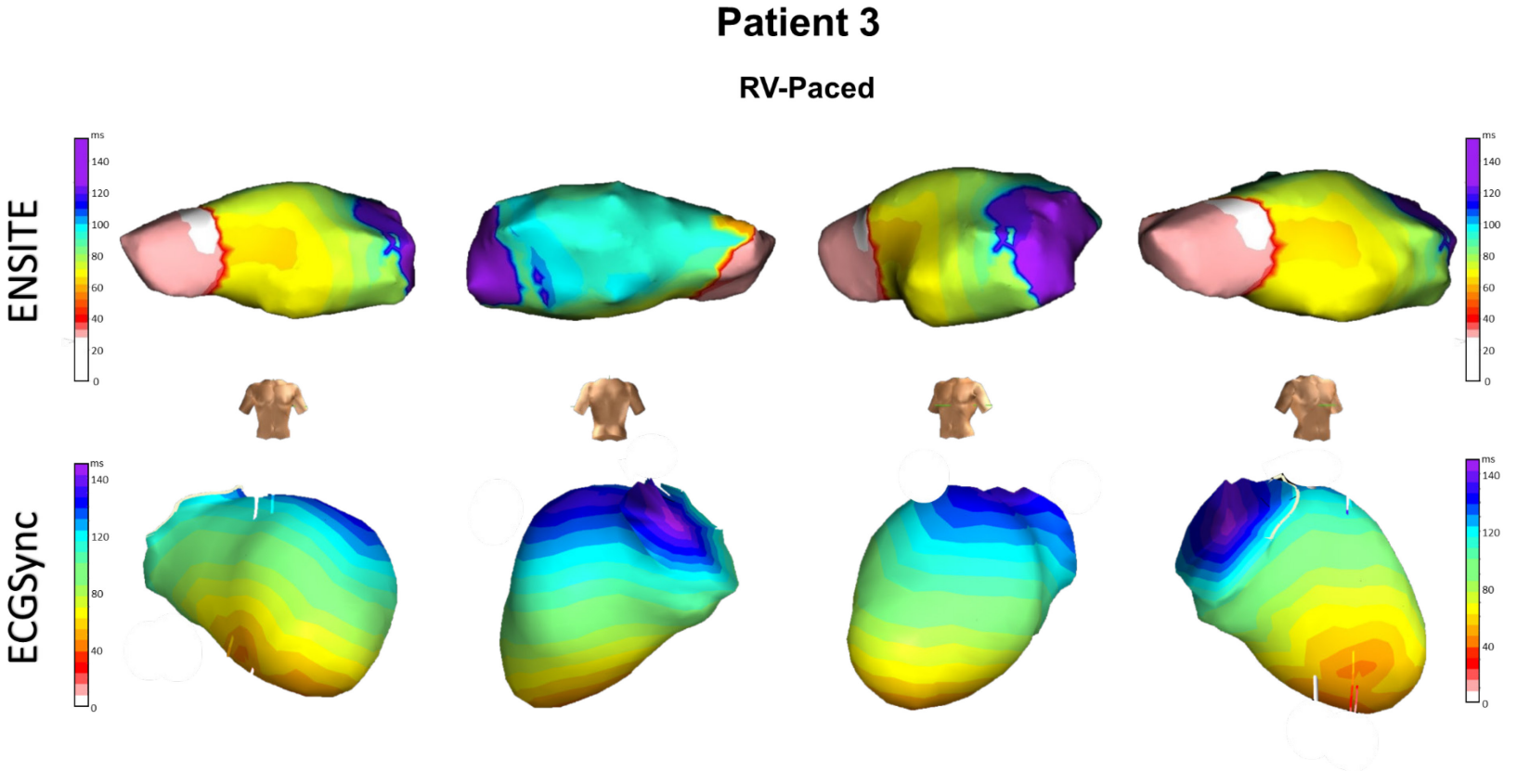
Patient 3
RV-Paced
ENSITE
ECGSync
ms
140
120
100
80
60
40
20
0

Patient 4 – Intrinsic

LBBB

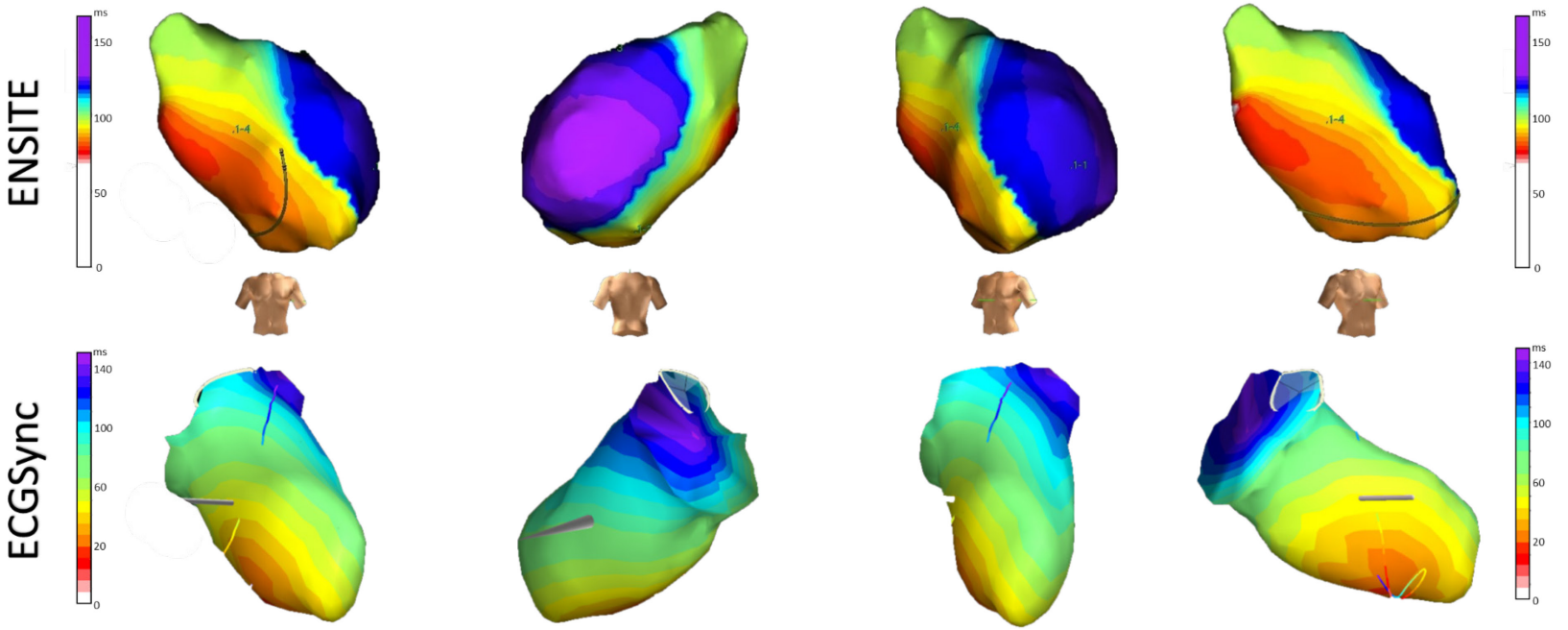

Patient 4

RV-Paced

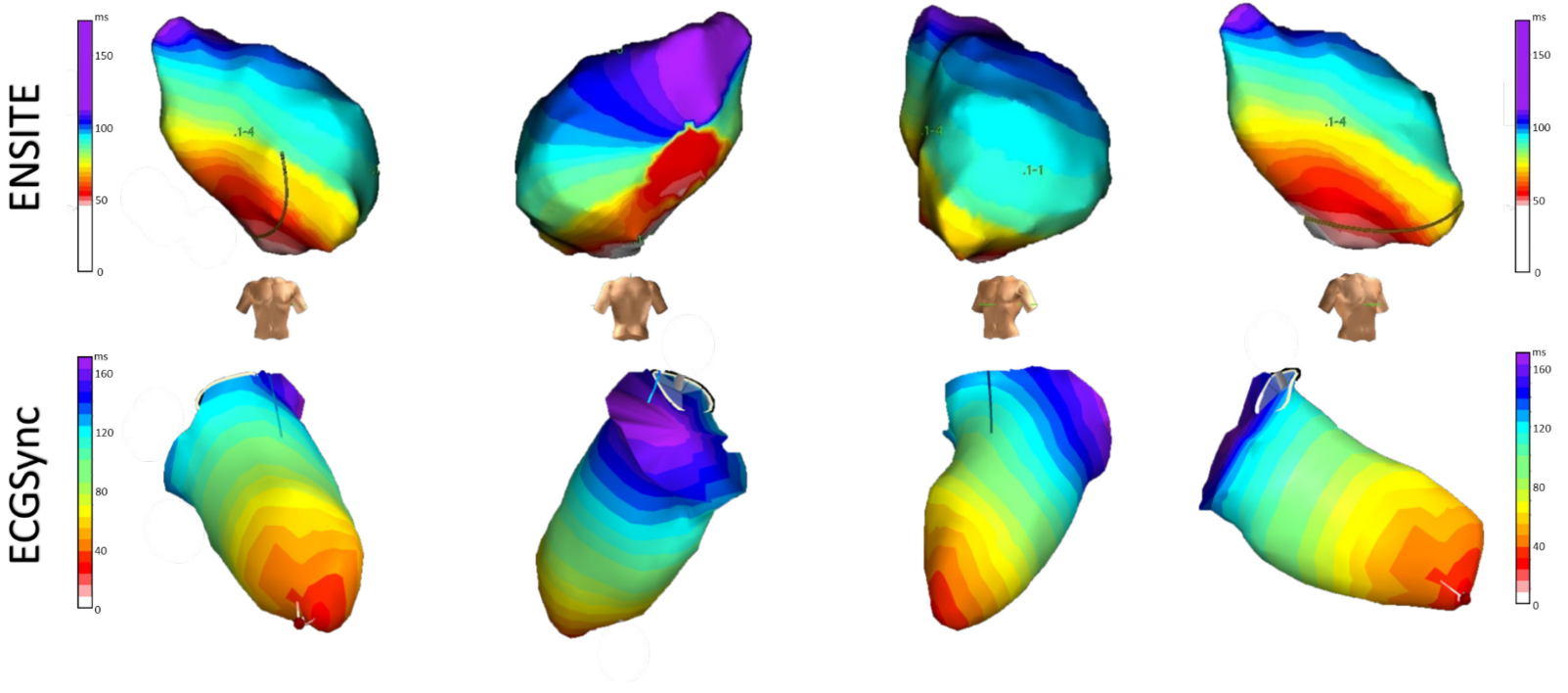

Patient 5 – Intrinsic

LBBB

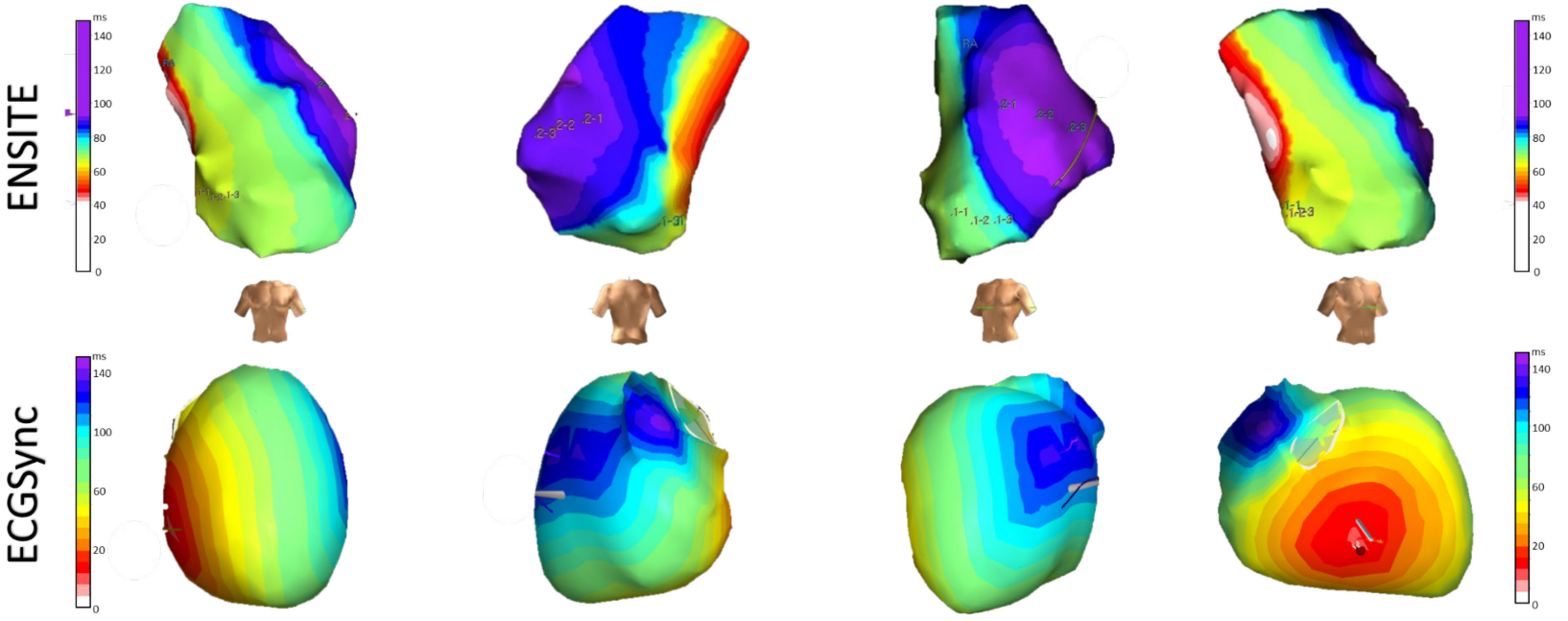

Patient 6 – Intrinsic

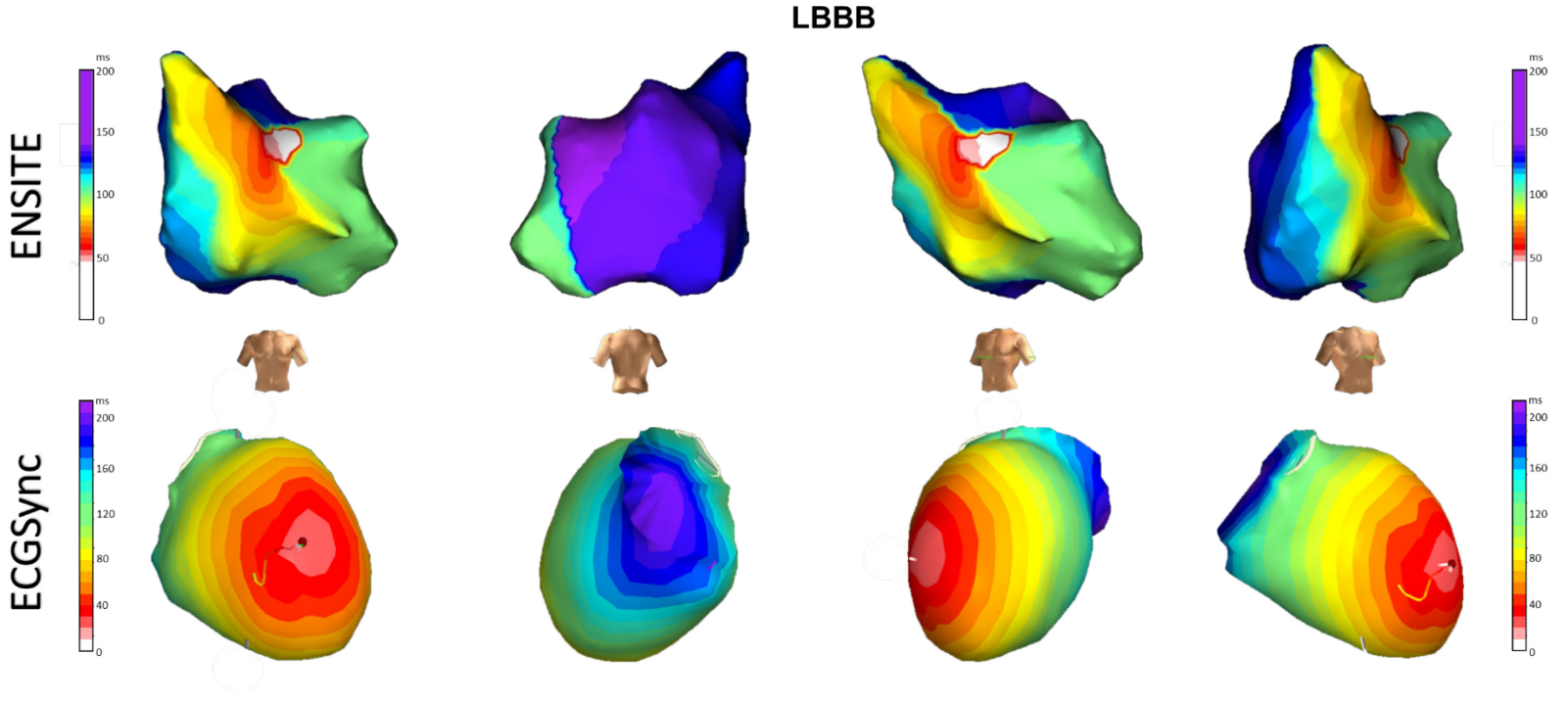

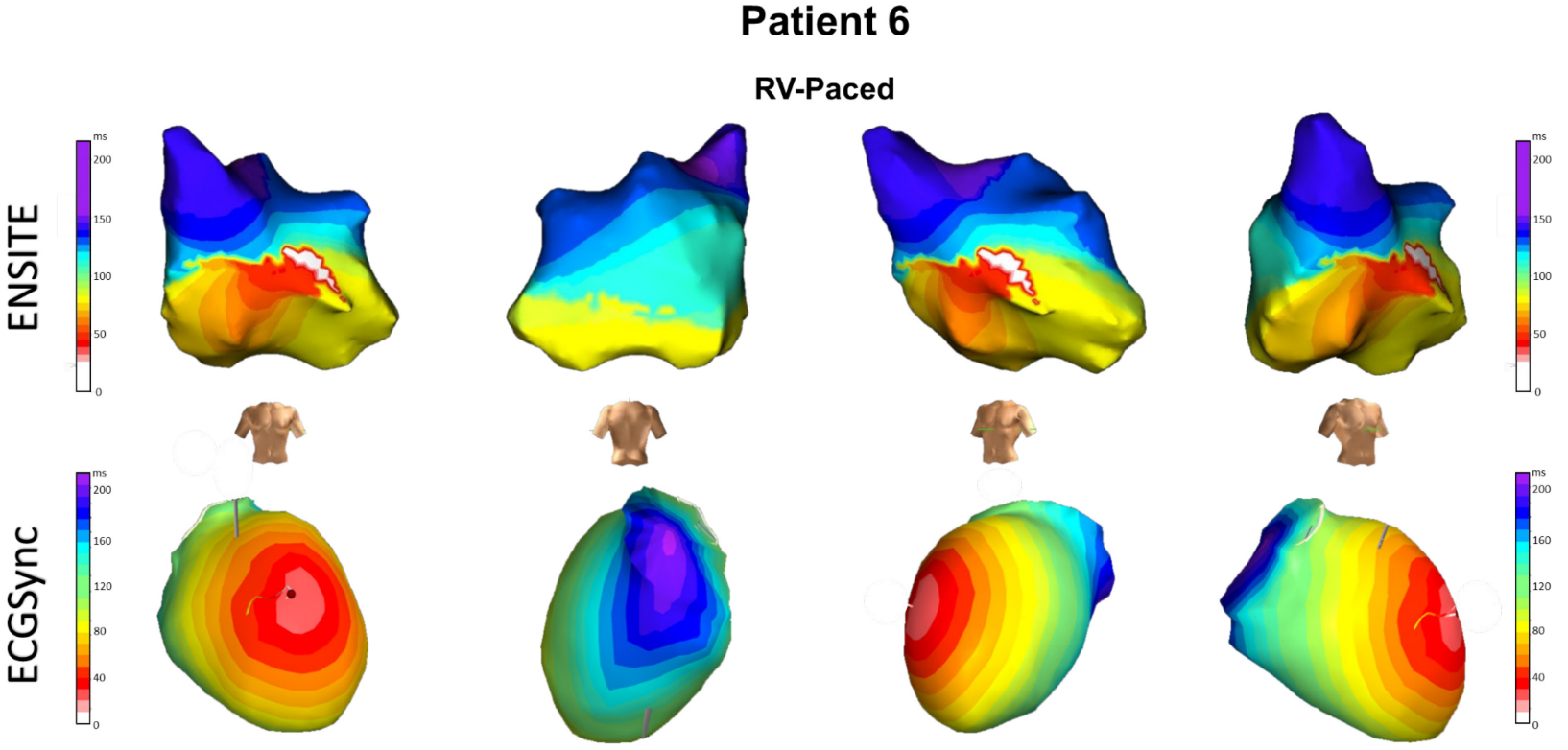
Patient 6
RV-Paced
ENSITE
ECGSync
ms
200
150
100
50
0
160
120
80
40

Patient 7 – Intrinsic

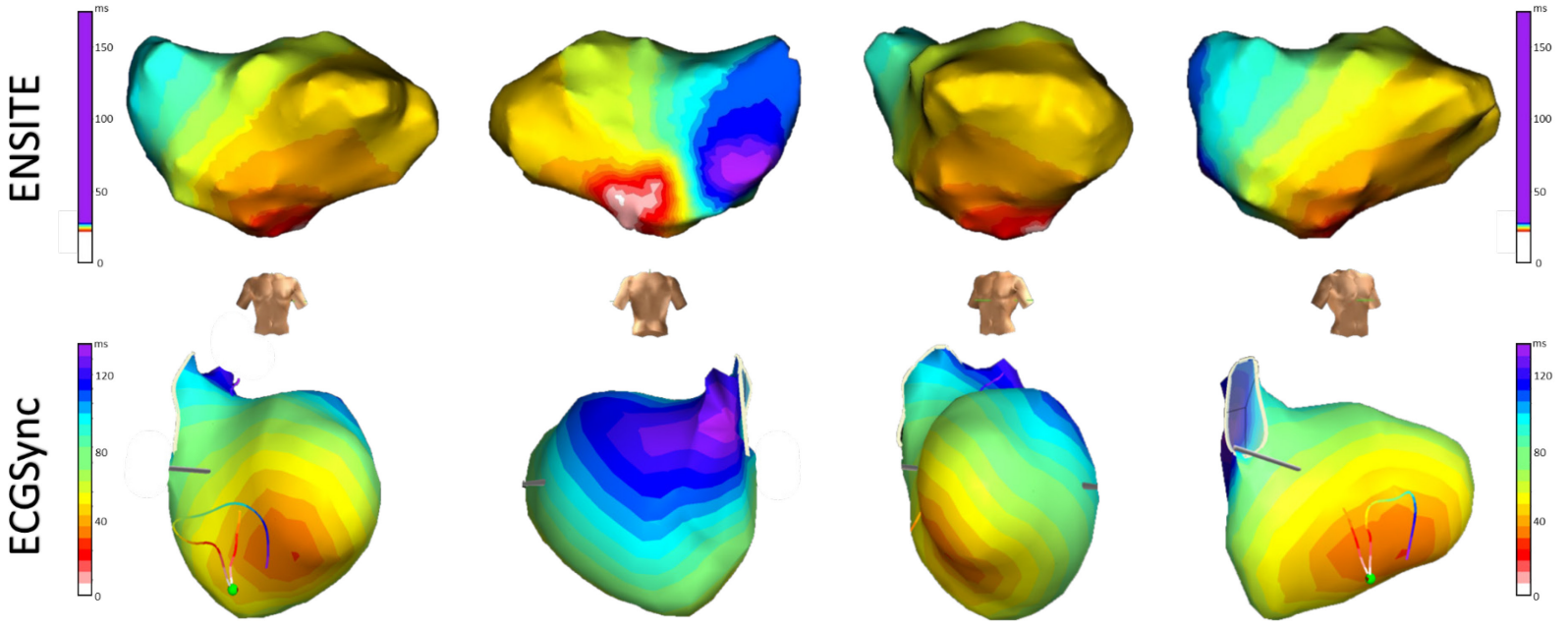

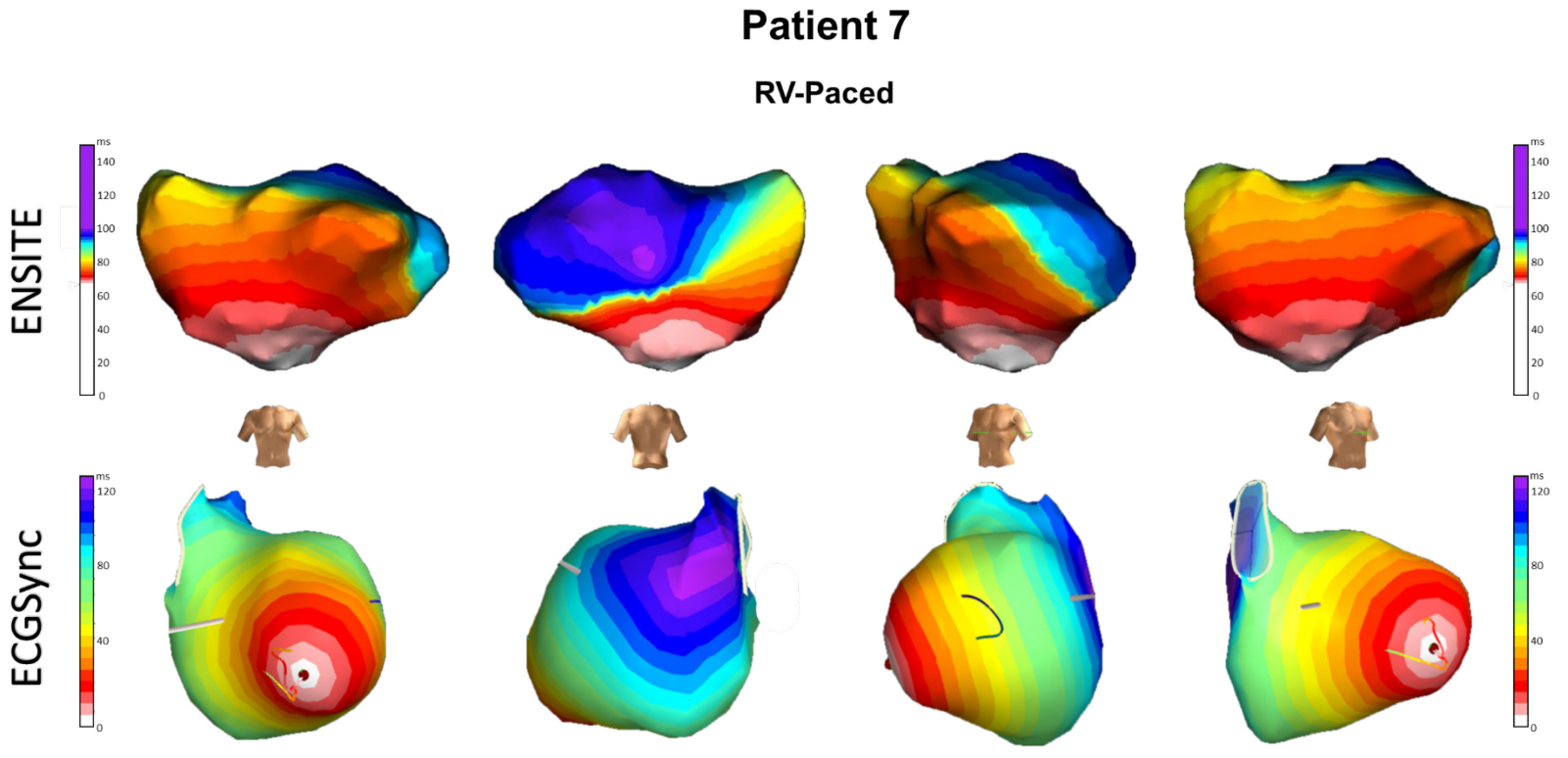
Patient 7
RV-Paced
ENSITE
ECGSync
ms
140
120
100
80
60
40
20
0

Patient 8 – Intrinsic

LBBB

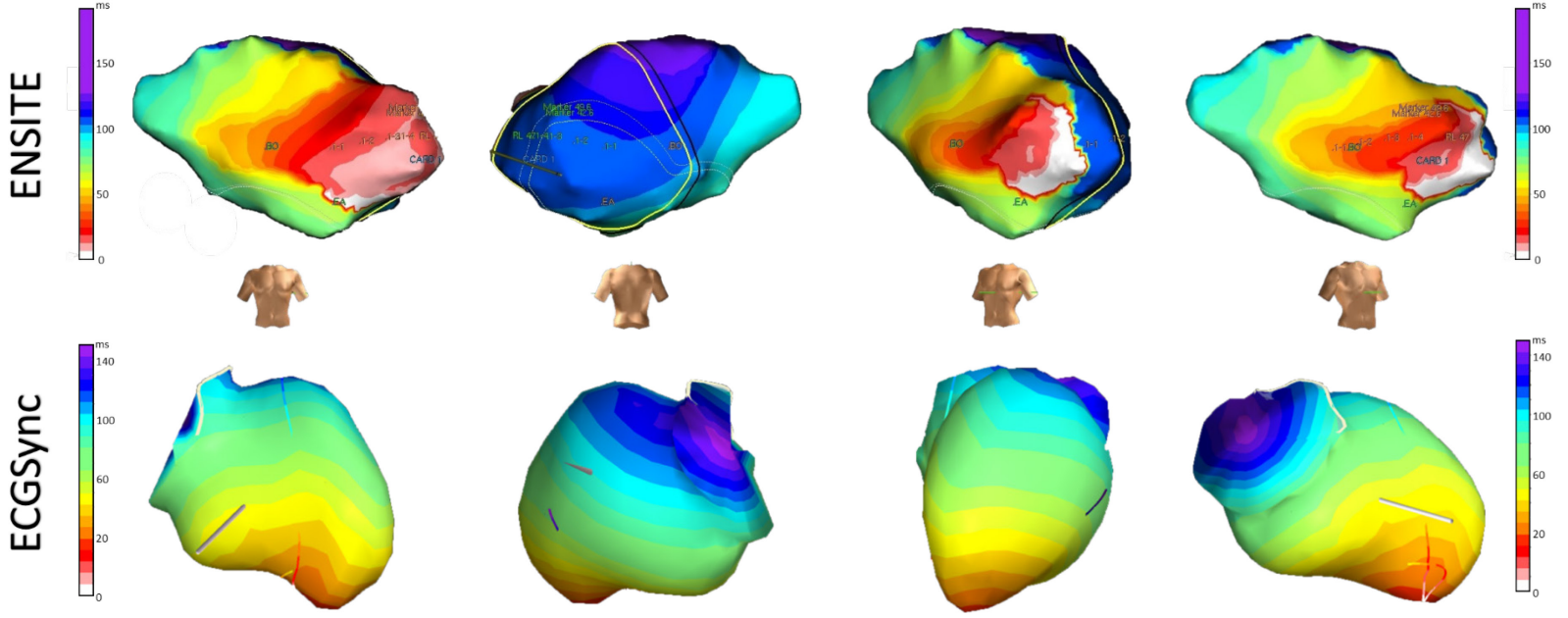

Patient 8

RV-Paced

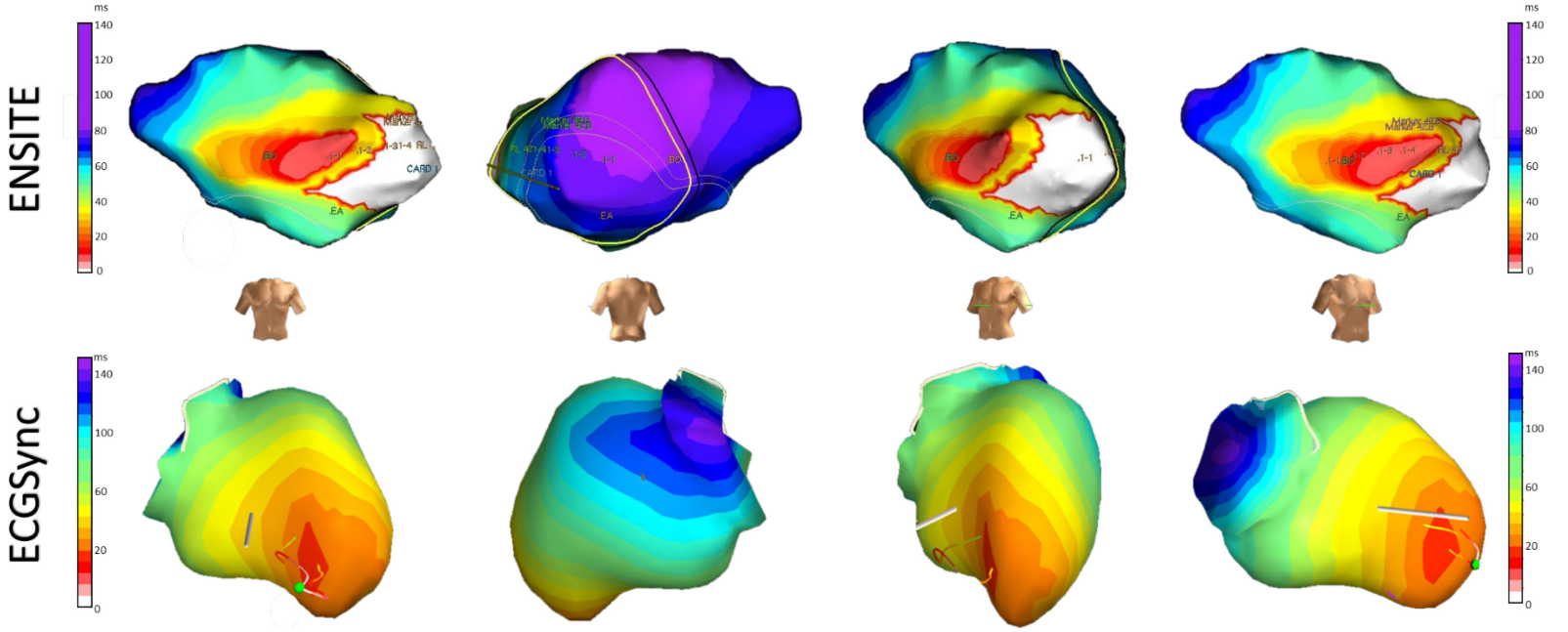

Patient 9 – Intrinsic

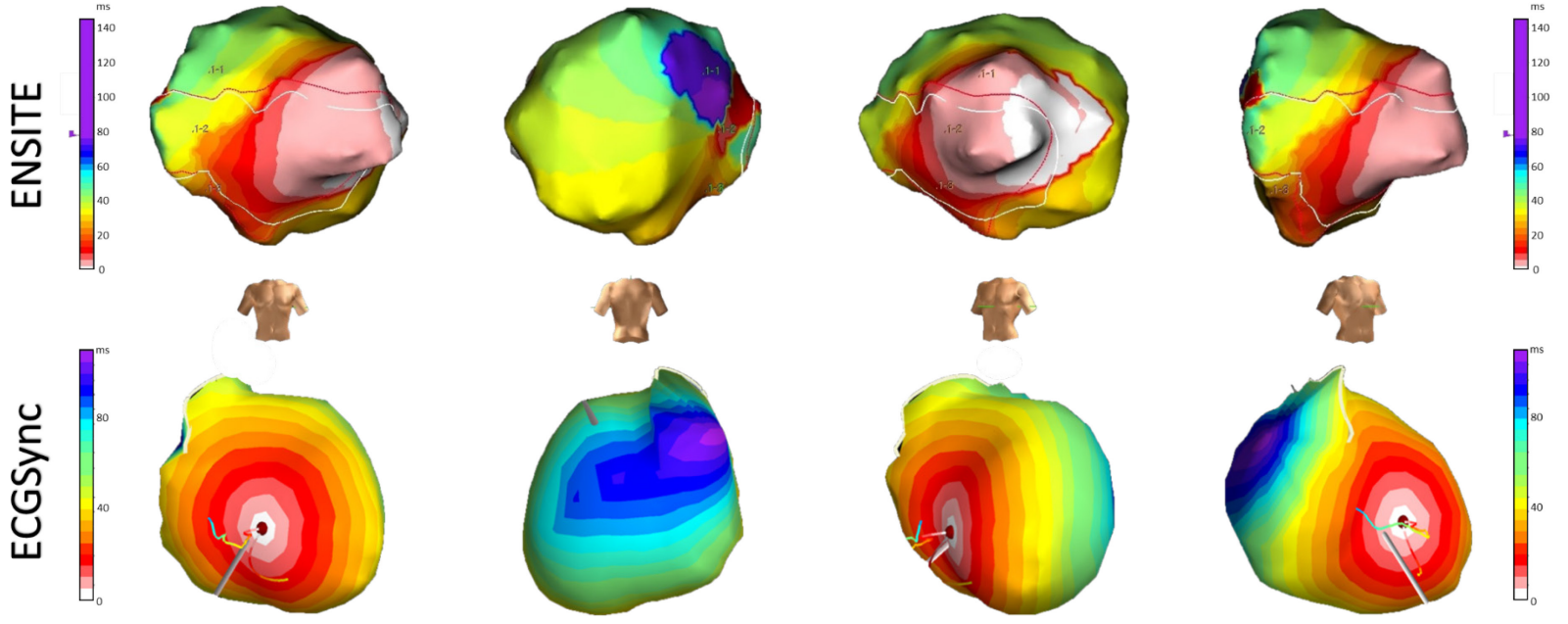

Patient 9

RV-Paced

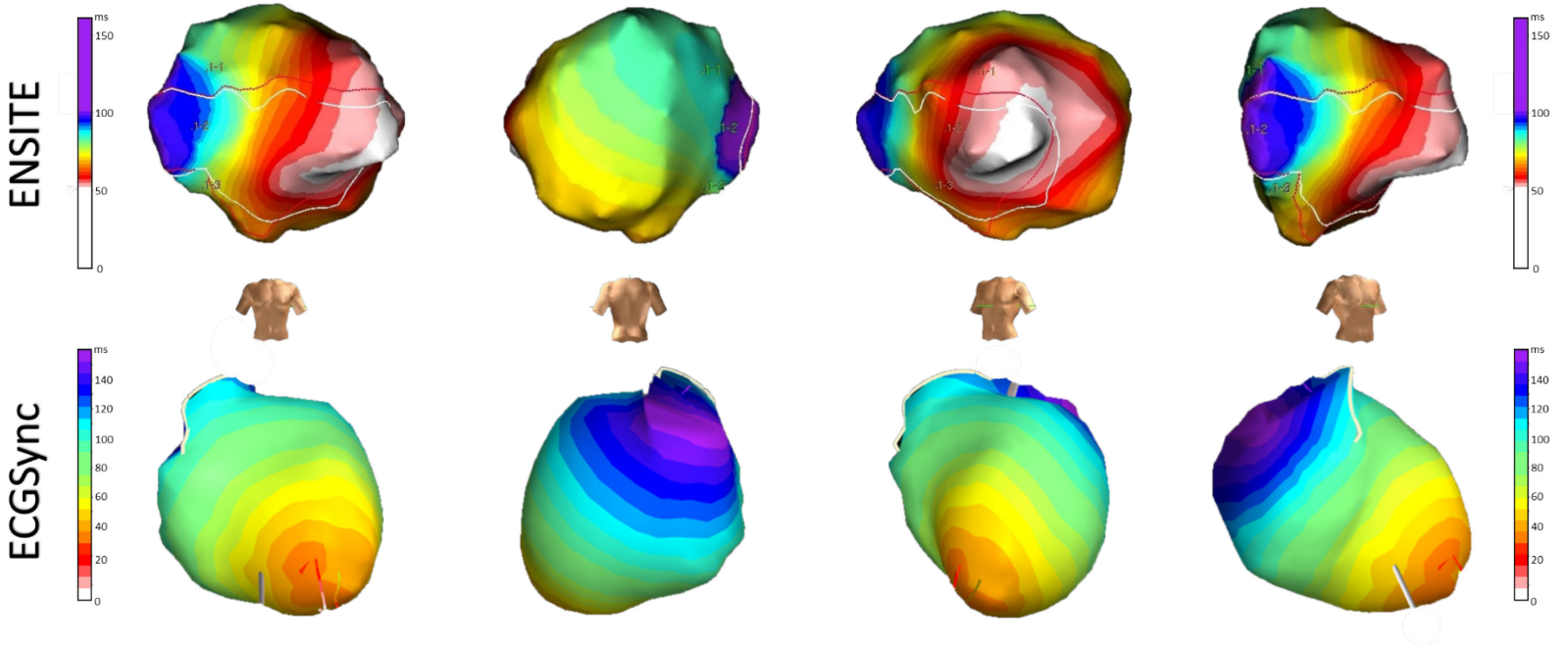

Patient 10 – Intrinsic

LBBB

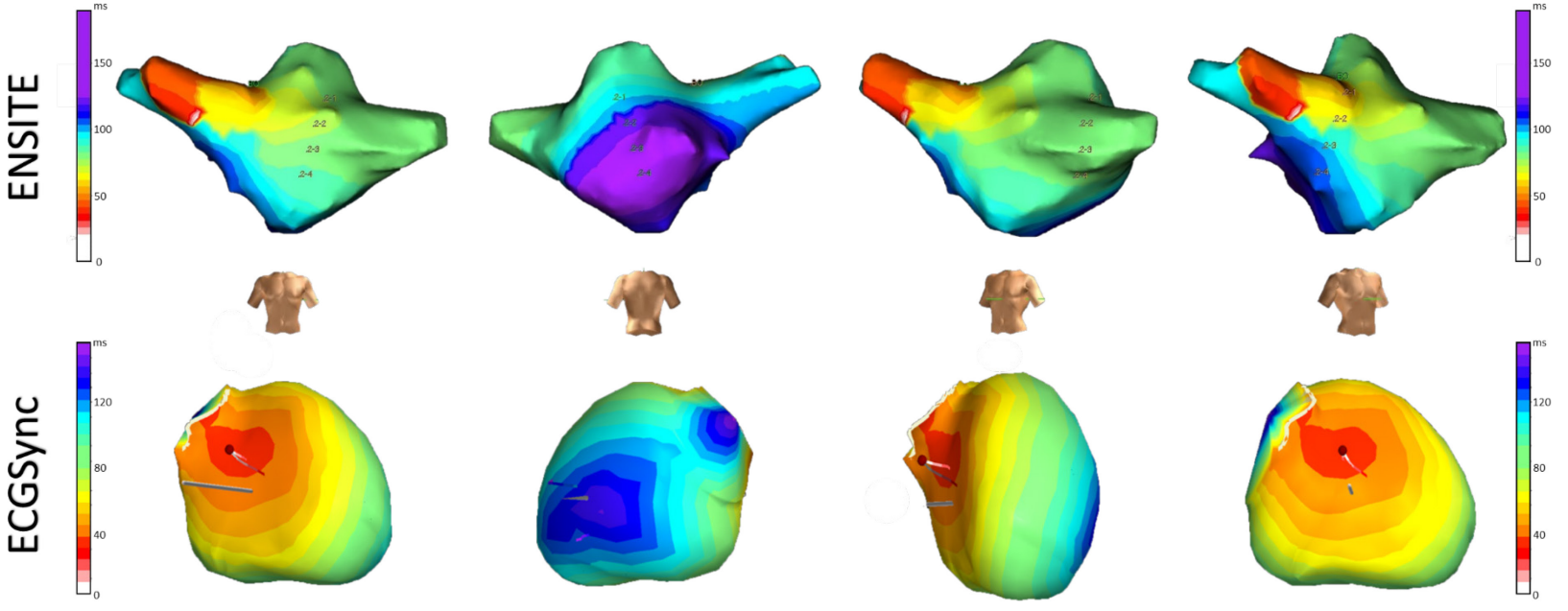

Patient 11 – Intrinsic

LBBB

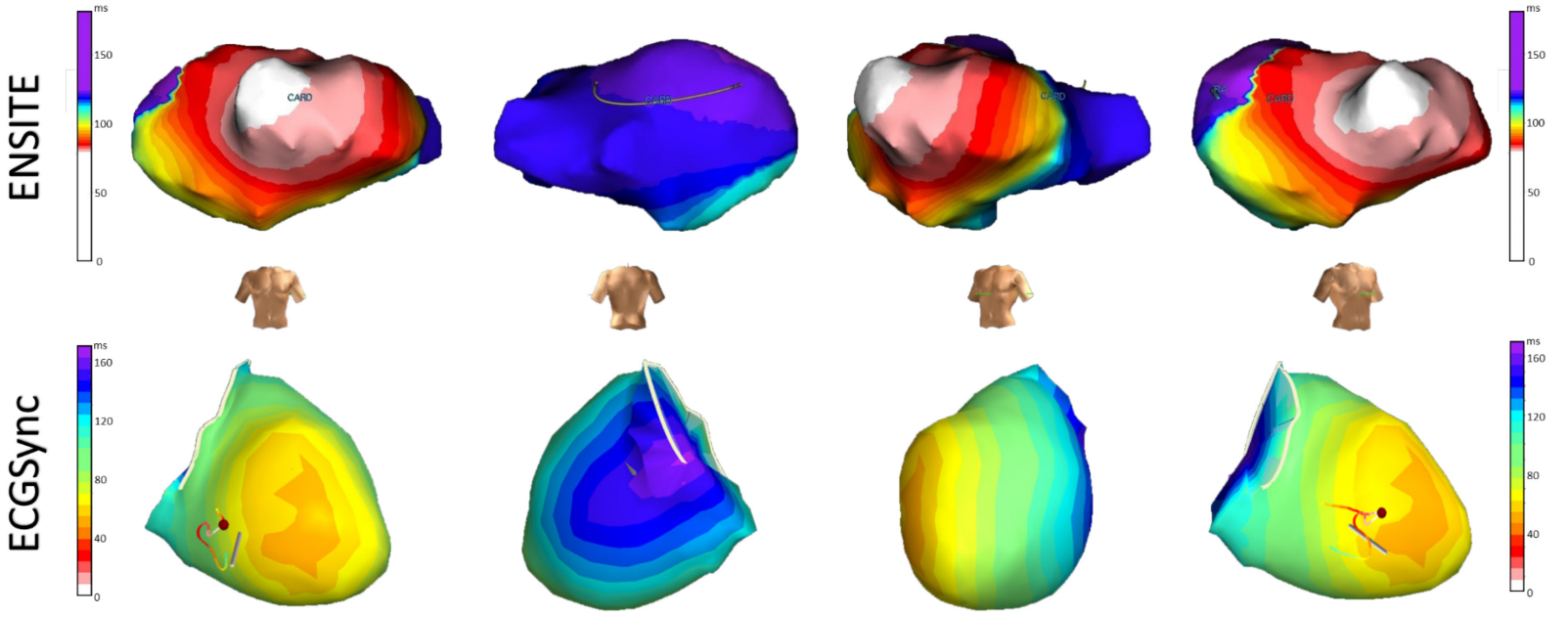

Patient 11

RV-Paced

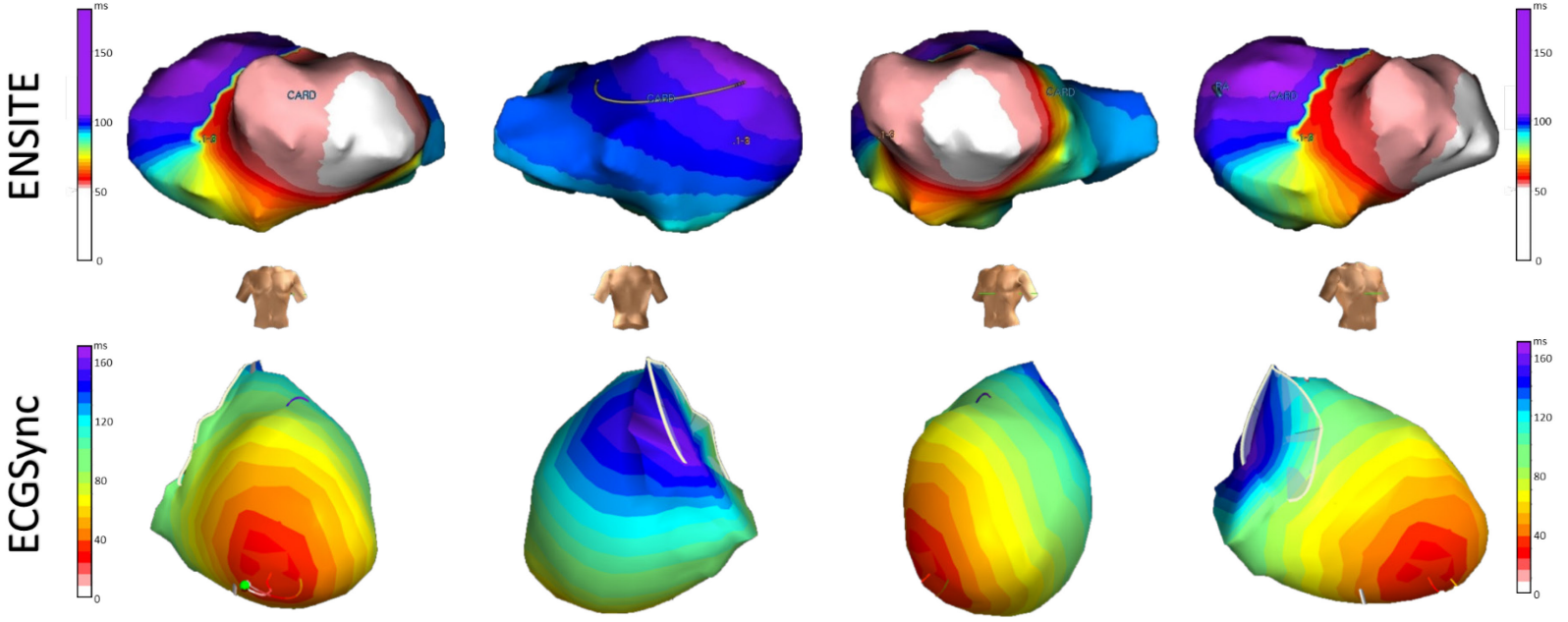

Patient 12 – Intrinsic

LBBB

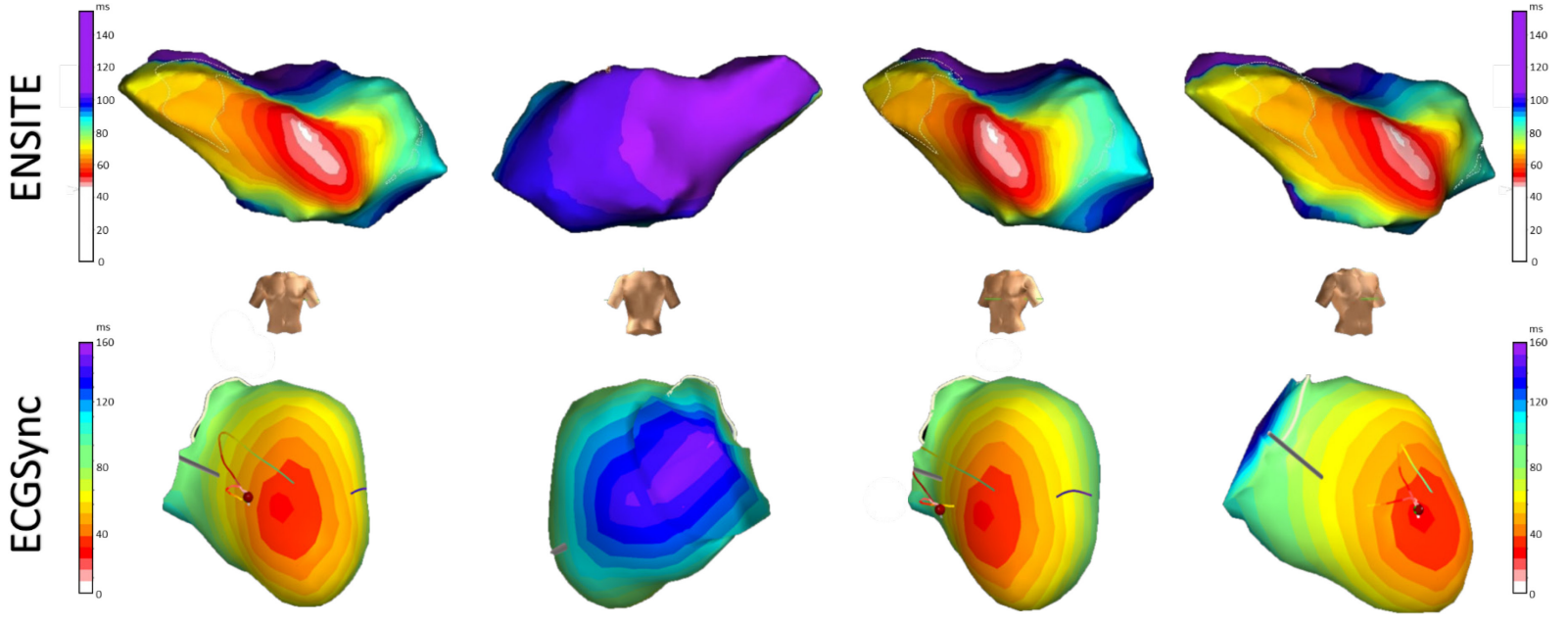

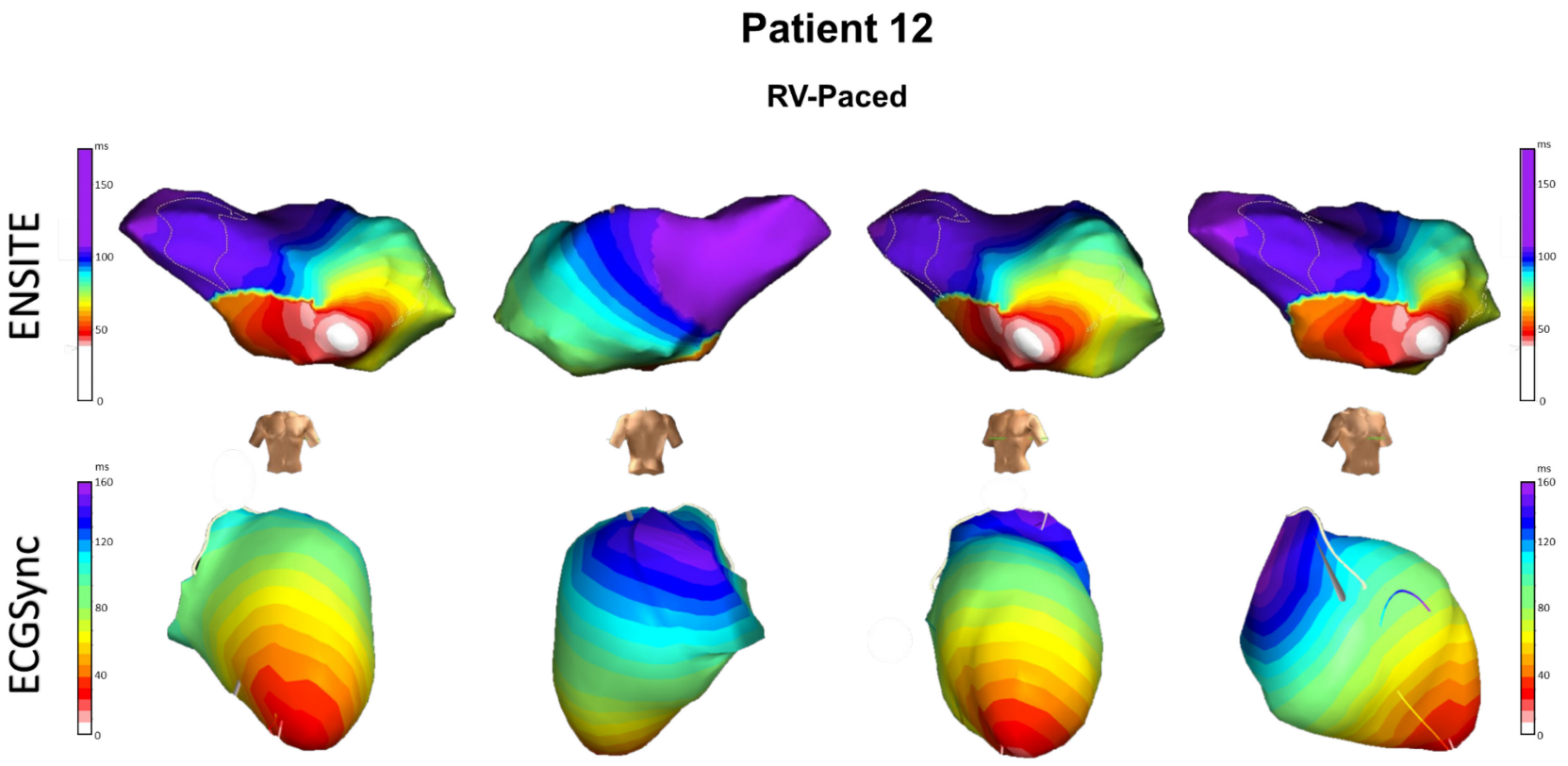
Patient 12
RV-Paced
ENSITE
ECGSync
ms
150
100
50
0
160
120
80
40

Patient 13 – Intrinsic

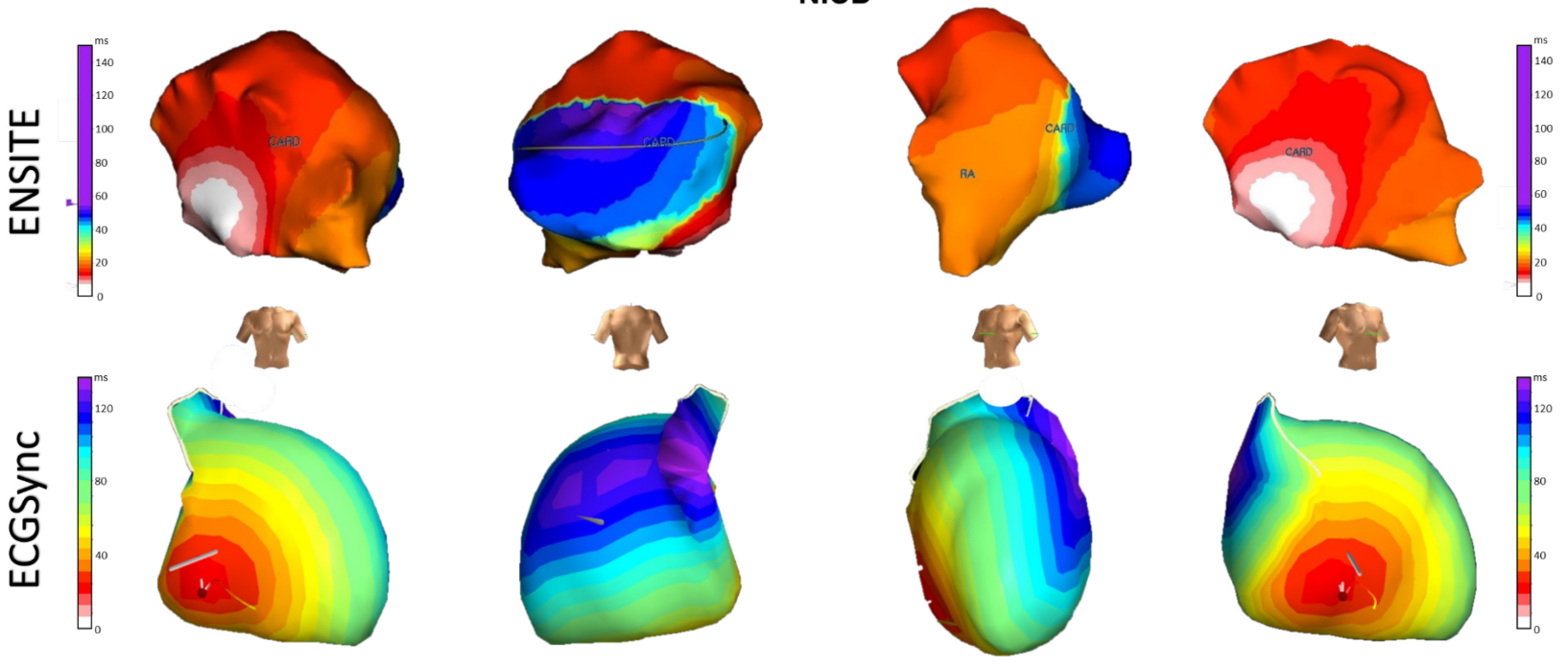

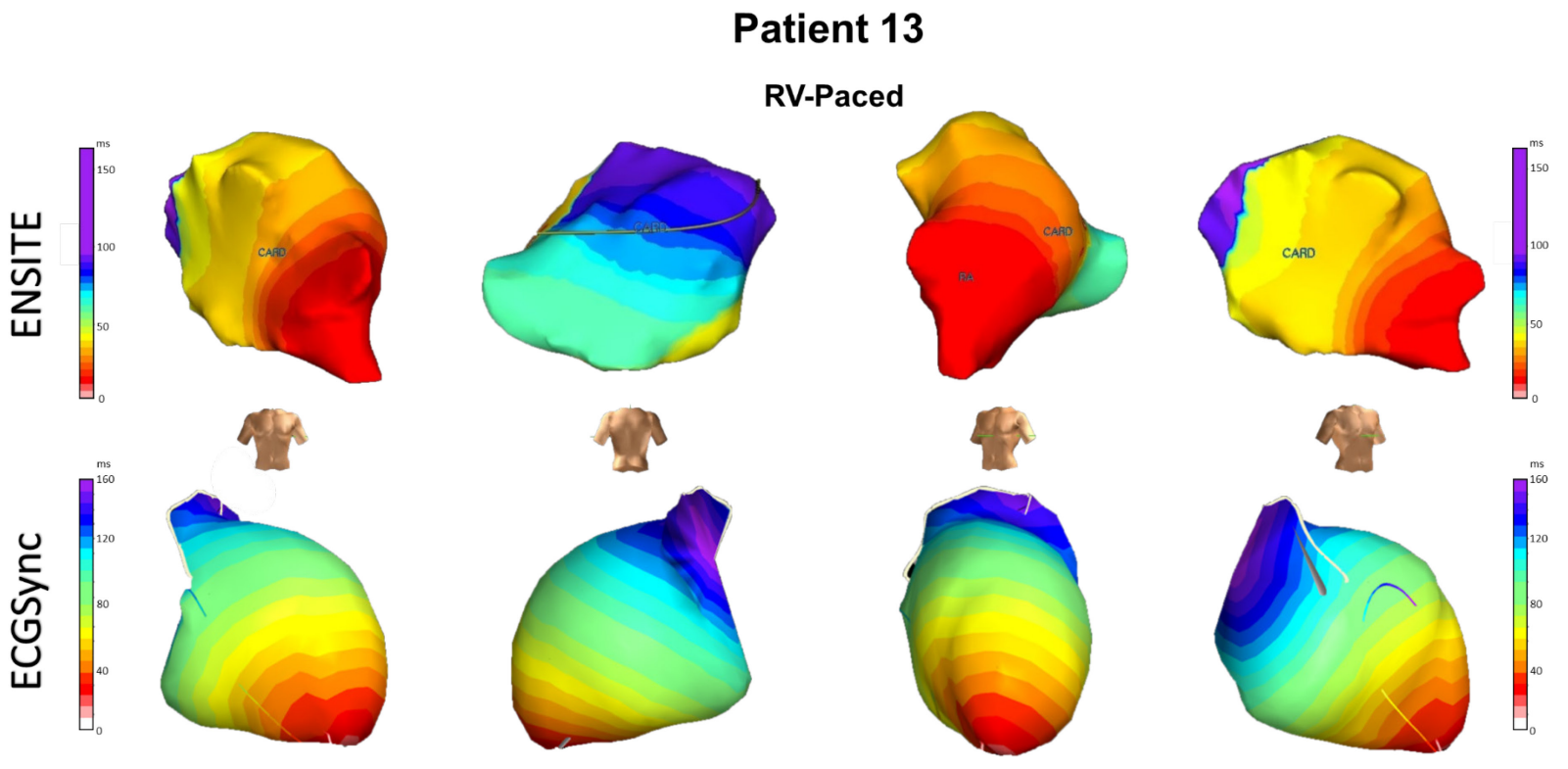
Patient 13
RV-Paced
ENSITE
ECGSync
ms
150
100
50
0
160
120
80
40
CARD
RA

Patient 14 – Intrinsic

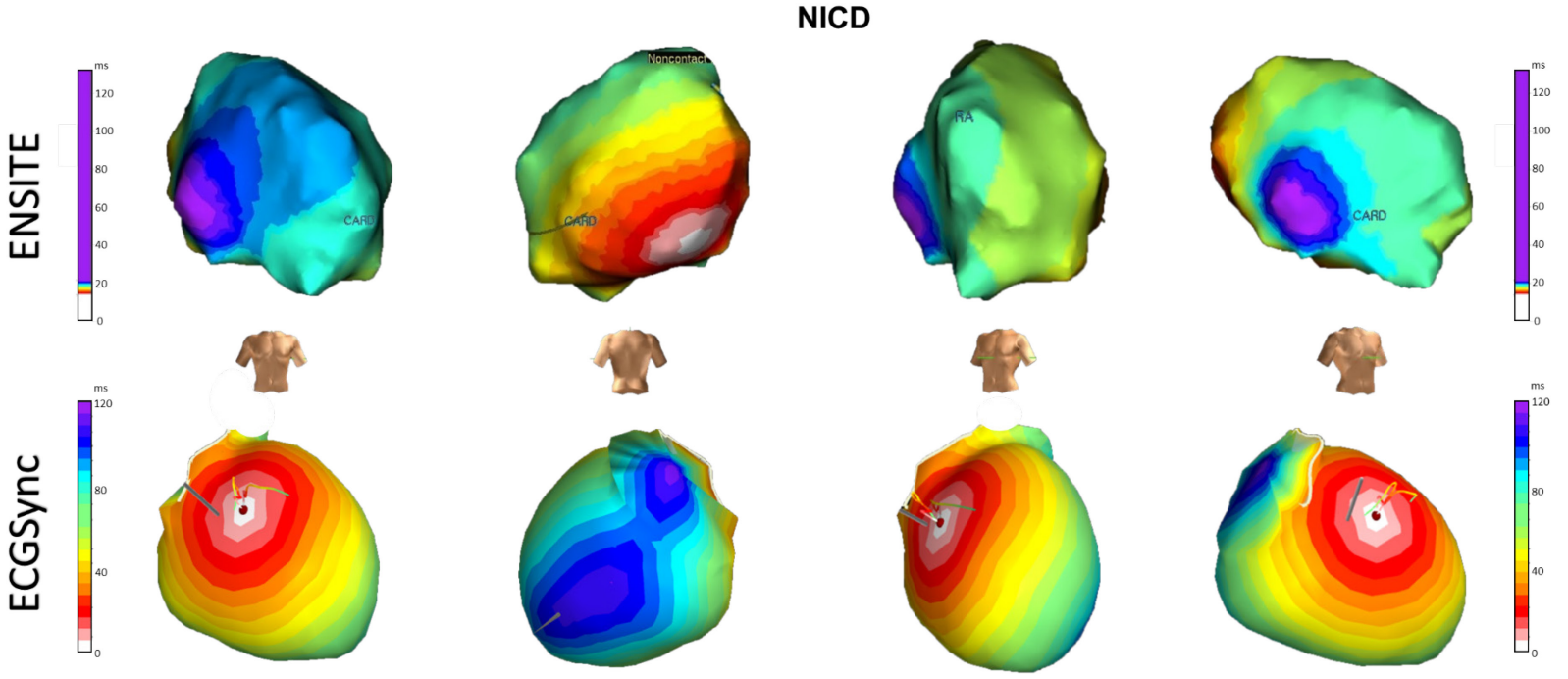

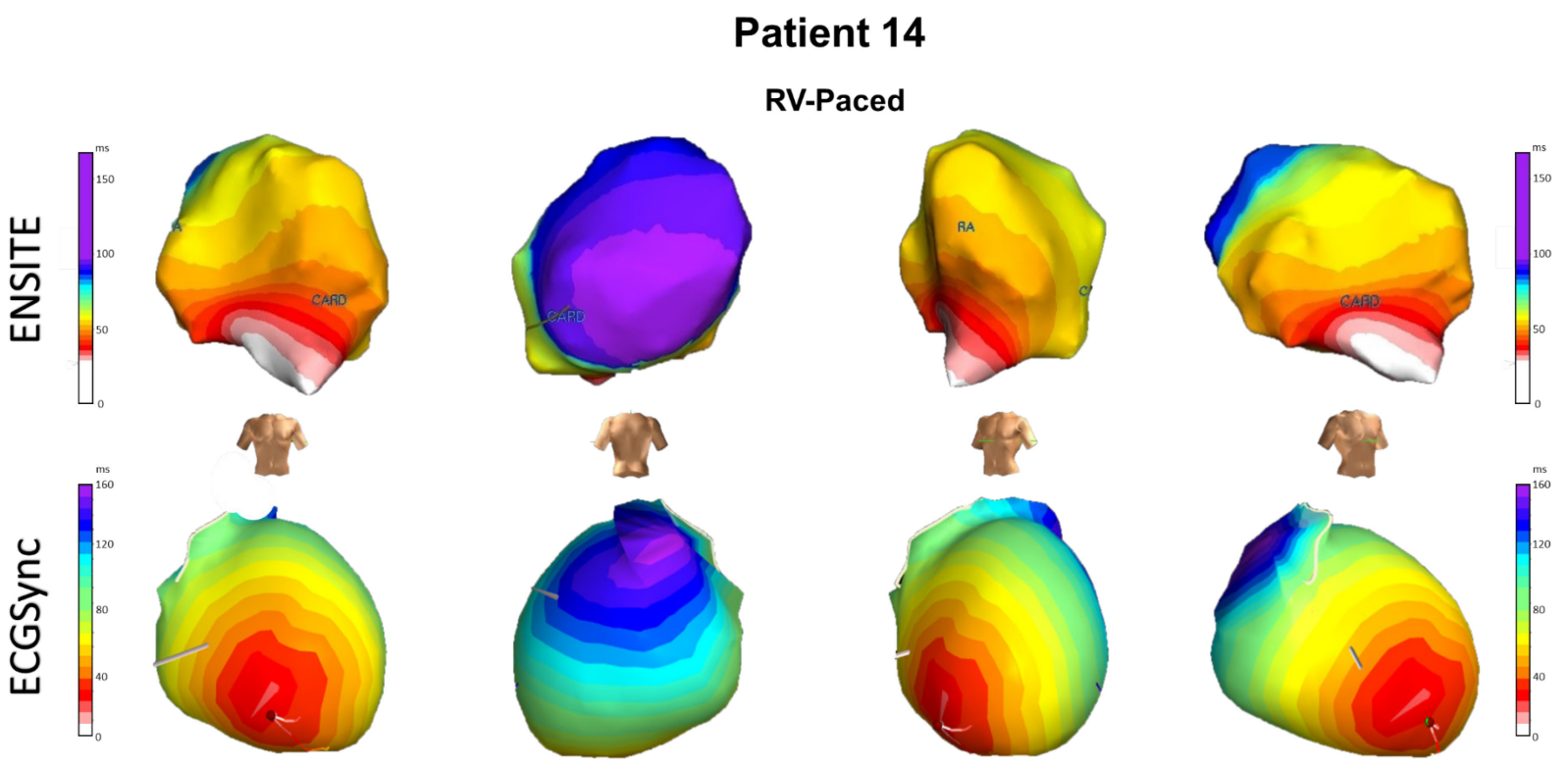
Patient 14
RV-Paced
ENSITE
ECGSync
ms
150
100
50
0
160
120
80
40
CARD
RA

Patient 15 – Intrinsic

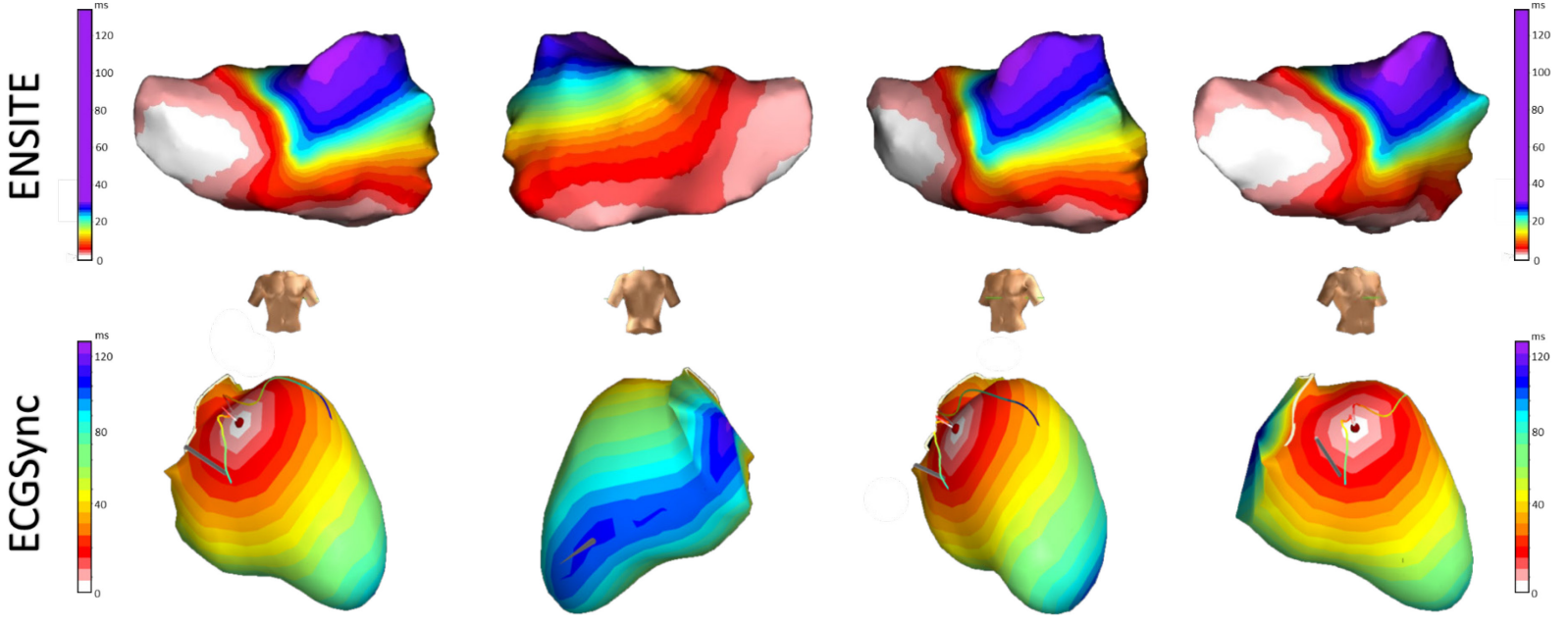

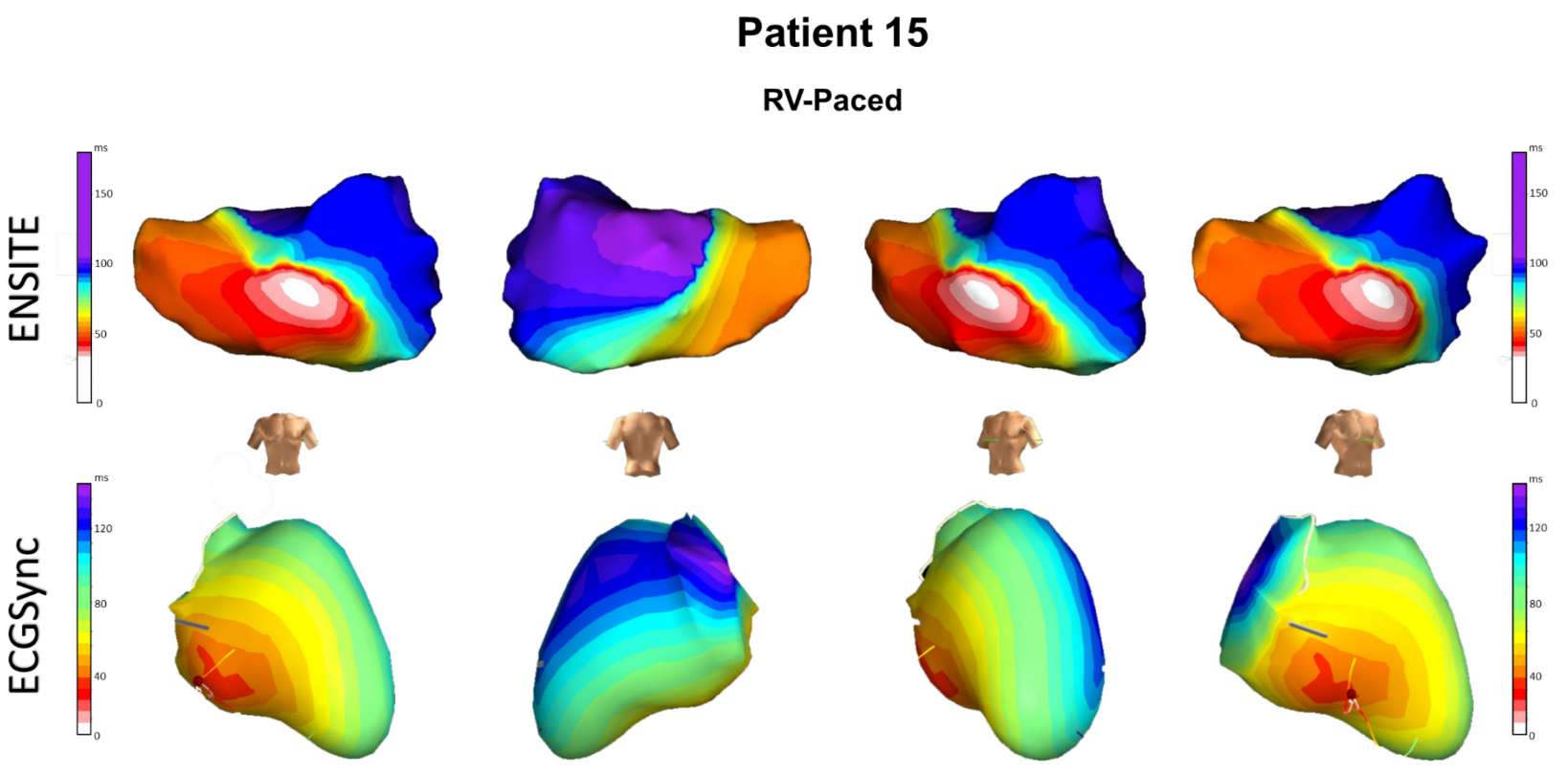
Patient 15
RV-Paced
ENSITE
ECGSync
ms
150
100
50
0
120
80
40

Patient 16 – Intrinsic

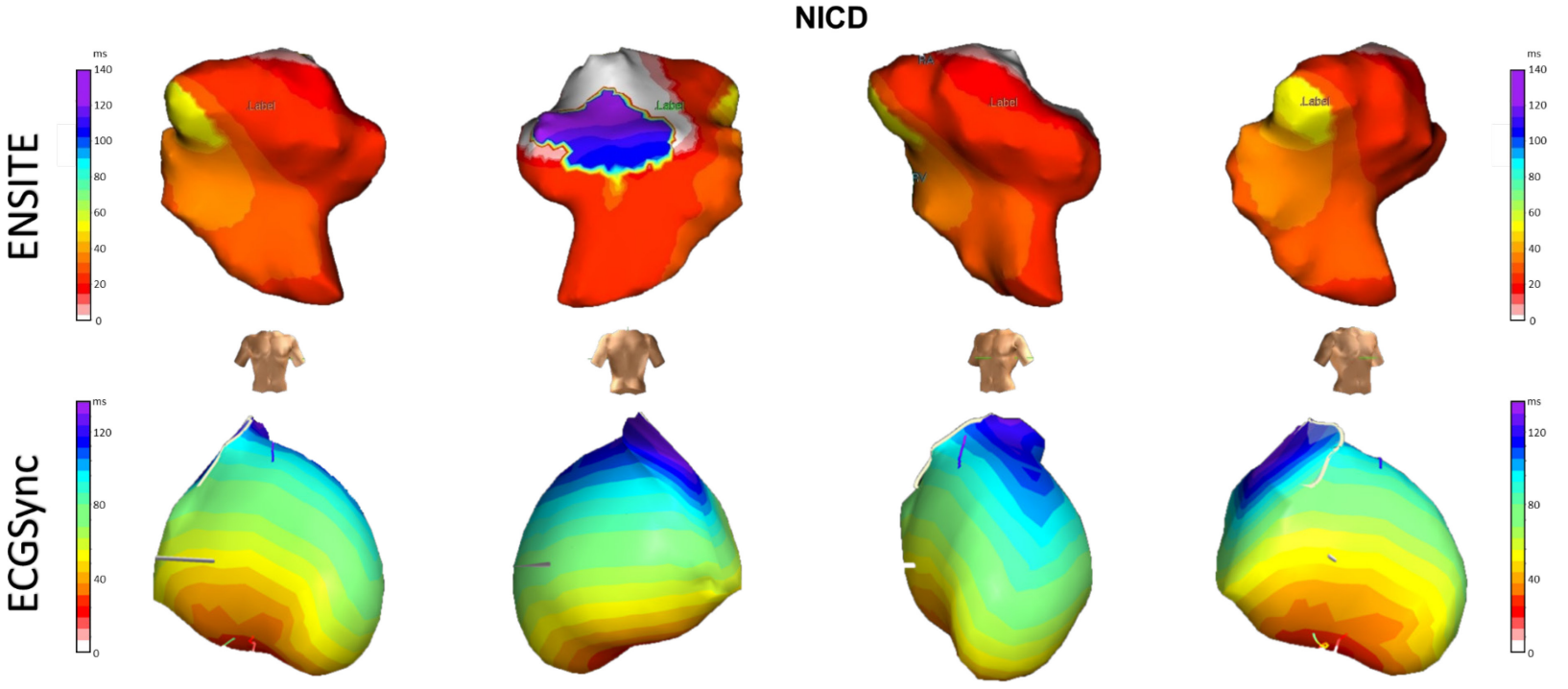

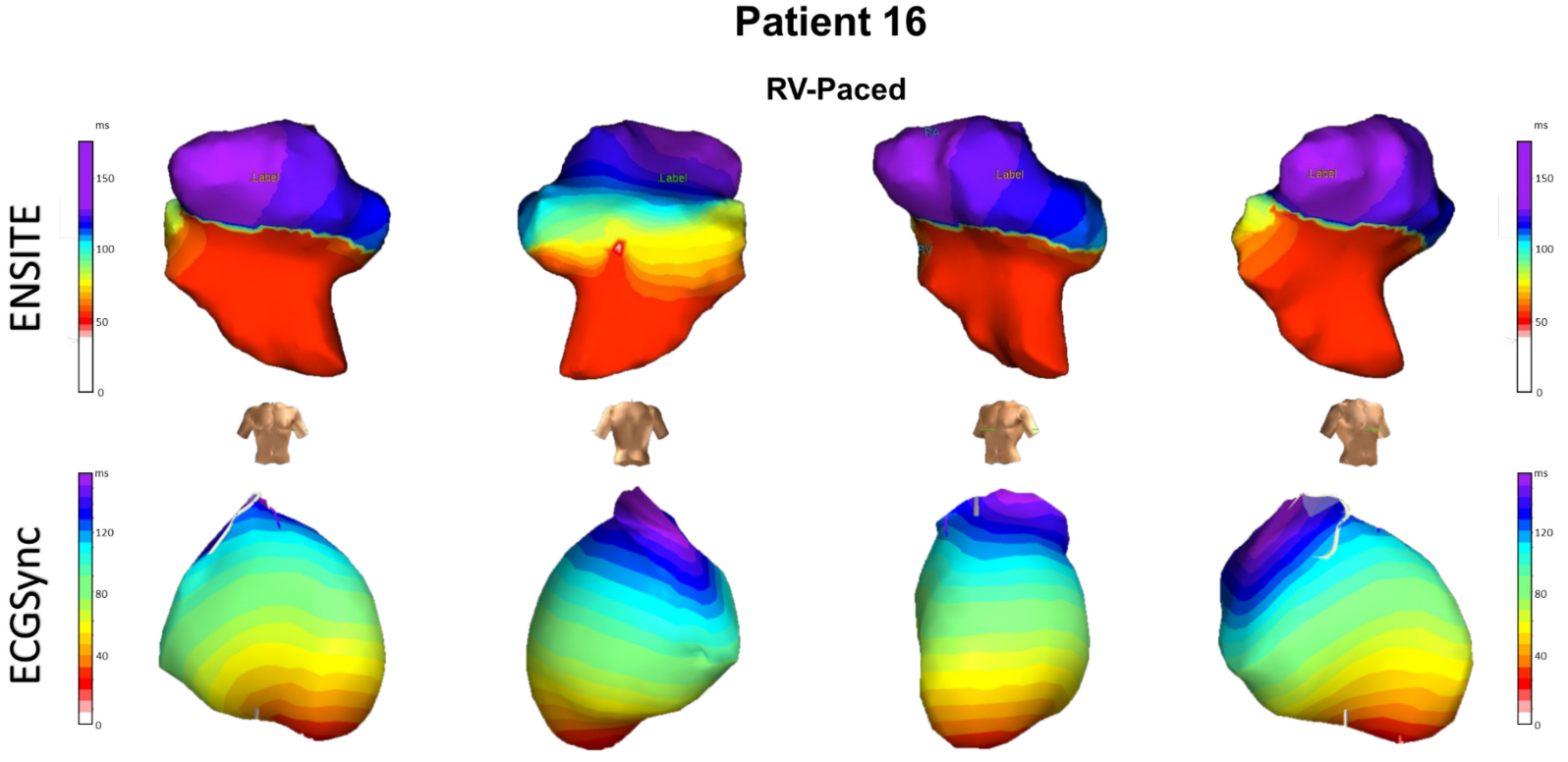
Patient 16
RV-Paced
ENSITE
ECGSync
ms
150
100
50
0
120
80
40
Label